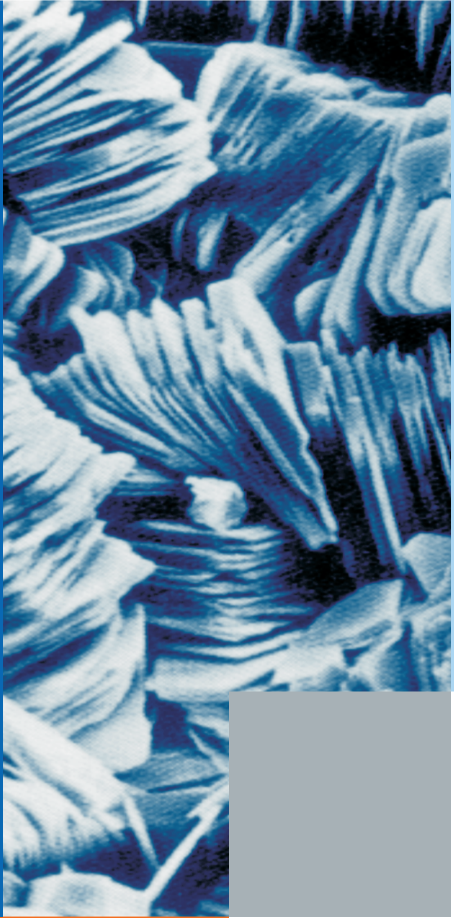

Universität Stuttgart

Numerical Analysis and Design Criteria of Embankments on Floating Piles

Syawal Satibi

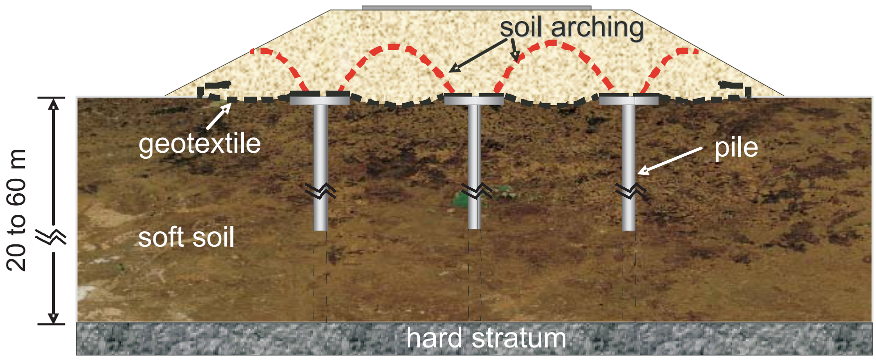

2009 Mitteilung 62
des Instituts für Geotechnik
Herausgeber P. A. Vermeer

IGS

Universität Stuttgart
Syawal Satibi
2009 - Mitteilung 62

Numerical Analysis and Design Criteria of Embankments on Floating Piles

Von der Fakultät für Bau– und Umweltingenieurwissenschaften
der Universität Stuttgart
zur Erlangung der Würde eines Doktors der Ingenieurwissenschaften (Dr.-Ing)
genehmigte Abhandlung,

vorgelegt von

SYAWAL SATIBI

aus Bengkalis, Indonesien

Hauptberichter: Prof. Dr.-Ing. P. A. Vermeer
Mitberichter: Prof. Dr. techn. H.-F. Schweiger, M. Sc.

Tag der mündlichen Prüfung: 13. Mai 2009

Institut für Geotechnik der Universität Stuttgart

2009

Mitteilung 62
des Instituts für Geotechnik
Universität Stuttgart, Germany, 2009

Editor:
Prof. Dr.-Ing. P. A. Vermeer

Institut für Geotechnik
Universität Stuttgart
Pfaffenwaldring 35
70569 Stuttgart

Keywords: Piled embankment, floating piles, numerical analysis

Printed by DCC Siegmar Kästl e. K., Ostfildern, Germany, 2009

ISBN 978-3-921837-62-7
(D93- Dissertation, Universität Stuttgart)

Preface

In recent years, the Institute of Geotechnical Engineering of Stuttgart University participated in a Marie Curie Research Training Network of the European Union named AMGISS (Advanced Modelling of Ground Improvement of Soft Soils) with the aim to advance numerical modelling of ground improvement. Within this well-coordinated research network of six different European universities, Stuttgart had to focus on embankments on floating piles, being the subject of this thesis by Syawal Satibi.

In 2004, Syawal Satibi wrote me an email in which he expressed his desire to do a PhD-study on soft soil improvement. He was motivated by the fact that some thirty percent of the surface of his home country, Indonesia, is covered with soft soils where I witnessed myself embankment construction on short floating piles. As the effectiveness of such piles is not so obvious, I suggested Syawal Satibi to study floating piles. The German Academic Exchange Service (DAAD) was so kind to fund this proposal and this made it possible for Syawal Satibi to come to Stuttgart in 2005.

For soft layers of limited depth, the use of end-bearing piles is obvious, but they become extremely costly when the bearing stratum is at great depth. In such cases, floating piles will be of advantage. In simple cases of relatively dense grids of piles of one particular pile length, the settlement calculation is straight forward and numerical analyses are not needed, but an optimal design is based on piles of different lengths as considered at the end of this thesis.

The final case study of this thesis is about a test embankment in Sweden, which requires a numerical study both because of the different pile lengths involved and the significant creep of the soft soil layers. In fact, that particular case study constitutes an extremely nice end of a fine PhD study, with whom I would like to congratulate Syawal Satibi.

This dissertation study also marks the end of a fruitful research period of the AMGISS research training network, which was well led by Dr. Minna Karstunen of Strathclyde University in Glasgow, UK. Within this network, research on soft soils in Stuttgart was not only conducted by Syawal Satibi, but also by Raymond van der Meij, Dr. Ayman Abed and last but not least by Dr. Martino Leoni. All of us liked working with Syawal Satibi very much. Now that he returns to Indonesia, he will continue his career in geotechnical engineering and I do hope to remain in contact.

Prof. Dr.-Ing. Pieter A. Vermeer

Stuttgart, June 2009

Acknowledgement

I am deeply indebted to my supervisor Professor Pieter A. Vermeer for his ultimate help and patient guidance during my doctoral study. Professor Vermeer has not only enriched my knowledge but also has opened my view on the high standard of scientific life. I have been given the opportunity to participate in the AMGISS (Advanced Modelling of Ground Improvement on Soft Soils), a Marie Curie research training network in which I gained valuable experiences of advanced geomechanics research community and learned about modelling and applications of soft soil improvement techniques. I am also thankful to my co-advisor Professor H. F. Schweiger for his suggestions on my research work on embankments on floating piles.

I am very grateful to the German Academic Exchange Service (DAAD) for granting me the scholarship for my doctoral study and for introducing me to the unique German culture. Universität Stuttgart and in particular my doctoral program "ENWAT" are highly acknowledged for providing me a very high standard of learning opportunity.

I would like to especially thank to Dr. Martino Leoni, Raymond van der Meij and Dr. Ayman Abed for the ultimate support and fruitful discussions in my research work and in my dissertation writing.

I also warmly thank all may colleagues at the Institute of Geotechnical Engineering (IGS) for the precious and pleasant time that I spent with them. I always felt like I were with my family.

My thank also goes to Indonesian community in Stuttgart for the support and the cordial relationship, which relief me from feeling homesick.

My most special thank to my mother and my late father for their love, care and encourage to me to remain motivated and optimistic in life.

Syawal Satibi

Stuttgart, June 2009

Contents

Abstract

The increasing need for infrastructure development often forces engineers to find safe ways of building on soft soils. Soft soil cannot sustain external loads without having large deformations. Thus, soil improvement is needed. One of the soil improvement techniques is a piled embankment. When the installed piles do not reach a hard stratum due to large thickness of the soft soil layer, the construction is called an "embankment on floating piles". The design of embankments on floating piles involve complex soil-structure interaction. Nowadays, numerical methods such as finite element analysis are available for solving complex soil-structure interaction problems. Nevertheless, there are no clear, uniform procedures or guidelines available for the design of embankments on floating piles using the finite element method.

This research is focused on establishing reliable calculation procedures for the design of embankments on floating piles using the finite element method. To fulfil this aim, several research topics were studied, including soil arching analysis, effects of pile installation process, and settlements analysis of embankment on floating piles using the finite element method with calibration to field measurements. Additionally, important design criteria of embankments on floating piles are highlighted.

The research findings on numerical analyses of soil arching clarify some uncertainties, which include: the influence of numerical geometrical idealizations, the influence of geotextile reinforcements, the influence of capping ratio, and the influence of constitutive models on soil arching action in piled embankment design in general. Moreover, sensitivity analyses are performed to identify which parameters have significant influence on the results of soil arching analysis. In addition, a clear and repeatable procedure to simulate the effects of displacement piles installation, which is called K − Pressure method, has been developed. The method is important especially for the analysis of displacement floating piles as used for soft soil improvement. It is developed for axisymmetrical analyses based on stress-controlled cavity expansion. The method is considered a sound method for displacement piles analysis and can be used within the realm of engineering practice. The applicability of this method is not limited to displacement piles, but can also be extended to other column type foundations. Furthermore, approaches for assessing the settlements and the effectiveness of embankments on floating piles using analytical methods and the finite element method have been shown. It is found that, generally, an embankment on floating piles is an effective method for soft soil improvement. A simple method for estimating the effectiveness of embankments on floating piles based on the concept of block behaviour has been presented. This method is very useful and easy to apply in practice. Based on analyses of a case study of embankments on floating piles, it was found that the use of long floating piles is essential for reducing long-term settlement due to creep of soft soil. For economic considerations, a construction combining short and long piles can represent the optimal balance between cost and settlement reduction. Finally, the research is concluded with recommendations for further research on the design of embankments on floating piles.

Zusammenfassung

Infolge einer ständig wachsenden Infrastruktur müssen immer mehr Bauvorhaben auf weichen Böden geplant und ausgeführt werden. Auf Grund der geringen Steifigkeit ist dies in der Regel mit großen Verformungen verbunden. Bei Infrastrukturmaßnahmen werden meisten Dammschüttungen erforderlich, bei denen die weichen Böden verbessert werden müssen. Eine mögliche Methode zur Bodenverbesserung ist eine Dammkonstruktion auf Pfählen. Erreichen die Pfähle, folge einer großen Mächtigkeit der weichen Bodenschichten, keine tragfähige Schicht, so wird diese Konstruktion als Damm auf schwimmenden Pfählen bezeichnet.

In Folge der Setzungsdifferenz zwischen den steifen Pfählen und dem umgebenden Untergrund bildet sich im granularem Dammkörper eine Gewölbe zwischen den Pfahlköpfen aus. Dieses Gewölbe transferiert die Last aus dem Eigengewicht des Damms in die Pfähle, welche die Last in tiefere und tragfähigere Schichten ableiten. Um die Konstruktion aus Damm und Pfählen effektiv zu entwerfen, muss der Lastumlagerungsmechanismus im Dammkörper im Detail bekannt sein. Wird zusätzlich ein Geotextil als Bewehrung verwendet, können die Zugkräfte aus der Gewölbewirkung an Dammsohle aufgenommen werden und die Konstruktion damit noch steifer ausgeführt werden. Durch das Geotextil wird der Anteil der Last der durch die weichen Böden abgetragen wird weiter verringert und die Setzungen weiter verringert.

In Süd-Ost Asien und Skandinavien gibt es große Gebiete in denen weiche Böden bis zu einer Mächtigkeit von 40 m vorkommen. In Indonesien befinden sich die weichen Böden vor allem an der Küste und umfassen ein Gebiet von 60 Millionen Hektar Land, also rund 30 Prozent der gesamten Landfläche Indonesiens. In diesem Gebiet befinden sich ebenfalls die meisten Großstädte. Im Osten von Sumatra, im Süden von Kalimantan und im Süden von Irian Jaya werden die weichen Tonböden typischerweise durch Torfschichten überlagert. In diesen Gebieten sind Dammschüttungen auf schwimmenden Pfählen eine ideale Konstruktion für Infrastrukturmaßnahmen.

Beim Entwurf eines Dammes auf schwimmenden Pfählen muss die komplexe Boden-Bauwerk Interaktion berücksichtigt werden. Dies kann mit numerischen Methoden wie z.B. der Finite-Elemente Methode im Detail untersucht werden. Dennoch sind klare und einheitliche Leitlinien für den Entwurf und die Berechnung der Dämme auf schwimmenden Pfählen mit Hilfe der Finite-Elemente Methode nicht vorhanden.

Dieses Forschungsvorhaben versucht zuverlässige Verfahren für den Entwurf von Dämmen auf schwimmenden Pfählen mit der Finite-Elemente Methode zu schaffen. Darüber hinaus wird die Gewölbewirkung im auf Pfählen gegründeten Dammkörper sowie der

Einfluss der verschiedenen Prozesse zur Herstellung von Verdrängungspfählen und die Verformungen der Dämme auf schwimmende Pfähle im Detail untersucht. Dabei werden die Ergebnisse der Finite-Elemente Untersuchungen mit in-situ Messungen verglichen. Zusätzlich werden die wichtigsten Kriterien für die Dimensionierung von Dämmen auf schwimmenden Pfähle herausgearbeitet. Hierbei werden die Kriterien für die Dimensionierung von Dämmen auf schwimmenden Pfähle hervorgehoben. In diesem Zusammenhang werden folgende Kapitel berücksichtigt:

Kapitel 2: Richtlinien zum Entwurf von Dämmen auf Pfählen

Diese Kapitel stellt ein Überblick über die wichtigsten Leitlinien für den Entwurf von Dämme auf Pfählen dar. Zwei Entwurfsmethoden aus dem British Standard BS8006 und der Deutschen Methode EBGEO 2004 sind in diesem Kapitel zusammengefasst und erläutert. Der British Standard BS8006 stellt einfache anzuwendende, auf der sicheren Seite liegenden Regeln dar und kann für einen konservativen Bemessung von Dämmen auf Pfählen verwendet werden. In der EBGEO 2004 wird ein neues Verfahren für den Entwurf der Dämme auf Pfählen dargestellt, welches auf einen sinvoller wissenschaftlichen Hintergrund in der Ermittlung der Belastung des Dammkörpers einsetzt. Diese beide Methoden konzentrieren sich auf die Ermittlung der Belastung des Dammkörpers auf die Pfähle und die Geotextillagen. Die Annahmen und Grenzen der Leitlinien vor allem zum Entwurf einen Damm auf schwimmenden Pfählen werden diskutiert.

Kapitel 3: Numerische Analyse der Gewölbewirkung

In diesem Kapitel wird die Gewölbewirkung in granularen Dämmen mit Hilfe numerischer Methoden untersucht. Zur Validierung der numerischen Studie wurde eine Versuchsreihe, die an der Universität Kassel durchgeführt wurde, nachgerechnet. Die Versuchsdurchführung gliedert sich folgender Maßen. Zwischen vier Pfählen, die in einem quadratischen Raster und einem Abstand von 0,5 m angeordnet waren, wurde weicher Boden schichtweise eingefüllt. Zwischen der obersten Lage aus Sand und dem weichen Boden wurde eine Kunststofffolie als ein Trennschicht eingelegt. Mit diesem Versuchsaufbau wurden zwei Testreihen durchgeführt. Bei einer Testreihe wurde zwischen Pfahlkopf und Sandschicht ein Geotextil angeordnet. Bei der anderen Testreihe wurde auf das Geotextil verzichtet.

Zur Validierung der Untersuchung der Gewölbewirkung wurden beide Testreihen mit Hilfe der Finite Elemente Methode simuliert. Es werden die wesentlichen Einflussfaktoren, d.h. die Geometrie, das Verhältnis von Pfahldurchmesser zum Durchmesser der Pfahlkopfplatte (pile capping ratio) sowie die verwendeten Stoffgesetze, der numerischen Untersuchung diskutiert. Außerdem wird der Einfluss der Anzahl der Geotextillagen auf die Ausbildung des Gewölbes im Dammkörper mit der Finiten Elemente Methode untersucht und diskutiert. Ferner wird die Dimensionierung der Geotextillagen in Bezug auf die Gewölbewirkung in der Praxis präsentiert.

Für einen wirtschaftlichen Entwurf von Dämmen auf Pfählen ist die Höhe des Gewölbes im Dammkörper von entscheidender Bedeutung. Diese Höhe des Gewölbes wird als Mindestmaß für die Dammhöhe angesetzt, um die volle Gewölbewirkung, die den Lastumlagerungsmechanismus bestimmt, zu gewährleisten. In den FE-Analysen wird die Höhe des Gewölbes mit Hilfe einer horizontalen Ebene im Dammkörper, welche gleiche vertikale Setzungen aufweist, bestimmt.

Im British Standard BS8006 und der deutschen EBGEO 2004 wird ebenfalls eine Vorgehensweise zur Bestimmung der Höhe des Gewölbes vorgestellt. Beide Richtlinien liefern eine gute Übereinstimmung mit den durchgeführten FE-Simulationen. Im Allgemeinen liegen die Ergebnisse aus der EBGEO 2004 näher an den Ergebnissen der Finite Elemente Berechnungen.

Prinzipiell können die numerischen Untersuchungen der Gewölbewirkung mit unterschiedlichen Arten von Berechnungen durchgeführt werden: axialsymmetrische Berechnungen, zweidimensionale oder dreidimensionale Berechnungen. Ohne Zweifel spiegelt eine dreidimensionale (3D) Berechnung die realen Verhältnisse im Dammkörper am besten wider. Eine solche Berechnung erfordert jedoch große Rechnerkapazitäten. Deswegen wurden für die Vergleichsberechnungen axialsymmetrische Bedingungen zu Grunde gelegt. Diese Annahme führte zu gleichwertigen Ergebnisse wie die 3D Geometrie. Auch der Vergleich mit den beiden Testreihen zeit eine gute Übereinstimmung. Der Vergleich mit den Ergebnissen der 2D Berechnungen (ebenes Ersatzsystem) zeigt deutlich, dass eine Analyse der Gewölbewirkung mit ebenen Systemen nicht möglich ist. Diese Systeme können die dreidimensionalen Verhältnisse nicht simulieren und führen in der Regel zu einem Durchstanzen der Pfähle durch den Dammkörper.

Durch den Einsatz von Geotextil kann das Setzungsverhalten sowie die Ausbildung des Gewölbes entscheidend verbessert werden. Die Untersuchungen zeigen, dass schon eine Lage von Geotextilien für die Bewehrung einer Dammkonstruktion mit schwimmenden Pfählen ausreichend ist. Für den Fall, dass mehr als eine Lage von Geotextilien verwendet wird – was einer konservativen Bemessung entspricht – sollten die Geotextillagen in der unteren Hälfte der prognostizierten Gewölbehöhe angeordnet werden. Je tiefer die Geotextillagen positioniert werden, desto effizienter können sie zur Verstärkung des Dammkörpers herangezogen werden.

Für die Untersuchung von Dämmen auf schwimmenden Pfählen ist die Verwendung von höherwertigen Stoffmodellen wie z.B. dem sogenannten Hardening Soil Modell (Modell mit zweifacher Verfestigung und einer Grenzbedingung nach Mohr-Coulomb) zu empfehlen. Durch die Verwendung von realistischen Baugrundparametern ist die Prognose von Setzungen realistischer, was der Vergleich der Ergebnisse mit den Messungen einer Fallstudie unterstreicht. Des Weiteren kann die Ausbildung des Gewölbes besser modelliert werden.

Bei Verwendung des Hardening Soil Modells sind verschiedene Baugrundparameter erforderlich, wobei der Einfluss der einzelnen Parameter auf die Gewölbewirkung unterschiedlich groß ist. Die numerischen Untersuchungen zeigen, dass der effektive Reibungswinkel (φ') und der Steifemodul (E_{oed}^{ref}) bei einer Referenzspannung von p^{ref} einen signifikanten Einfluss auf das Ergebnis haben. Der Reibungswinkel φ' bestimmt maßgeblich die Lastumlagerung vom Damm in die Pfähle. Die Setzungen hingegen werden hauptsächlich von der ödometrischen Steifigkeit E_{oed}^{ref} bestimmt.

Basierend auf den numerischen Untersuchungen wurden folgende Kriterien für die Konzeption eines Dammes auf schwimmenden Pfählen, welche besonders der Ausbildung eines stabilen Gewölbes im Dammkörper Rechnung tragen, gefunden:

- Das Dammmaterial sollte einen effektiven Reibungswinkel von $\varphi' \geq 30°$ haben.
- Die Höhe des Dammes muss größer als die Höhe des sich ausbildenden Gewölbes sein. Diese Höhe kann aus einer FE-Analyse abgeleitet werden, wobei eine Ebene im Dammkörper mit gleichen Setzungen bestimmt wird. Alternative kann die Höhe des Gewölbes mit $h = 0,7 \cdot s_d$ abgeschätzt werden, wobei s_d der diagonale Abstand der Pfähle ist.
- Das Verhältnis von Pfahldurchmesser zum Durchmesser der Pfahlkopfplatte (pile capping ratio) sollte größer als 10 Prozent sein
- Die Verwendung einer starkeren Geotextillage ist in der Regel ausreichend.

Kapitel 4: Einfluss des Herstellungsprozesses von Verdrängungspfählen

Zur Verbesserung eines weichen Bodens kommen hauptsächlich Verdrängungspfähle zur Anwendung. Anders als bei Tiefgründungen für Bauwerke werden die Pfähle zum Zwecke der Bodenverbesserung in einem sehr dichten Raster mit einem Abstand von nicht mehr als drei Metern angeordnet. Die Pfähle haben normalerweise eine relativ geringe Tragfähigkeit, welche typischerweise nicht mehr als 300 kN beträgt. Daher werden in der Regel Mikropfähle mit einem Durchmesser kleiner 30 cm verwendet. Zu den Mikropfählen zählen Holzpfähle, Ortbetonpfähle, Fertigbetonpfähle sowie vermörtelte Schotterstopfsäulen. Alle Pfahlarten haben gemein dass durch die Herstellung Boden verdrängt wird und damit das Spannungsfeld um den Pfahl wesentlich verändert wird.

Will man den Rammvorgang numerisch simulieren, so kann dies nicht mittels der herkömmlichen Finite Elemente Methode erfolgen, da die sehr großen Verformungen nicht abgebildet werden können. Hierfür müssen spezielle Verfahren, welche die großen Verformungen abbilden können, wie beispielsweise die sogenannte Material-Point Methode verwendet werden. Diese Methoden benötigt jedoch große Rechnerkapazitäten und ist noch nicht in die Ingenieurpraxis eingegangen. Um den Herstellungsprozess des Pfahles mit Hilfe der standardmäßigen FE-Methode abbilden zu können, müssen Vereinfachungen getroffen werden. Erst dann ist es möglich die Einflüsse der Herstellung von Verdrängungspfählen zu simulieren.

Die Änderung der radialen Spannungen um den Pfahl, welche die Tragefähigkeit des Pfahles vergrößern, ist ohne Zweifel die wesentliche Folge der Pfahlherstellung. Zusätzlich kann bei der Herstellung von vorgefertigten Pfählen eine Mantelreibung sowie ein

Spitzendruck nach der Herstellung verbleiben. Besonders für kleine und relative kurze Verdrängungspfählen, die in weichen Böden verwendet werden, können die verbleibende Mantelreibung wie auch der verbleibende Spitzendruck vernachlässigt werden. Aus den vorgenommenen Untersuchungen geht hervor, dass bei Verdrängungspfählen in weichen Böden die Mantelreibung nach Pfahlherstellung nahezu Null ist und der Spitzendruck dem Pfahlgewicht entspricht. Aus diesem Grund wurde bei den numerischen Simulationen ausschließlich ein Augenmerk auf die Vergrößerung der radialen Spannungen in Folge der Herstellung gelegt.

Im Rahmen dieser Arbeit wurde die sogenannte K-Druck Methode entwickelt, welche sich besonders für die Analyse von Verdrängungspfählen, welche zur Bodenverbesserung in weichen Böden eingesetzt werden, eignet. Diese Methode wurde mit Hilfe axialsymmetrischer Berechnungen entwickelt, welche auf einer spannungsgesteuerten Aufweitung des Pfahlschafts basiert. Hierbei wird die Vergrößerung der Radialspannung infolge einer Pfahlherstellung durch einen radialen Druck $p_r = K \cdot \sigma'_{v0}$ am Pfahlmantel simuliert, wobei σ'_{v0} die effektive, vertikale Initialspannung ist. Die Konstante K kann durch eine Kalibrierung an einer Pfahlprobebelastung rückgerechnet werden. Bei Verwendung dieser Methoden kann ein realistisches Spannungsfeld nach Herstellung des Pfahles gewonnen werden. Anhand einer Fallstudie in Wijchen, Niederlande, wird die Anwendung der K-Druck-Methode für Mikropfähle aufgezeigt.

Die K-Druck Methode ist nicht nur für die Simulation von Verdrängungspfählen unter drainierten Bedingungen anwendbar, sondern auch unter undrainierten Bedingungen. So entwickeln sich während der Herstellung im undrainierten Fall Porenwasserüberdrücke innerhalb einer plastischen Zone um den Pfahl herum. Bei einer darauffolgenden Konsolidationsphase werden die Porenwasserüberdrücke relativ schnell abgebaut, was auch in der Realität beobachtet wird. Der Vergleich der Berechnung mit drainierten Verhältnissen und der Berechnung mit undrainierten Verhältnissen und einer Konsolidationsphase nach der Pfahlherstellung zeigt nur geringe Unterschiede. Es sei hier angemerkt, dass die Erfassung von Porenwasserüberdrücken in Folge Pfahlherstellung nur sehr schwer möglich ist. Aus diesem Grund sollte die Simulation der Herstellung von Verdrängungspfählen mittels K-Druck Methode unter drainierten Bedingung durchgeführt werden, wobei die Konstante K aus einer Probebelastung rückgerechnet werden sollte. Bei den Berechnungen zur Entwicklung der K-Druck Methode wurde auch der Einfluss unterschiedlicher Stoffgesetze untersucht. Für die vorliegende Untersuchung wurde wiederum das sogenannte Hardening-Soil (HS) Modell verwendet. Darüber hinaus wurde auch das sogenannte HS-Small Model verwendet, worin im Gegensatz zum HS Modell die höhere Steifigkeit bei kleinen Dehnungen berücksichtigt wird. Der Vergleich des Last-Setzungsverhaltens mittels der zuvor genannten Modelle zeigt, dass das HS-Small Modell eine bessere Übereinstimmung mit den Messungen ergibt. Bei den Berechnungen mit dem HS-Small Modell zeigt sich eine Hysterese beim Be- bzw. Entlasten, was in der Realität ebenfalls zu beobachten ist.

Kapitel 5: Setzungsanalyse von Dämmen auf schwimmenden Pfählen

Um eine effiziente Konstruktion von Dämmen auf schwimmenden Pfählen zu erzielen müssen die auftretenden Setzungen untersucht werden. Um den Nutzen der setzungsminimierenden Konstruktion zu bewerten, müssen ebenfalls Setzungsanalysen vor der Baumaßnahme durchgeführt werden. In der Regel führt das Auftreten von ungleichmäßigen Setzungen zu Problemen. In diesem Kapitel werden daher die Setzungen von Dämmen auf schwimmenden Pfählen untersucht.

Die Installation von schwimmenden Pfählen im dicken, weichen Böden reduziert prinzipiell die Gesamtsetzung der Dammkonstruktion. Zweifelsohne führt eine Reduzierung der Gesamtsetzung auch zu einer Reduzierung der Differenzsetzung. Durch die schwimmenden Pfähle wird die Last des Dammes in tiefere und steifere Bodenschichten, welche sich in der Nähe der Pfahlspitzen befinden, geleitet. Zusätzlich werden die Spannungen in den weichen Schichten durch die Herstellung der Verdrängungspfähle erhöht. Durch diese Effekte werden die weichen Bodenschichten homogenisiert. Ein idealer, homogener Zustand ist erreicht, wenn sich die Pfähle und der dazwischenliegende weiche Boden wie ein Block verformen.

Die Berechnung von Setzungen und die Beurteilung der Effektivität von Dämmen auf schwimmenden Pfählen kann sowohl mit analytischen als auch mit numerischen Methoden durchgeführt werden. Diese Methoden werden in diesem Kapitel vorgestellt. Außerdem werden wichtige Konstruktionsregeln für derartige Konstruktionen beschrieben. Dabei wird zum Beispiel auf das Verhältnis von Pfahllänge zur Mächtigkeit der weichen Bodenschicht unter dem Damm eingegangen. Es wird eine Beziehung zwischen der erforderlichen Länge der Pfähle und der Schichtdicke des weichen Bodens aufgestellt.

Die Effektivität der Dammkonstruktion auf Pfählen kann mit der Setzungsreduzierung im Vergleich zu einer Dammkonstruktion ohne Pfähle bewertet werden. Trotz vereinfachenden Annahmen sind analytische Ansätze für das allgemeine Verständnis des Setzungsverhaltens der Konstruktion geeignet. Außerdem sind analytisches Verfahren wichtig für die Einschätzung der kritischen Pfahllänge im Vorfeld einer Baumaßnahme. Die kritische Pfahllänge ist die Länge eines Pfahles, bei der die Pfahltragfähigkeit gleich der entsprechenden Dammlast ist.

Zweifelsohne werden mit der FE-Methode bessere und genauere Abschätzungen des Setzungsverhaltens erzielt. Die FE-Berechnungen zeigen, dass die Effektivität und damit die Setzungsreduzierung bei Dämmen auf schwimmenden Pfählen mit zunehmender Pfahllänge ansteigt. Je weiter sich die Pfahllänge an die kritische Pfahllänge annähert, desto geringer sind die Gesamtverformungen. Wird die kritische Pfahllänge überschritten, so findet eine Verringerung der Effektivität statt. Die günstigste Variante ist die, bei der die Pfähle eine Längen von 30 bis 50 Prozent der Dicke der weichen Bodenschicht aufweisen. Dennoch sollte die Pfahllänge genau überdacht werden, denn die auftretenden Dammsetzungen können trotz der vorher beschriebenen Regeln beträchtlich sein. Die maximal zulässigen Setzungen müssen daher während der Planungsphase festgelegt werden, um eine effektive Konstruktion hinsichtlich der Wirtschaftlichkeit und der Gebrauchstauglichkeit zu erzielen.

Ab einer gewissen Pfahllänge verhält sich der weiche Boden, welcher mit schwimmenden Pfählen verbessert wurde, wie ein starrer Block, bei dem sich Boden und Pfähle gleichmäßig setzen. Es wurde herausgefunden, dass dieser Effekt eintritt, wenn die Pfahllänge 75 Prozent der kritischen Pfahllänge l_{crit} beträgt. Die kritische Pfahllänge l_{crit} kann analytisch aus dem Gleichgewicht in vertikaler Richtung ermittelt werden. Des Weiteren wurde ein einfaches, analytisches Verfahren, welches auf dem Konzept des Blockverhaltens beruht, zur Bestimmung der Effektivität von Dämmen auf schwimmenden Pfählen vorgestellt. Diese Methode ist sehr hilfreich und zudem äußerst einfach in der Anwendung.

Kapitel 6: Fallstudie eines Dammes auf schwimmenden Pfählen

Im Westen von Schweden liegt ein Testdamm der im Rahmen eines Ausbauvorhabens instrumentiert wurde. Bei dem Vorhaben handelt es sich um den Bau einer Autobahn sowie einer zweigleisigen Bahnstrecke für Hochgeschwindigkeitszüge. Der Testdamm liegt im östlichen Göta-Tal in Nödinge. Die im Bereich des Dammes anstehenden Böden sind bekannt für ihre sehr geringe Steifigkeit und reichen bis in sehr große Tiefen. Um die Gebrauchstauglichkeit des Bauwerks während der gesamten Lebensdauer zu gewährleisten, muss eine Bodenverbesserung vorgenommen werden. In der ersten Entwurfsphase wurden schwimmende Pfähle als die am besten geeignete Alternative zur Stabilisierung des Dammes angesehen. Um nähere Erkenntnisse über des Setzungsverhaltens von schwimmenden Pfählen in den weichen Tonen zu gewinnen, sowie zur Qualitätsverbesserung der Setzungsberechnung, wurden unterschiedliche Testdämme auf schwimmenden Pfählen errichtet. Für die hier präsentierte Fallstudie wurde ein Damm in Nödinge ausgewählt. Die Verformungen des Dammes auf schwimmenden Pfählen wurde mit einer dreidimensionalen FE Berechnung analysiert und die Berechnungsergebnisse mit den Messergebnissen verglichen. Die Ergebnisse der Studie werden in diesem Kapitel vorgestellt und diskutiert.

Für die Verbesserung des weichen Bodens in Nödinge wurden Kalk-Zement-Säulen ausgeführt. Insgesamt wurden 153 Kalk Zement-Säulen (LCCs) in einem quadratischen Raster von 1,5 m (Mittelpunktabstand) eingebracht. Jede zweite Reihe der LCCs hat eine Länge von 20 m. Die dazwischenliegende Reihe weist eine Länge von 12 m auf. Der Durchmesser der LCCs beträgt 0,6 m. Hergestellt wurden die LCCs aus einer trockenen Mischung, die aus 45 kg Kalk und 45 kg Zement pro Kubikmeter Kalk-Zement-Boden-Gemisch besteht. Die LCCs wurden im Mai 2001, ca. 7 Monate vor der Schüttung des Dammes hergestellt.

Der Damm an sich hat an der Krone eine Länge von 25 m sowie eine Breite von 13 m und wurde in zwei Lagen geschüttet. Die erste Lage weist eine Höhe von 1,5 m auf, was einer Belastung an Unterkante Damm von 25 kPa auf die verbesserte, weiche Bodenschicht entspricht. Knapp zwei Jahre später wurde die zweite Lage des Dammes geschüttet, was zu einer weiteren Belastung der verbesserten, weichen Bodenschicht von 25 kPa führte. Vor der Dammschüttungen wurden Setzungsschläuche, Piezometer und Inklinometer in den weichen Tonen sowie in den Kalk-Zement-Säulen installiert. Der wurde über einen Zeitraum von 6 Jahre überwacht und sämtliche Daten wurden aufgezeichnet. Mit Hilfe dieser Daten war es möglich das Langzeit-Setzungsverhalten des Dammes auf schwimmenden Pfählen im Detail zu untersuchen und mit Hilfe der FE Methode nachzurechnen.

Für die Analyse des Kriechverhaltens der weichen Schichten wurde das sogenannte Soft-Soil-Creep Modell benützt. Die meisten Parameter des Stoffgesetzes können aus den Ergebnissen üblicher Laborversuche bestimmt werden. Zur Ermittlung der Steifigkeitsparameter können die Ergebnisse von sogenannten CRS-Oedometer Versuchen herangezogen werden. In Schweden führt man diese CRS-Oedmeter Versuche häufig durch, so auch im Rahmen dieses Testdammes. Aus dem CRS-Oedometer ergeben sich im Vergleich zum Standard Oedometer andere Werte für den Überkonsolidierungsgrad (OCR) des Bodens. Aus diesem Grund muss eine Kalibrierung der aus dem CRS-Oedometer bestimmten Parameter mit der FE Methode durchgeführt werden. Ein detailliertes Berechnungsverfahren zur Gewinnung der richtigen OCR-Werte für das Soft-Soil-Creep Modell aus einem CRS-Oedometer Versuch wird in diesem Kapitel vorgestellt. Darüber hinaus stellt die FE-Simulation des CRS-Oedometer Versuchs ebenso sicher, dass die restlichen verwendeten Parameter das reale Bodenverhalten richtig wiedergeben.

Nach der Kalibrierung der Parameter kann die eigentliche FE-Berechnung der Fallstudie des Dammes auf schwimmenden Pfählen durchgeführt werden. In der FE-Analyse wird der komplette Bauablauf simuliert. Nach Generierung der Initialspannungen werden die schwimmenden Pfähle hergestellt. Anschließend wird die erste Lage des Dammes bis zu einer Höhe von 1,5 m in einer Zeit von acht Stunden geschüttet. In dieser Phase wird rein undrainiertes Materialverhalten angenommen. D.h. dass auf Grund der Belastung Porenwasserüberdrücke entstehen. Anschließend folgt eine 660 Tage lange Konsolidationsphase. Daraufhin folgt die zweite Bauphase des Dammes, bei der eine weitere gleichmäßige Flächenlast von 25 kPa aufgebracht wird. Diese Berechnungsphase erfolgt ebenfalls in acht Stunden unter komplett undrainierten Bedingungen. Abschließend folgt eine weiter Konsolidationsphase bis zu 2142 Tagen.

Die Ergebnisse der FE-Simulation hinsichtlich des Setzungsverhaltens zeigen gute Übereinstimmungen im Vergleich zu den Messungen. Zusätzlich wurden weitere Berechnungen des Testdammes zur Prognose der Langzeitverformungen sowie Vergleichsberechnungen ohne Pfähle durchgeführt. Diese Ergebnisse werde in diesem Kapitel ebenfalls im Detail präsentiert und diskutiert.

In weiteren Parameterstudien wurde der Einfluss der Pfahllänge auf das Verformungsverhalten des Testdammes untersucht. In der ausgeführten Variante befinden sich in jeder zweiten Reihe Pfähle mit einer Länge von 20 m und in den zwischenliegenden Reihen 12 m lange Pfähle. Es ist wichtig den Einfluss der Pfahllänge sowohl auf das primäre als auch auf das sekundäre Setzungsverhalten der weichen Böden zu untersuchen. Für diesen Zweck wurde die Spannungsverteilung an Geländeoberkante und das Setzungsverhalten des Dammes für die Fälle der ausgeführten Variante und der Varianten mit konstanten Pfahllängen von 12 m und 20 m verglichen.

Die FE Simulation zeigt, das längere Pfähle keiner Erhöhung der Stabilität der Konstruktion bewirken. Die Ergebnisse der Langzeitberechnungen verdeutlichen die hohe Effizienz der ausgeführten Konstruktion im Vergleich zu den anderen Varianten. Die aktuelle Pfahllänge beweist dass die Langzeitsetzungen im Vergleich zu kurzen Pfählen (12 m) erheblich reduziert werden können. Werden lange Pfähle verwendet, ist die Setzungsreduzierung im Vergleich zur ausgeführten Konstruktion nur minimal. Damit zeigt die aktuelle Konstruktion einen klaren Vorteil hinsichtlich der Wirtschaftlichkeit und der Effektivität. An Hand dieser Fallstudie ist zu erkennen, dass lange Pfähle für die Reduzierung der Kriechsetzungen wichtig sind. Eine Kombination von langen und kurzen Pfählen ist hingegen optimal, da sowohl die Baukosten als auch die auftretenden Verformungen reduziert werden können.

Kapitel 7: Schlussfolgerung und Ausblick

Im letzten Kapitel werden die Ergebnisse dieser Arbeit noch einmal zusammengefasst und mit die wichtigsten Schlussfolgerungen gezogen. Anschließend wird ein Ausblick auf weitere, fortführende Forschungsthemen gegeben.

Chapter 1

Introduction

The increasing need for infrastructure development often forces engineers to build on soft soils. Soft soils cannot sustain external loads without having large deformations. Hence, a soft soil improvement measure is often a prerequisite. Several techniques have been introduced and applied for soft soil improvement. One of the techniques is a piled embankment as shown in Figure 1.1. The embankment can be supported by end-bearing piles, i.e. piles that reach a hard stratum, or floating piles, which are piles that do not reach a hard stratum. When the installed piles do not reach a hard stratum due to large thickness of the soft soil, the construction is called an "embankment on floating piles". A well designed piled embankment has the advantages that it requires less construction time and yields little embankment settlement. Moreover, its construction process causes minimal disturbance to the natural environment. This technique is extremely time effective and it is considered an environmental friendly technique (Dumas, 2002).

1.1 Piled embankments

Since ancient times, piles have been embedded in soft soils as a means of soft soil improvement. For example, in Germany, closely spaced timber piles known as " Spickpfähle" were used for soil improvement at Gifhorn castle in the 12th century (Wichert, 1988). In Indonesia, the use of timber piles, which are known as "Cerucuk", is a familiar traditional way of soft soil improvement (CUR, 2001).

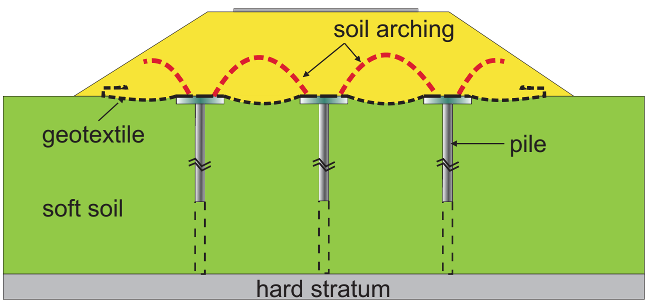

Figure 1.1: Piled embankment method

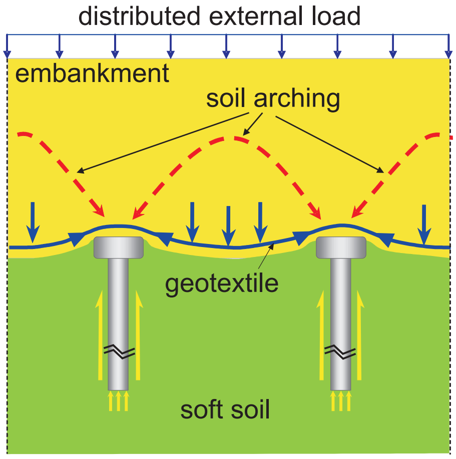

Figure 1.2: Load transfer mechanism in piled embankments

Unlike piles for deep foundations of buildings, piles for soil improvement are characterized by their installation in a very dense grid with centre to centre spacing of not more than 3 m, generally. In addition, soil improvement piles have low load carrying capacity. The required load carrying capacity of the piles is typically less than about 300 kN. This implies that the piles used for soil improvement are often micropiles, i.e. a pile with diameter less than 30 cm. Many types of non-deformable columns can be considered as piles for soft soil improvement such as timber piles, prefabricated or cast-insitu concrete piles, deep mixing lime cement columns, as well as grouted stone columns.

Nowadays, embankments of granular soils supported by piles are often used for road and railway constructions. Geotextile layers are usually applied on top of pile caps as reinforcement. This method is known as a piled embankment. Due to differential settlement between the stiff pile caps and the soft soil surface, the stresses in the granular embankment are redistributed and reoriented to form arches. This is known as soil arching. The soil arching mechanism transfers the embankment load above the arches and the external load directly to the piles as illustrated in Figure 1.2. When a geotextile is used, it holds the remaining load of the embankment and also transfers the load to the piles via its tension. The pile transfers the embankment load and the external load down to the deeper and firmer soil stratum. Hence, the soft soil bears less force and therefore produces less settlements. The piles that support the embankment can be end-bearing piles or floating piles. This thesis is mainly focused on the design of embankments on floating piles. Nevertheless, several aspects that relate the design of piled embankments in general are also considered. For floating piles, the settlement reduction is not as large as for end-bearing piles, but they create a homogenization that render settlements more uniform. Here, it should be noted that settlements are mostly acceptable a long as they are uniform.

Piled embankments have existed for a long time, but they have become more popular since 1970s. Several piled embankments implemented in practice have been reported, e.g. by Holtz and Massarsch (1976), Smoltczyk (1976), Tan et al. (1985), Wood (2003)

Figure 1.3: Location of soft soils in Indonesia

and Van Eekelen et al. (2008). Most of the piled embankments incorporate geotextiles as reinforcements. Since the 1980s, increasing interest in piled embankments has led to an increase in research on rational approaches for soil arching in granular embankments. The aim of previous research was mainly to determine the amount of load transferred from the embankment to the piles, as well as the requirement of the geotextiles tensile strength. Some published research on soil arching can be seen in Terzaghi (1941), Carlsson (1987), Guido et al. (1987), Hewlett and Randolph (1988), Vermeer et al. (2001) and Zaeske (2001). Today, some of the research findings have been adopted as guidelines for piled embankments design such as Nordic guidelines, British standard BS8006, and the German method EBGEO 2004.

In recent decades, numerical methods such as finite element analysis with the support of computer technology have been increasingly used in the field of geotechnical engineering. Since around 1990, the importance of numerical analysis in investigating piled embankments has constantly grown (Jones et al., 1990; Russel and Pierpoint, 1997; Jenck et al., 2007). Nowadays, numerical analysis of piled embankments is strongly recommended, especially for detailed designs. Nevertheless, guidelines for a proper numerical analysis of piled embankments are not yet available.

1.2 Motivation

Strong and stiff soils are preferable as foundations for embankments and buildings. However, these types of foundation soils are not always available on site. For example, in South East Asia and Scandinavia, many areas are covered by thick soft soil layers, which can reach 40 metres or even more. As shown in Figure 1.3, in Indonesia, soft soils cover most of the coastal areas, which contain many densely populated cities and the need for infrastructure development is high. Especially east of Sumatra, south of Kalimantan and south of Irian Jaya, the soft areas are mainly dominated by peat soil overlaying soft clay soils, whereas in other places, they are mainly soft clay soils. The total area of soft soils in Indonesia is about 60 million hectares, which is about 30 percent of the total land area. Considering the available soft soils, the piled embankments method is an attractive soft soil improvement technique. The increasing interest in the use of piled embankments in Indonesia can be seen from several projects carried out in Sumatra and Java (see for example Rahardjo, 2005). Moreover, from 1996 to 2001, a large scale collaborative project on soft soil improvement was carried out between the government of Indonesia and the Netherlands. This project includes several piled embankments trials performed at Bereng Bengkel, Kalimantan (The et al., 2002).

In order to construct effective and efficient piled embankments, design guidelines are needed. Guidelines for piled embankments design exist. However, there are uncertainties and inadequacies in the design guidelines especially for embankments on floating piles. The design of an embankment on floating piles involves complex soil-structure interaction. For such problems, numerical methods such as finite elements analysis can be utilised. Nevertheless, clear procedures or guidelines for finite elements analyses of embankments on floating piles are not available. Hence, research is required to find proper procedures for finite elements analysis as well as design criteria for embankments on floating piles.

1.3 Research aims

This research is focused on establishing reliable calculation procedures for the design of embankments on floating piles using the finite element method. To achieve this aim, several research topics are studied using the finite element method with calibration to field measurements. Topics studied include: soil arching analysis, effects of pile installation process, and settlements analysis of embankments on floating piles. In addition, important design criteria of embankments on floating piles are highlighted. The established calculation procedures are seen as guidelines for finite element analysis of embankments on floating piles.

1.4 Layout of thesis

In addition to this introduction, the thesis is arranged in 7 chapters as indicated below:

Chapter 2 reviews the most relevant guidelines for piled embankments design. Two design guidelines, which are the British Standard BS8006 and the German method EBGEO 2004 section 6.9 are summarized. The design procedures in the guidelines focus on the determination of load transfer from an embankment to piles and geotextiles tensile strength requirements. At the end of this chapter, several uncertainties and limitations of the current design guidelines are discussed.

Chapter 3 presents numerical analyses of soil arching development in granular embankment soil. Several aspects which influence the numerical analyses of soil arching such as geometrical representation, capping ratio and soil constitutive models are discussed. In relation to soil arching, the design of geotextile reinforcement layers in practice is presented. Moreover, the influence of the number of geotextile layers on soil arching development in an embankment is analyzed using the finite element method. At the end, criteria for the design of granular embankments, which regard the stability of soil arching mechanism are given.

Chapter 4 suggests a method to simulate the effects of installation of floating piles. To begin with, several alternative simulation methods are introduced. A preferred method, which is called the *K-Pressure* method is then presented in detail. The simulation, which uses stress-controlled cavity expansion in axisymmetrical geometry, is performed with the standard small strain finite elements algorithm. This method is considered to be applicable within the realm of engineering practice.

Chapter 5 covers the topic of settlement analyses of an embankment on floating piles. Analytical and finite elements settlement analyses of embankment on floating piles are presented. Moreover, important design criteria of embankments on floating piles with respect to pile length and soft soil thickness are shown.

Chapter 6 contains a case study of a test embankment on floating piles. The test embankment was constructed in Nödinge, Sweden. A long term monitoring of the embankment settlements was conducted. Finite elements creep analysis of the embankment is performed. The analysis covers a method to back-calculate material properties from laboratory CRS tests and creep settlement calculations of the embankment. Moreover, it is also shown how pile length influences the creep settlement behaviour of the embankment.

Chapter 7 finally presents the main findings to conclude this study of embankments on floating piles.

Chapter 2

Current design procedures for piled embankments

Several procedures for piled embankments design exist. The design procedures according to the British standard 8006 (BS8006) and the German method (EBGEO 2004 section 6.9) are described in this chapter. Despite some uncertainties in the procedure, BS8006 is often used in design practice worldwide. BS8006 is familiar to engineers, simple to apply and generally, it gives a conservative design of piled embankments. The EBGEO 2004 section 6.9 is a new design procedure for piled embankments with a more scientific approach on the soil arching assumption.

The design of a piled embankment includes the design of an embankment, geotextiles and piles. The embankment is designed in such a way that it satisfies the requirements of geometry, e.g. the required embankment height, stability and load transfer mechanism via soil arching. The geometry is chosen so that it suits the construction requirements, embankment stability and soil arching development. The embankment stability can be assessed using the common slope stability analyses such as Bishop's method, Fellenius's method or using numerical analysis such as the finite element method. Since the design of geometry and embankment stability are relatively clear and definite, most attention of the piled embankments design is focused on the design of the load transfer mechanism through soil arching action. Based on the soil arching action, the geotextile tensile strength requirement is determined. The piles that support the embankment are generally assumed to be end-bearing piles. In case of floating piles, the influence of the pile caps settlements on soil arching is represented by an additional coefficient.

2.1 British standard BS8006

The British Standard for piled embankment design is documented in BS8006 with the title of "Code of practice for strengthened/reinforced soils and other fills". It is issued by the British Standard Institution in 1995. The piled embankment design procedure adopts an empirical method, which is originally developed by Jones et al. (1990). For the safety in the design, certain partial factors are applied to the load and the resistance

Table 2.1: Summary of partial factors used in the design of piled embankments (after BSI, 1995)

Partial factors		Ultimate limit state	Serviceability limit state
Load factors	Soil unit mass, e.g. embankment fill	$f_{fs} = 1.3$	$f_{fs} = 1.0$
	External dead load, e.g. line or point loads	$f_f = 1.2$	$f_f = 1.0$
	External live load, e.g. traffic loading	$f_q = 1.3$	$f_q = 1.0$
Soil material factors	To be applied to tan φ'_{cv}	$f_{ms} = 1.0$	$f_{ms} = 1.0$
	To be applied to c'	$f_{ms} = 1.6$	$f_{ms} = 1.0$
	To be applied to c_u	$f_{ms} = 1.0$	$f_{ms} = 1.0$
Reinforcement material factor	To be applied to the reinforcement base strength	The value f_m depends on the type of material and its design life time. See also BS 8006 Section 5.3.3 and Annex A for the details	
Soil / reinforcement interaction factors	Sliding across surface of reinforcement	$f_s = 1.3$	$f_s = 1.0$
	Pull-out resistance of reinforcement	$f_p = 1.3$	$f_p = 1.0$

properties of the embankments, geotextiles and piles. The summary of the partial factors used in the design of piled embankments is listed in Table 2.1. Further details on the partial factors can be seen in BS8006 Section 8.

2.1.1 Embankment and load transfer

The embankment should be made of granular soils. Hence, the embankment materials should have a high shear strength with effective critical state friction angle φ'_{cv} of more than 30° for granular soils. The embankment height h is recommended to be at least $0.7 \cdot (s - a)$ to ensure that differential deformation cannot occur at the surface of the embankment.

Through soil arching action, the external and embankment loads are transferred to the pile caps. The effective pressure acting on top of pile caps σ'_c as shown in Figure 2.1a is determined as follows:

$$\sigma'_c = \sigma'_v \cdot \left(\frac{C_c \cdot a}{h}\right)^2 \quad with \quad \sigma'_v = f_{fs} \cdot \gamma_{emb} \cdot h + f_q \cdot q \tag{2.1}$$

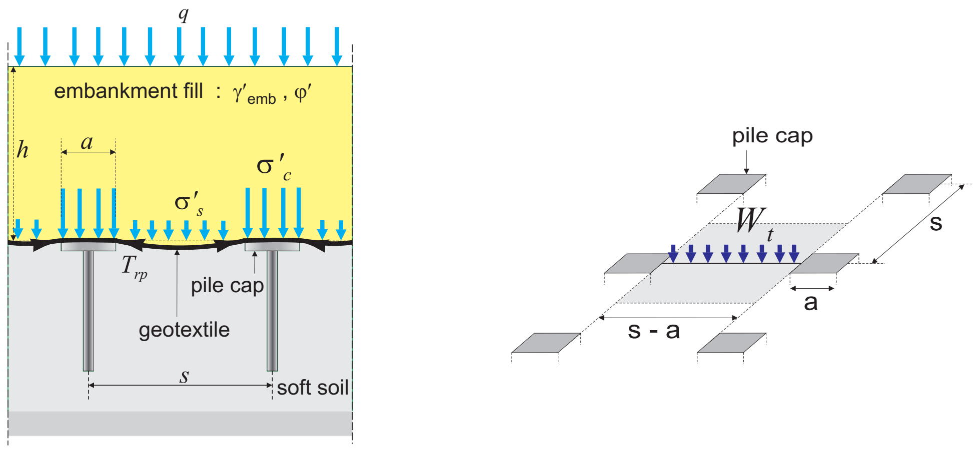

(a) (b)

Figure 2.1: Piled embankment loads according to BS8006

where C_c is the soil arching coefficient, a is the pile cap width, h is the height of the embankment and q is the uniformly distributed external load on the embankment surface. The soil arching coefficient is given as

$$C_c = 1.95\,h/a - 0.18 \quad \text{for embankment on end-bearing piles} \tag{2.2}$$

$$C_c = 1.5\,h/a - 0.07 \quad \text{for embankment on floating piles} \tag{2.3}$$

Equation 2.1 is a modified empirical formula, which is originally proposed by Marston in 1913 for plane strain approximation of soil arching on top of an infinitely long buried pipe (Love and Milligan, 2003). Marston suggested that the pressure ratio $\sigma'_c/\sigma'_v = (C_c \cdot a/h)$. In BS8006, the right hand term is squared to consider the three dimensional situation in a piled embankment. Based on the formulation of arching action above, the arching depends only on the geometry of the embankment and the pile grid. It is independent of the strength of the embankment material and the geotextile.

2.1.2 Geotextile tensile load

The geotextile holds the remaining portion of the embankment and external loads, which is not transferred to the pile caps. To calculate the tensile load in the geotextile, it is assumed that the pressure σ'_s over an area of $(s-a)\cdot s$ can be transformed into a uniformly distributed line load W_t as shown in Figure 2.1b. The line load W_t is calculated as follows:

$$W_t = \frac{1.4 \cdot f_{fs} \cdot \gamma_{emb} \cdot s \cdot (s-a)}{s^2 - a^2}\left[s^2 - a^2\left(\frac{\sigma'_c}{\sigma'_v}\right)\right] \quad for \quad h \geq 1.4 \cdot (s-a) \tag{2.4}$$

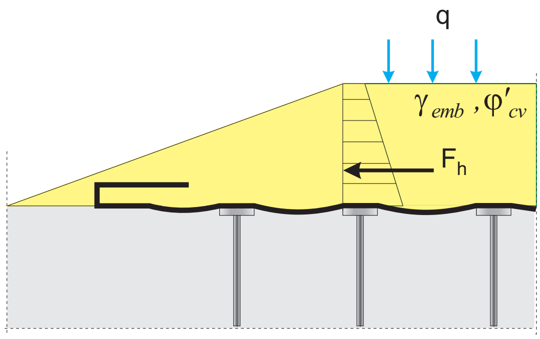

Figure 2.2: Horizontal force at the side of embankment (after BS8006)

and

$$W_t = \frac{s \cdot (f_{fs} \cdot \gamma_{emb} \cdot h + f_q \cdot q)}{s^2 - a^2} \left[s^2 - a^2 \left(\frac{\sigma'_c}{\sigma'_v} \right) \right] \quad for \quad 0.7 \cdot (s-a) \leq h \leq 1.4 \cdot (s-a) \tag{2.5}$$

Equation 2.4 considers that arching action is fully developed when $h \geq 1.4 \cdot (s-a)$. Hence, the uniformly distributed external load q does not have influence on the line load W_t. On the other hand, in Equation 2.5, the uniformly distributed external load q has influence on the line load W_t as arching action is not considered fully developed. Due to the line load, the tensile load in the geotextile T_{rp} is mobilized. T_{rp} is determined using Catenary equation for tension of a uniformly loaded flexible cable.

$$T_{rp} = \frac{W_t \cdot (s-a)}{2a} \cdot \sqrt{1 + \frac{1}{6\varepsilon}} \tag{2.6}$$

where ε is the strain in the geotextile. The strain in the geotextile is determined to not exceed 5% at the end of construction and 5% to 10% at the end of design life of the piled embankment. It should be noted that the support of soft soil to the geotextile is not taken into account in Equation 2.6, which leads to inconsistent assumption when designing embankment on floating piles. In addition to tension load T_{rp}, the geotextile should also resist the horizontal outward thrust due to horizontal force at the side of the embankment (Figure 2.2) . The geotextile tensile load needed to resist the horizontal force of the embankment T_{ds} is

$$T_{ds} = 0.5 \cdot K_a \cdot (f_{fs} \cdot \gamma_{emb} \cdot h + 2 \cdot f_q \cdot q) \cdot h \quad with \quad K_a = tan^2(45° - \varphi'_{cv}/2) \tag{2.7}$$

where K_a is the active lateral earth pressure coefficient and φ'_{cv} is effective friction angle at critical state or at large strain. Hence the total load that should be considered in the geotextile is $T_{total} = T_{rp} + T_{ds}$.

2.2 German method EBGEO 2004

The German method EBGEO 2004 Section 6.9 is a recommendation for piled embankments design procedure issued by the Deutsche Gesellschaft für Geotechnik (DGGT) in July 2004. The method adopts the so-called multi-shell arching theory based on the work of Zaeske (2001). Like the design requirements in BS8006, for the safety, certain partial factors for the load and resistance properties of the embankments, piles and geotextiles are also applied in the German method. However, the use of the partial factors in the design calculations is much more specific. In general, the calculations of loads and resistances in geotechnical design are performed using the so-called characteristic values of the loads and the material resistance properties. The characteristic values of material resistance properties are determined from the 5 percent lower value of the statistic material properties data for ultimate limit state. This means that statistically there is only five percent probability that the material properties are lower than the characteristic properties. For serviceability limit state, the mean values of the statistic material resistance data are taken as the characteristic values. The characteristic load values are taken as the 95 percent of the upper bound statistic load data, which imply that there is only 5 percent probability that the actual load is higher than the characteristic load. The partial factors applied in design calculations are distinguished in three conditions: during construction stage, after construction and in special cases, e.g. in case of earthquake. The partial factors applied for the design of piled embankment is summarized in Table 2.2. For serviceability limit state, all partial factors are equal to 1.

The German method EBGEO 2004 is recommended for the design of embankment on rigid end-bearing piles. For the design of embankment on floating piles, further elaboration of the design procedure is required.

2.2.1 Embankment and load transfer

To ensure the development of arching action, the embankment height h should be at least $0.7 \cdot s_d$, where s_d is the centre to centre diagonal pile spacing. In case of high dynamic external loads, higher embankments should be considered. The embankment should be made of granular materials with characteristic effective friction angle $\varphi'_k \geq 30°$ based on the values of critical state effective friction angle φ'_{cv}, at least up to a height of $0.7 \cdot s_d$. Above this height, other materials may be used for the fill materials.

To determine the arching action in the granular embankment, the arches are assumed to take the shape of hemispherical domes spanning between the pile caps, which is similar to the previously assumed single shell hemispherical arching suggested by Hewlett and Randolph (1988). The difference in the EBGEO 2004 is that the arches consist of multi-shell domes (Figure 2.3). The topmost arching shells take the shape of hemispherical domes with a radius of $0.5 \cdot s_d$. Inside the topmost shells, there are multi-spherical shaped arching shells with radius of larger than $0.5 \cdot s_d$ to infinite for the lowest arching shells. The lowest arching shells are tangential to the surface of the soft subsoil. By the

Table 2.2: Summary of partial factors used in the design of piled embankments (after DIN-1054 Revision 4)

Load factors		Load conditions[a]		
GZ 1B: Limit condition for construction failure		**LF 1**	**LF 2**	**LF 3**
Influence of dead load	γ_G	1.35	1.20	1.10
Influence of live load	γ_Q	1.50	1.30	1.10
GZ 1C: Limit condition for lost of overall stability				
Influence of dead load	γ_G	1.00	1.00	1.00
Influence of live load	γ_Q	1.50	1.30	1.10
Resistance factors				
GZ 1B: Limit condition for construction failure				
Pile resistance from pile loading tests	γ_{Pc}	1.20	1.20	1.20
Geotextile tensile resistance	γ_M	1.15	1.15	1.15
GZ 1C: Limit condition for lost of overall stability				
To be applied to tan φ'	γ_φ	1.25	1.15	1.10
To be applied to cohesion c'	γ_c	1.25	1.15	1.10
Geotextile pull-out resistance	γ_B	1.40	1.30	1.20

[a]LF 1 : end of construction. LF 2 : during construction, LF 3 : special cases, e.g. earthquake

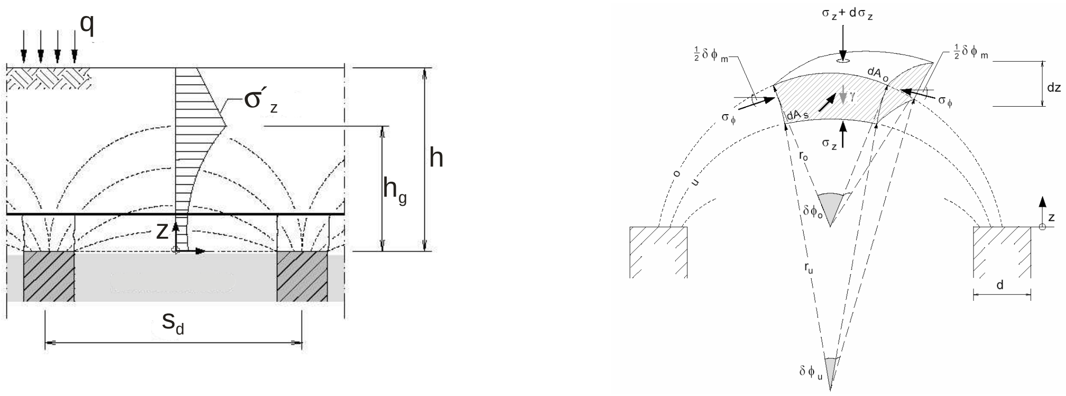

(a) (b)

Figure 2.3: Multi-shell arching theory (after Zaeske, 2001)

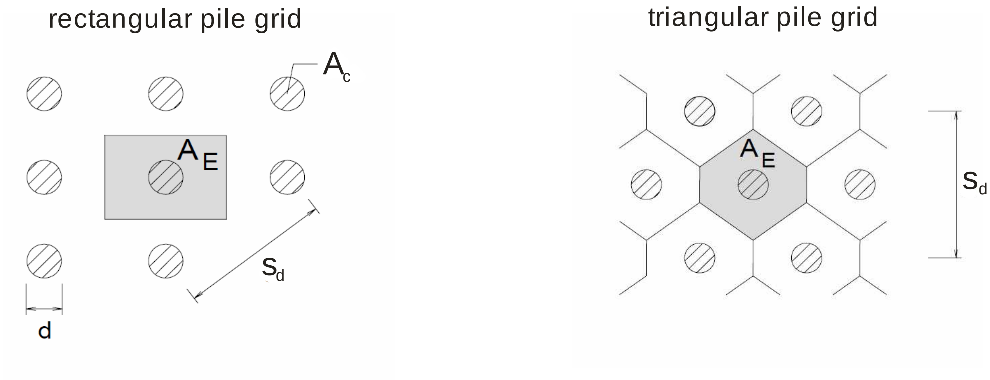

Figure 2.4: Area of one cell pile embankment (after DGGT, 2004)

evaluation of the vertical force equilibrium of an element in the middle of the arching dome, a solution for determining the vertical stress at the lowest arching shells or at the surface of the soft subsoil σ'_{z0} is obtained as shown in Equation 2.8

$$\sigma'_{z0} = \lambda_1^{\chi} \cdot \left(\gamma_{emb,k} + \frac{q_k}{h}\right) \cdot \left[h \cdot (\lambda_1 + h_g^2 \cdot \lambda_2)^{-\chi} + h_g \cdot \left(\left(\lambda_1 + \frac{h_g^2 \cdot \lambda_2}{4}\right)^{-\chi} - \left(\lambda_1 + h_g^2 \cdot \lambda_2\right)^{-\chi}\right)\right] \quad (2.8)$$

with

$$\lambda_1 = \frac{1}{8} \cdot (s_d - d)^2 \;\; ; \quad \lambda_2 = \frac{s_d^2 + 2 \cdot d \cdot s_d - d^2}{2 \cdot s_d^2} \;\; ; \quad \chi = \frac{d \cdot (K_p - 1)}{\lambda_2 \cdot s} \quad (2.9)$$

and

$$h_g = {}^{s_d}/_2 \;\; for \;\; h \geq {}^{s_d}/_2 \;\; ; \quad h_g = h \;\; for \;\; h < {}^{s_d}/_2 \quad (2.10)$$

The subscript k denotes the characteristic value and d is the diameter of the pile cap. In the case where the pile cap is not circular, d is taken as equal to $\sqrt{4 \cdot A_c/\pi}$ with A_c is the pile cap area. K_p is the passive lateral earth pressure, which is equal to $tan^2(45° + \varphi'_k/2)$ and h_g is the arching height. The characteristic effective pressure acting on top of pile cap is determined as follows:

$$\sigma'_{c,k} = ((\gamma_{emb,k} \cdot h + q_k) - \sigma'_{z0}) \cdot \frac{A_E}{A_c} + \sigma'_{z0} \quad (2.11)$$

where A_E is the area of one cell pile embankment as shown in Figure 2.4. $\sigma'_{c,k}$ is not the design value of pressure on pile cap. The design value of pressure on pile cap $\sigma'_{c,d}$ is determined from the pressure on pile cap under the influence of only dead load $\sigma'_{c,G}$ and from the pressure on pile cap under the influence of both dead load and external distributed live load q_k. The design pressure on pile cap is written as follows

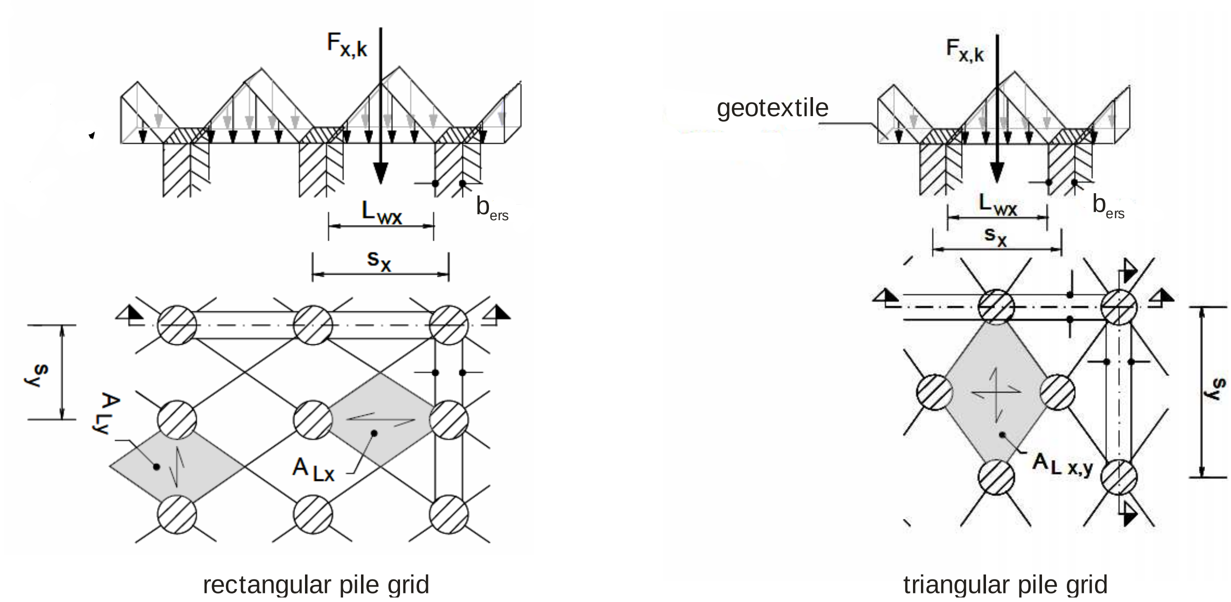

Figure 2.5: Vertical force on geotextile (after DGGT, 2004)

$$\sigma'_{c,d} = \sigma'_{c,G} \cdot \gamma_G + (\sigma'_{c,G+Q} - \sigma'_{c,G}) \cdot \gamma_Q \tag{2.12}$$

$\sigma'_{c,G}$ is calculated using Equation 2.11 with $q_k = 0$ and $\sigma'_{c,G+Q}$ is equal to $\sigma'_{c,k}$.

2.2.2 Geotextile tensile load

To determine the tensile load on the geotextile layer, the vertical force F as a result of vertical pressure on the subsoil σ'_{z0} acting on an influenced area A_L, is calculated. The vertical force F is considered to act on a strip geotextile with a width of b_{ers} and a length of L_w as shown in Figure 2.5. b_{ers} is equal to $0.5 \cdot d \cdot \sqrt{\pi}$ and L_w is equal to $s - b_{ers}$. Since it depends on the influenced area, the vertical force is determined according to the direction of reinforcement. For a rectangular pile grid,

$$F_x = A_{Lx} \cdot \sigma'_{z0} \quad ; \quad F_y = A_{Ly} \cdot \sigma'_{z0} \tag{2.13}$$

and for triangular pile grid,

$$F_x = \frac{J_x}{J_x + J_y} \cdot A_{Lxy} \cdot \sigma'_{z0} \quad ; \quad F_y = \frac{J_y}{J_x + J_y} \cdot A_{Lxy} \cdot \sigma'_{z0} \tag{2.14}$$

The influenced area of a rectangular pile grid is determined using Equation 2.15 with variables as described in Figure 2.5.

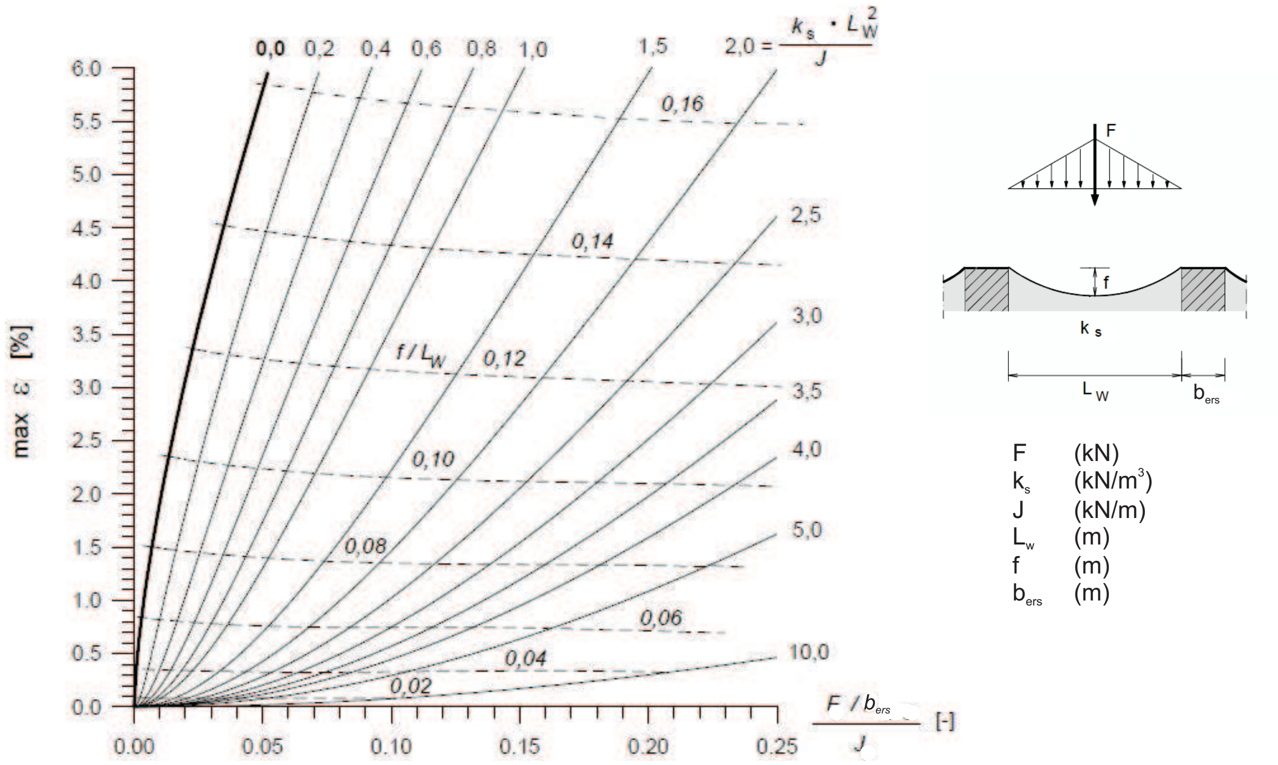

Figure 2.6: Maximum strain in the geotextile (after DGGT, 2004)

$$A_{Lx} = \frac{1}{2} \cdot (s_x \cdot s_y) - \frac{d^2}{2} \cdot \arctan\left[\frac{s_y}{s_x}\right] \cdot \frac{\pi}{180} \quad ; \quad A_{Ly} = \frac{1}{2} \cdot (s_x \cdot s_y) - \frac{d^2}{2} \cdot \arctan\left[\frac{s_x}{s_y}\right] \cdot \frac{\pi}{180} \tag{2.15}$$

For a triangular pile grid, the influenced area is determined using Equation 2.16

$$A_{Lxy} = \frac{1}{2} \cdot (s_x \cdot s_y) - \frac{d^2}{4} \cdot \pi \tag{2.16}$$

J is the time-dependent stiffness modulus of the geotextile. The maximum geotextile strain ε_{max}, in correspondence with the chosen stiffness modulus, can be determined graphically using Figure 2.6. It can be seen that the maximum strain ε_{max} is not only influenced by the vertical force F on the geotextile and the chosen stiffness modulus J, but also by the modulus of sub-grade reaction of the soft subsoil k_s. Hence, the support of subsoil to the geotextile is taken into account. In the design of piled embankment, the long term maximum strain ε_{max} due to creep is limited to less than 2%. This, however, does not include the short term strain after construction, which is limited to 6%. It is worth noting that Figure 2.6 is drawn from the numerical solution of the geotextile tensile load analysis, which is based on embedded beam theory after Emde (1995). The analysis leads to a differential equation that needs to be solved numerically. For design purpose, the numerical solution is presented graphically.

Once the maximum strain ε_{max} is determined, the characteristic tensile load $T_{rp,k}$ required in the geotextile to resist the vertical force can be determined,

$$T_{rp,k} = \varepsilon_{max} \cdot J \tag{2.17}$$

The design geotextile tensile load $T_{rp,d}$ is calculated as follows

$$T_{rp,d} = T_{rp,G} \cdot \gamma_G + (T_{rp,G+Q} - T_{rp,G}) \cdot \gamma_Q \tag{2.18}$$

where $T_{rp,G}$ is determined in the same way as $T_{rp,k}$ with $q_k = 0$ and $T_{rp,G+Q}$ is equal to $T_{rp,k}$.

Similar to BS8006, the geotextile should also resist the outward thrust due to horizontal force at the side of the embankment. The design geotextile tensile load to resist the horizontal force is determined using Equation 2.19

$$T_{ds,d} = (0.5 \cdot \gamma_{emb} \cdot (h - z) \cdot \gamma_G + q \cdot \gamma_Q) \cdot (h - z) \cdot K_{agh} \tag{2.19}$$

K_{agh} is the active lateral earth pressure coefficient according to DIN 4085, which is defined as

$$K_{agh} = \left(\frac{\cos \varphi'_k}{1 + A_a} \right)^2 \quad with \quad A_a = \sqrt{\frac{\sin(\varphi'_k + \delta_{a,k}) \cdot \sin \varphi'_k}{\cos \delta_{a,k}}} \tag{2.20}$$

$\delta_{a,k}$ is active wall friction angle, which is equal to φ'_k for piled embankment case and z is the vertical distance of the geotextile layer to the surface of soft subsoil. The total design tensile load on the geotextile is the superposition of both $T_{rp,d}$ and $T_{ds,d}$.

2.3 Limitations in the current design procedures

The current design procedures are written such that they are simple to use in practice and give conservative design result. They are good for preliminary design of piled embankments. However, for the detailed design, the reliability of the design procedure is questionable. This is mainly due to simplifications adopted in the procedures, which lead to uncertainties in the design result.

On the first place, both design methods explained previously assume that the soil arch is hemispherical. The arch is most likely to take an inverse cable deflection (catenary) shape. A hemispherical shape arching will produce bending moment, which may lead to instability of the arching structure as the embankment material cannot resist tension.

Handy (1987) states that in a gravity field, catenary presents an advantageous shape for a free standing arch in having no bending moment, and a natural arch therefore may tend to seek that advantage if it is required for stability. In addition to that, based on the orientation of principal stresses in a piled embankment, numerical studies on soil arching as will be shown in the next chapter also show that the arching is not a hemispherical. Furthermore, the assumption of arching action suggested in BS8006 using modified arching action on an infinitely long buried pipe, leads to many critics (Love and Milligan, 2003; Van Eekelen et al., 2003, etc).

Since the arching assumption determines the distribution of load transfer in the embankment body, this also leads to uncertainty on the amount of load which is supported by the geotextile layer. Hence, the design result of geotextile tensile load becomes uncertain. Considering the design of geotextile, it exposes further the limitation in the current design procedures. Both procedures present the design of embankment with one geotextile layer, whereas in practice, three layers of geotextile are often used. The reasons for this is probably because it gives more safety and confidence during the construction process, especially when using a low embankment or larger pile spacing. It can also be because the tensile strength requirement becomes lower. This will then lead to economic optimization. Nevertheless, the adequacy of this practice should be verified. In addition to that, to propagate tension in the geotextile, some allowable strain is required. Both design procedures mentioned previously suggest a maximum allowable strain of maximum of 5 to 6 percent. In practice, it is often applied to design with maximum geotextile strain of 3 to 4 percent. The use of geotextile strain of about the half of the maximum allowed strain shows the level of uncertainties in the design of geotextiles.

Another crucial limitation in the current design procedures is that they are suitable only for the design of embankments on end-bearing piles. BS8006 does consider embankments on floating piles. However, the design procedure is inconsistent (Van Eekelen et al., 2003). The arching action in an embankment on floating piles is reduced by means of a lower empirical arching coefficient as shown in Equation 2.3. This is then followed by the design of geotextile tensile load with an assumption that the geotextile is spanning on rigid piles with no subsoil support. In EBGEO 2004, it is stated that further elaborations are required in the procedure for designing embankments on floating piles.

As described in Section 1.2, the design of embankments on floating piles is very important. The design of embankments on floating piles leads to the question of the degree of arching action related to the settlement of piles (head-settling piles), for example, when using timber piles. It is worth to note that particularly in the South East Asian region, this pile can be a very important option. The consequence of considering the piles as head-settling piles can be that the load on the geotextiles due to soil arching is less. This is due to the slight settlement of the pile head, which leads to smaller differential settlement between the pile head and the surrounding soil. Thus, there will be more counter support from the sub soil to the geotextile layer. Finally, it leads to the choice of geotextile tensile strength requirement.

In addition to that, displacement piles are often used for embankments on floating piles construction. This leads to the requirement to include the effects of pile installation process in the design analysis. The understanding of the effects of pile installation process and to take them into account are important especially for the design of floating piles.

Another important aspect that is not covered by the current design procedures is the settlement behaviour and horizontal movement of an embankment on floating piles. This is very important considering the serviceability of the construction. Hence, short and long term settlement behaviour will be of most importance when designing embankments on floating piles.

There are more uncertainties in the design practice that are not covered in details here such as the influence of dynamic loading and local failure of a floating pile on the overall performance of the embankment on floating piles. These and other uncertainties can be added to the limitation of the current design procedures.

No doubt that the design of embankments on floating piles involves complex soil structure interaction. Current design procedures use some assumptions to simplify the design. Therefore, some influencing factors are not taken into account. Nowadays, advanced method such as finite element analysis are available for solving complex problems. Therefore, a proper finite element analysis of piled embankment design can be an adequate and reliable way to model the complex soil-structure interaction involved in the design.

Chapter 3

Numerical analysis of soil arching

As stated by Handy (1987), “arching” in civil engineering is defined as the transfer of stress from a yielding part of soil mass to adjoining less-yielding or restrained parts of mass (CGTDSM, 1958). Arching effect in soil is a familiar phenomenon and its existence has been considered in many fields of geotechnical engineering design. For example, arching effect behind retaining structures (Handy, 1985, Vermeer et al., 2001) and arching effect in the design of a buried conduit (Spangler and Handy, 1982). In addition to that, Ruse (2004) shows increasing arching effect in front of tunnel face with increasing soil friction angle.

In piled embankments design, arching in the granular embankment is a crucial mechanism for load transfer, which ensure that significant differential settlements will not occur on the embankment surface. The amount of load transfer depends on the assumed shapes of the arching and its corresponding formulations of the arching action. Various arching shapes for estimation of load transfer in piled embankments have been summarized in Satibi et al. (2007). Van der Stoel et al. (2006) show that different arching assumptions give a large difference in the amount of load transferred from the embankment to the pile caps. In addition to that, Van Eekelen et al. (2008) show a comparison of piled embankment design calculations using current design procedures described in Chapter 2 for the field test of the Kyoto road piled embankment. Both procedures give significant difference in the design results, although they are both on the safe side compared to measurements.

Nowadays, numerical methods such as finite element analysis have become more popular in geotechnical engineering design. The use of numerical methods for soil arching analysis in piled embankments designs is recommended. Some studies on numerical analysis of soil arching in piled embankments exist. However, guidelines for an adequate and reliable procedure of soil arching analysis using numerical methods are not available.

This chapter presents numerical analyses of soil arching in general piled embankments focused on the investigation of the influence of geometrical idealizations, the influence of geotextile reinforcements, the influence of capping ratio, the influence of constitutive models on soil arching action in a piled embankment. Moreover, sensitivity analyses are performed to know which parameters give significant influence on the results of soil

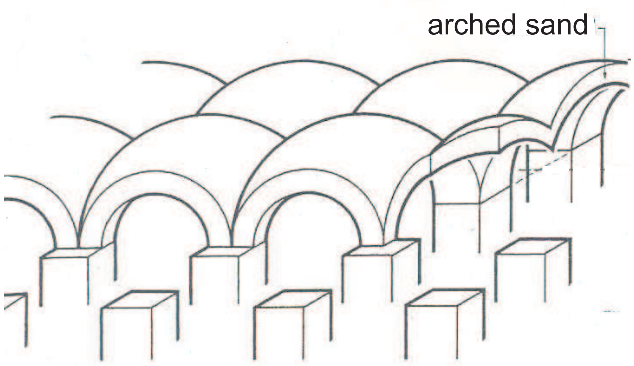

Figure 3.1: Assumed arching dome after Hewlett and Randolph (1988)

arching analysis. Particular important guides for the design of the embankment and geotextiles are highlighted.

It worth mentioning that the numerical analyses presented in this thesis are performed using the finite element method. It is assumed that the reader is familiar with the concept of the finite element method. Hence, in the present thesis, the concept of the finite element method is not primarily discussed. It is intended to present important aspects on the numerical analysis of embankments on floating piles with the use of the finite element method.

3.1 Influence of geometrical idealizations with validation of FE-model

In reality, natural arches in piled embankments represents dome-like structures spanning between pile caps. Hewlett and Randolph (1988) approximate the natural arches in piled embankments as hemispherical domes as shown in Figure 3.1. When performing a numerical analysis of arching in piled embankments, the three dimensional situation of the arching in reality can therefore be best analyzed using three dimensional (3D) geometry. This implies that neither a plane strain nor an axisymmetrical analysis can accurately represent the actual situation. Axisymmetrical analysis will produce an “umbrella” shape arch resting on a single central pile cap (Kempton et al., 1998) and plane strain analysis will produce half-tube type arching. On the other hand, many recent studies and designs of piled embankments are performed using axisymmetrical or plane strain analyses (Han and Gabr, 2002; Plomteux and Porbaha, 2004; Arwanitaki and Triantafyllidis, 2006). Moreover, Zaeske (2001) shows that the three dimensional situation can well be approached using plane strain analysis with the geometrical idealization as suggested by Bergado and Long (1994).

Axisymmetrical or plane strain analysis of soil arching in piled embankment requires less computer power and is much easier to perform compared to three dimensional (3D)

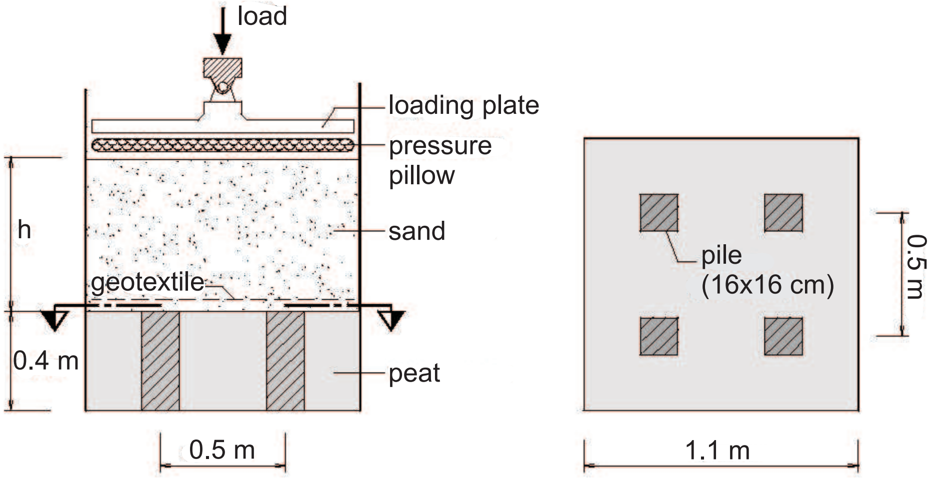

Figure 3.2: Layout of small scale piled embankments tests (Zaeske, 2001)

analysis. Because of this, a practical but accurate axisymmetrical or plane strain analysis has significant advantages. One needs to make sure, though, that the axisymmetrical or plane strain approach is a good representation of what happens in reality. This implies that research is required to compare the results of soil arching analyses from different idealizations i.e. axisymmetrical, plane strain and 3D geometries especially related to field measurements. In order to do so, numerical analyses using the finite element method of a piled embankment with different geometrical idealizations are performed. As a reference case study, the piled embankment tests performed by Zaeske (2001) are chosen.

3.1.1 Reference case study

The piled embankment tests performed by Zaeske (2001) is set up as follows: First, four rigid piles with square grid are arranged in a 1.1 m x 1.1 m box as shown in Figure 3.2. The squared piles have a size of 0.16 m x 0.16 m with 0.5 m centre-to-centre spacing. Soft peat soil is filled in between the piles up to the level of pile head. A thin plastic foil is laid on top of the peat as a separator.

In the tests, two series of experiments, one with and one without a geotextile reinforcement have been performed. In the assessment of the influence of geometrical idealizations in numerical analysis of soil arching, pile embankment tests without geotextile reinforcements are considered. Nonetheless, it is worth mentioning that in the case with geotextile reinforcement, one layer of strong geogrid with stiffness of 1000 kN/m at a strain of less than 1.5 percent is laid on top of the piles. On top of it, sand is filled up to a certain height of the embankment body. The height of the embankment varies. However, a test with an embankment height of 0.7 m is chosen as the reference for the finite element analyses. The sand is filled with pluviation (rain fall) method. It is poured in every 5 cm layer and for each layer the fall height is kept constant. With the fall height of 50 cm at every layering. It is estimated that the sand density will be around 0.5 and the embankment fill unit weight will be around 18 kN/m^3 based on preliminary fall height tests. The surface of the sand embankment is then loaded uniformly using a loading plate as shown in Figure 3.2. Underneath the loading plate, a pressure pillow containing water is applied to ensure a uniformly distributed pressure on the sand surface.

A set of measurements is taken during the test. These include the measurements of surface settlements at the top of the loading plate, the force on the pile head and the tension in the geotextile when it is used. Compared to piled embankment in practice, this test embankment is a low embankment with the ratio of embankment height to centre to centre pile spacing (h/s) of 1.4.

3.1.2 Geometrical idealization

Four geometrical idealizations used for soil arching analysis in piled embankments have been found in literature. The geometrical idealizations include axisymmetrical, plain strain model according to Bergado and Long (1994), plain strain model with equivalent pile stiffness and 3D geometries as illustrated in Figure 3.3. The idealization of the actual piled embankment test geometry can be described as follows:

- *Axisymmetric geometry:* The three dimensional one cell of the pile embankment is transformed into a circular cell with the area of pile and the soil remain the same. Figure 3.3a shows the transformation of the squared cell to a circular cell. For the axisymmetrical finite element (FE) analysis, one radian of the circular piled embankment cell is used.

- *Plane strain after Bergado:* According to Bergado and Long (1994), the three dimensional grid of piles can be transformed into continuous walls with an equivalent thickness t_{eq} in plane strain geometry (Figure 3.3b). The thickness of the continuous wall is calculated based on the consideration that the ratio of improved area i.e. the ratio of pile cap area to the one cell soil area (A_c/A_E) is kept constant. Hence,

$$\frac{A_c}{A_E} = \frac{t_{eq} \cdot s_y}{s_x \cdot s_y} \tag{3.1}$$

  For the current reference case, the pile is therefore transformed into a thin continuous wall with equivalent thickness t_{eq} of 5.1 cm. Due to symmetry, only half of the plane strain geometry is used for the FE-calculations.

- *Plane strain with equivalent pile stiffness:* Alternative method that has been found in literature to transform the three dimensional grid of piles into a continuous wall in plane strain condition is by assuming equivalent wall stiffness. In this method the thickness of the wall is the same as the width of the original pile as shown in Figure 3.3b. The equivalent stiffness of the wall E_{eq} is taken as the proportional average of

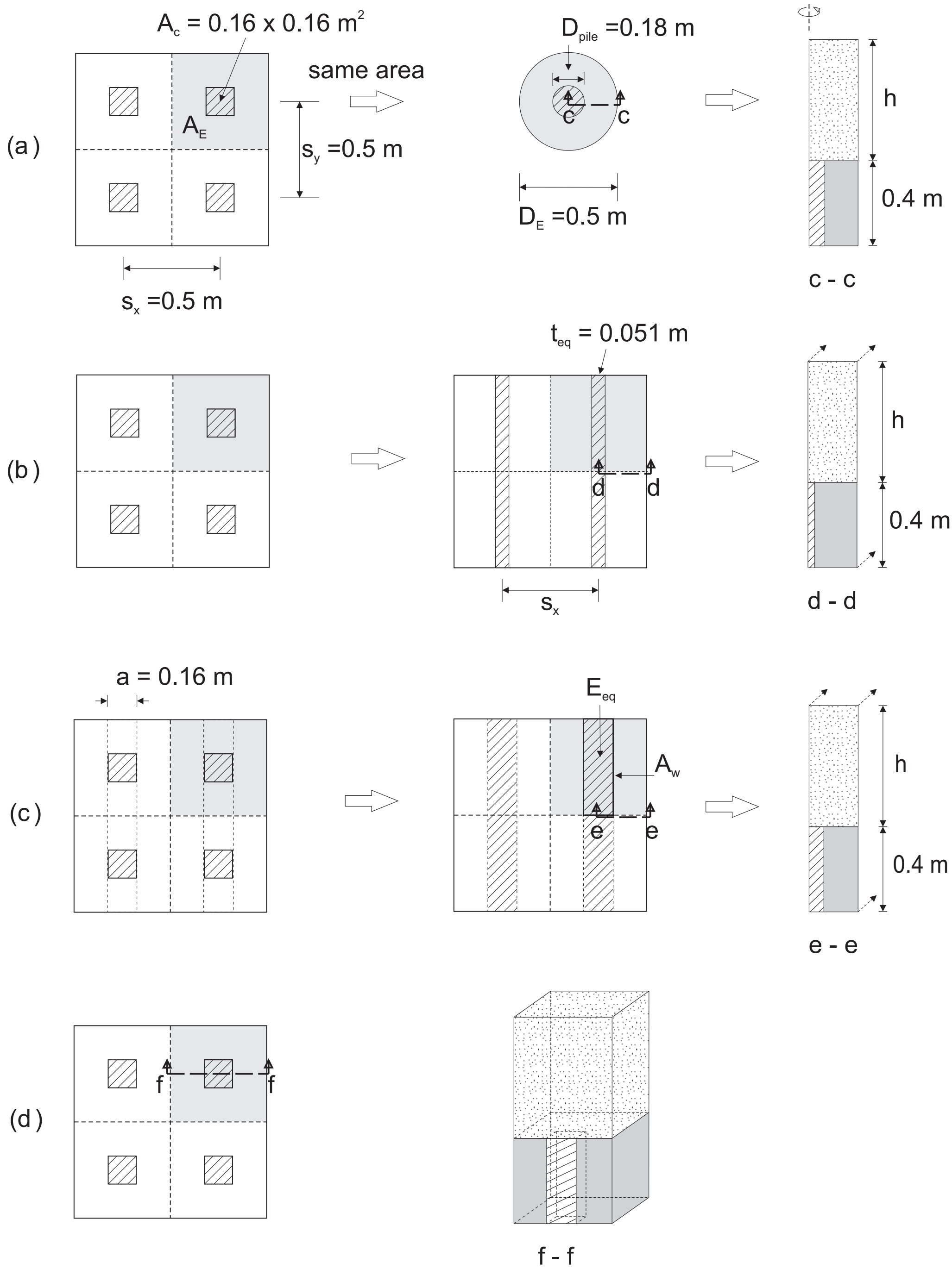

Figure 3.3: Geometrical idealizations of one cell piled embankment (a) Axisymmetrical idealization (b) Idealization for plane strain after Bergado (c) Idealization for plane strain with equivalent stiffness (d) 3D geometry

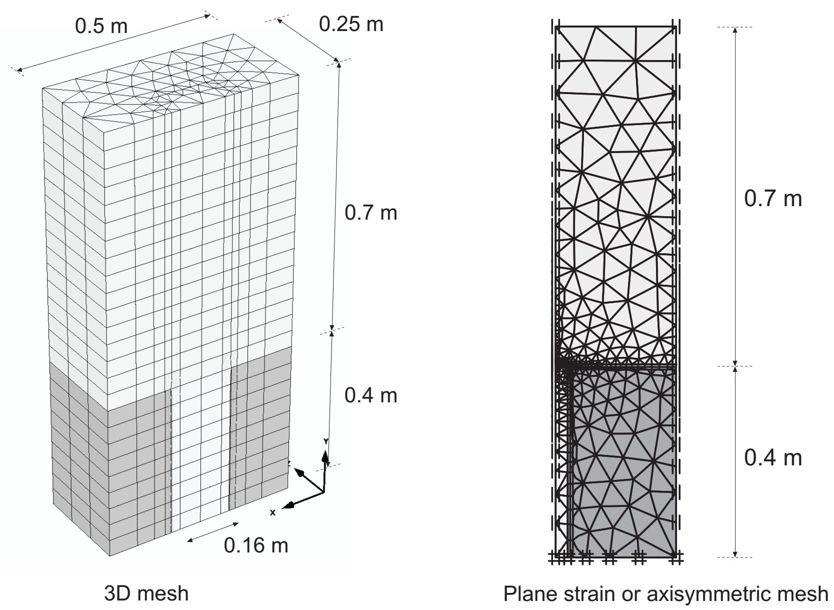

Figure 3.4: Typical FE meshes as used for the analyses of the influence of geometrical idealization

the pile and soil stiffness. Thus,

$$E_{eq} = \frac{E_c \cdot A_c + E_s \cdot (A_w - A_c)}{A_w} \tag{3.2}$$

where E_c, E_s and A_w are pile stiffness, soft subsoil stiffness, and wall area as shown in Figure 3.3c respectively. It worth noting that on using this method, the improved area ratio (or area of the pile) becomes larger. As a consequence, the volume of embankment fill below the arch becomes less compared to actual three dimensional condition. Therefore, this method is not considered for the present soil arching analyses.

- *3D geometry:* The three dimensional dimension of the actual case can be best analyzed using 3D geometry. Half of the piled embankment cell is considered for the 3D finite element analyses (Figure 3.3d). The 3D half cell geometry is used because it is the most efficient geometry offered by the FE-program that include the possibility of using interface elements between the pile shaft and the peat.

3.1.3 FE-piled embankment calculation

Figure 3.4 illustrates the meshes used in the FE-analyses. The meshes are refined around the pile head where the stress gradient is expected to be high. For axisymmetrical and plane strain analyses, six-noded triangular elements with three Gaussian integration points are used. Fifteen-noded wedge elements with six Gaussian integration points are used for the 3D analyses. Around 350 elements are used for the axisymmetrical and plane strain analyses, whereas the 3D FE-mesh consist of about 3000 elements. Interface elements are applied to simulate pile-soil contacts both at the shaft and the top of the pile. However, for the 3D analyses, interface elements are used at the contact between the soft soil and pile. The description about the interface elements behaviour is not described primarily in this thesis. However, it can be found in Appendix B.

Boundary conditions

For present FE analyses, the boundary conditions applied are described as follows. At the nodes of all side (vertical) boundaries, roller fixities are applied. This means that vertical displacement is let free and horizontal displacement is restricted. This implies that normal stress is allowed, but no shear stress. For the bottom boundaries, all nodes have total fixities, which allow no displacement in both horizontal and vertical directions. As a consequence, both normal and shear stress may occur. The top boundaries have no fixities. Therefore, the nodes at the top boundaries are fully free to displace.

Initial conditions

The initial stresses conditions of the homogeneous peat soil with horizontal soil surface is generated according to K_0-condition. This means that the effective vertical soil stress σ'_v and the effective horizontal soil stress σ'_h are assumed to follow the relation

$$\sigma'_v = \gamma' \cdot z \tag{3.3}$$

$$\sigma'_h = K_0 \cdot \sigma'_v \quad with \quad K_0 = 1 - (\sin \varphi') \tag{3.4}$$

where z is the depth below soil surface.

Material constitutive models and properties

Material constitutive model is an important constituent part of FE-analysis. It governs the material stress-strain behaviour in the analysis. In this chapter, the so-called Hardening Soil model is used for modelling the material constitutive behaviour of the embankment fill and the peat. Detail description of the soil constitutive model is not discussed here, it can be found in Appendix A. This advanced soil model is used because it can simulate both stiff and soft soil behaviour. It accommodates stress-dependent stiffness and yielding formulations for simulating volumetric compression and shear hardening. For the details of the soil model, the reader is referred to Schanz et al. (1999). The material properties for the Hardening Soil model as used in the finite element calculations are listed in Table 3.1. The material properties are based on the available test data. For the stiff concrete pile, linear elastic non-porous behaviour is considered with pile Young's modulus of 26 GPa.

Table 3.1: Material parameters for the Hardening Soil model (see Appendix A.1)

Properties		Sand	Peat
φ'	$[°]$	38	24
c'	$[kPa]$	0.1	8.5
ψ	$[°]$	11	0
γ'	$[kN/m^3]$	18	8
E_{50}^{ref}	$[MPa]$	23	1.7
E_{oed}^{ref}	$[MPa]$	28	0.85
E_{ur}^{ref}	$[MPa]$	112	12.75
ν_{ur}	$[-]$	0.2	0.2
m	$[-]$	0.5	1
R_{inter}	$[-]$	1	0.35

Calculation procedure

The calculation begin with the generation of initial stresses conditions of the homogeneous peat soil. After that, the embankment fill elements are activated. In the case where a geotextile is used, it is applied simultaneously with the embankment fill. Finally the external load is applied on the surface of the embankment fill.

3.1.4 Load on pile

Figure 3.5a shows the principal stresses due to the arching action from an FE-axisymmetric analysis. The stresses are redistributed and reoriented to form arches. It can be seen that the orientations of principal stresses show inverse catenary-like shaped arches. In addition to that, as illustrated in Figure 3.5b, the differential vertical displacements in the embankment only occur up to a certain height. Beyond this height the vertical settlements are uniform.

Through arching action, the embankment and uniformly distributed external loads are largely transferred to the pile. Figure 3.6a shows the calculated load on pile from axisymmetrical and 3D analyses. It is shown that calculated load on pile from both axisymmetrical and 3D analyses give the same result. Moreover, the calculated loads on pile give good agreements with measurements from the reference case. In addition to that, the amount of load transfer in piled embankments can be determined using the so-called *efficacy*, defined as the ratio of load on pile cap to the total embankment and external load of the corresponding unit cell piled embankment as shown previously in

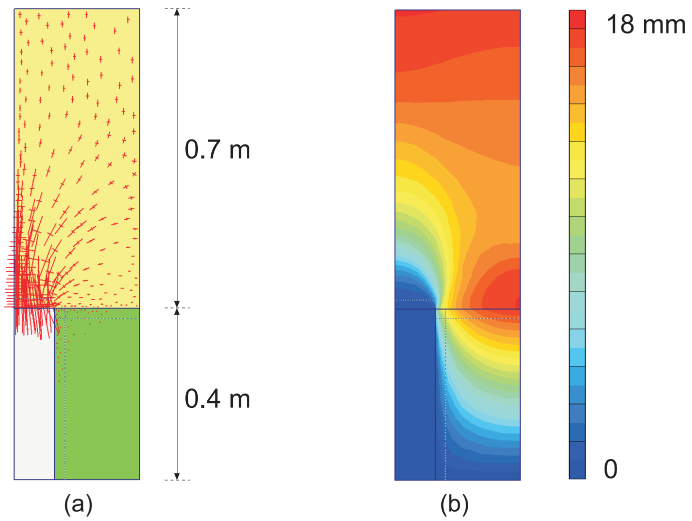

Figure 3.5: Developed arching action from an FE-axisymmetric analysis (a) Principal stresses (b) Vertical settlements shadings

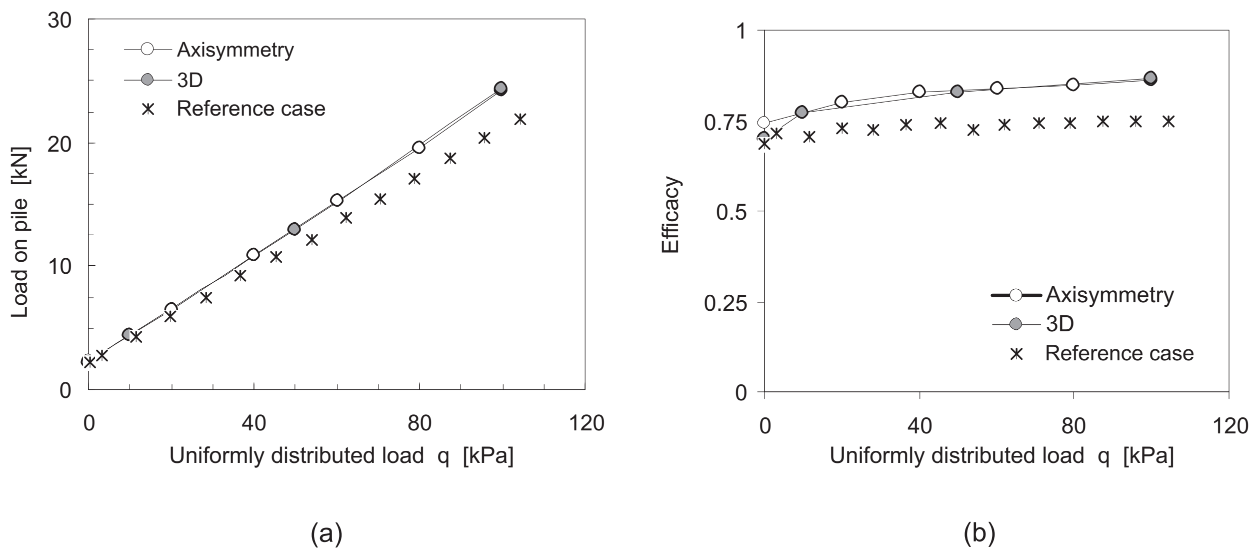

Figure 3.6: Calculated load on pile and efficacy

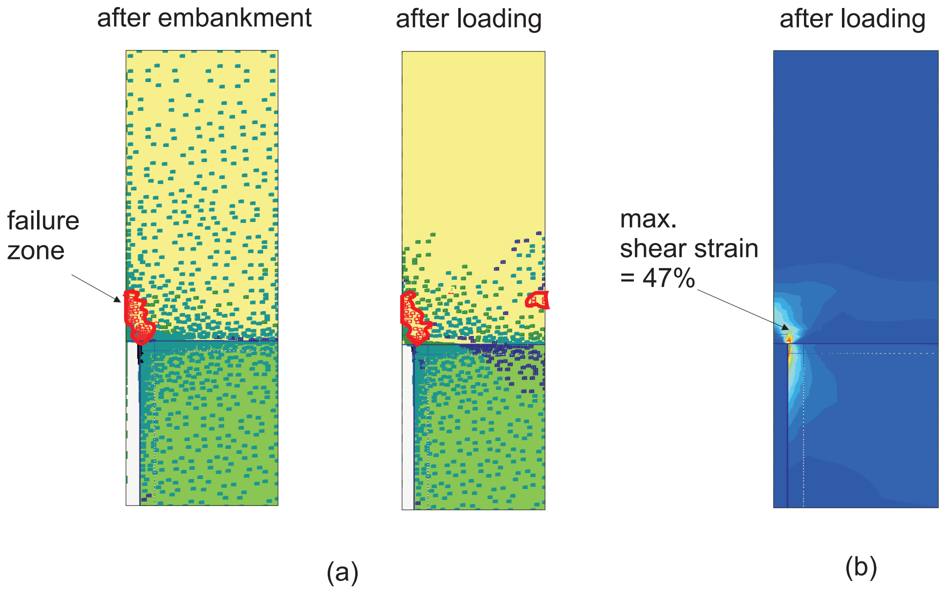

Figure 3.7: Failure mechanism of the plane strain after Bergado

Figure 2.4. Efficacy E can be expressed as

$$E = \frac{P}{(\gamma'_{emb} \cdot h + q) \cdot A_E} \tag{3.5}$$

where P is the vertical force on pile cap and q is the uniformly distributed load on the embankment surface. Hence, efficacy describes the portion of total load that is carried by pile. Figure 3.6b shows the calculated and measured efficacy for the present case.

In contrast to the axisymmetrical and 3D geometry, the FE-analysis with plane strain geometry leads to calculation instability and a wrong failure mechanism. The calculation fails just after applying uniformly distributed load q of about 5 kPa on embankment surface. Hence, the load on pile and efficacy cannot be plotted. The reason for this is that the plane strain geometry using the Bergado method transforms the actual squared pile to a thin wall. If no cap is considered on the pile head, this causes pile punching failure into the embankment instead of soil arching. This particular failure mechanism is visualized with the Gaussian points, which reach Mohr-Coulomb failure condition as illustrated in the failure zone in Figure 3.7a. Furthermore, the contour plot of total shear strains confirms that the pile is penetrating into the embankment instead of supporting it (Figure 3.7b). With some modification in the calculation procedure, it is possible to force the calculation to continue and to obtain load-settlement curve, which may give good agreement with the measurements as presented by Zaeske (2001). However, the punching failure indications observed from the plasticity and strain condition of the embankment soil stress points, will occur since the very beginning. Moreover, the obtained load-settlement curve distorts, which shows a deceptive result. Hence, in this study, the plane strain analysis with geometrical idealization put forward by Bergado and Long (1994) is not applicable.

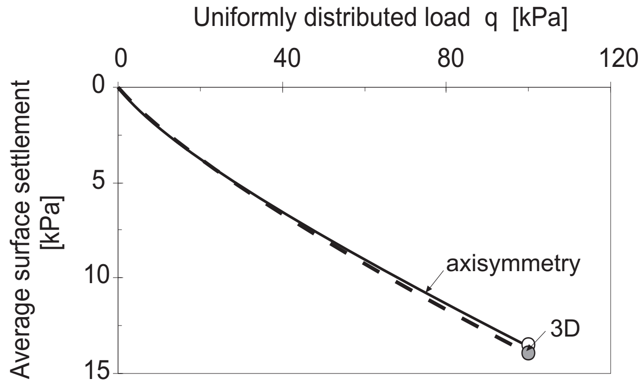

Figure 3.8: Calculated load-embankment surface settlement curves

3.1.5 Embankment settlements

Figure 3.8 shows the calculated load-settlements curve at the surface of the embankment. For the current material data, good agreements with the measured load-settlements data could not be achieved. It may probably because the stiffness of the pluviated sand for the embankment fill is lower than the data obtained from triaxial tests. Nonetheless, when a calibration is made, a reasonably good agreement of calculated load-settlements curve can be obtained by reducing the stiffness properties of the sand to about a half of the values as listed in Table 3.1. This result will be shown in Section 3.4.

As the main focus of the study is to compare the results of different geometrical idealizations, it is shown from Figure 3.8 that calculated load-settlements from axisymmetrical and 3D FE-analyses almost coincide. This suggests that both analyses are equivalent. Further evaluation of the calculation results show that axisymmetrical and 3D analyses do not show significant differences. Figure 3.9 shows that the vertical settlement shadings from 3D and axisymmetrical analyses are very much alike. Moreover, both analyses produce the same arching height, which is indicated by a plane of equal settlement (Figure 3.10). A plane of equal settlements is a horizontal plane in the embankment body, which has equal vertical settlements. In piled embankments analysis, the plane of equal settlement has been used for determining soil arching height as originally proposed by Marston (Naughton, 2007).

Soil arching height in a piled embankment analysis has been considered as the minimum height h_{min} of an embankment to ensure the development of full arching action. Several criteria have been proposed for determining h_{min}. For example, British standard BS8006 suggests $h_{min} = 1.4 \cdot (s - a)$ for full aching action and the German method EBGEO 2004 proposes that $h_{min} = 0.7 \cdot s_d$. In this particular case, both criteria and the result of FE-analyses are in a good agreement with h_{min} of about 0.5 m. As illustrated in Figure 3.11, generally the criteria from the German method gives a conservative and better agreement with FE-analyses especially for pile capping ratio of more than 10 percent. Pile capping ratio is the ratio of pile cap area A_c to the cross section area of one cell of the piled embankment A_E.

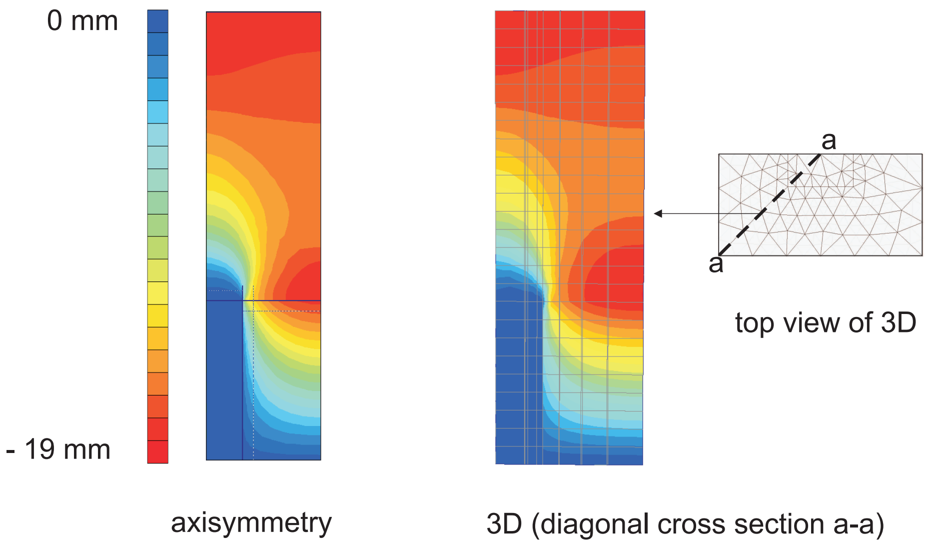

Figure 3.9: Comparison of vertical settlements shadings after applying external load q of 100 kPa

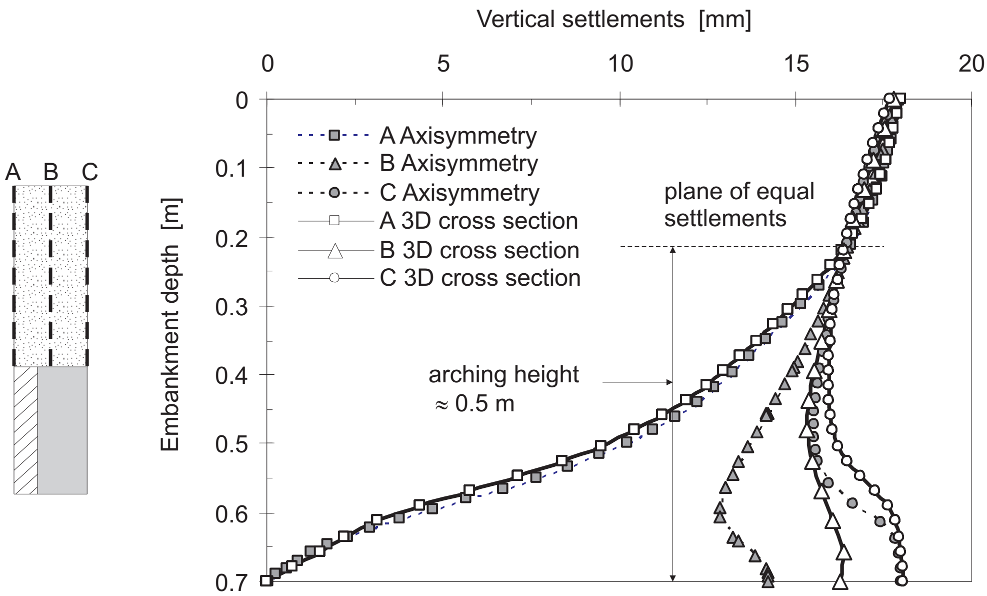

Figure 3.10: Vertical settlements profiles at three cross section from axisymmetrical and 3D (cross-section a-a) outputs

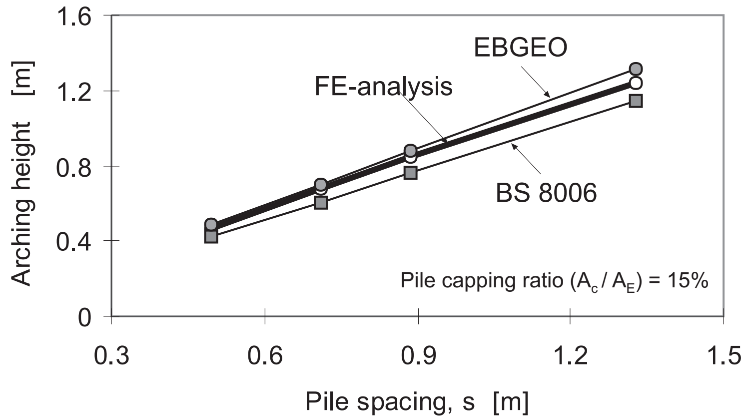

Figure 3.11: Comparison of arching height in piled embankments from FE-analyses and the current design guidelines

3.2 Influence of geotextile reinforcement

Most of piled embankment constructions use geotextile reinforcements. For the FE-analyses of piled embankments with a geotextile reinforcement, axisymmetrical idealisation of the reference case as described in Section 3.1.1 is used. Hence, the calculation procedure is similar. In addition, one geotextile layer with a tensile stiffness of 1000 kN/m is applied on top of the pile cap. Three noded-line elements with three Newton-Cotes integration points for each element are used for the geotextile layer. Each node of the geotextile elements has two translational degree of freedoms. Moreover, the geotextile elements posses only tensile stiffness.

Since the geotextile is laid horizontally and the embankment loading is acting perpendicular on the geotextile layer, updating the geometry of the mesh during the stepwise incremental loading in the finite elements calculations is necessary. With this procedure, the mobilized tensile strains in the geotextile elements are captured. Since the geometry of the mesh are updated after each calculation step, the geotextile is no longer horizontal. Hence, tensile strains in the geotextile develop due to vertical embankment load. The presently used FE-program provides a calculation procedure for that purpose, which is based on updated Lagrange formulation. In general, the procedure is considered for analyses of problems where the influence of the shape of the geometry is significant. For example, in the case where large deformations are expected to happen. In FE-analysis with updated Lagrange procedure, the stiffness matrix is based on the deformed geometry. Hence, at each load step, the stiffness matrix is updated due to the new geometrical positions of the deformed elements. In addition to that, a special definition of stress rate is adopted that includes rotational terms. Therefore, the updated Lagrange procedure involves more complex formulations and requires more computational time compared to the standard FE-calculation procedure. For a further details of geotextile elements and

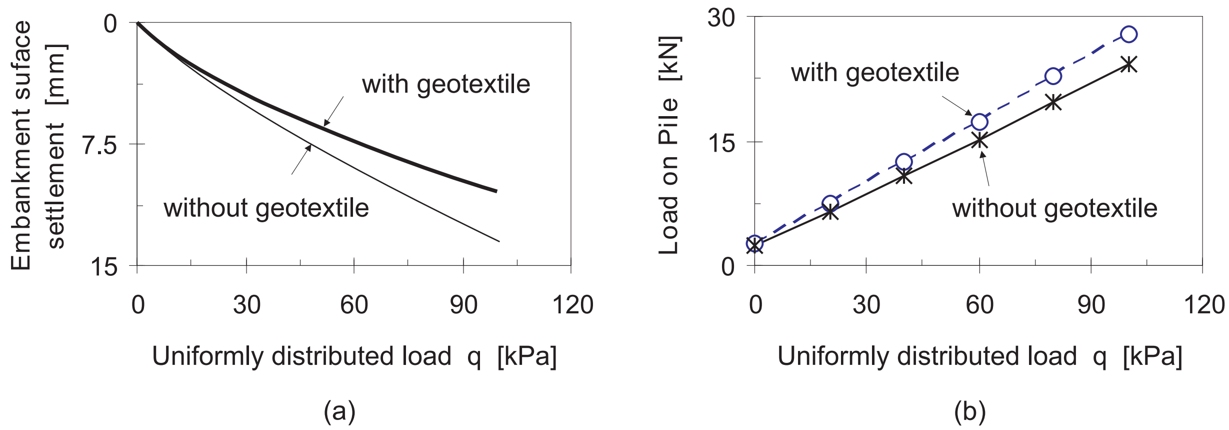

Figure 3.12: Influence of geotextile reinforcement on embankment surface settlements and load on pile

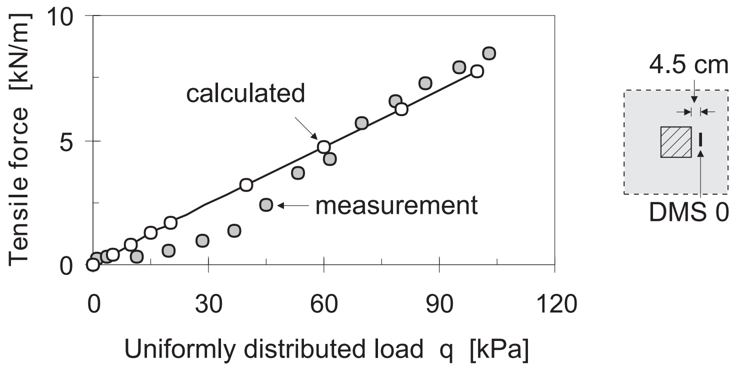

Figure 3.13: Calculated and measured geotextile tensile force at location DMS 0

updated Lagrange procedure, the reader is referred to Brinkgreve (2002).

The influence of a geotextile reinforcement on piled embankments is illustrated in Figures 3.12a and 3.12b. The use of geotextile reduces the embankment settlements and increase the load carried by pile. Furthermore, by applying geotextile reinforcements, the tendency of punching failure as described in Section 3.1.4 is reduced. Hence, it improves the stability of soil arching. This will be shown more clearly in the next section. For the reference case, the calculated tensile force in the geotextile is in a good agreement with measurement as shown in Figure 3.13.

3.2.1 Applied layers of geotextiles

In piled embankments design practice, it is often that up to three layers of geotextiles are used, although the current design procedures described in Chapter 2 are based on one layer geotextile reinforcement. FE-analyses of piled embankments with one strong geotextile layer also show that one layer reinforcement is sufficient. Hence, there is no need to apply more geotextile layer. The current practice of using more than one layer of geotextile may be because it is intended to have a conservative design due to uncertainties in the available strength of materials and the possible damage during construction process. When conservative design by applying more than one geotextiles layer is needed, the geotextiles are laid with a certain distance. In practice, the distance between geotextile layers are between 10 cm to about 50 cm depending on the geometry of the piled embankment. According to the German method, when two geotextile layers are used, the distance between the geotextile layers should be between 15 to 30 cm.

To observe the influence of the number of geotextile layers on settlements and load transfer behaviour of a piled embankment, axisymmetrical FE-piled embankment analyses are performed using the geometry of the reference case. Instead of the previous medium dense sand, a loose sand with low effective friction angle of 30° is used for the embankment fill. The reference oedometer stiffness E_{oed}^{ref} of the sand is taken equal to its reference secant triaxial loading stiffness E_{50}^{ref} of 12 MPa. The reference unloading-reloading stiffness E_{ur}^{ref} of the sand is taken as 48 MPa. The superscript ref denotes that the stiffness is measured at a reference pressure, which is 100 kPa. Moreover, one to three layers of geotextile with tensile stiffness of 333 kN/m are applied. For the pile embankment geometry of the reference case, three different distance of geotextile layers of 5 cm, 10 cm and 15 cm are considered in the FE-analyses.

Embankment settlements

Figure 3.14a illustrates the comparison of calculated settlements of a piled embankment with different number of geotextile reinforcements due to external load. The settlements are evaluated at the middle of the sub-soil surface in between pile heads as the settlement at this point relates to the geotextile tensile load. It is shown that the more geotextile layers used the less settlements occur. However, when the distance of the geotextile layer is made larger, the settlements become similar to sub-soil settlements in the case of only one geotextile layer is applied. For the present piled embankment geometry, Figure 3.14b shows that when the distance of geotextile layers of 15 cm is used, there is no considerable difference between the sub-soil settlements of embankment with three geotextile layers and of embankment with one geotextile layer. The reason is that 15 cm distance is too high that the second and the topmost geotextile layers mobilize only little strains due to little differential settlements in the embankment at the level of the two upper geotextile layers. The differential settlements is maximum at sub-soil surface and reduce significantly to zero at the plane of equal settlements, which is also the arching height. Figure 3.15 shows that the current arching height is 0.42 m above the sub-soil surface, whereas the level of the top most geotextile layer is 0.3 m above sub-soil surface when 15 cm distance is used. Therefore, the topmost geotextile layer does not develop much tension. Typically, large differential settlements accumulate at the lower half of

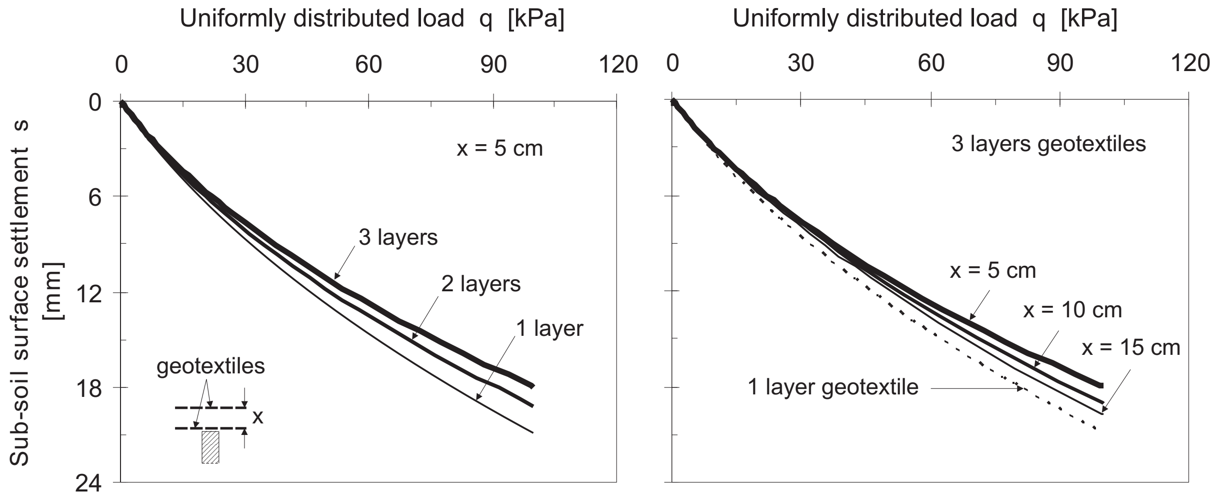

(a) (b)

Figure 3.14: Sub-soil settlements with different number and distance of geotextile reinforcements

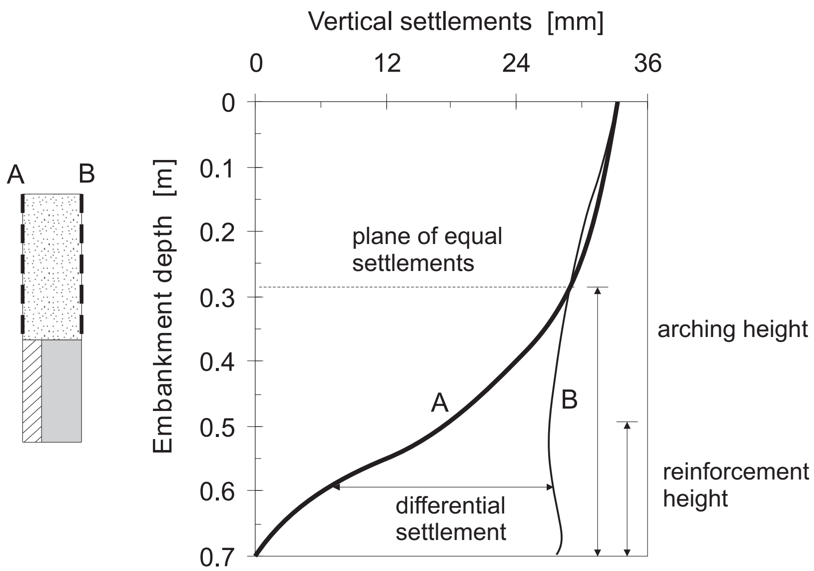

Figure 3.15: Differential settlements below plane of equal settlements

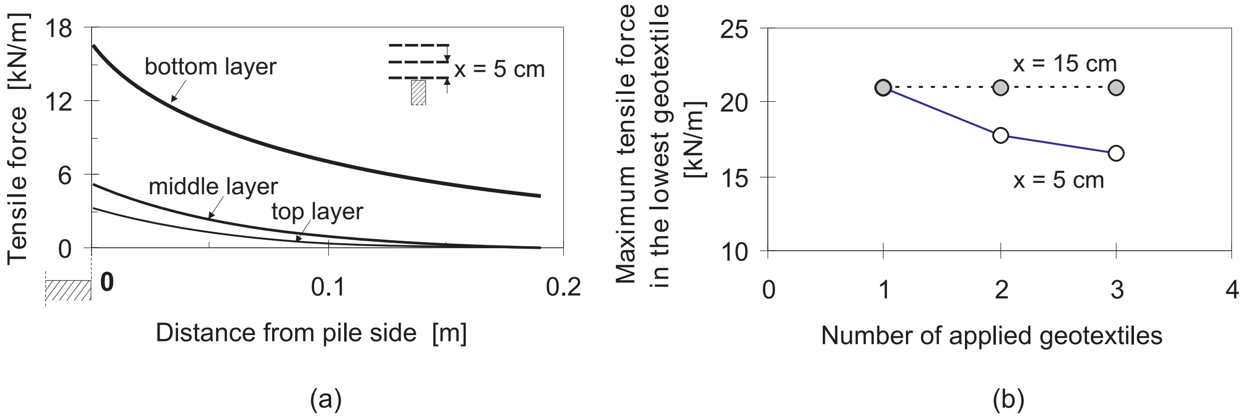

Figure 3.16: Tensile forces from different number and distance of geotextile layer

the arching height. Hence, to apply additional layer of geotextiles effectively, it should be placed at the lower half of the arching height as described in Figure 3.15. The distance between geotextile layers may be taken as the possible minimum distance from practical or installation point of view.

Geotextile tensile force

The bottom geotextile exerts the largest tensile force due to the largest differential settlements at this level. Higher positioned geotextiles exert less tensile force as described in Figure 3.16a. It is obvious that the maximum tensile force occurs just around the pile. Economic saving can be obtained when the reinforcement is focused on this area. In addition, Figure 3.16b shows the maximum tensile force in the lowest geotextile with different number of applied geotextiles. Again, it can be seen that when the distance of geotextile is high, the influence of adding more geotextile layers to the amount of maximum tensile force exerted in the lowest geotextile is negligible. On the other hand, when the distance of geotextile layers is small, additional layers of geotextile reduce the amount of tensile force in the lowest layer.

Punching failure problem

When a small pile cap is used, instead of the development soil arching action, the embankment may tend to have a punching failure as described in Section 3.1.4. The tendency of punching reduces when geotextile reinforcement is used. Figure 3.17 illustrates the total shear strains contours after loading of 100 kPa from piled embankments with different number of geotextile reinforcements. It can be seen that using more geotextile layers increases the stability against punching. Nevertheless, adding more geotextile layer might not be economic since one strong geotextile is generally already sufficient.

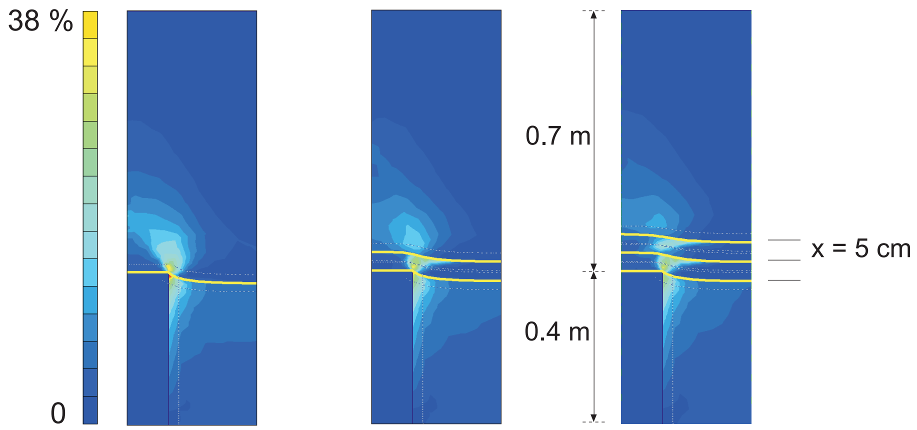

Figure 3.17: Total shear strain contours after loading 100 kPa from embankment with different number of geotextile layers

3.3 Influence of capping ratio

Capping ratio is defined as the ratio of pile cap area A_c to the cross section area of one cell of the piled embankment A_E. In some literature, capping ratio is also known as improvement area ratio or pile cap coverage. In piled embankments, a certain capping ratio is required to ensure that a stable arching action is developed. It is known that a small capping ratio can lead to punching failure that damages the arching structure. In practice, 5 to 25 percent capping ratio has been used for piled embankment constructions. Han and Gabr (2002) summarize applied capping ratios of several actual piled embankments with geotextile reinforcements as described in Figure 3.18. In addition to that, a comparison of the percentage of capping ratio of piled embankments without geotextile reinforcement that is put forward by Rathmayer (1975) is shown. It can be seen that piled embankments with geotextile reinforcement requires less capping ratio. 10 percent of capping ratio may be considered as the minimum capping ratio for piled embankment with geotextile reinforcement.

Based on the piled embankment case as described in Section 3.2.1 with one geotextile reinforcement, FE-analyses are performed to evaluate the influence of capping ratio. In the analyses, the size of pile is varied to give capping ratio of 5 to 15 percent. Figure 3.19a shows the total shear strain shadings after applying uniformly distributed load q of 100 kPa from piled embankments with different capping ratios. Although all calculations do not show failure, the tendency of punching is clearly seen when using 5 percent capping ratio. The shear strain accumulation is cutting through the centre of axisymmetry to the side of pile head, whereas with the use of larger capping ratios, this does not occur. The plot of plasticity points that show the zones in which the stress points reach Mohr-Coulomb failure condition as depicted in Figure 3.19b confirm the theory. Hence, the results of FE-analyses also suggest that a minimum of 10 percent capping ratio may be considered as a minimum capping ratio to obtain a stable arching action in piled embankments with a strong geotextile reinforcement. Moreover, it is worth mentioning that

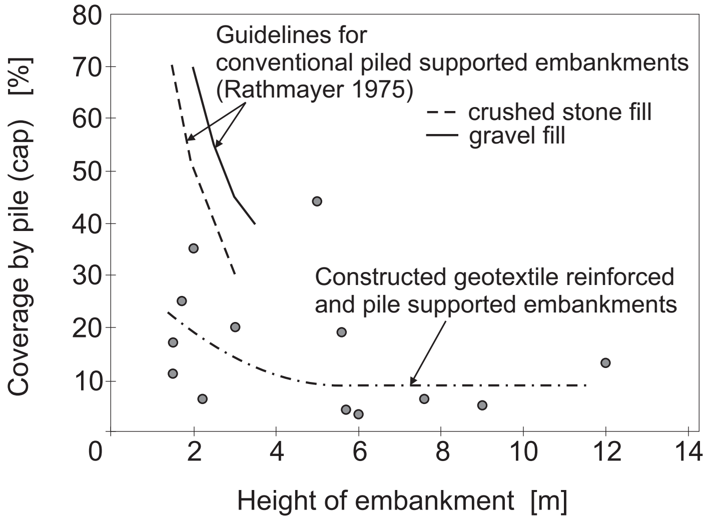

Figure 3.18: Capping ratio for piled embankment constructions after Han and Gabr (2002)

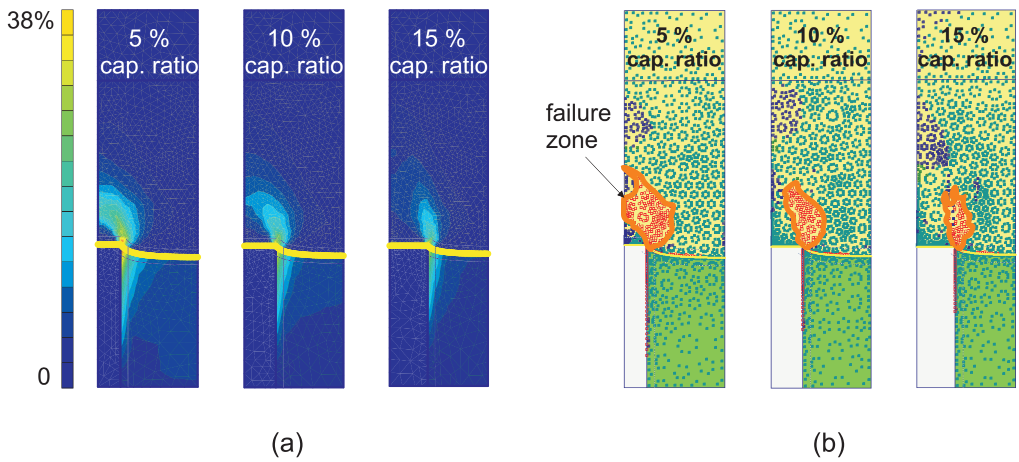

Figure 3.19: FE-analyses outputs from embankment with different capping ratio (a) Total shear strain shadings (b) Plasticity points showing Mohr-Coulomb failure zone

from previous FE-analyses, punching failure can be avoided by applying more geotextile layers within the lower half of the predicted arching height.

For piled embankment without a strong geotextile reinforcement, a larger capping ratio need to be used. Numerical analysis results suggest that minimum capping ratio of 20 percent is save from punching failure. However, conservative considerations should be taken for embankment without geotextile reinforcement as the risk of collapse of soil arching, which can lead to severe damage of the piled embankment is high. On the other hand, as long as a strong geotextile is used, the risk of soil arching collapse is low although the tendency of punching problem identified.

3.4 Influence of soil constitutive models

Nowadays, several constitutive models are available for modelling the behaviour of granular embankment fill. Hence, different constitutive models have been used for numerical analyses of soil arching in piled embankments. For example, the well known Mohr-Coulomb (MC) model has been used by Russel and Pierpoint (1997) and Van der Stoel et al. (2006) among others. Jenck et al. (2007) used a modified MC model with stress dependent stiffness and Han and Gabr (2002) applied the hyperbolic soil model after Duncan and Chang (1970). Nevertheless, to the writer knowledge, there is no comparison has been made so far on the influence of different soil constitutive models on the results of a piled embankment analysis especially related to measurements from a case study.

At the Institute for Geotechnical Engineering, University of Stuttgart, various soil constitutive models have been developed. For the evaluation of the influence of soil constitutive models on soil arching analysis, two advanced models, which can accurately simulate the behaviour of granular materials will be compared to the well-known MC model. The advanced soil models are the Hardening Soil (HS) model as briefly described in 3.1.3 and the Hardening Soil Small (HS-Small) model. The HS-Small model is a small strain stiffness extension of the HS model that accounts for higher stiffness of soils at small strains. At small strain levels most soils exhibit a higher stiffness than at engineering strain levels. This stiffness varies non-linearly with strain. The stiffness decays as the strain increases. The importance of the high stiffness at small strains and its use in geotechnical engineering have been shown by researchers, e.g. by Benz (2006). His work has led to the development of the HS-Small model. Further description of the HS-Small model can be found in Appendix A.2.

Similarly to the previous section, axisymmetrical FE-analyses of piled embankment with the reference case geometry as described in Section 3.1.1 are performed to analyze the influence of soil constitutive models. Table 3.2 shows the embankment material properties for the soil models as used in the current FE-analyses. The embankment material properties are back-calculated values, which give the best approximations to the load-settlement measurements of the reference piled embankments test with and without geo-

Table 3.2: Embankment material properties for different soil models as used in the FE-analyses (see also Appendix A)

Properties		MC model	HS model	HS-Small model
φ'	[°]	38	38	38
c'	kPa	0.1	0.1	0.1
ψ	[°]	8	8	8
γ'	[kN/m^3]	18	18	18
E_{50}^{ref}	[MPa]	-	12	12
E_{oed}^{ref}	[MPa]	-	12	12
E_{ur}^{ref} / E	[MPa]	- / 7.5	48 / -	48 / -
ν_{ur} / ν	[-]	- / 0.2	0.2 / -	0.2 / -
m	[-]	-	0.5	0.5
G_0^{ref}	[MPa]	-	-	80
$\gamma_{0.7}$	[-]	-	-	10^{-4}

textile reinforcement. The material parameters as well as the constitutive models for the pile, peat and geotextile remain the same as described in Section 3.1.1.

Figure 3.20 shows calculated curves of applied uniformly distributed external load against average embankment surface settlement from different soil models. The curve from analyses with the MC model show a linear load-settlement behaviour, whereas the curves from analyses with the HS and the HS-Small models are non-linear. The curvature of the the latter curves is closer to what is observed from measured data. The load-settlement curves from analysis with the HS and the HS-Small models coincide. This indicates that most of the strains occurred in the piled embankment are not very small that the small strain stiffness has decayed. Hence, it gives no significant influence on the load-settlement curve. Similarly, the other calculation outputs from the analysis with the HS and the HS-Small models are almost the same.

As depicted in Figure 3.21a, the predicted load on pile from analysis with the MC model and the HS model are more or less the same. Moreover, when performing analyses with geotextile reinforcement, both models gives no considerable difference of the geotextile tensile force as described in Figure 3.21b. Hence, provided that a suitable stiffness is chosen, the piled embankment analysis with the MC model gives similar results compared to analyses with the more advanced models.

However, a reliable stiffness for the MC model can hardly be chosen compared to the choice of stiffness for the HS model where reliable correlations for typical granular materials are available (see for example Vermeer et al. 1999). Moreover, when using the MC model for an axisymmetrical piled embankment analysis, one might consider hi-

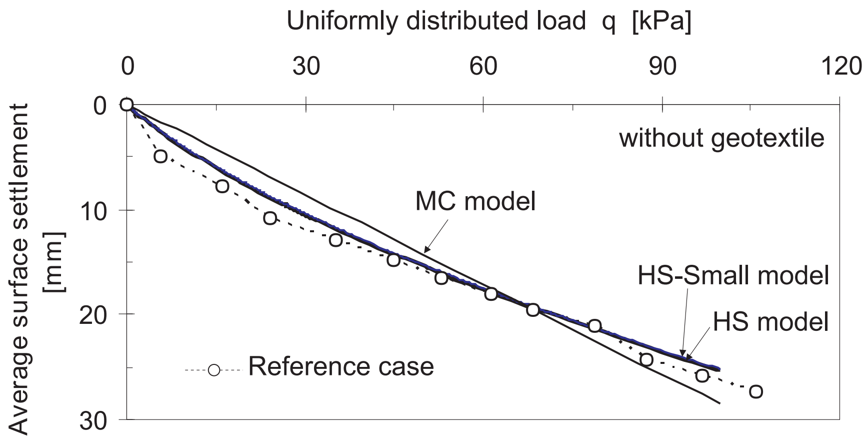

Figure 3.20: Load-settlement curves from analyses with different soil models

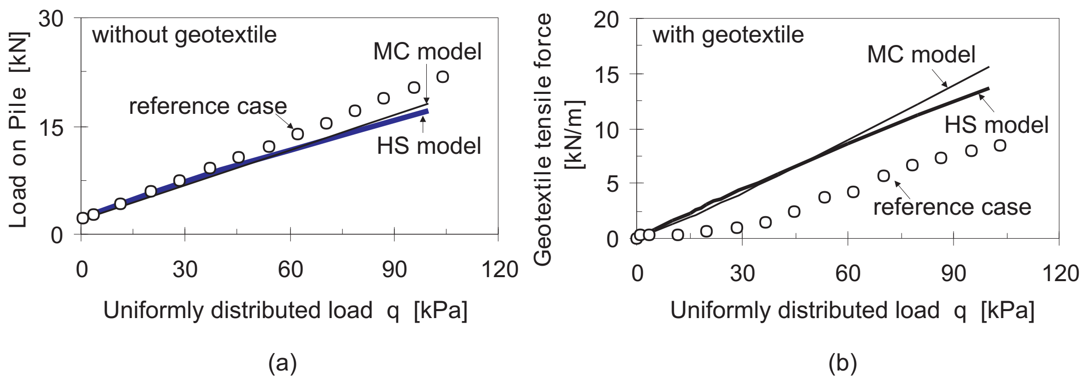

Figure 3.21: Calculated load on pile and geotextile tensile force from analyses with different soil models

gher Poisson's ratio ν than the real value to obtain a proper K_0-value for the generation of horizontal stresses. The Poisson's ratio ν can be obtained using the relation

$$\nu = \frac{K_0}{1 + K_0} \tag{3.6}$$

where K_0 can be taken using Jaky's formula, which is $K_0 = 1 - \sin\varphi'$. Hence, the horizontal stresses in the MC model depend on the Poisson's ratio ν. On the other hand, when using the HS model, K_0-value according to Jaky's formula is an independent input. Hence, when using HS model, realistic unloading reloading Poisson's ratio ν_{ur} can be used. Furthermore, indications of pile punching problem are less obvious compared to when using the HS model. Hence, the use of advanced soil model such as the HS model for piled embankments analysis is recommended compared to the simpler MC model, which is an elastic-perfectly plastic model with Mohr-Coulomb failure criterion.

3.4.1 Sensitivity analysis

In the previous section, the use of the HS model for analysis of soil arching in piled embankments is recommended. The Hardening Soil model entails several material parameters. The parameters consist of shear strength parameters, which are effective friction angle φ', dilatancy angle ψ and effective cohesion c'. In addition to that, the model uses three stiffness parameters which are the secant deviatoric loading stiffness E_{50}^{ref}, oedometer loading stiffness E_{oed}^{ref}, and unloading-reloading stiffness E_{ur}^{ref}. The superscript ref denotes that the stiffness is measured at a reference pressure p^{ref}, which is generally taken as 100 kPa. Moreover, the model also uses unloading-reloading Poisson ratio ν_{ur} and a power law m (see Appendix A.1). In order to understand which parameters give large influence in a piled embankment analysis, sensitivity analyses are performed by evaluating the changes of load-settlement curve, load on pile as well as indication of punching problem due to independent variation of the parameters.

Influence of shear strength parameters

For granular embankment materials, effective cohesion c' can be assumed zero. Hence, evaluation is focused on the variation of φ' and ψ. For the influence of φ', all other parameters are kept constant and ψ is taken as zero. Calculation results show that φ' has significant influences on the results of piled embankment analyses. Figure 3.22a shows that the influence of φ' on load-settlement taken at the level of soft sub-soil surface. The same behaviour is also observed for the settlement at the surface of the embankment. The higher φ' leads to less settlements in the embankment. Moreover, φ' influence significantly the amount of embankment and external load transferred to the pile as illustrated in Figure 3.22b. Hence, the higher φ' the stronger the arching action in the embankment. Furthermore, the curve in Figure 3.22b shows two lines with different slopes.

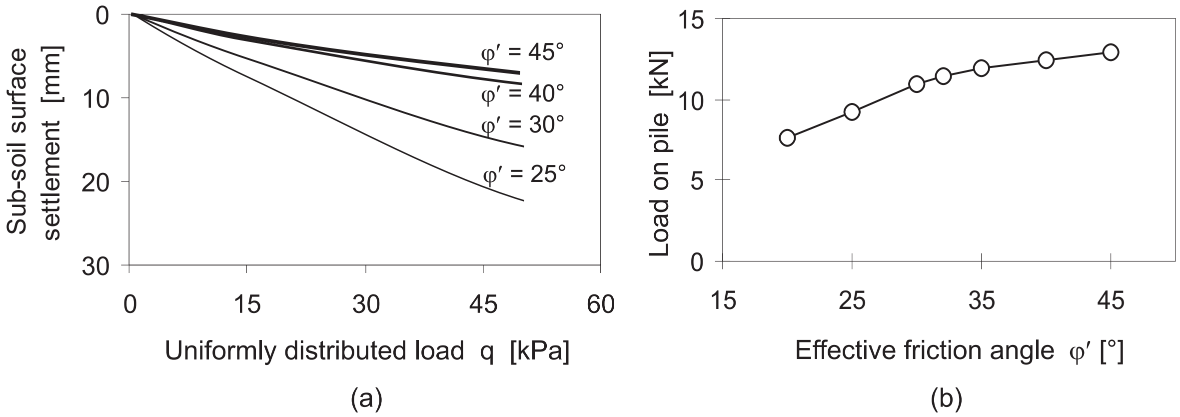

Figure 3.22: Influence of effective friction angle φ' (a) Sub-soil surface settlements at the centre of pile spacing (b) Load on pile after applying uniformly distributed load q of 50 kPa

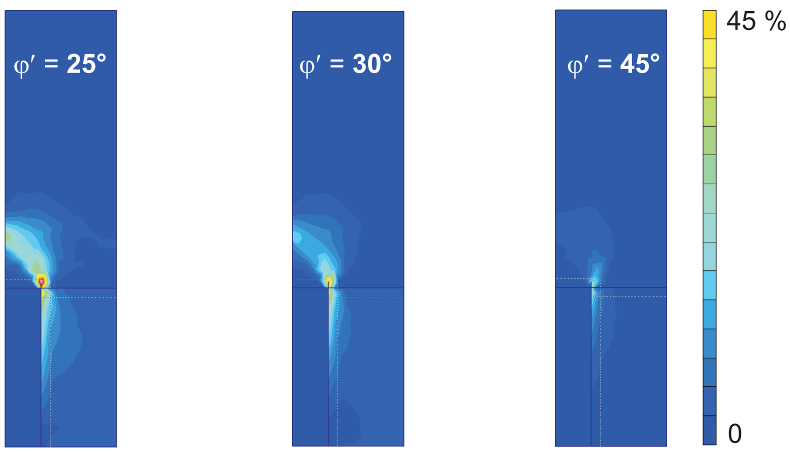

Figure 3.23: Total shear strain shading after applying uniformly distributed load q of 50 kPa

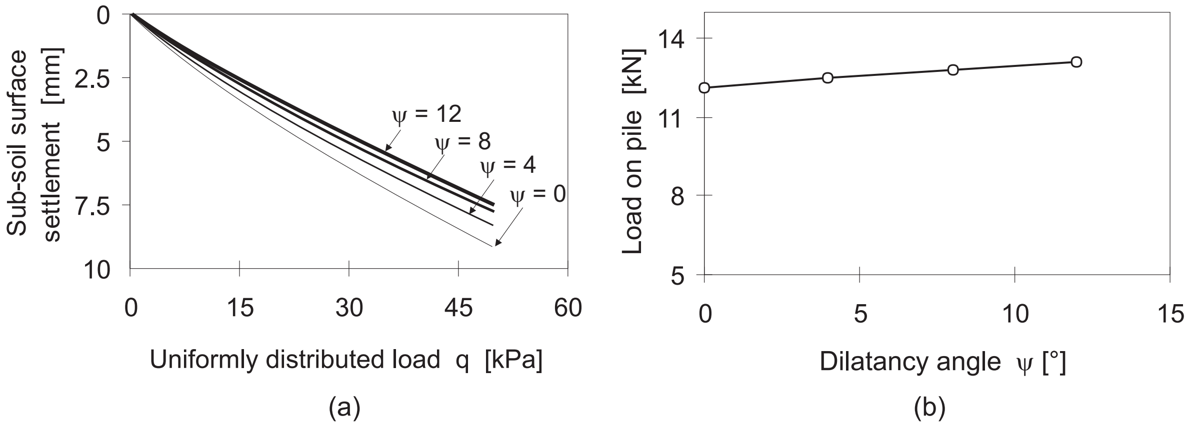

Figure 3.24: Influence of dilatancy angle ψ (a) Sub-soil surface settlements at the centre of pile spacing (b) Load on pile after applying uniformly distributed load q of 50 kPa

For an embankment with φ' lower than 33°, the increase of load on pile is relatively high with the increase of φ'. This increase is much less if the φ' is higher than 33°. Similar findings are also shown by Jenck et al. (2007) from small scale model tests. It is shown that the increase of load transfer is high as φ' increase up to 30°. Beyond that value, the increase of load transfer is less. In addition to that, a high effective friction angle reduce the possibility of punching as illustrated in Figure 3.23. Hence, numerical analyses results confirm the requirement of the embankment fill material with minimum effective friction angle of 30° as stated in the current design procedures described in Chapter 2.

The influence of the dilatancy angle ψ on piled embankment analysis results is much less significant. Figure 3.24a show the load-settlement variation due to variation of ψ. Moreover, its influence on the amount of load transfer is very small as depicted in Figure 3.24b.

Influence of stiffness parameters

Among the three stiffness parameters, the oedometer loading stiffness E_{oed}^{ref} is the only stiffness that shows a noticeable influence on the calculation results of piled embankment analyses. As illustrated in Figure 3.25a, the differential settlements at the sub-soil surface reduce as E_{oed}^{ref} increases. Similar tendency also shown for the settlements at the embankment surface. However, the variation of E_{oed}^{ref} does not seem to have much influence on the arching action, i.e. the load transferred to the pile as described in Figure 3.25b. Particularly for granular embankment with E_{oed}^{ref} larger than 30 MPa, which implies a medium dense soil, the influence of E_{oed}^{ref} on the settlement as well as load transfer is no longer significant. Hence, E_{oed}^{ref}, particularly with a value of lower than 30 MPa influences the settlement of the embankment.

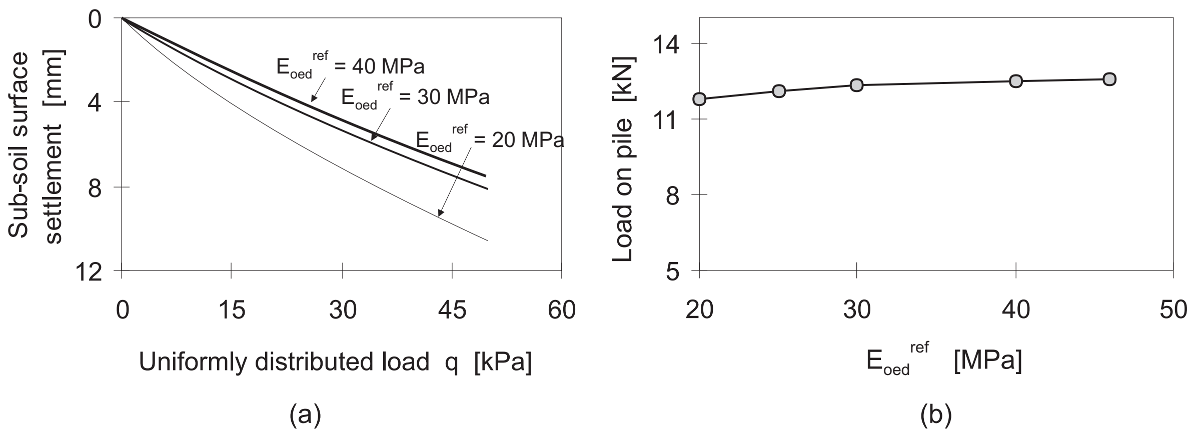

Figure 3.25: Influence of E_{oed}^{ref} (a) Sub-soil surface settlements at the centre of pile spacing (b) Load on pile after applying uniformly distributed load q of 50 kPa

Unlike E_{oed}^{ref}, the influence of E_{50}^{ref} and E_{ur}^{ref} are hardly noticed especially in this case where cyclical loading is not considered. Variation of those stiffness parameters lead to very little difference on embankment settlement as well as load transfer.

Influence of parameters m and ν_{ur}

The power law parameter m governs the stress level dependent stiffness of the soil. The typical value of m ranges between 0.5 to 1. For sand, m value of 0.5 is usually adopted whereas m value of 1 is generally considered for clay. The Lower m value implies the stiffer the soil. For granular embankment material, variation of m around 0.5 show only little influence on the embankment settlements and no considerable influence on the load on the pile is observed after applying uniformly distributed load q.

Observation on the variation of the unloading-reloading Poisson's ratio ν_{ur} shows that it has no influence at all on the calculated settlements as well as load on pile. It is worth mentioning that this is not the case when using the MC model where influence of Poisson's ratio is high. Figure 3.26 shows the influence Poisson's ratio on load-embankment surface settlement curves.

In conclusion, on using the HS model, parameter effective friction angle φ' and reference oedometer loading stiffness E_{oed}^{ref} are the most sensitive parameters for analyses of soil arching action around the middle of a piled embankment.

3.5 Conclusions on numerical analysis of soil arching

Research on numerical analysis of soil arching have been performed. The research findings clarify some of the uncertainties in soil arching analysis in piled embankments.

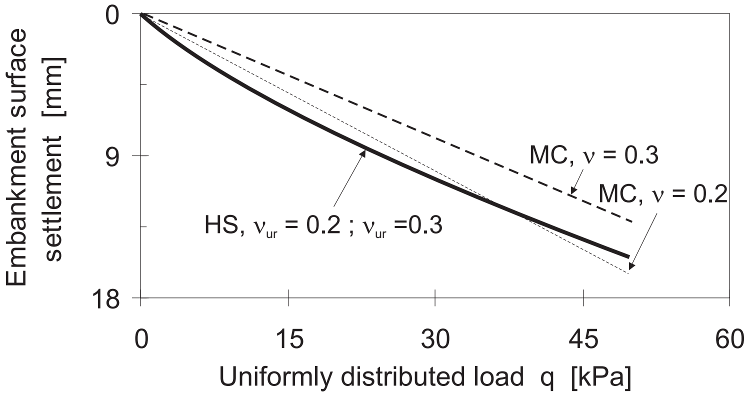

Figure 3.26: Influence of Poisson's ratio on embankment surface settlements

Moreover, the findings are considered as guides for numerical analysis and design criteria of soil arching in piled embankments.

Numerical analysis of soil aching in piled embankments can be done with different geometrical idealizations i.e. 3D geometry, axisymmetrical geometry and plane stain geometry. No doubt that the analysis is best performed using 3D geometry. However, this requires much computer power. Alternatively, the analysis can be done in axisymmetrical idealization which give equivalent results to the 3D analysis. Moreover, both results shows good agreements with measurement from a reference case study. In contrast, the analysis with plane strain geometry leads to soil arching instability in the form of punching failure. Hence, in this study, plane strain geometry is not applicable for soil arching analysis. In addition to that, it is shown that soil arching stability can be identified through plasticity conditions and shear strain at the soil stress points in the embankment.

The use of geotextile reinforcements improve embankment settlement and soil arching stability. One layer of strong geotextile is sufficient as piled embankment reinforcement. For the case where a conservative design by applying more than one layer of geotextile is needed, The geotextile layers should be placed within the lower half of the predicted arching height to ensure the effectiveness of the geotextile reinforcement. In general, the lower the geotextile is placed the more effective the reinforcement. Moreover, more than one geotextile layer placed within the specified height avoid punching failure.

In numerical analysis of soil arching, the use of advanced soil constitutive model such as the Hardening Soil model is recommended. It allows a more realistic choice of soil parameters, gives a better approximation of embankment settlement compared to reality and a clear identification of soil arching stability. On using the Hardening Soil models, it involves several soil parameters. However, not all of them have significant influence on the results of soil arching analysis. It has been shown that variations of effective friction angle φ' and oedometer loading stiffness E_{oed}^{ref} have significant influence on the calculation results. φ' has significant influence on load transfer from embankment to pile and embankment settlement, whereas E_{oed}^{ref}, particularly with lower value of less than 30 MPa, has only significant influence on the settlement of the embankment.

Numerical analysis results support the suggestion of using a minimum of 10 percent capping ratio with a strong geotextile reinforcement. When no geotextile is applied, a conservative consideration should be taken by using much larger capping ratio. This is because of high risk of soil arching collapse, which can lead to severe damage of the piled embankment.

Based on the evaluation of punching failure indications, the following criteria for the design of a piled embankment are recommended to ensure a stable arching mechanism:

- The embankment material has an effective friction angle $\varphi' \geq 30°$.
- The embankment height are larger than arching height. This can be well estimated using the criteria from the German method EBGEO 2004 that is $h_a = 0.7 \cdot s_d$, where s_d is the diagonal spacing of the piles.
- Pile capping ratio is larger than 10 percent.
- One strong geotextile reinforcement.

Chapter 4

Analysis of the effects of displacement piles installation

Different from piles for deep foundations of buildings, piles for soil improvement, e.g. for piled embankments, are characterized by their installation in a very dense grid with centre to centre spacing of not more than 3 m, generally. In addition, soil improvement piles have low load carrying capacity. The required load carrying capacity of the piles is typically less than about 300 kN. This implies that the piles used for soil improvement are often micropiles, i.e. a pile with diameter less than 30 cm. Many types of non-deformable columns can be considered as piles for soft soil improvement such as timber piles, prefabricated or cast-insitu concrete piles, deep mixing lime cement columns, as well as grouted stone columns. These types of piles are displacement piles.

Displacement piles are often used for the construction of piled embankments. A displacement pile is a pile that changes the stress fields in the soil around the pile due to its installation. Displacement piles can be distinguished between cast-in-place piles, precast piles and timber piles. In this analysis, the attention is focused on the effects of installation of cast-in-place displacement piles, such as lime-cement columns, tube-installed micropiles and screw micropiles (Van Impe, 1994). In addition to that, small diameter precast concrete pile and timber piles that are driven or jacked in soft soils are also considered. These types of piles are commonly used for piled embankments constructions. A proper analysis of a displacement pile leads to a good prediction of the pile capacity. Especially for floating piles, it is important to take into account the effects of installation process of displacement piles.

This chapter discusses the effects of displacement pile installation process and propose a reliable and repeatable calculation procedure to account for the effects of displacement pile installation using the standard finite element method. The calculation procedure requires a calibration on pile loading tests.

4.1 Effects of displacement piles installation

On the assessment of the effects of displacement piles installation, cast-in-place piles can be considered as full-displacement piles or partial-displacement piles and they induce

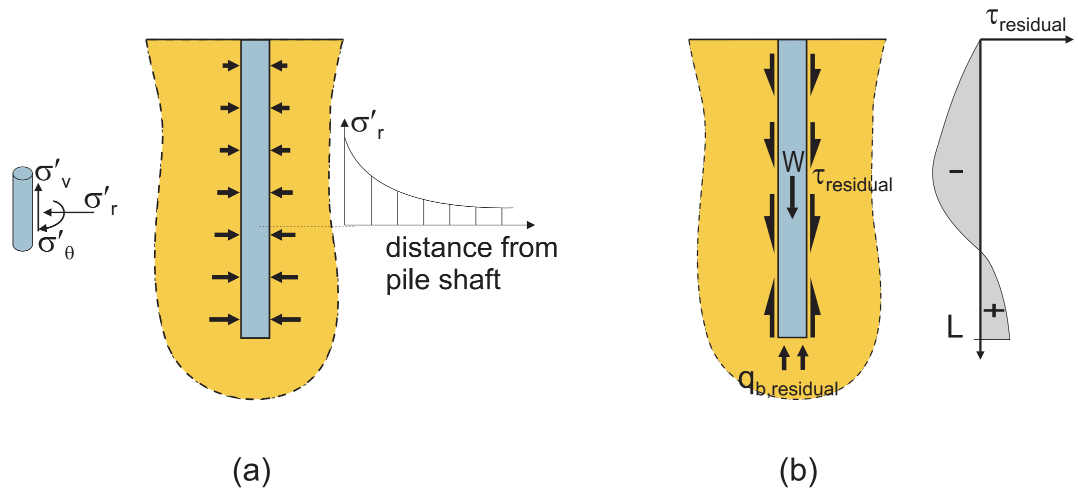

Figure 4.1: Stresses after displacement piles installation (a) Increased radial stress (b) Residual skin friction and pile-tip pressure for driven piles

an increase of the radial stress around the piles. Apart from that, precast-pile installation also creates residual shear stress along the pile shaft and an initial mobilization of the pile-tip resistance.

Radial stress increase

No doubt that the main effect of the installation process of displacement piles is the increase of the radial stress in the soil around the pile as result of displaced and compressed surrounding soil to accommodate the volume of the pile (Figure 4.1a). The prediction of radial stress increase that leads to the determination of limiting skin friction of the pile is extremely difficult. This is because the complexity of the nature and the soil-pile interaction from different type of piles with different installation procedures. When considering the prediction of limiting skin friction of a displacement pile, three main empirical approaches have been suggested and used in practice (e.g. Lancellotta, 1995). The approaches include the total stress approach, where the limiting skin friction is a function of the soil undrained shear strength c_u, the effective stress approach, where the limiting skin friction is a function of the effective radial stress σ'_r on the pile shaft and combination of total and effective stress approach. Although these approaches are used in practice, none of them is fully satisfactory and their application depend largely on field experiences.

The effective radial stress governs the contact friction between the pile and the surrounding soil. Hence, in the present analysis, effective stress approach is considered. Knowing that the frictional surface is vertical and friction failure is limited by Mohr-Coulomb failure criterion, one uses the expression (Chandler, 1968; Kulhawy, 1984)

$$\tau_s = \sigma'_r \cdot \tan\delta = K \cdot \sigma'_{v0} \cdot \tan\delta \qquad (4.1)$$

Table 4.1: Some measured and suggested value of K (after Said, 2006)

Type of pile	K-value (loose sand)	K-value (dense sand)	Reference
Steel pile	0.5	1	FOND. (1972)
Rough concrete pile	1	2	
Smooth concrete pile	0.5	1	
Conical wooden pile	1.5	4	
Jacked pile	1.5 (I_D< 20%)	3.8 (I_D > 70%)	Puech et al. (1979)
Driven pile	2 to 3 (I_D< 30%)	3 to 5 (I_D > 70%)	Eissautier (1986)
Bored pile	0.75 to 1.5 (I_D< 30%)	1 to 2 (I_D > 70%)	

where τ_s is the unit skin friction, K is the lateral earth pressure coefficient, which is defined as the ratio of the effective radial stress to the initial effective vertical stress σ'_r/σ'_{v0} and δ is the wall friction angle. Since the initial soil effective vertical stress σ'_{v0} and the wall friction angle δ can be determined relatively accurately, the most uncertainty lies in the determination of K-value, which describes the amount of radial stress increase. Some measured and suggested values of K for sand are listed in Table 4.1. The K-value depends on the relative density I_D[(1)] or the stiffness of the sand, the type of pile and the pile installation method. Burland (1973) uses Equation 4.2 to estimate unit skin friction τ_s.

$$\tau_s = \beta \cdot \sigma'_{v0m} \tag{4.2}$$

where σ'_{v0m} is the average initial effective vertical stress along the pile. He presented experimental data from pile load tests in soft clay, which show β-value in the range of 0.24 to 0.4. When considering an effective friction angle φ' of 20° for soft clay and assuming a rough pile, this gives K-value of 0.7 to 1.

On using the effective stress approach, for relatively homogeneous soil, the radial stress is assumed to increase linearly with depth. Beside this practice, there are several other methods to determine the radial stress increase such as based on CPT data (Jardine et al., 2006) or using analytical strain path method (Baligh, 1985).

Residual pile-tip pressure and skin friction

During the driving process of precast-piles, the shear stress along the pile skin as well as pile-tip resistance (force) are mobilized. Upon removal of the driving force, the pile will slightly rebound due to the elastic decompression of the pile as well as the unloading of

[1]The relative density is defined as $I_D = (n_{max} - n)/(n_{max} - n_{min})$, where n_{max}, n_{min} and n is the maximum, the minimum and the actual porosity of the soil

the soil around the pile-tip. The static condition of the pile is achieved after the weight of the pile, the residual mobilized skin resistance and the residual pile-tip resistance balance and reach equilibrium. Residual pile-tip pressure and skin friction may occur in significant amount after installation of a driven pile (Figure 4.1b). The importance of the residual resistances particularly for precast-pile driven in sand have been shown by several researchers (e.g. Briaud and Tucker, 1984; Alawneh and Malkawi, 2000). To estimate the residual pile-tip pressure $q_{b,residual}$, Briaud and Tucker (1984) suggest the following empirical relation

$$q_{b,residual} = 533.4 \cdot L \cdot \beta \quad with \quad \beta = \sqrt{\frac{K_\tau \cdot p}{A_b \cdot E_{pile}}} \quad and \quad K_\tau = 188.9 \cdot (N_{side})^{0.27} \tag{4.3}$$

where L is the pile length (in m), p is the perimeter of the pile (in cm), A_b is the cross-section of the pile (in m^2), E_{pile} is the elastic modulus of the pile (in kPa), N_{side} is the uncorrected average SPT blow-count within the pile shaft length considered and K_τ is initial friction modulus, which is determined in kPa/cm. Alternatively, one can also estimate the pile-tip pressure based on the flexibility of the pile η as suggested by Alawneh and Malkawi (2000)

$$q_{b,residual} = 13158 \cdot (\eta)^{0.724} \qquad with \qquad \eta = \left(\frac{L}{D}\right) \cdot \left(\frac{A_{shaft}}{A_b}\right) \cdot \left(\frac{G}{E_{pile}}\right) \tag{4.4}$$

where D is the diameter of the pile, A_{shaft} is the surface area of the pile side and G is the shear modulus of the soil.

For the determination of the residual skin friction, one may use the approximation method as suggested by Alawneh and Malkawi (2000). The other way is one can determine the average residual skin friction $\tau_{mean,residual}$ along pile shaft by evaluating the static vertical force equilibrium of the pile. Hence,

$$\tau_{mean,residual} = \frac{A \cdot q_{b,residual} - W_{pile}}{A_{shaft}} \tag{4.5}$$

where W_{pile} is the weight of the pile.

As can be seen for example in Equation 4.4, the residual pile-tip pressure is a function of the ratio of soil shear modulus and pile stiffness. Hence, when considering short and small diameter piles installed in soft soil for the embankments on floating piles , the influence of the residual stresses is not important. Furthermore, when using cast-in-place piles, the residual skin friction is almost zero and the pile-tip pressure is proportional to the weight of the pile.

4.2 Alternative methods for FE-simulation of radial stress increase around displacement piles

Upon penetration of a displacement pile, the soil is severely sheared. Hence, the soil experiences very large straining and drastic changes of stresses in the soil occur. To simulate a pile penetration properly, one needs an advanced numerical method, which takes into account very large strains. Chopra and Dargush (1992) wrote the following about such pile installation:

"Classical finite-element algorithms used in analysing the behaviour of soils assume that small strain occurs in the soils due to the applied loads. However, the assumption is no longer valid for problems involving the penetration of large scale cylindrical objects such as piles, into the soil. The excessive movement of the medium, particularly around the boundaries of the pile, during the embedment process causes substantial alterations in the geometry of the solution domain. As a result, strains are no longer linearly related to displacement gradients in such regions, and the equilibrium equations must be modified to take into account these changes in geometry. Of course, irreversible plastic deformation is also prevalent".

In addition to that, it might be added that dynamic effects due to pile driving or pile vibration also need to be taken into account. Moreover, such a large strain analysis needs a constitutive model that is capable to handle large deformation and density changes correctly. Large strain numerical analyses have been applied for pile penetration by researchers (Henke and Grabe, 2006; Mabsout et al., 1995; Wieckowsky, 2004). However, due to the lack of availability of the code for large strain numerical algorithm, the complexity of the analysis and excessive computational time-cost, large strain FE-analysis is from the point of view of practical engineers not yet popular.

No doubt that the major effect of a particular pile installation procedure is the resulting stress fields around the pile. Indeed, bored piles will hardly disturb the initial geostatic stress fields, but the installation of displacement piles creates an increase of the radial stress around the pile. One uses the expression of $\sigma'_r = K \cdot \sigma'_{v0}$ (e.g. Lancellotta, 1995). If direct empirical data on K is missing, its value can be back-analyzed from a pile loading test. Even in times of growing computer power and advanced numerical modelling, pile loading tests remain of utmost importance as even advanced numerical models need field calibration. Hence, it is not believed that numerical models will ever be suited for the analysis of pile foundation without field calibration.

On having field data on the K-value, it is no longer necessary to simulate the precise pile installation process. Instead, the back-analysed K-value can be used to initialise the appropriate stress fields around the pile. For that purpose, several alternative methods as illustrated in Figure 4.2 can be applied using standard FE-analysis as will be described next.

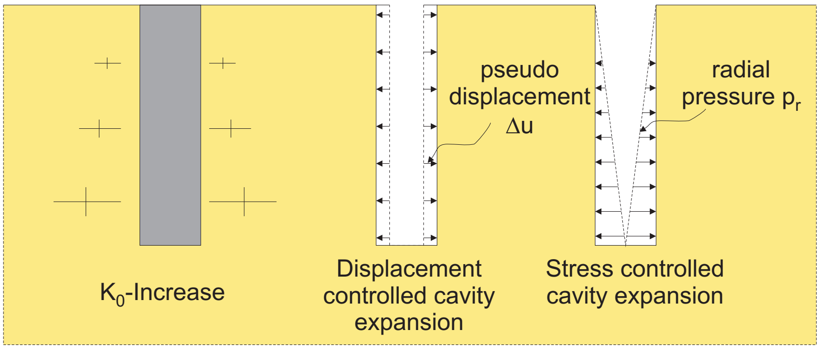

Figure 4.2: Alternative methods for simulating radial stress increase using standard FE-analysis

K_0-increase approach

The simplest procedure is to use the back-analysed K-value as a K_0-value, i.e. as a coefficient for the lateral earth pressure at rest all around the soil as for instance used by Russo (2004). On using this approach, it should be realized that radial stress is increased at the entire soil where the increase of K_0-value is applied. As a consequence, the shear strength of the soil is also mobilized for the entire soil. Moreover, not only the effective radial stress σ_r', but also the effective circumferential stress σ_θ' is increased at the same amount. Hence, the resulting stress fields do not represent a cavity expansion due to pile penetration.

Cylindrical cavity expansion approach

Considering cavity expansion, one has the option of using either a stress-controlled expansion or a displacement-controlled one. Pile penetration is a displacement-controlled problem. It is not possible to properly simulate the actual expansion of the cavity using the standard small strain FE-analysis. Hence, on using a displacement controlled cavity expansion, one has to find a suitable pseudo displacement that will give a best approach of the available measured load-settlement curve. On the other hand, one can use stress-controlled cavity expansion to initialize the radial stress increase by imposing radial pressure of p_r on the cavity wall. Upon using this method, it will be shown that realistic stress fields after pile installation and after pile loading simulation are obtained up to an appropriate K-value, which is in the range of practical experiences. This method is considered more sound and within the realm of engineering practice. Moreover, the method is fully suitable for the application with the standard small strain FE-analysis. In addition, one has the option of using various different constitutive models in the FE-simulation of a cylindrical cavity expansion.

The preferred stress-controlled cavity expansion method, which is named as *"K-Pressure"* method will be explained in details in the next section. In this thesis, the comparison of

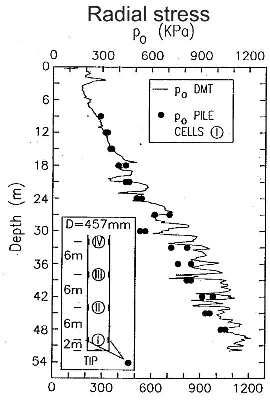

(a)

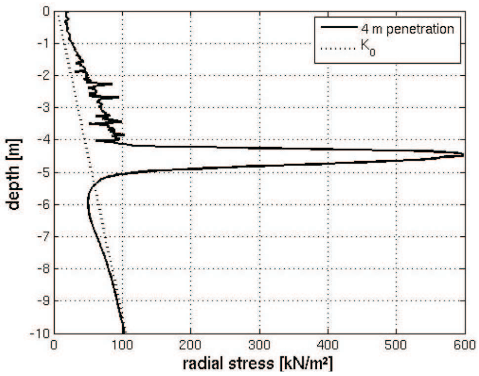

(b)

Figure 4.3: Linearly increase radial stress after pile installation (a) Total radial stress during pile installation (after Totani et al., 1994) (b) Effective radial stress from numerical analysis of a pile jacking of 4 m depth (after Henke and Grabe, 2006)

FE-analysis results with the alternative methods is not discussed in detail. However, it has been reported in Satibi et al. (2007).

4.3 K-Pressure Method

The increase of radial stress due to pile installation is a major concern in the analysis of a displacement pile. The increased effective radial stress is commonly expressed as $\sigma_r' = K \cdot \sigma_{v0}'$ in engineering practice. In literature, the K-value ranges between 0.5 to 5 depending on the density of the soil, the type of pile and its displacement magnitude (Lancellotta, 1995; Said, 2006). Upon using the K-Pressure method, the increase of radial stress due to pile installation is created by imposing radial stress with $p_r = K \cdot \sigma_{v0}'$ on the cavity wall. The K-value will be back-calculated from the measured load-settlement data from pile loading tests up to a reasonable value based on field experience. Thus, Pile loading tests are required. For homogeneous soil, the imposed radial stress is assumed to increase linearly with depth. An example of measured data on total radial stress due to pile driving presented by Totani et al. (1994) indicates that the radial stress can be assume to approximately increase linearly with depth especially at the first 20 m depth where the soil is homogeneous plastic clay layer (Figure 4.3a). Beside that, one of the research findings on numerical analyses of a jacked pile performed by Henke and Grabe (2006) also shows that the radial stress increases almost linearly with depth following a constant K-value after installation (Figure 4.3b). For a particular loose sand and a pile diameter of 30 cm, they obtained a K-value of 1.25. To show the detailed implementation of the K-Pressure method, a FE-analysis of a displacement pile loading test is presented in following sections.

4.3.1 Pile load test in Wijchen

Several small diameter piles (D = 18 cm) so called HSP piles with embedment depth of about 6.25 m have been installed in Wijchen, the Netherlands. The soil at the site consists of well packed fluvial layers of medium fine to coarse sand, which were deposited during the Pleistocene era (Vermeer and Schad, 2005). The soil is considered as medium dense to loose sand. The piles are installed by jacking a steel tube at constant speed, if necessary supported by vibration. Once the tube has reached the required depth, the tube is withdrawn and high slump concrete is pumped continuously into the cavity (Figure 4.4a). The tube withdrawal can only start when a predetermined minimum concrete pressure has been reached.

Due to the installation process, the radial stress around the pile increases. In addition to that, as the tube is withdrawn, high slump concrete is filled into the cavity. This leads to no residual skin friction between the pile and the soil. Furthermore, the residual pile-tip pressure can be assumed to be proportional to pile weight.

In order to determine the carrying capacity of the piles, several load tests have been performed. Figure 4.4b presents the data from the load-settlement measurements. In the figure, the whole measured data are plotted, which include the creep phases, where the initial and end settlements at maintained load steps are recorded.

4.3.2 FE-analysis of pile load test with K-Pressure method

The FE-analysis of pile load tests described in Section 4.3.1 is performed in axisymmetrical condition. Figure 4.5 shows the FE-mesh used for the analyses. Six-noded triangular elements with second-order interpolation function for the displacements and three Gaussian integration points are used. The mesh is refined along the shaft and at the bottom of the pile where the stress gradient is expected to be high. For the contact between pile and soil, three-pair-noded interface elements with three Newton-Cotes integration points are applied.

The advantage of using the interface elements has been shown by Wehnert and Vermeer (2004) that it reduces significantly the sensitivity of the load-settlement calculation results to mesh refinement. Moreover, on using the interface element, unrealistic high stress concentration around a sharp corner can be avoided (Van Langen and Vermeer, 1991). In addition to that, when considering a smooth prefabricated pile, the interface friction angle is lower than the soil friction angle and the interface cohesion should always close to zero to account for the remolded soil around the pile.

For the material constitutive behaviour, the Hardening Soil model is used for the soil and the interface behaviour follows the Mohr-Coulomb model[(2)]. The pile is considered as elastic with Young's modulus of 15 GPa and Poisson's ratio of zero. The unit weight of the pile is 23.5 kN/m^3. Table 4.2 shows the material parameters for soil and interface as used in the analyses. The subscript *in* denotes interface properties. As can be seen in

[2] A more detailed description on the MC-interface model can be found in Appendix B

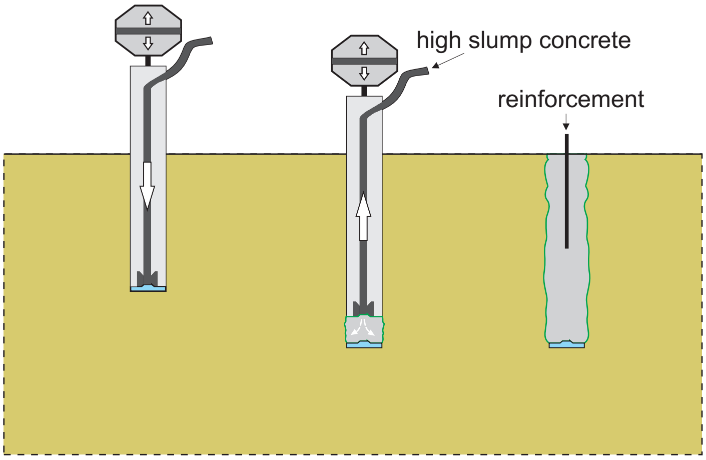

(a)

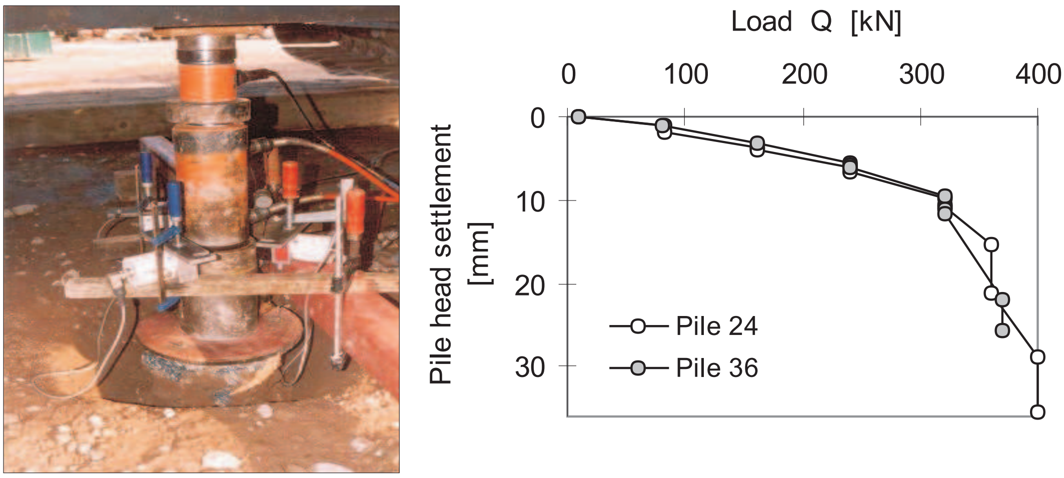

(b)

Figure 4.4: HSP-micropile (a) Installation process (b) Static load test

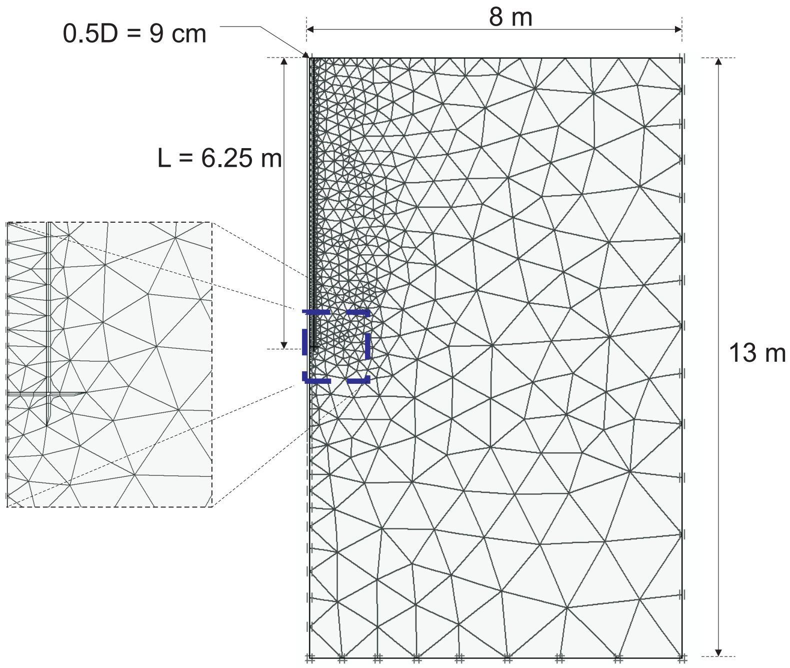

Figure 4.5: Geometry and FE-mesh for pile load test analyses

Table 4.2: Material properties as used for the FE-analysis of pile load test

Parameters		HS soil	MC interface
γ_{unsat}	[kN/m^3]	18	-
φ' / φ'_{in}	[°]	39	39
c' / c'_{in}	[kPa]	0.1	0.1
ψ / ψ_{in}	[°]	6	6
E_{50}^{ref}	[MPa]	17.5	-
E_{oed}^{ref}	[MPa]	17.5	-
$E_{ur}^{ref} / E_{in}^{ref}$	[MPa]	70	70
ν_{ur} / ν_{in}	[-]	0.2	0.45
m	[-]	0.5	-
t_{in}	[mm]	-	26
Tensile strength	[kPa]	0	0
Dilatancy cut-off	[-]	active	-

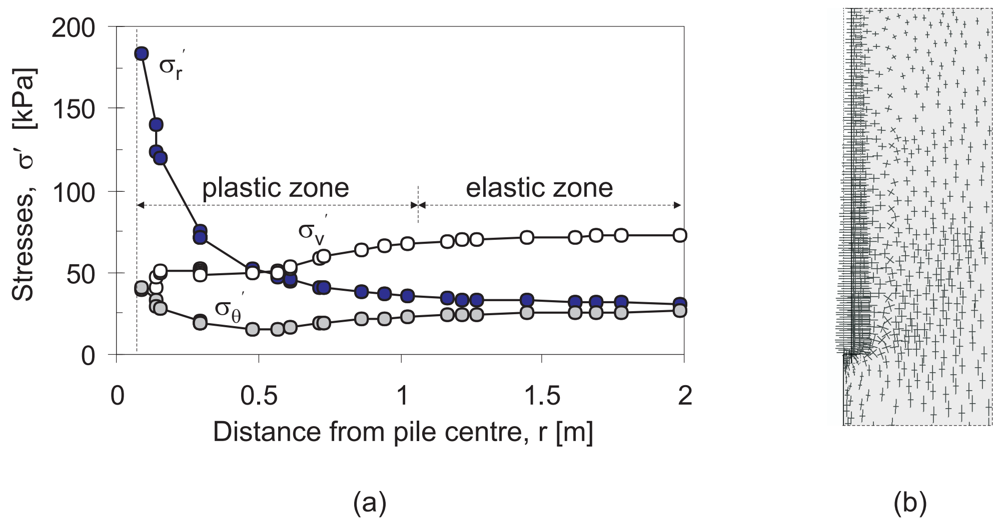

Figure 4.6: Stresses after imposing K-Pressure with K = 2.6 and using the HS model (a) Stress fields at at 4 m depth (b) Principal stresses around pile-tip

the table, the dilatancy cut-off is activated. This option is used to limit the dilation of the soil. Detailed discussion on the use of dilatancy cut-off is presented in Section 4.3.2.3.

The initial in-situ soil condition is geostatic stress state with initial effective vertical stress of $\sigma'_{v0} = \gamma_{unsat} \cdot z$, where γ_{unsat} is the moist unit weight of the soil and z is the depth below the ground surface. For the corresponding horizontal stress, it yields $\sigma'_h = K_0 \cdot \sigma'_{v0}$. The K_0-value is taken according to the Jaky's formula $K_0 = 1 - \sin\varphi'$ for normally consolidated soil. For φ' = 39°, this gives K_0 = 0.371. The ground water table is far below the surface; hence the water table is set at the bottom side of the mesh. As for the boundary condition, horizontal displacement is prevented everywhere. In addition, vertical displacements are prevented at the bottom of the mesh as shown in Figure 4.5.

4.3.2.1 Pile installation with K-Pressure method

The increase of effective radial stress due to pile installation process is simulated using stress-controlled expansion of a cylindrical cavity. This process can be described as follows: First, in-situ soil conditions are set as described previously. After that, elements are removed to create a cavity along the centre-line and subsequently a radial pressure is imposed to the cavity wall. This radial pressure increases with depth according to $p_r = K \cdot \sigma'_{v0}$, where K is taken to be 2.6 for the present calculation. This value is obtained from back-calculation of measured load-settlement curves. In addition to the imposed radial pressure, at the bottom of the cavity, a vertical stress of $\sigma'_v = \gamma_{unsat} \cdot L$ is applied, where L is the pile embedment length. After imposing the radial pressure, the pile material is placed into the cavity. At the same time, the radial pressure as well as the vertical stress at the bottom of the cavity are removed.

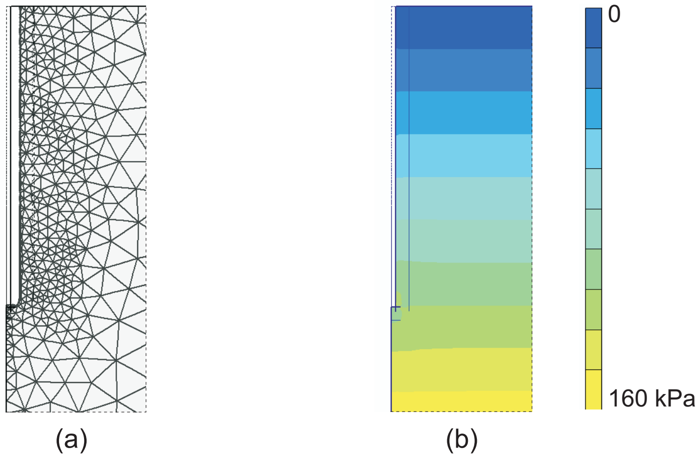

Figure 4.7: Elastic cavity expansion after imposing K-Pressure with $K = 2.6$ (a) Deformed mesh (scaled to 20 times) (b) Vertical stress shading

In the above process, the Hardening Soil model can directly be applied. However, on using the Hardening Soil model, the cavity expansion is significantly non-uniform. Moreover, the resulting effective vertical stress in the soil decreases significantly in the plastic zone around the cavity, as shown in Figure 4.6a. The decrease of the vertical stress is initiated from the tension and distortion of stresses at around the corner of the pile-tip due to cavity expansion, which rotates the principal stresses around the pile (Figure 4.6b). When considering the installation of the pile where the tube is jacked into the soil and then withdrawn again as the concrete is filled, it is hardly believed that the decrease of the vertical stress is realistic.

Stress-controlled cavity expansion using elasticity

In order to minimize a disturbance of the vertical stress, an additional procedure is applied. The cavity expansion is first done in elastic material, where the vertical stress remains constant during the expansion. the soil stiffness is assumed to increase linearly with depth. This gives a reasonably uniform cavity expansion as can be seen in Figure 4.7a. As the FE-code used for the analysis does not allow an input of zero stiffness. An arbitrary small value of $1 \cdot 10^{-8}$ kPa is applied as Young's modulus at the surface ($E_{surface}$). The Young's modulus of the elastic material increases with an arbitrary amount of 5000 kPa per meter depth. The Poisson's ratio ν of the material is zero, which is chosen aiming to have no vertical deformation during the cavity expansion.

The results of the FE-analysis show a perfectly constant vertical stress even in the region close to the cavity as shown in Figure 4.7b. As for the evolution of vertical, radial and circumferential stress with distance from the centre-line, these are indicated in Figure 4.8. For the cylindrical cavity expansion in elasticity, the analytical solutions for stress

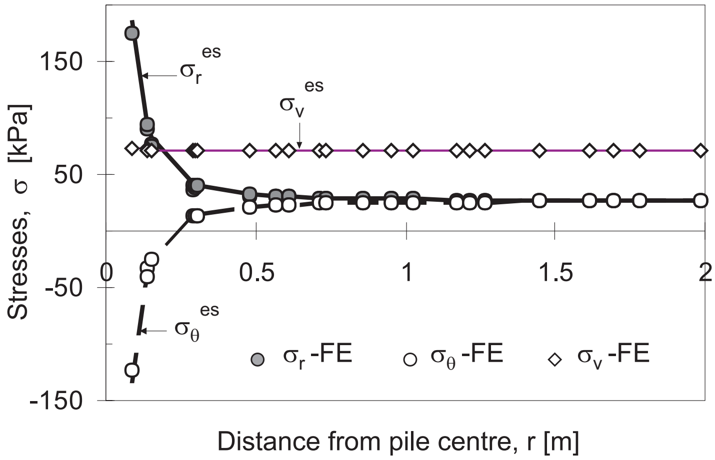

Figure 4.8: Stresses at 4 m depth after elastic cavity expansion using K-Pressure with K=2.6

fields can be obtained as the following equations (Vesic, 1972)

$$\sigma_r^{es} = \sigma_{r0} + (p_r - \sigma_{r0})\,\frac{r^2}{R^2} \qquad and \qquad \sigma_\theta^{es} = \sigma_{\theta 0} - (p_r - \sigma_{\theta 0})\,\frac{r^2}{R^2} \tag{4.6}$$

where σ_r^{es} and σ_θ^{es} are the radial and circumferential stress from elastic solution, σ_{r0} and $\sigma_{\theta 0}$ are the initial radial and circumferential stress in the elastic material. p_r is the radial pressure imposed on the cavity wall, r is the radius of the cylindrical cavity and R is the distance to the cavity centre. As shown in Figure 4.8, the calculated radial stress and circumferential stress have good agreements with the results from elastic solution, which shows that the results of FE-calculations are valid.

Returning stresses to Mohr-Coulomb yield surface

On using an elastic constitutive model, the stresses due to K-Pressure will be violating the Mohr-Coulomb failure criterion. This will give problems later when the elastic constitutive model for the soil is replaced by the Hardening Soil model. Therefore, the stresses that violate the Mohr-Coulomb failure criterion are mapped back to the Mohr-Coulomb failure line. For that purpose, the elasticity model is replaced with elasto-plastic Mohr-Coulomb model with increasing stiffness with depth. The material properties for the Mohr-Coulomb model are presented in Table 3.1. After applying the Mohr-Coulomb model, the decrease of effective vertical stress still occurs. However, it is less pronounced than using directly the Hardening Soil model. The installation process is therefore best simulated by imposing the radial K-Pressure on an elastic soil and subsequently replacing it with Mohr-Coulomb (MC) material. On using this procedure

Table 4.3: Mohr-Coulomb soil parameters for installation simulation

Parameters		Value
γ_{unsat}	[kN/m^3]	18
$^{dE}/_{dz}$	[kN/m^2/m]	5000
$E_{surface}$	[kPa]	$1{\cdot}10^{-8}$
c'	[kPa]	0.1
φ'	[°]	39
ψ	[°]	0
ν	[-]	0
Tensile strength	[kPa]	0

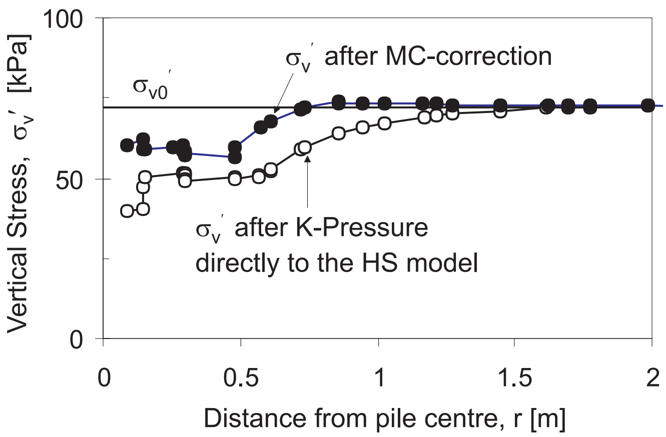

Figure 4.9: Vertical stresses at 4 m depth after K-Pressure with K = 2.6 for different soil models

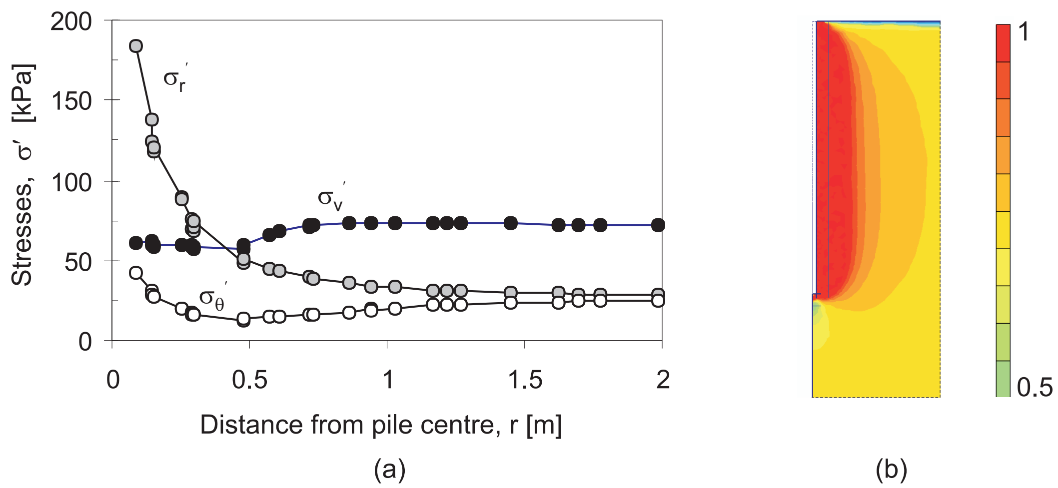

Figure 4.10: Stresses and mobilised shear strength after MC-correction (a) Stresses at 4 m depth (b) Mobilized shear strength

only a small disturbance of effective vertical stress around a distance of 0.7 m from the centre-line is observed as shown in Figure 4.9.

Figures 4.10a shows the stresses at 4 m depth after elastic cavity expansion and MC-correction. The disturbance of the effective vertical stress is much less pronounced. The effective radial and circumferential stresses at 4 m depth appear to be almost the same to the ones obtained from K-Pressure with directly using the HS model (Figure 4.6). From Figure 4.10b, it is shown that the soil shear strength is almost fully mobilized up to a distance of about 0.7 m or about 3.9 pile diameter from the centre of axisymmetry due to cavity expansion. Mobilized shear strength is the ratio of the actual shear stress, i.e. the radius of the Mohr stress circle to the maximum value of shear stress for the case where Mohr's circle is expanded to touch the Coulomb failure envelope keeping the intermediate principal stress constant. Thus, mobilized shear strength indicate the proximity of stress point to the failure envelope.

The principal stresses along the pile shaft shown in Figure 4.11a and b are not rotated, showing that there is no shear at the pile shaft. This is in agreement with the fact that there is no shear stress occurs as the tube is withdrawn and the pile material is placed into the cavity. This case is different if the pile is driven. The installation process using elastic material and corrected by Mohr-Coulomb computation forms a reasonably uniform horizontal displacement along the pile cavity as aimed (Figure 4.11c and d). After elastic cavity expansion followed by MC-correction, the pile material is then placed into the cavity and the soil elements are switched from the MC model to the Hardening Soil model. Furthermore, the displacements are set back to zero since it is aimed to initialize the stress fields after pile installation and not modelling the displacement. On removing the imposed K-Pressure, the pile will be loaded by the soil and this leads to some compression of the pile and a slight reduce of the K-Pressure. However, because the stiffness

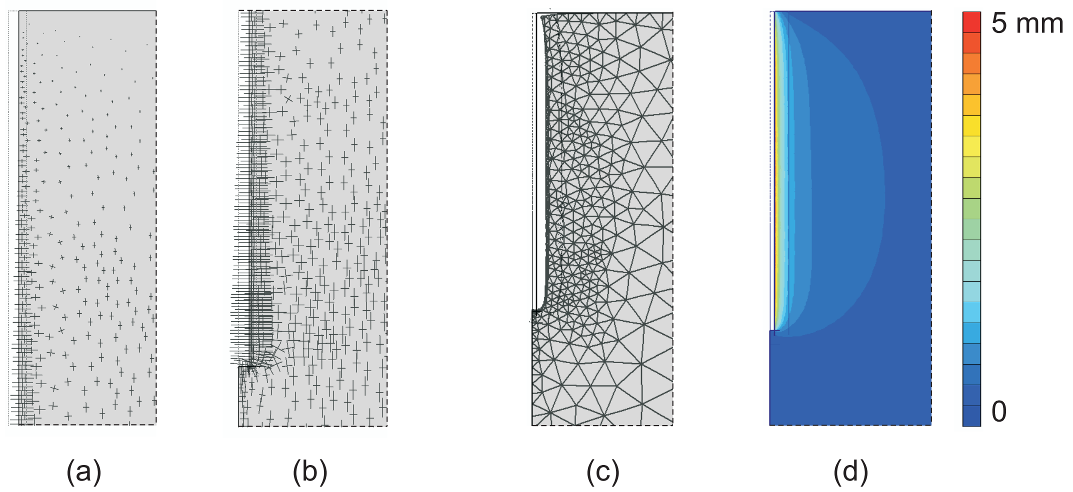

Figure 4.11: Principal stresses and deformation outputs after MC-correction (a) Principal stress around pile top (b) Principal stresses around pile tip (c) Deformed mesh (scaled to 50 times) (d) Horizontal displacement shading

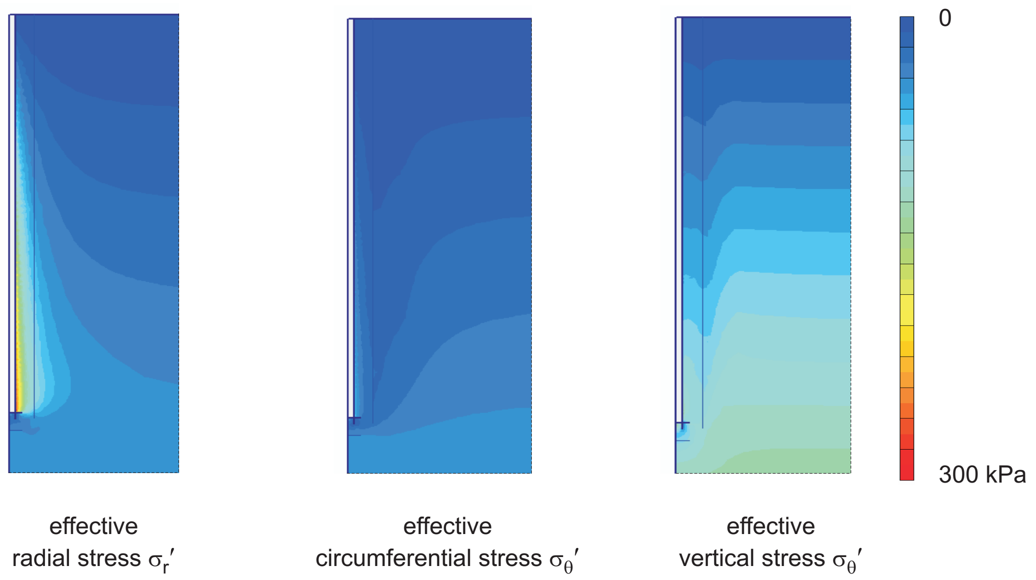

Figure 4.12: Stress fields after MC-correction

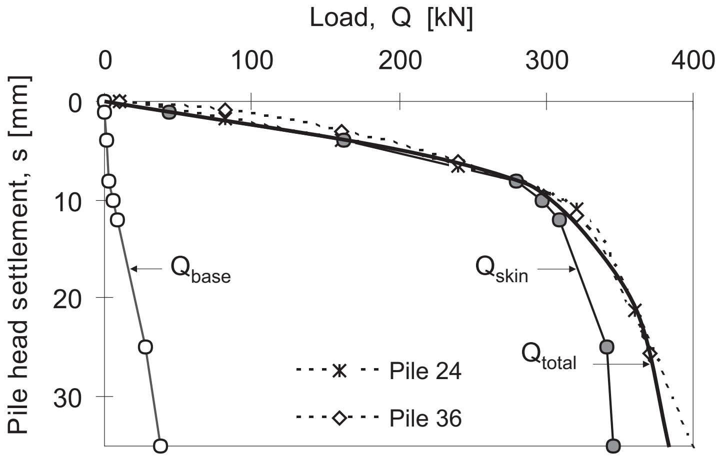

Figure 4.13: Calculated and measured load-settlement curve (K= 2.6)

of the pile is high, the reduction of the K-Pressure is observed to be very small; it reduces from K = 2.6 down to K = 2.59. The resulting stress fields after replacing with the Hardening Soil model appear to be almost the same as the ones from MC-correction as illustrated in Figure 4.12.

4.3.2.2 Pile loading after K-Pressure method

After pile installation process and set displacement back to zero, the loading is performed using displacement control. The displacement is prescribed at the pile head. According to the measured data, the pile loading is stopped when the pile head settlement reaches about 20 percent of the pile diameter. Based on this, the prescribed pile head settlement is taken as 35 mm. The soil model used in this pile loading process is the Hardening Soil model. Figure 4.13 shows the calculated load-settlements curve. It is in good agreement with the measured ones, which is not a surprise as the K-value and some soil parameters used are based on a preliminary back-calculations of the load-settlement curves of the pile load tests. It should be mentioned that in the figure, the measured data are plotted without including the data from the creep phases, which is commonly done for plotting load-settlements curve. Apart from the load-settlement curve, it is also important to see the resistance components of the pile, which are the skin resistance and the pile-tip resistance. As can be seen in Figure 4.13, up to a load of 280 kN almost all of the load is taken by the skin resistance and at a pile head settlement s of 35 mm the load is still mainly taken by the skin resistance (about 90 percent). A pile with this type of behaviour is generally known as *skin friction* pile.

Figure 4.14a shows the deformed mesh after pile loading up to s = 35 mm. It can be seen that along the pile-soil interface, the nodes of pile elements and the nodes of soil elements are not in the same position showing that some slip along the interface occurs. Moreover, the soil elements next to the interface are significantly distorted due to shear

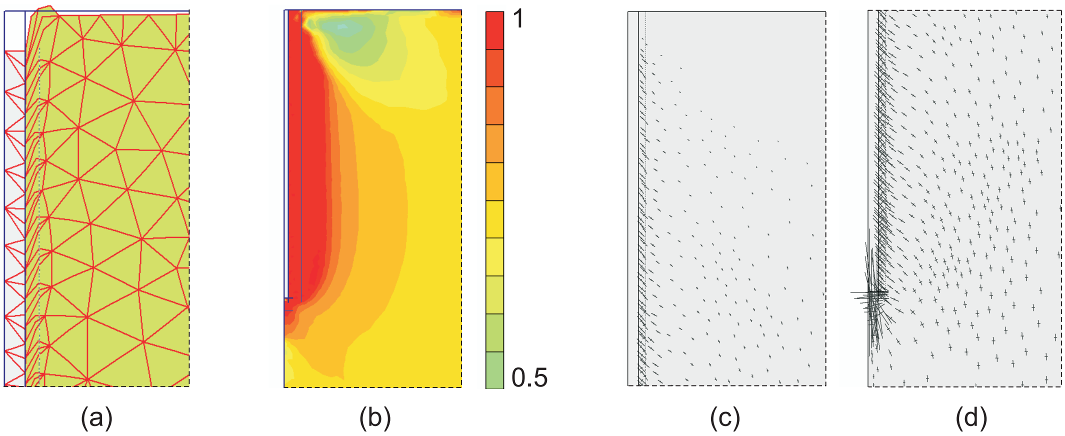

Figure 4.14: Calculation outputs after pile loading at pile head settlement s of 35 mm (a) Deformed mesh (scaled to 5 times) (b) Mobilized shear strength (c) Principal stresses around pile-top (d) Principal stresses around pile-tip.

deformation in the soil. The plot of mobilised shear strength contours of the soil at 35 mm pile head settlement as shown in Figure 4.14b is slightly different from the ones after installation process (Figure 4.10b). The area where the soil shear strength is almost fully mobilized, moves slightly downward. Figure 4.14c and d show the rotated principal stresses around pile-top and around pile-tip due to mobilized shear resistance in the soil after pile loading up to s = 35 mm.

Figure 4.15 show the calculation results of interface shear and radial stresses along the pile shaft. The distribution of shear stress in the interface have a curved shape which is in agreement with the shape of skin friction distribution, as first published by O'Neil and Reese (1972) and Vesic (1970). The smooth curves of the shear and radial stresses as shown in Figure 4.15 represent polynomial functions that give a least square fit to the zigzagging computed stress distributions. The polynomial functions used in this case are of fourth order. The zigzagging stress distribution is the result of numerical integration in the interface elements after intensive shearing when no smoothing is applied. Thus, the polynomial curves represent a smoothing of the interface stress distribution.

As for the ultimate skin resistance of a pile Q_{skin}, it is calculated according to the formula

$$Q_{skin} = \pi \cdot D \cdot \tan \delta_w \cdot \int_0^L \sigma'_r \, dz = \pi \cdot D \cdot \tan \delta_w \cdot \int_0^L K \cdot \sigma'_{v0} \, dz \tag{4.7}$$

where D is pile diameter and δ_w is wall or pile-soil interface friction angle. In practice K is often assumed to be constant with depth, although Figure 4.15 shows that this is not the case. For such situation, it is possible to introduce an average K-value. It can be back calculated as follows:

$$K_{average} = \frac{\int_0^L \sigma'_r \, dz}{\int_0^L \sigma'_{v0} \, dz} \tag{4.8}$$

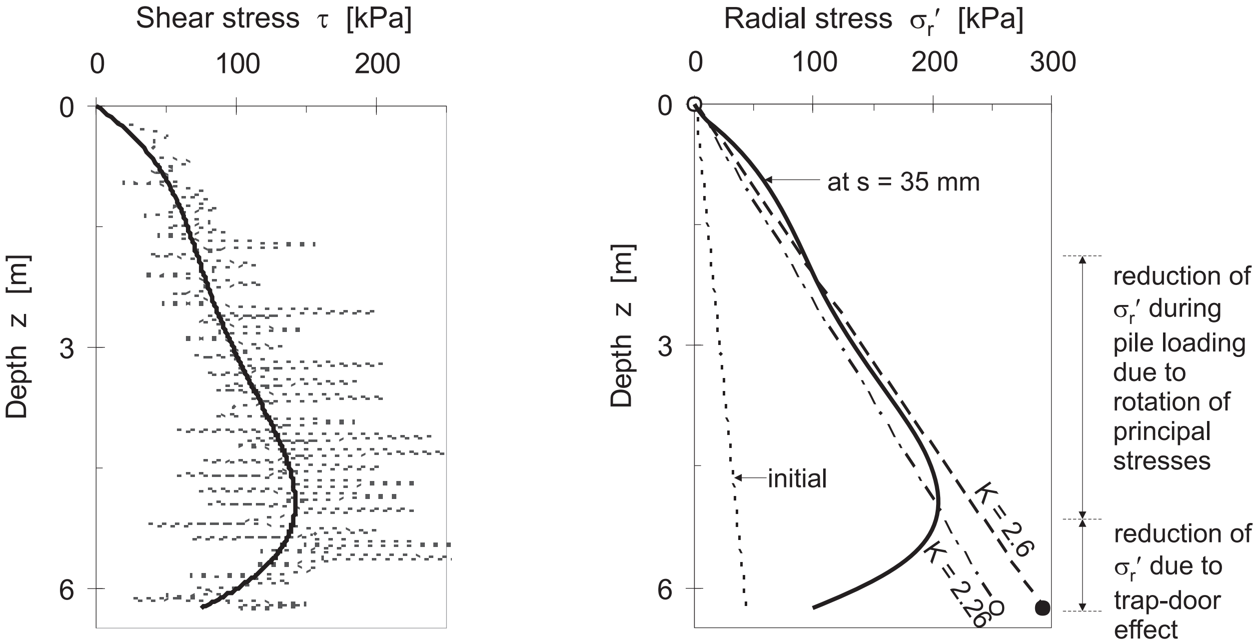

Figure 4.15: Interface stresses at 35 mm pile head settlement

The integral of the radial stress can be obtained by numerical integration whereas the integral of initial vertical stresses can be evaluated analytically to give $0.5 \cdot \gamma_{unsat} \cdot L^2$. In this analysis $K_{average}$ at the end of loading is found to be 2.26. Hence, K drops from K = 2.6 after installation down to $K_{average}$ = 2.26 for a pile head settlement of s = 35 mm. The significant reduction of the radial stresses at around the bottom of the pile is caused by the so-called trap-door effect. Terzaghi (1936) explained this effect with his experiment on a sand box with a trap-door at the base of the box (Figure 4.16a). As long as the downward movement of the trap-door remains very small, it merely produces a vertical expansion of the lower part of the body of sand located above the trap-door. As a result of this deformation, the sand located on both side of this body is allowed to expand laterally, thus reducing the lateral stress in this area. A similar effect also occurs to the pile loading as first introduced by Vesic (1963) and Touma and Reese (1974). The pile base settlement drags down the soil at the side of the pile. The vertical stretching of soil at the pile side just above the pile-tip causes the reduction of effective vertical stress. The effective radial stress also reduces as this soil is in a failure state with Mohr-stress circle moving to the apex. The soil below the pile-tip displaces to the side of the pile, which then forms a kind of arching effect around the pile-tip as described in Figure 4.16b. In addition to that, the reduction is also induced by the rotation of principal stresses due to the developed shear stress (skin friction) along the pile shaft. This reduction of radial stress is particularly shown at around the middle part of the pile as depicted in Figure 4.15.

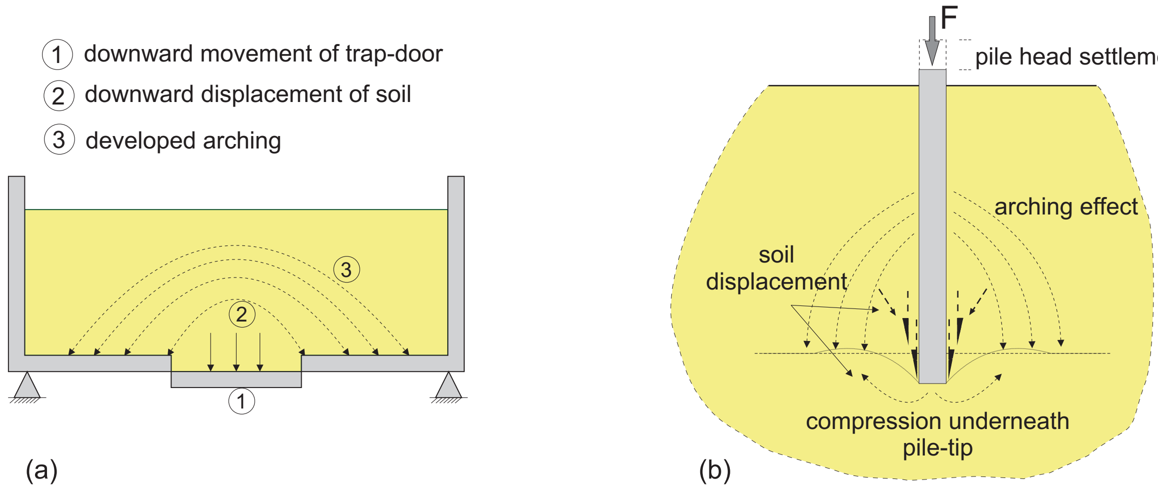

Figure 4.16: Description of trap-door effect (a) Terzaghi sand box (b) Pile loading

4.3.2.3 Parametric study

K-Pressure method involves back-calculation of measured load-settlement curves as a basis for initializing stress fields due to pile installation. Therefore, several trial calculated load-settlement curves need to be made. The resulting calculated load-settlement curves depend on the applied K-value and the soil properties. Some soil properties such as strength properties are known relatively accurately. Hence, they are not variables. Other parameters, for example the soil stiffness parameters, may need to be first assumed from a reliable correlation. While back calculating the measured load-settlement curves, they are then adjusted to achieve a best fit calculated load-settlement curve. Several calculations have been performed to show a general picture of the influence and the significance of the soil parameters as well as the used K-value on load-settlement curves.

Influence of dilatancy cut-off in interface

Since the K-pressure was performed in a pile load test analysis in a drained sand, the use of dilatancy cut-off to limit the dilation of the shear zone, i.e. the interface between the pile and the sand needs to be accounted for. This is however not necessary when considering pile installation in soft soil. The use of dilatancy cut-off for the present pile loading test analysis is described next.

After extensive shearing, dilating materials in the shear zone arrive in a state of critical density where dilatancy has become fully mobilized. Upon reaching this state, no further dilation occur. This behaviour is taken into account in the Hardening Soil model by means of *dilatancy cut-off*. Dilatancy cut off option in interfaces is available in combination with the Hardening Soil model where mobilized dilatancy with respects to the change in interface void ratio is accounted for (Brinkgreve, 2002). In order to specify the

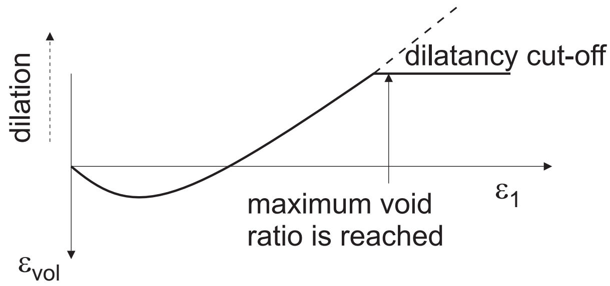

Figure 4.17: Strain curve for a standard drained triaxial test including dilatancy cut-off

behaviour, the initial void e_0, the minimum void ratio e_{min}, and the maximum void ratio e_{max}, of the material are required. As soon as the volume change results in a state of maximum void, the mobilized dilatancy angle ψ_m, is automatically set back to zero, as indicated in Figure 4.17. The limitation of the dilatancy follows the criteria

$$\sin\psi_m = \frac{\sin\varphi_m - \sin\varphi_{cv}}{1-\sin\varphi_m\cdot\sin\varphi_{cv}} \quad for \quad e < e_{max}$$

$$\sin\psi_m = 0 \qquad for \quad e = e_{max} \tag{4.9}$$

where φ_m is the mobilized friction angle and φ_{cv} is friction angle at critical state or at large strain. On using the logarithmic strain measure, the void ratio is related to the volumetric strain ε_{vol} by the relationship

$$\varepsilon_{vol} = -\ln\frac{1+e}{1+e_0} = -\ln\left(1+\frac{\Delta e}{1+e_0}\right) \tag{4.10}$$

with compression is considered as positive. For small strains, it yields $\Delta e/\left(1+e_0\right) < 0.1$ and one obtains the usual small strain definition

$$\varepsilon_{vol} \approx \frac{-\Delta e}{1+e_0} \tag{4.11}$$

The pile considered in this study has a very rough interface with the surrounding soils. This implies the occurrence of a more or less usual shear band around the pile. Soil shear bands have a thickness of about 10 to 12 times d_{50}, where d_{50} is the average grain size of the soil. Unfortunately, no grain size distribution is available. However, for a medium fine to coarse sand, it can be assumed that the d_{50} is around 0.4 mm. Thus, the shear band thickness is found to be about 4 mm. It is further assumed that the void ratios of the sand are as follows:

$$e_0 = 0.65\,; \quad e_{min} = 0.4\,; \quad e_{max} = 0.9$$

This sand can therefore dilate no more than $\Delta e_{max} = 0.9 - 0.65 = 0.25$. For a shear band, this implies that it can have maximum volumetric strain $\Delta\varepsilon_{vol}^{max} = -\Delta e_{max}/(1+e_0) = 0.15$. Since the shear band thickness is t = 4 mm, it gives $\Delta t_{max} = t\cdot\varepsilon_{vol}^{max} = 0.6$ mm.

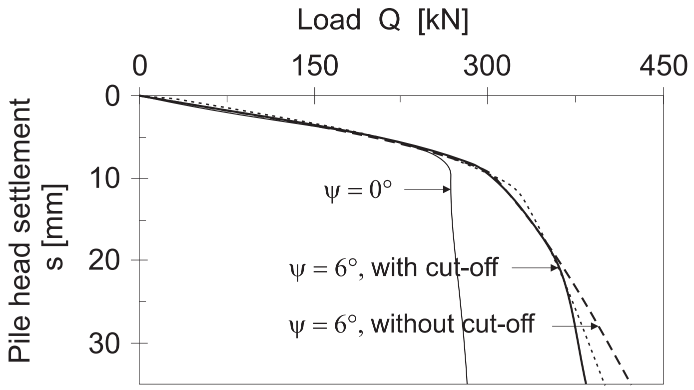

Figure 4.18: Effect of dilatancy cut-off on load-settlement curves

The FE-mesh being used involves an interface thickness of t_{in} = 26 mm, which is beyond the real shear band thickness of 4 mm. Hence, a numerical scaling should be applied to obtain an equal amount of dilation. This thick FE-interface may therefore dilate up to Δt_{in}^{max} = 0.6 mm. In order to achieve that, the volumetric interface strain has to be restricted to a low value of $\varepsilon_{vol}^{max} = \Delta t_{in}^{max}/t_{in}$ = 0.6 mm / 26 mm = 0.023. Based on the maximum volumetric strain, the void ratio of the interface may increase up to Δe_{max} = 0.034. This implies that the maximum void ratio of the interface should be $e_{max} = e_0 + \Delta e_{max}$ = 0.684 $\approx$ 0.7. Thus, to realize the dilatancy cut-off the following input of void ratios of $e_0 = 0.65$, $e_{min} = 0.4$, and $e_{max} = 0.7$ are applied to the Hardening soil model.

Figure 4.18 shows the load-settlement curves for the case of dilatancy zero, dilatancy 6° with the dilatancy cut-off and dilatancy 6° without dilatancy cut-off option. The Load-settlement curve from soil without dilatancy drops suddenly after a load of 280 kN, which implies that the skin friction has been fully mobilized. The very small increase of load with settlement after the sudden drop is due to some increase of pile-tip resistance. It can be seen from the figure that when the soil has dilatancy and the dilatancy cut-off is applied, the load-settlement curve show two times drops. The first drop happens suddenly at the load of about 300 kPa showing that the skin friction is fully mobilized. After that, the curve show some increase due to dilatancy and pile-tip resistance. At a load of 360 kPa, the curve drops again, which indicates that dilation is cut off. In the case of without dilatancy cut-off, there is no second drop showing that the soil continues to dilate. Hence, dilatancy cut-off has an important role in pile loading analysis in dilating soil.

Influence of K-value for the K-pressure

In the K-Pressure method, a reasonable predicted value of K in the back-calculation process of the measured load-settlement curves is important to ensure that a realistic stress fields are obtained. Figure 4.19 illustrates the influence of varying K-value to the calcu-

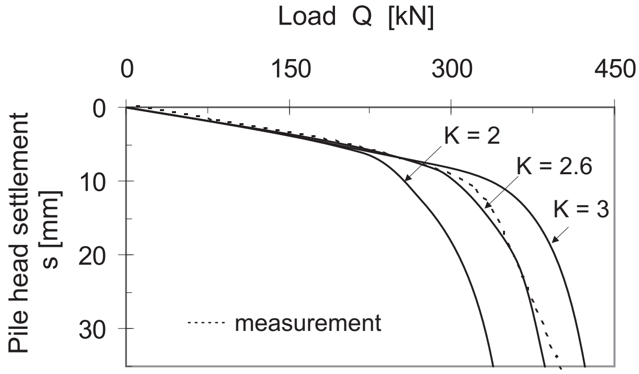

Figure 4.19: Influence of *K*-value on the load-settlement curves

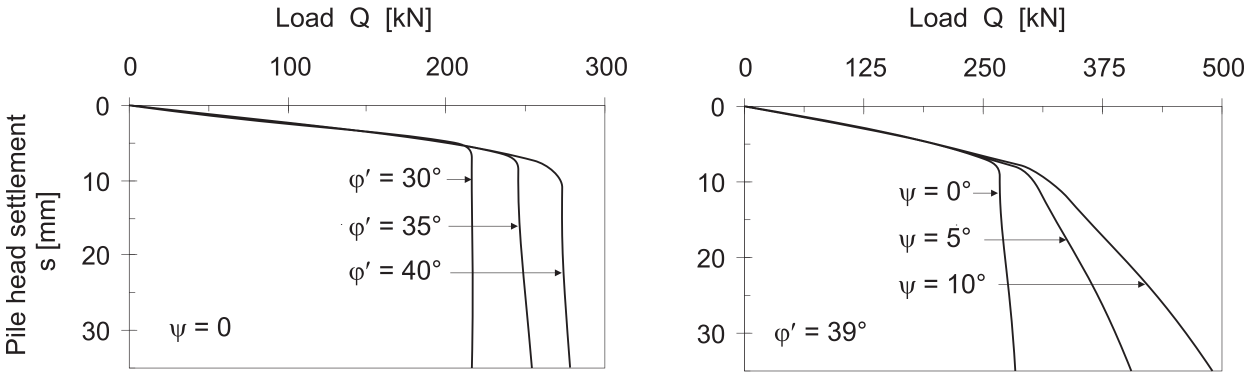

Figure 4.20: Influence of strength parameters on load-settlement curves

lated load-settlement curves. In general, each curve has two significant different slopes. The first part of the curve has low steepness and it is called elastic response part. The rest part of the curve that show large steepness is named as plastic response part. It is obvious that the larger the *K*- value, the longer the elastic response part of the curve. The slopes of all curves remain unchanged due to variation of *K*-value.

Influence of strength parameters

Since cohesion is approximately zero around the pile to account for remolding of soil during the pile penetration, the behaviour of load-settlement curves are focused on the variation of effective friction angle φ' and dilatancy angle ψ. Figure 4.20 left describes the influence of φ' on the load-settlement curves. It is shown that the larger the soil effective friction angle the longer the elastic response part of the curves. On the other hand, as shown in Figure 4.20 right, the amount of dilatancy in the soil determine the slope of the plastic response part of the curve. Dilatancy angle ψ shows only marginal influence on the elastic response part of the curve.

Influence of stiffness parameters as used in the Hardening Soil model

In many soil laboratory test reports, it is rarely found that the stiffness parameters are available especially for the stiffness parameters as used in the Hardening Soil model. Nevertheless, as first assumptions, one can use the values from reliable correlations such as given by Vermeer et al. (1999).

Upon calibrating the load-settlement curves using the K-Pressure method, the stiffness parameters of the soil are automatically adjusted. Once a best-fit calculated load settlement curve is obtained, the used stiffness values are considered reasonably representative for the soil provided that they are not deviating from the correlation by far. For the adjustment of stiffness values, the typical influence of stiffness as used in the Hardening Soil model on the load-settlement curves is shown in Figure 4.21. It can be seen that varying E_{50}^{ref} gives little influence on the load-settlement curves (Figure 4.21a). On the other hand, E_{oed}^{ref} has significant influence on the load-settlement curves. Increasing E_{oed}^{ref} leads to stiffer behaviour of the load-settlement curves. Higher value of E_{oed}^{ref} results in a longer and stiffer elastic response part of the curve as shown in Figure 4.21b. On the plastic response part of the curve, it is shown that there is only little change due to the variation of E_{oed}^{ref}, which can be understood that the pile is of the type of skin friction pile where pile-tip resistance is small. In Figure 4.21c, it is shown that E_{ur}^{ref} has some influence on the load-settlement curves. Increasing E_{ur}^{ref} causes a stiffer behaviour of the elastic response part of the curve. However, the increase of E_{ur}^{ref} also reduces the elastic response part of the load-settlement curve.

Influence of small strain stiffness

In order to investigate the influence of small strain stiffness, pile loading tests is performed using the HS-Small model instead of the Hardening Soil model. As described in Section 3.4, the HS-Small model is an extension of the Hardening Soil (HS) model that account for higher stiffness of soil at small strain level.

For the HS-Small model, the properties as used in the HS model, which are listed in Table 4.2 are used. In addition to that, two additional small strain parameters, which are G_0^{ref} and $\gamma_{0.7}$ are applied (see also Appendix A.2). For medium dense to loose sand, the initial Young's modulus E_0 may for instance be assumed to be about 3.5 times the reference unloading-reloading modulus E_{ur}^{ref}. This gives E_0 of 245 MPa. The G_0^{ref} can be obtain using the relation

$$G_0^{ref} = \frac{E_0}{2 \cdot (1 + \nu_{ur})} \tag{4.12}$$

which gives a value of G_0^{ref} of about 100 MPa. For the $\gamma_{0.7}$, a value of $8 \cdot 10^{-5}$ is chosen. In addition to that, K-value of 2.3 is applied, which gives a best-fit load-settlement curves.

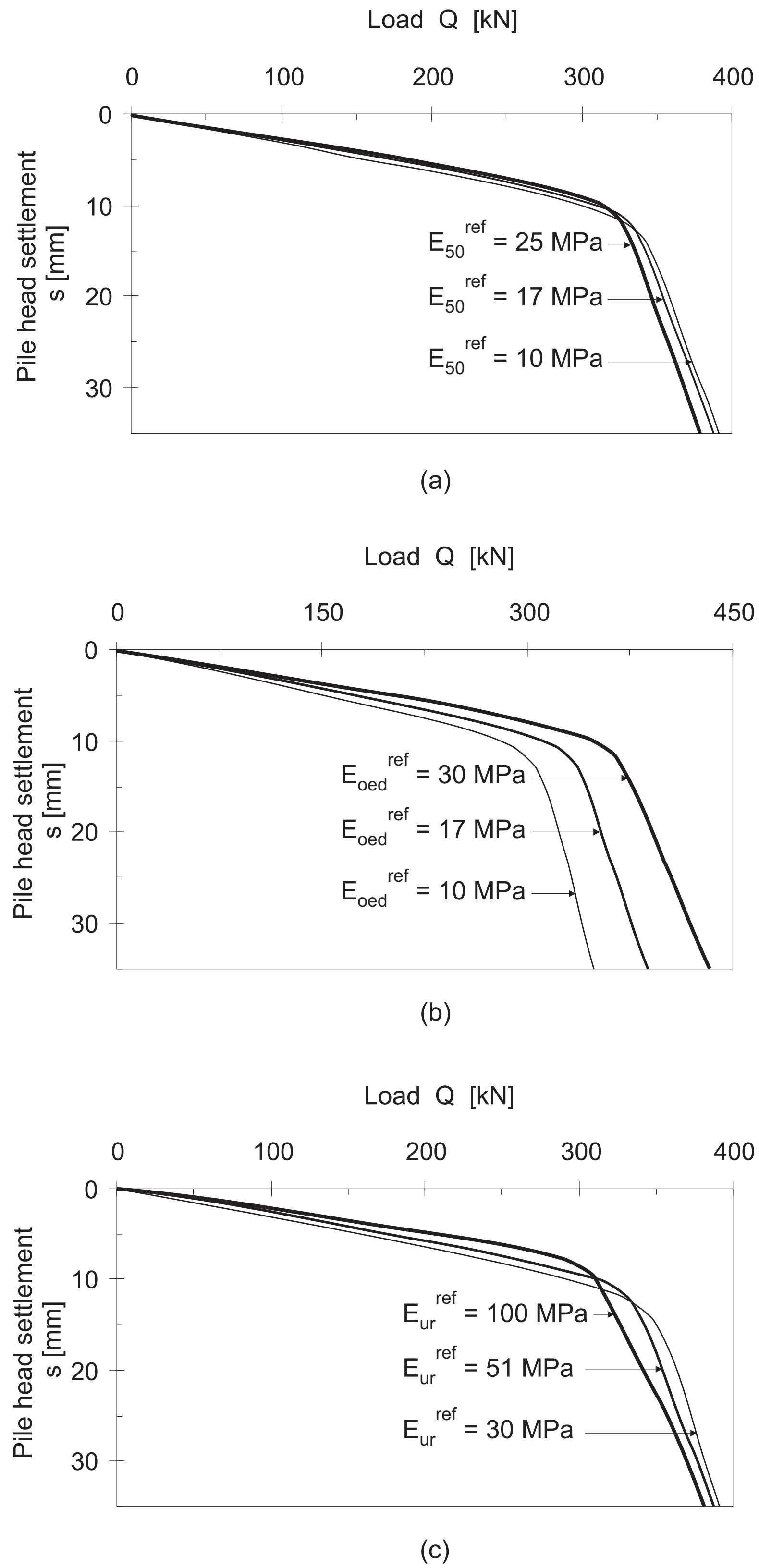

Figure 4.21: Influence of stiffness parameters on load-settlement curves (a) Variation of E_{50}^{ref} (b) Variation of E_{oed}^{ref} (c) Variation of E_{ur}^{ref}

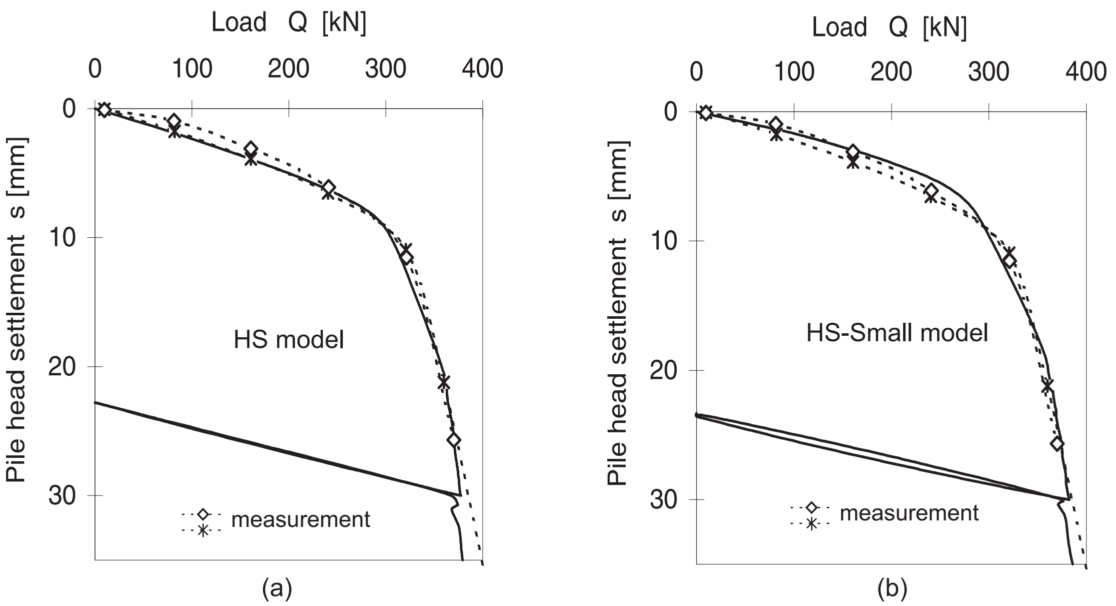

Figure 4.22: Load settlement curves with unloading-reloading (a) using HS model (b) using HS-Small model

Figure 4.22a and b show the comparison of load-settlement curves with unloading-reloading using the HS model and the HS-Small model. It can be seen that the additional small strain stiffness causes the elastic response part of the load-settlement curve to be slightly higher than the one using the HS model which is as expected. Up to a load of about 300 kN the HS-Small model gives a more curvature to the load-settlement curve. Other difference between the HS-Small model and the Hardening Soil model can be seen in the case of unloading-reloading. In contrast to the HS model, the HS-Small model show some hysteresis during unloading-reloading. Hence, the use of the HS-Small model shows a better results of pile loading test and the use of the model is therefore recommended. Computational results on deformed mesh and mobilized shear strength as well as the orientations of principal stresses appear to be very similar to those from the HS-computations. In addition, It is worth showing that the load reversal due to unloading causes the irregular directions of the principal stresses along the interface as shown in Figure 4.23.

During unloading and reloading of the pile, the stresses along the pile shaft changes. As shown in Figure 4.24a, due to unloading the shear stress reduces to a total value of about zero and it increases again to its maximum distribution after reloading. Figure 4.24b shows radial stresses along the interface due to unloading-reloading. After unloading, the radial stress decreases slightly. Apart from around pile-tip, the distribution of the radial stress along the pile shaft after unloading shows a linear increase following a constant K-value. This indicates that the use of K-Pressure with a constant K-value is realistic. When the pile is reloaded, the radial stress increases again to about the same amount as in the previous loading phase.

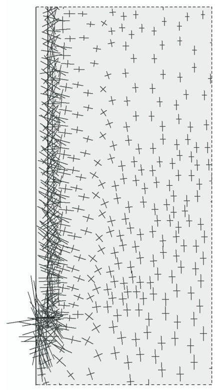

Figure 4.23: Principal stresses around pile after unloading

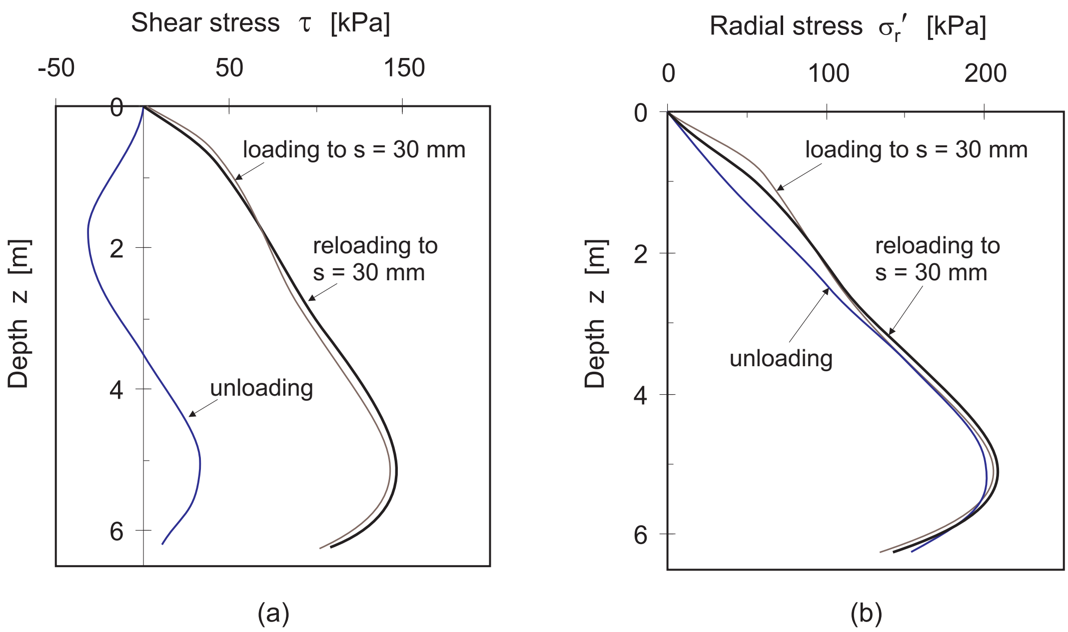

Figure 4.24: Stresses along interface during unloading-reloading phases (a) Shear stresses (b) Radial stresses

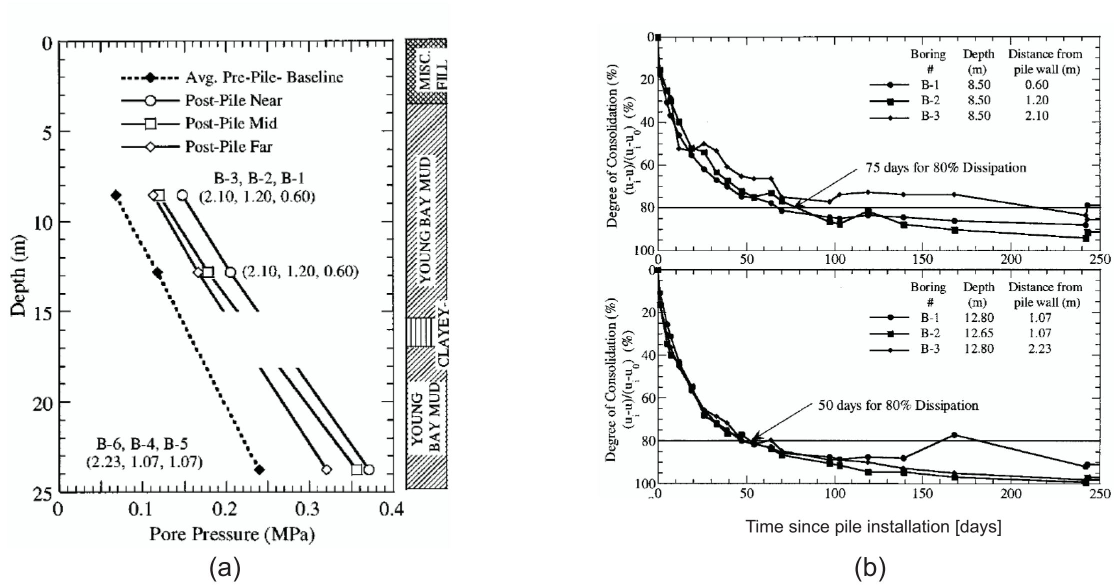

Figure 4.25: Pore water pressure measurement after pile driving and after consolidation (a) Pore water pressure 2 hours after pile installation (b) Dissipation of excess pore water pressure in time at three depths (after Pestana et al. 2002)

4.3.3 Undrained FE-analysis of a pile load test with K-Pressure method

During displacement pile installation in saturated soft clay, excess pore water pressure develops due to the pressure to displace some volume of the soil for the pile. Several field measurements on the developed excess pore water pressure due to pile installation have been reported. Field measurements performed by Holtz and Lowitz (1965) suggest an increase of pore water pressure within a distance of 1.5 to 2 pile diameter from pile shaft immediately after pile installation. Beyond a distance of 2 to 3 pile diameter from the pile shaft, pore water pressure seems to be largely unaffected due to pile installation. This observation is consistent with the field measurement performed by Roy et al. (1981), which shows that negligible excess pore water pressure occurs beyond a distance of 8 times pile diameter from the pile shaft.

Pestana et al. (2002) conducted a field test of a 61 cm diameter closed ended pile installed into a deep deposit of Young Bay Mud, where the soil is a soft to medium plasticity sensitive marine clay. Measurements of development and dissipation of excess pore water pressure just after and at some time after pile installation are presented. The pore water pressure measurements are very consistent. Figure 4.25a shows a linear fit of pore water pressure immediately after pile driving. They are grouped into their locations. The "Near" values are from piezometer B-1 and B-5. "Mid" values are from B-2 and B-4 and "Far" values correspond to piezometers in B-3 and B-6. It can be seen that higher excess pore water pressure occurs near the pile shaft and it decreases with increasing distance from the pile shaft. As illustrated in Figure 4.25b, all piezometers seem to show an exponential decay of excess pore water pressure. The excess pore pressures have already reached 80 percent dissipation within 50 to 80 days. The rapid dissipation of excess pore water pressure after pile installation is also shown by Morison (1984) whose findings show almost full dissipation of excess pore water pressure within only few days after pile installation.

From practical point of view, when the time lag of pile installation to pile loading takes more than about 3 months, it may be considered that the effects of pile installation process is equivalent to the effects of a drained pile installation where there is no excess pore water pressure developed. Hence, when performing FE-analysis, simulation of the effects of a pile installation in drained condition is valid to be applied and it is simpler to perform. However, if the pile loading test is only a few days after the pile installation, developed excess pore water pressure in the soil around the pile cannot be neglected. Thus pile installation analysis needs to be performed in undrained condition where the developed excess pore water pressure is considered.

Up to now, FE-analysis of the effects of pile installation has been performed in drained condition. In this section, FE-analysis of the effects of pile installation with K-Pressure method in undrained condition and then followed by consolidation analysis is presented. A comparison to a drained FE-analysis of the effects of pile installation is also shown. In addition to that, pile loading analyses in undrained as well as in drained conditions are discussed.

4.3.3.1 Calculation procedure

For the undrained analyses of a displacement pile installation and loading, a tentative pile loading test case is assumed. For that purpose, the geometry of the Wijchen pile loading test as described in Section 4.3.2 is chosen. However, the soil in this case is assumed to be a saturated normally consolidated soft clay, with the ground water table at the ground surface. The FE-Mesh used for the current analyses is the same as in the previous analysis as illustrated in Figure 4.5. In addition, a closed consolidation boundary at the left side of the mesh i.e. at the centre of axisymmetry is applied for the consolidation calculation. It is assumed in this case that the excess pore water pressure can dissipate everywhere except to the centre of axisymmetry. As for the displacement boundary condition, horizontal displacement is prevented everywhere and vertical displacements are prevented at the bottom of the mesh. The material of the non-porous linear elastic pile is taken the same. For the soft clay, its behaviour is simulated using the Hardening Soil model and interface follows the Mohr-Coulomb model. The material properties for soft clay and interface are listed in Table 4.4. The subscript *in* denotes interface material property and k is the permeability of the soft clay.

The pile installation simulation follows the K-Pressure procedure as described in Section 4.3.2. However, the material behaviour for the soft clay and for the materials used in the K-Pressure procedure are set to undrained condition, where upon loading, excess pore pressure is generated and dissipation of the excess pore pressure takes some time.

Table 4.4: Material properties as used for the undrained pile installation analysis

Parameters		Clay (HS model)	Interface (MC model)
γ'	[kN/m^3]	7	-
$\gamma_{saturated}$	[kN/m^3]	17	-
φ' / φ'_{in}	[°]	25 / -	- / 25
c' / c'_{in}	[kPa]	0.1 / -	- / 0.1
ψ / ψ_{in}	[°]	0	0
E_{50}^{ref}	[MPa]	2	-
E_{oed}^{ref}	[MPa]	1	-
$E_{ur}^{ref} / E_{in}^{ref}$	[MPa]	12 / -	- / 12
ν_{ur} / ν_{in}	[-]	0.2 / -	- / 0.45
m	[-]	1	-
t_{in}	[mm]	-	26
k	[m/day]	$1{\cdot}10^{-4}$	-
Tensile strength	[kPa]	0	0

An exception is applied to the soil below the pile, where its behaviour is set to drained behaviour. This is done to avoid suction pore water pressure during the K-Pressure procedure. The calculation is started with generation of initial soil geostatic stress state with an initial effective vertical stress of $\sigma'_{v0} = \gamma' \cdot z$, where γ' is the effective unit weight of the soil. For the corresponding horizontal stress, it yields $\sigma'_h = K_0 \cdot \sigma'_{v0}$. The K_0-value is taken according to the Jaky's formula $K_0 = 1 - \sin\varphi'$ for normally consolidated soil. For φ' = 25°, this gives K_0 = 0.58. After initialization of the initial stresses, the K-Pressure procedure is performed with K-value is chosen to be 1.5 considering the normally consolidated soft clay soil. Hence, the stress controlled cavity expansion in elasticity is applied and then followed by the MC-correction as illustrated in Section 4.3.2. After that, the original materials for the undrained soft clay with the Hardening Soil model and pile are placed. At the same time the K-Pressure stresses are removed. Following the later calculation phase, consolidation calculation is performed to observe the changes of stress fields due to excess pore water pressure dissipation and the required time for full dissipation. Hence, the consolidation calculation is performed up to a full dissipation of excess pore water pressure.

After undrained pile installation simulation with K-Pressure procedure and followed by consolidation, pile loading is in undrained condition is performed using displacement controlled method. A prescribed displacement of 35 mm is applied at the pile head. In addition to that, pile loading in drained condition is also evaluated as a comparison.

4.3.3.2 Undrained pile installation followed by consolidation

After undrained pile installation simulation with K-Pressure method, the resulting stress fields as illustrated in Figure 4.26a are obtained. The effective stresses distributions and active pore water pressure at 4 m depth are depicted in Figure 4.26b. Looking from the outer radius of the mesh to the pile shaft, the effective radial stress increases and effective circumferential stress decreases at the same amount up to a distance of about 2 times pile diameter from the pile shaft. After that, the effective radial and circumferential stresses change slightly and then they seems to level off. In the same distance within a radius of 2 times pile diameter to the pile shaft, the vertical stress decreases and beyond this distance the vertical stress remains constant. This indicates that the soil within the radius of 2 times pile diameter from the pile shaft is in plastic condition due to the applied K-pressure. Beyond that radius, the soil behave elastically.

In this undrained analysis, excess pore water pressure is generated due to K-Pressure loading. In Figure 4.26b, it can be seen that significant excess pore water pressure $\triangle u$ occurs close to the pile shaft within the plastic zone. This result is in agreement with the assumption given by Randolph and Wroth (1979) that excess pore pressure occurs only in plastic zone due to cylindrical cavity expansion. In the elastic zone, the excess pore water pressure should be zero since the total radial and circumferential stress change in the same size and in the opposite direction while the total vertical stress remains the same. This means that the total mean stress $p = {}^{1}\!/_{3}(\sigma'_r + \sigma'_\theta + \sigma'_v) + u$ remains constant.

Figure 4.27a shows the principal stresses of the excess pore water pressure with depth. The excess pore water pressure increases just around and along the pile shaft. Some negative (suction) pore water pressure occurs just around the corner of the pile-tip. This is due to the imposed radial K-Pressure, which causes some tension in the soil around the corner of the pile-tip. As illustrated in Figure 4.27b, the developed excess pore water pressure along the pile shaft increase linearly with depth. Approximately linear increase of excess pore pressure distribution along the pile shaft is also described by Pestana et al. (2002) from field measurements (see Figure 4.25a). Since the excess pore water pressure is developed, the increase of effective radial stress is not the same as the imposed K-Pressure. However, the total radial stress i.e. the sum of the effective radial stress and the excess pore pressure is equal to the imposed K-Pressure as illustrated in Figure 4.27b. The interface shear stress remains almost zero after the undrained pile installation simulation with K-Pressure method. The resulting stress fields obtained from the undrained analysis of pile installation with K-Pressure are reasonably representative for the effects of the installation of tube-installed type piles as the chosen tentative pile load test case.

After the undrained pile installation procedure, consolidation analysis is performed. Figure 4.28a shows the interface stresses after consolidation analysis. The consolidation is performed up to full dissipation of excess pore water pressure. The calculation results predict that full dissipation of the excess pore pressure takes 27 days to complete. Hence, a rapid dissipation of excess pore water pressure after pile installation in a saturated clay is shown from numerical analysis. The full dissipation of the excess pore water pressure does not increase the effective radial stress to the value of the imposed radial stress p_r.

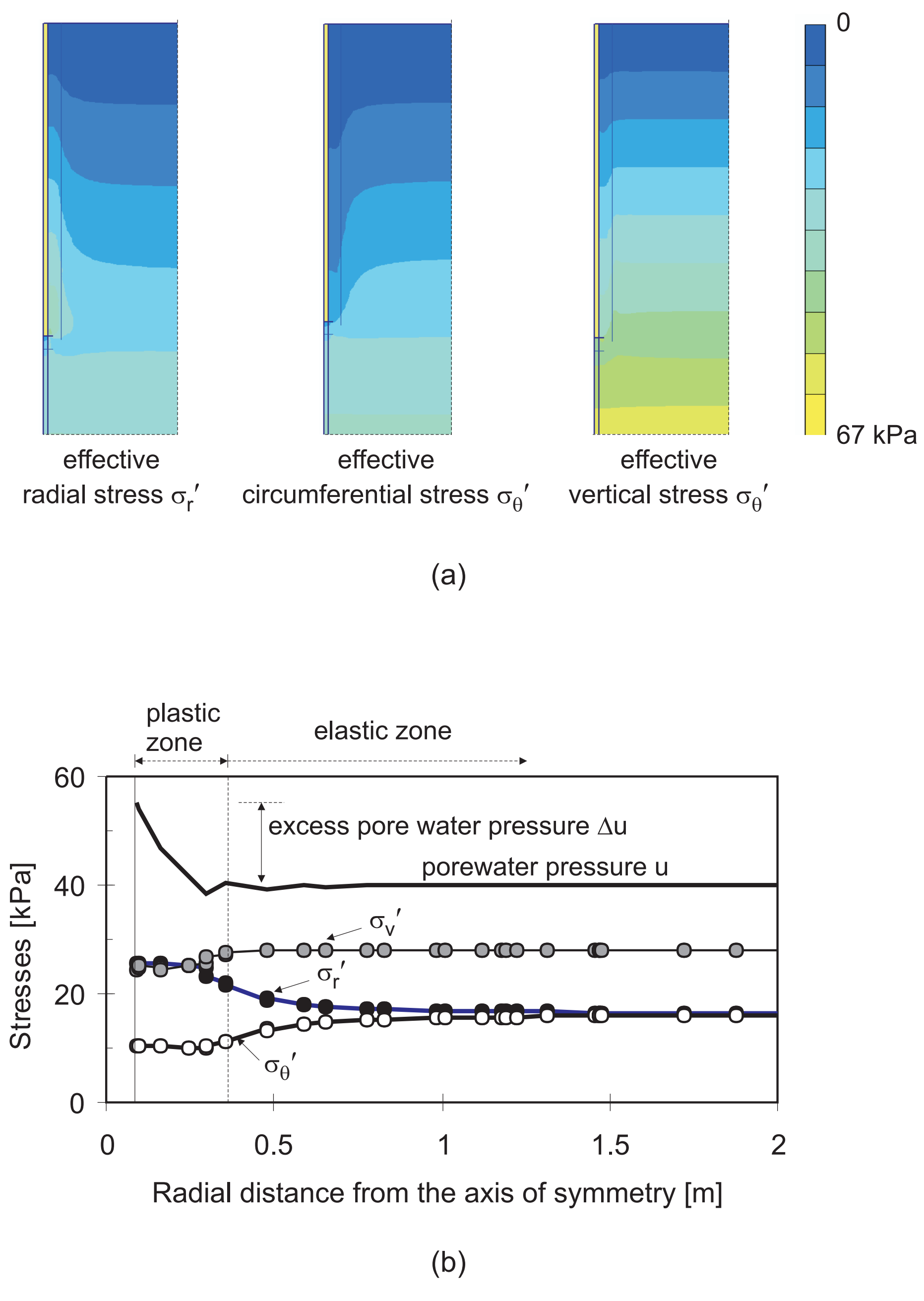

Figure 4.26: Stresses after undrained pile installation simulation using K-Pressure method with K = 1.5 (a) Effective stresses along the pile (b) Effective stresses and pore water pressure at 4 m depth

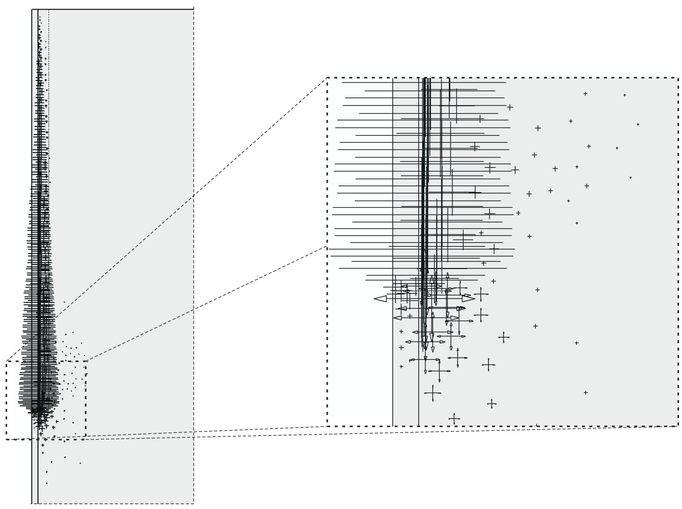

(a)

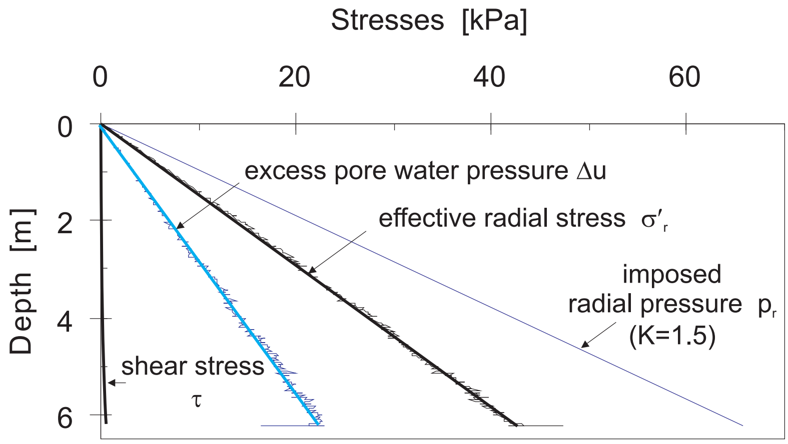

(b)

Figure 4.27: Stresses after undrained pile installation with K-Pressure method (a) Developed excess pore water pressure (b) Interface stresses after K-Pressure with $K = 1.5$

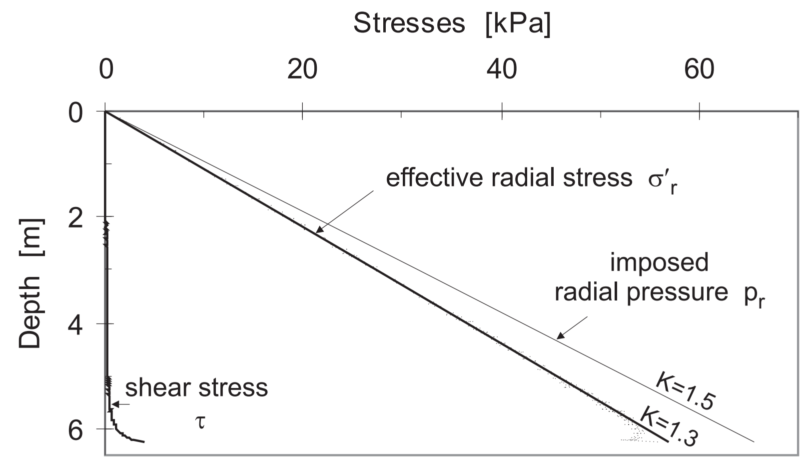

(a)

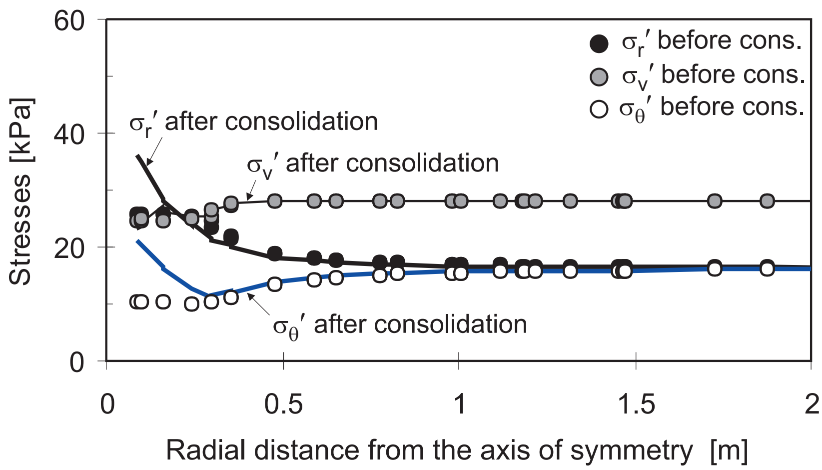

(b)

Figure 4.28: Stresses after consolidation (a) Interface stresses (b) Effective stresses at 4 m depth

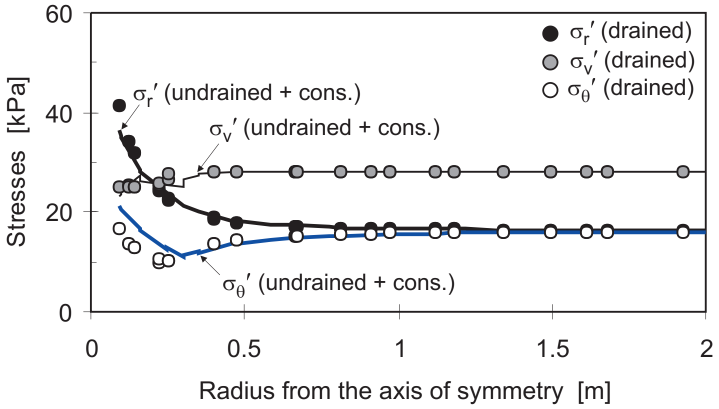

Figure 4.29: Comparison of stress fields at 4 m depth between undrained analysis followed by consolidation and drained analysis of pile installation

The reason for this is shown from the comparison between effective stresses distributions with distance from the pile centre at 4 m depth before and after consolidation as depicted in Figure 4.28b. It can be seen that the dissipation of excess pore water pressure due to consolidation causes the increase not only for the effective radial stress, but also for the effective circumferential stress. The effective vertical stress does not seem to change.

It is of interest to compare the resulting stress fields from undrained pile installation analysis and followed by consolidation to allow full dissipation of excess pore water pressure to the resulting stress fields of a drained pile installation analysis. In Figure 4.29, the comparison between the resulting stress fields at 4 m depth from undrained pile installation followed by consolidation (undrained + cons.) with the resulting stress fields from drained analysis of pile installation is presented. It can be seen that upon applying K-Pressure with the same *K*-value, the resulting stress fields from undrained analysis followed by consolidation to full dissipation of excess pore water pressure are slightly different from the resulting stress fields obtained from a drained analysis. The effective radial stress from undrained analysis followed by consolidation is slightly lower compared to the effective radial stress from drained analysis. On the other hand, the effective circumferential stress from undrained analysis followed by consolidation is slightly higher than the one from drained analysis. The effective vertical stress from both analyses are more or less the same. Nevertheless, the differences between the resulting stress fields from both analyses are not significant.

4.3.3.3 Pile loading

When the pile loading is performed relatively quickly as in the case of pile load tests, the process is considered in undrained condition. Figure 4.30 shows two load settlement curves from pile loading in undrained condition. The two curves are from different conditions of previous pile installation simulation. The thick curve is from pile instal-

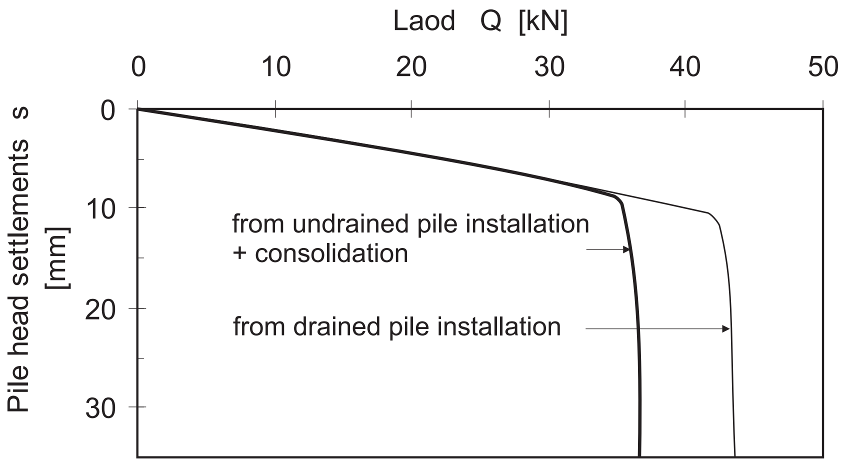

Figure 4.30: Pile loading results in undrained condition

lation simulation in undrained condition and followed by consolidation up to full dissipation of excess pore water pressure. The thin curve is from drained pile installation simulation. It can be seen that the load-settlement curve from drained pile installation gives 7 kN higher pile bearing capacity compared to the one from undrained analysis followed by consolidation. This can be understood since the resulting effective radial stress after drained pile installation is slightly higher compared to the one from undrained pile installation simulation followed by consolidation.

If the pile loading is performed very slowly, the analysis can be considered as in drained condition. The load-settlement curves from drained pile loading are similar to the ones shown in Figure 4.30. The resulting bearing capacity from drained pile loading after drained pile installation is slightly higher the one from drained pile installation after undrained pile installation followed by consolidation. However, the difference of the pile bearing capacities is less compared to the results shown in Figure 4.30.

Generally, it is very difficult to have good measurements on the development of excess pore water pressure during pile installation as well as pile loading. This requires robust and precise piezometer tools as well as a very careful and well controlled procedure during the measurement. Hence, verification of the developed excess pore water pressure from numerical analysis to the reality is also difficult. Comparison of numerical analyses results from undrained pile installation followed by consolidation up to a full dissipation of excess pore water pressure and drained pile installation shows only marginal difference. In addition to that, after the pile installation simulation, the load-settlement curves from pile loading analyses, especially in drained condition, may be considered not significantly different. Therefore, drained pile installation simulation using K-Pressure method where the K-value is back-calculated from load-settlement measurements is suggested. Afterwards, pile loading simulation can be done in drained or undrained condition.

4.4 Conclusions on analysis of the effects of displacement piles installation

The main effect of displacement piles installation is the increase of radial stress around the pile, which later increases the pile capacity. Apart from that, precast pile installations also create some residual skin friction and residual pile-tip pressure. However, for typical small and relatively short displacement piles installed in soft soils as in the case of embankments on floating piles, the residual skin friction and pile-tip pressure are insignificant.

For analysis using the standard small strain finite element, it is not possible to simulate full pile penetration. Hence, an alternative method is necessary. A clear and repeatable procedure to simulate the effects of displacement piles installation, which is called $K - Pressure$ method has been developed. The method is important especially for the analysis of displacement floating piles as used for soft soil improvement. The method has been developed for axisymmetric displacement pile analysis, which is based on stress controlled cavity expansion. The increase of radial stress due to pile installation can be created by applying radial stresses on the cavity wall, with $p_r = K \cdot \sigma'_{v0}$. The constant K-value is calibrated using the load settlement measurements from pile loading tests. Hence, *the K-Pressure method requires calibration by pile loading tests*. Upon using this method, realistic stress fields after pile installation as well as after pile loading are obtained up to an appropriate K-value, which is in the range of practical experiences.

The K-Pressure method is not only suitable for displacement pile analysis in drained condition but also for analysis in undrained condition. On applying K-Pressure method in undrained condition, excess pores pressure develops around the pile within the plastic zone after pile installation simulation. When consolidation take place afterwards, the excess pore pressure dissipates relatively rapidly as also observed from field experience. The resulting stress fields after applying K-Pressure and followed by consolidation up to full dissipation of excess pore water pressure do not show significant difference compared to applying K-Pressure procedure in drained condition. In addition to that, good data on excess pore water pressure after pile installation and pile loading are hardly obtained. Hence, validation of numerical analysis is also difficult. Therefore, pile installation simulation with K-Pressure method in drained condition, where the K-value is back-calculated from load-settlement measurements, is preferable. Afterwards, pile loading simulation can be performed either in drained or undrained condition.

With the K-Pressure method, the option of using different advanced constitutive models in the numerical simulation are available. In the present analyses, the Hardening Soil (HS) model has been used. In addition to that, the analyses with the HS-Small model, where small strain stiffness is taken into account are also performed. It is found that the resulting load settlement curve from displacement piles analyses with HS-Small model give better curvature compared to the ones from analyses with the HS model. Moreover, analyses with the HS-Small model shows hysteresis when unloading-reloading cycle is performed. Hence, the use of the HS-Small model give better results especially when unloading-reloading cycle is considered.

In general, The K-Pressure method is considered a sound method for displacement piles analysis and within the realm of engineering practice. The applicability of this method is not limited to displacement piles but can be also extended to other column type foundations.

Chapter 5

Settlement analysis of embankments on floating piles

A piled embankment with end-bearing piles is known as an effective method for soft soil improvement. However, end-bearing piles can be applied only when the soft soil thickness is relatively small, e.g. up to 20 m. In many areas such as in Scandinavia and in some region in South East Asia, the soft soil thickness can be very large up to 40 m or even more (e.g. Poulos, 2007). In such case, it is not economically possible to use end-bearing piles. Therefore, floating piles (friction piles) are used instead of end-bearing piles. Embankments on floating piles will settle depending on the pile length (penetration depth) and embankment load. For that reason, when designing an embankment on floating piles, attention is focused on evaluating the effectiveness of the system. So that the final tolerated embankment settlement and relative differential settlements can be achieved within acceptable technical and financial limitations.

The effectiveness of embankments on floating piles can be determined using its relative settlement reduction (RSR). The relative settlement reduction is defined as

$$RSR = \frac{S_0 - S}{S_0} \tag{5.1}$$

where S_0 is embankment settlement constructed on soft soil without the support of piles and S is the settlement of embankment supported by piles. Thus, the effectiveness describes the gained embankment settlement reduction when floating piles are installed in the soft soil relative to the embankment settlement without installing piles. Indeed, settlements become a problem when it implies differential settlements. The installation of floating piles reduce the total settlements of the piled embankments. No doubt that a reduction of total settlements will also reduce differential settlements. Moreover, the floating piles transfer the main embankment load to the deeper and stiffer stratum around the piles-tip. This gives the effect of bridging soft spots in the soft soil around the surface in between the piles. Hence, the floating piles render the soft soil in between the pile to become more homogeneous. This is apparently shown when the floating piles and the surrounding soft soil has reached a block behaviour. Further description on the block behaviour will be in Section 5.3.3.

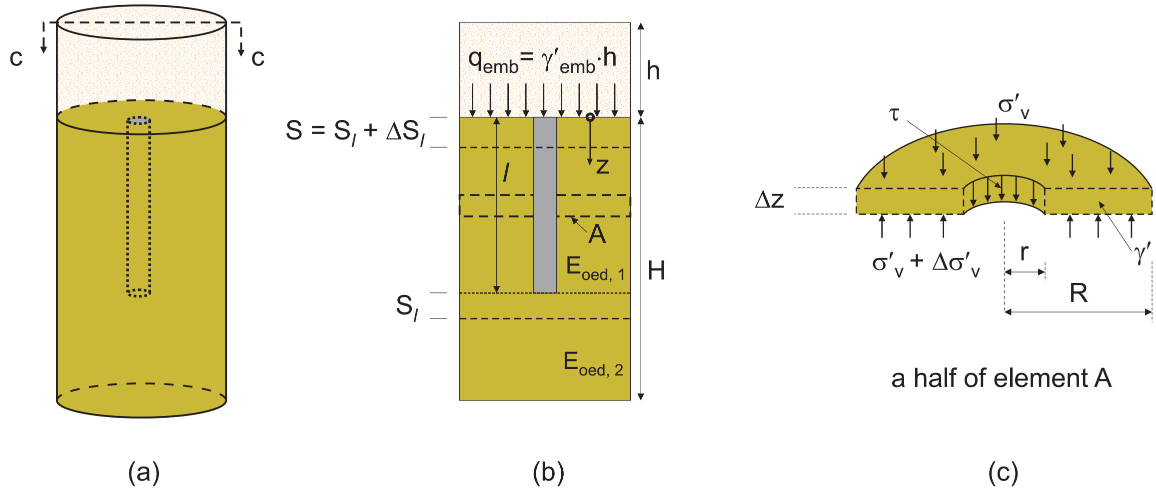

Figure 5.1: Settlement analysis of one cell embankment on floating piles (a) One circular cell idealization (b) Vertical cross-section c-c (c) Vertical effective force equilibrium of element A

To evaluate the effectiveness of the embankment on floating piles, one can use an analytical approach as well as using advanced method such as FE-analysis. Both approaches for determining the effectiveness of an embankment on floating piles are discussed next.

5.1 Analytical approach for settlement of embankments on floating piles

On using an analytical approach for evaluating the settlement of embankments on floating piles, a circular idealization of one cell rigid embankment on a floating pile as illustrated in Figure 5.1a is considered. Figure 5.1b and c show the vertical cross section of the circular cell and vertical effective force equilibrium of element A respectively. Assuming the embankment is rigid, the settlement is then evaluated at the surface of the soft soil. When no pile is installed, the soft soil surface settlement due to embankment load can be simply calculated using the Hooke's law. Hence;

$$S_0 = S_l + \Delta S_0 = \frac{q_{emb} \cdot (H - l)}{E_{oed,2}} + \frac{q_{emb} \cdot l}{E_{oed,1}} \tag{5.2}$$

The subscript "0" describes that no pile is installed. Thus, S_0 is the total settlement at the surface of soft soil in the case of without installed pile. ΔS_0 is the settlement of the soft soil part until a depth of l, where l is the length of pile when it is installed. S_l is the settlement of the soft soil below the depth l. q_{emb} and H are the embankment load and the total thickness of the soft soil respectively.

When the embankment is supported by a floating pile, the settlement of the soft soil can be determined through vertical effective force equilibrium analysis of the soft soil surround the pile. Considering the ground water at the surface of the soft soil, the vertical effective force equilibrium of element A as shown in Figure 5.1c can be written as follows:

$$\left[\left(-\sigma'_v + \sigma'_v + \Delta\sigma'_v - \gamma' \cdot \Delta z\right) \cdot \pi \left(R^2 - r^2\right)\right] - 2\pi r \cdot \tau \Delta z = 0 \tag{5.3}$$

where R is the radius of the circular cell, r is the radius of the pile and τ is pile skin friction. Rewriting Equation 5.3, it gives

$$\frac{d\sigma'_v}{dz} - \gamma' = \frac{2r}{R^2 - r^2} \cdot \tau = \frac{2r}{R^2 - r^2} \cdot K \cdot \sigma'_v \cdot \tan\delta \tag{5.4}$$

where K is the coefficient of lateral earth pressure and δ is the wall friction angle. Vermeer and Sutjiadi (1985) give an analytical solution for ultimate shear stress at a shear band that depends on effective friction angle φ' and dilatancy ψ as follows

$$\tau_f = \sigma'_n \cdot \frac{\sin\varphi' \cdot \cos\psi}{1 - \sin\varphi' \cdot \sin\psi} \tag{5.5}$$

where σ'_n is effective normal stress. For non-dilating soil as the case in soft soil, $\tan\delta$ in Equation 5.4 is equal to $\sin\varphi'_{softsoil}$ for ultimate skin friction. The equilibrium described in Equation 5.4 can be rearranged to form a linear non-homogeneous first order differential equation

$$\frac{d\sigma'_v}{dz} - \beta \cdot \sigma'_v = \gamma' \quad \textit{with} \quad \beta = \frac{2r}{R^2 - r^2} \cdot K \cdot \sin\varphi'_{softsoil} \tag{5.6}$$

The differential equation can be solved for σ'_v to find

$$\sigma'_v = -\frac{\gamma'}{\beta} + C \cdot e^{\beta z} \tag{5.7}$$

where C is the constant that can be solved by applying the boundary condition. On evaluating the boundary condition at the pile-tip where the entire embankment load q_{emb} is transferred to this depth, it is known that at $z = l$; $\sigma'_v = q_{emb} + \gamma' \cdot l$. Inserting this boundary condition to Equation 5.7, one finds the complete solution of the effective vertical stress

$$\sigma'_v = \left(q_{emb} + \gamma' \cdot l + \frac{\gamma'}{\beta}\right) \cdot e^{\beta(z-l)} - \frac{\gamma'}{\beta} \tag{5.8}$$

On defining the additional effective vertical stress along the pile due to embankment load $\Delta\sigma'_v = \sigma'_v - \gamma' \cdot z$, it is found that

$$\Delta\sigma'_v = \left(q_{emb} + \gamma' \cdot l + \frac{\gamma'}{\beta}\right) \cdot e^{\beta(z-l)} - \frac{\gamma'}{\beta} - \gamma' \cdot z \tag{5.9}$$

In order to achieve that the entire embankment load q_{emb} is supported by the floating pile, the pile length l should be chosen such that $\Delta\sigma'_v$ at the surface of soft soil (z = 0) is zero. Pile length that satisfies this criterion is called critical pile length l_{crit}, which can be determined from Equation 5.9 to give

$$q_{emb} + \gamma' \cdot l_{crit} + \frac{\gamma''}{\beta} = \frac{\gamma'}{\beta} \cdot e^{\beta l_{crit}} \tag{5.10}$$

On approximating $e^{\beta l_{crit}} \approx 1 + \beta \cdot l_{crit} + \frac{1}{2} \cdot \beta^2 \cdot l_{crit}^2$, it is found that

$$l_{crit} \approx \sqrt{\frac{2q_{emb}}{\beta \cdot \gamma'}} \tag{5.11}$$

Assuming an elastic soil body, the settlement due to the embankment load at the surface of the soft soil improved with floating piles can be calculated as follows:

$$S = \int \varepsilon \cdot dz = S_l + \int_0^l \frac{1}{E_{oed,1}} \cdot \left(q_{emb} + \gamma' \cdot l + \frac{\gamma'}{\beta}\right) \cdot e^{\beta(z-l)} dz - \int_0^l \frac{\gamma'}{E_{oed,1} \cdot \beta} dz - \int_0^l \frac{\gamma'}{E_{oed,1}} \cdot z\, dz$$

$$= S_l + \frac{\left(q_{emb} + \gamma' \cdot l + \frac{\gamma'}{\beta}\right)}{E_{oed,1} \cdot \beta} \cdot (1 - e^{-\beta l}) - \frac{\gamma' \cdot l}{E_{oed,1} \cdot \beta} - \frac{\gamma' \cdot l^2}{2 \cdot E_{oed,1}} \tag{5.12}$$

Once the settlement has been determined, the effectiveness of the embankment on floating piles based on the relative settlement reduction RSR can be evaluated.

5.2 Effectiveness of embankments on floating piles from analytical approach

Despite the use of simplifications, an analytical approach is useful to have a preliminary estimation of critical pile length and its corresponding effectiveness for soft soil improvement. Moreover, it is also useful for understanding the general behaviour of a floating pile foundation. Indeed, for a detailed and more accurate design of an embankment on floating piles, an advanced method such as finite elements is required.

For the evaluation of the effectiveness of an embankment on floating piles using an analytical approach, a circular cell geometry as illustrated in Figure 5.1 is considered, with R is equal to 0.5 m and pile radius r is 0.1 m. The embankment consists of stiff material with γ'_{emb} = 18.5 kN/m^3. The soft soil has effective unit weight γ' of 7 kN/m^3 and effective friction angle $\varphi'_{softsoil}$ of 25°. Due to the installation effect of the displacement floating pile, the coefficient of lateral earth pressure K is assumed to be 1. For the settlement calculations, the soft soil is divided into two layers, which are the upper layer with a thickness of l and the lower layer with a thickness of $H - l$. The oedometer or compression modulus of the soft soil layers E_{oed} is taken as tangent modulus. This can be determined using the power law relation as originally suggested by Ohde (1930)

$$E_{oed} = E_{oed}^{ref} \cdot \left(\frac{\sigma_v'}{p^{ref}}\right)^m \tag{5.13}$$

where E_{oed}^{ref} is the reference oedometer stiffness taken at the reference pressure p^{ref}. Considering a typical E_{oed}^{ref} of 1 MPa at p^{ref} of 100 kPa and m value of 1 for soft soils, Equation 5.13 reduces to $E_{oed} = 10 \cdot \sigma_v'$. σ_v' is the effective vertical stress calculated at the middle of the soft soil layer and it depends on the amount of embankment load. In this case, the compression modulus of the soft soil layers is calculated as follows:

$$E_{oed,1} = 10 \cdot (0.5 \cdot l \cdot \gamma' + 0.5 \cdot q_{emb})$$

$$E_{oed,2} = 10 \cdot (0.5 \cdot (H + l) \cdot \gamma' + 0.5 \cdot q_{emb}) \tag{5.14}$$

In the design of embankment such as road embankment, the required final height of embankment h' measured above the original ground level after settlement due to embankment load is specified. Therefore, the calculations of critical pile length l_{crit}, and designed embankment height h need to be done iteratively. The critical pile length and designed embankment height are updated during the iterative calculations to compensate the settlement until the specified embankment height h' is obtained. Thus, the calculation involves geometrical changes of the embankment on floating piles. Since the embankment is assumed to be built of a stiff coarse material, its compressibility due to self-weight is negligible. Therefore, the embankment settlement is observed at the surface of soft soil. A simple algorithm for the iterative calculation of the effectiveness of an embankment on floating piles with embankment geometry changes is shown in Algorithm 5.1. In the algorithm, the calculation steps are arranged for pile of critical length, where critical length changes due to the iteratively updated new embankment height h_{new}.

For a shorter pile with its length is kept constant the settlement in calculation step 4g in the algorithm, is then calculated for pile of length l instead of l_{crit}. In addition to that, calculation step 4d is not in the loop as the pile length is not the critical pile length and it is kept constant as the initial pile length.

Figure 5.2 shows the relative settlement reduction against pile length for embankment of 2 m height with different soft soil thickness. The bold curves are from calculation with geometrical changes (iterative procedure) whereas the thin curves are from calculations with constant geometry. The latter means that the relative settlement reductions are calculated with embankment height constant as the initial embankment height. The curves show the effectiveness, which is evaluated using the relative settlement reduction, increases rapidly as the pile length is closer to the critical length. Similar findings are also obtained for embankment of 1 and 4 m height. In general, the effectiveness is less than 60 percent. The effectiveness of embankment on floating piles can be analysed

Algorithm 5.1 Simple Procedure for effectiveness calculation with geometrical changes for pile of critical length

1. Input properties: γ'_{emb}, γ', $h_{initial}$, H, K, $\varphi'_{softsoil}$, R, r
2. Calculate $\beta = \frac{2r}{R^2-r^2} \cdot K \cdot \sin\varphi'_{softsoil}$, $q_{emb} = \gamma'_{emb} \cdot h_{initial}$
3. Initialize: $S = 0$, $S_0 = 0$
4. DO WHILE TOL ≥ 0.01
   a) $h_{new} = h_{initial} + S$
   b) $q_{emb} = q_{emb,new}$
   c) $q_{emb,new} = \gamma'_{emb} \cdot h_{new}$
   d) $l_{crit} \approx \sqrt{\frac{2 \cdot q_{emb,new}}{\beta \cdot \gamma'}}$
   e) $E_{oed,1} = 10 \cdot (0.5 \cdot l_{crit} \cdot \gamma' + 0.5 \cdot q_{emb,new})$
   f) $E_{oed,2} = 10 \cdot (0.5 \cdot (H + l_{crit}) \cdot \gamma' + 0.5 \cdot q_{emb,new})$
   g) $S \approx \frac{q_{emb,new} \cdot (H - l_{crit})}{E_{oed,2}} + \frac{q_{emb} + \gamma' \cdot l_{crit} + \frac{\gamma'}{\beta}}{E_{oed,1} \cdot \beta} \cdot \left(1 - e^{-\beta l_{crit}}\right) - \frac{\gamma' \cdot l_{crit}}{E_{oed,1} \cdot \beta} - \frac{\gamma' \cdot l_{cirt}^2}{2 \cdot E_{oed,1}}$
   h) TOL = $\left| \frac{q_{emb,new} - q_{emb}}{q_{emb,new}} \right|$

   END DO
5. Initialize for calculating S_0: $S_0 = 0$, $q_{emb} = \gamma'_{emb} \cdot h_{initial}$
6. DO WHILE TOL ≥ 0.01
   a) $h_{new} = h_{initial} + S$
   b) $q_{emb} = q_{emb,new}$
   c) $q_{emb,new} = \gamma'_{emb} \cdot h_{new}$
   d) $S_0 = \frac{q_{emb,new} \cdot (H - l_{crit})}{E_{oed,2}} + \frac{q_{emb,new} \cdot l_{crit})}{E_{oed,1}}$
   e) TOL = $\left| \frac{q_{emb,new} - q_{emb}}{q_{emb,new}} \right|$

   END DO
7. $RSR \approx \frac{S_0 - S}{S_0}$

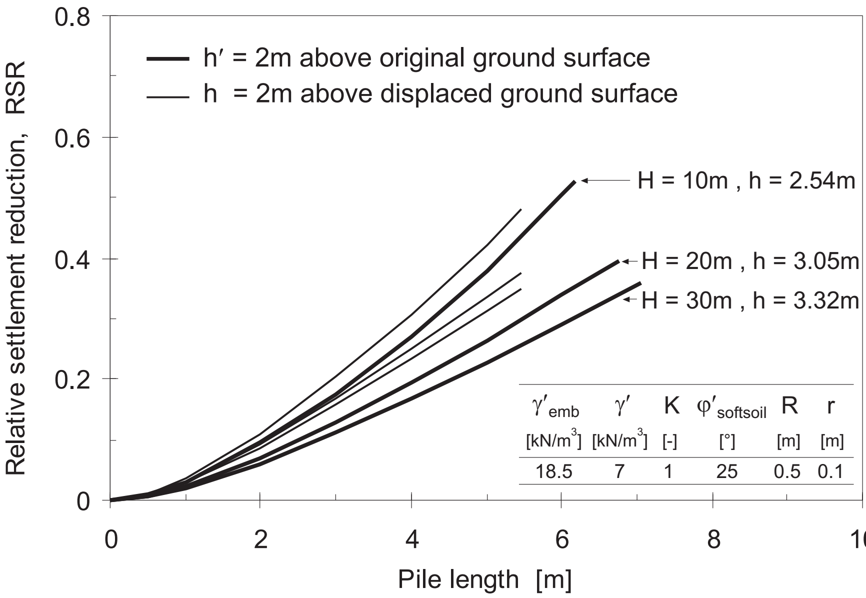

Figure 5.2: Effectiveness of floating piles for 2 m embankment height and different soft soil thickness

maximum up to pile length equal to critical length. It should be noted that the analysis of the effectiveness of embankment on floating piles with pile length longer than the critical length is not possible with the analytical method. This is because the vertical equilibrium condition as described in Section 5.1 is not satisfied with pile length longer than the critical length.

5.3 FE-settlement analysis of embankments on floating piles

For a more detailed and accurate settlement analysis of embankment on floating piles, an advanced method such as FE-analysis can be used. On using FE-analysis for evaluating the effectiveness of embankment on floating piles, the complexities of the embankment-pile-soil interaction can be accounted for. Moreover, finite elements can evaluate the effectiveness of embankment on floating piles with any length beyond critical length.

To assess the effectiveness of an embankment on floating piles using FE-method, the circular cell geometry as in the analytical approach is used. The details of the calculation procedure are described next.

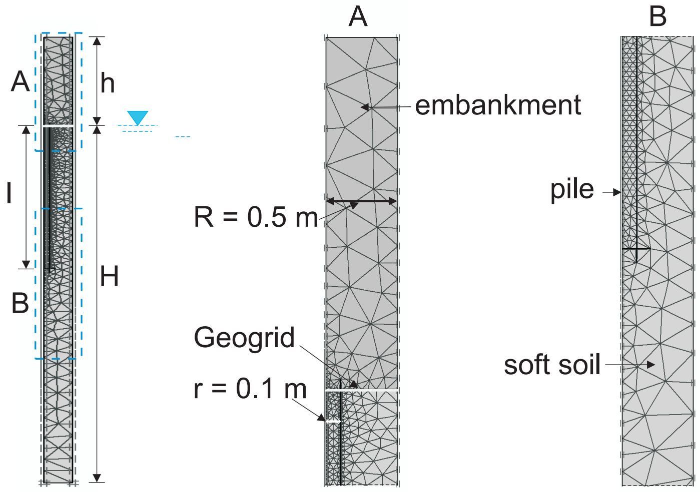

Figure 5.3: FE-mesh for embankment on floating piles analyses

5.3.1 Calculation procedure

In order to perform FE-settlement analyses of embankment on floating piles, axisymmetrical geometry with typical mesh as shown in Figure 5.3 is used. The mesh has a radius of 0.5 m and the radius of the pile is 0.1 m. The embankment height h and pile length l and soft soil thickness H are varied. A strong geogrid is applied on the soft soil surface as the reinforcement of the embankment. The same as in the previous FE-calculations presented in this thesis, 6-noded triangular elements are used and interface elements are applied to simulate pile-soft soil, soft soil-geogrid and embankment-geogrid contacts. The strength of the interface is taken equal to the strength of the surrounding soil.

As for the boundary conditions, at the side of the mesh, the horizontal displacement is prevented and at the bottom of the mesh both horizontal and vertical displacements are prevented. The phreatic water level is set at the soft soil surface. The initial condition is generated assuming a K_0^{NC}-condition for the soft soil, with K_0^{NC}-value according to Jaky's formula. In addition to that, the phreatic water pressure is also initialized.

For the material constitutive model, the Hardening Soil model is used for the embankment and the soft soil. Pile and geogrid materials are considered to follow linear elastic behaviour with stiffness of 15000 MPa and 1000 kPa respectively. The soil material properties as used in the FE-calculations are listed in Table 5.1. The R_{inter} is the interface shear strength factor relative to the soil shear strength.

The same as in the analytical approach, FE-analyses of effectiveness of embankment on floating piles are performed for embankment with geometrical changes. This means that the FE-analyses need to be performed iteratively so that the specified embankment height above the original soft soil surface h' is obtained. For this reason, the FE-calculations are divided into two parts. First, trial calculations are done to determine the final embankment height h, which gives the specified embankment height above original

Table 5.1: Material properties for the HS model as used in the FE-settlement analyses of embankment on floating piles

Properties		Embankment	Soft soil
φ'	[°]	40	25
c'	[kPa]	0.1	0.1
ψ	[°]	10	25
γ_{unsat}	[kN/m^3]	18.5	15
$\gamma_{saturated}$	[kN/m^3]	20	17
E_{50}^{ref}	[MPa]	40	2
E_{oed}^{ref}	[MPa]	40	1
E_{ur}^{ref}	[MPa]	120	8
ν_{ur}	[-]	0.2	0.2
m	[-]	0.5	1
R_{inter}	[-]	1	1

ground level h', after settlements have taken place. After that, the calculations with the final embankment height h are performed to find the relative settlement reduction of the soft soil with floating pile improvement compared to without any soft soil improvement. In the analyses, the calculations are performed under drained condition and settlement due to creep effect is not considered. Moreover, to take into account large deformation during the settlement of the soft soil, updated Lagrange procedure as described in Section 3.2 is applied. In addition to that, it is assumed that the phreatic ground water level remains constant at its initial level. In order to do so, the updated pore water pressure option is activated. Hence, after the settlements have taken place, some lower part of the embankment will be under the phreatic water level.

The sequence of the trial calculations is illustrated in Figure 5.4a. After the initial phreatic water pressure and effective stresses have been generated, the K-Pressure procedure as described in Section 4.3 is performed with K-value is taken as 1. After the K-Pressure procedure, geogrid elements are applied and embankment with its initial height $h_{initial}$ is activated. Starting from this calculation phase, updated Lagrange procedure in combination with updated pore water pressure option are applied. This is done to account for large settlements, to obtain a realistic tension in the geogrid and to maintain the phreatic water level at a constant level as in reality. After that, a unit distributed load is applied on top of the embankment. This load is then multiplied to determine the amount of applied load that is equal to embankment surface settlement times embankment unit weight, $q_{applied} = S_{emb} \cdot \gamma_{unsat}^{emb}$. The embankment settlement S_{emb} is taken as additional embankment height Δh that will be added to the initial embankment height for the final calculation (see Figure 5.4b). Indeed, the additional embankment height Δh will also

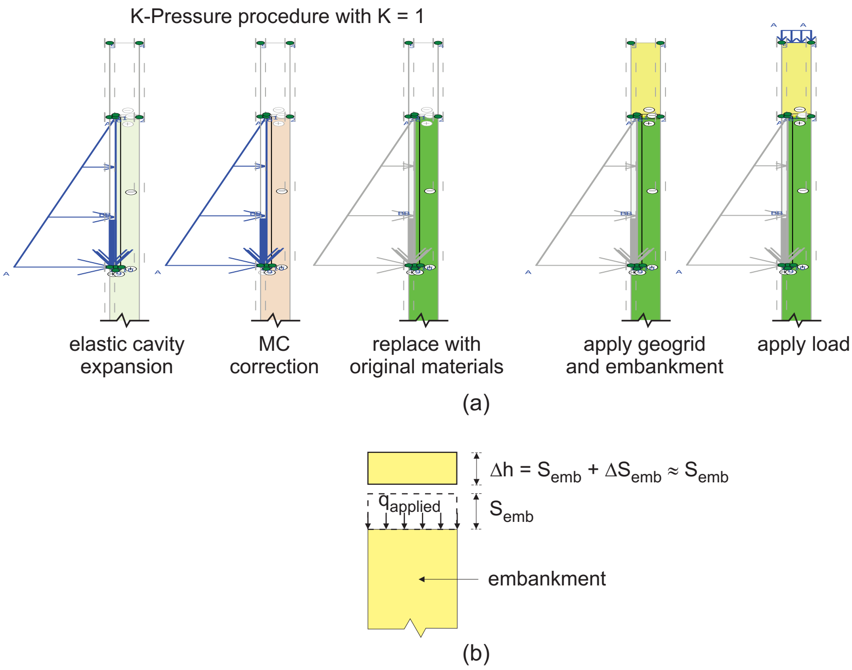

Figure 5.4: Trial calculation procedure for embankment of floating piles (a) calculation sequence (b) additional embankment height for the final calculation.

settle slightly in the amount of $\Delta S_{emb} = 0.5 \cdot \gamma_{unsat}^{emb} \cdot \Delta h^2 / E_{oed}^{emb}$, where E_{oed}^{emb} is the compression modulus of the embankment material. However, this settlement is negligible as the embankment material is stiff. Hence, $\Delta h \approx S_{emb}$.

The final calculation procedure is almost the same as the trial calculation procedure. After initial conditions are generated and the K-Pressure procedure is performed, it is then followed by applying geogrid and embankment with the final height $h = h_{initial} + \Delta h$. At this calculation phase, updated Lagrange procedure and updated water pressure option are used. After the average settlement at the soft soil surface is determined, the relative settlement reduction can be calculated.

5.3.2 Effectiveness of embankments on floating piles from FE-analyses

FE-calculation results show that an embankment on floating piles is an effective method for soft soil improvement. Figure 5.5 shows the relative settlement reduction against pile length for different soft soil thickness and for specified embankment height above original soft soil surface $h' = 2$ m. It can be seen that the effectiveness of embankment on floating piles, which is determined from relative settlement reduction *RSR*, increases with pile length up to almost one when the pile is end-bearing pile. Indeed, the *RSR* will reach one if a stiff plate is used in between the pile heads and the embankment. It is also shown in the figure that the smaller the soft soil thickness leads to the higher effectiveness.

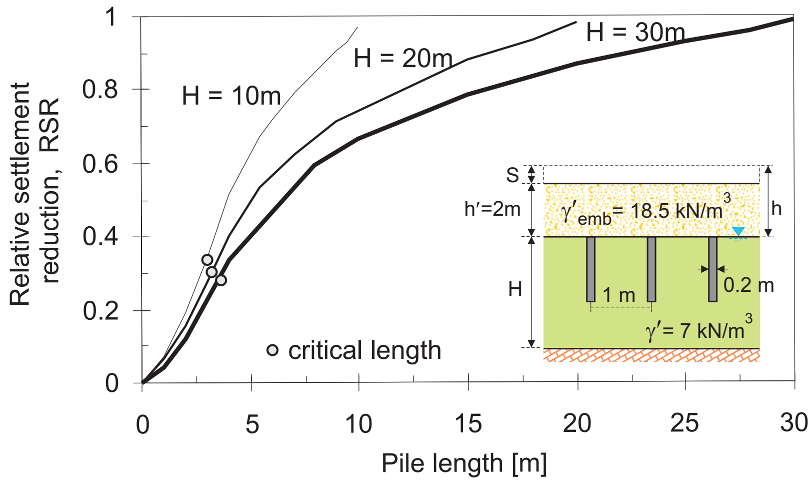

Figure 5.5: Effectiveness of embankment on floating piles for $h' = 2$ m and different soft soil thickness

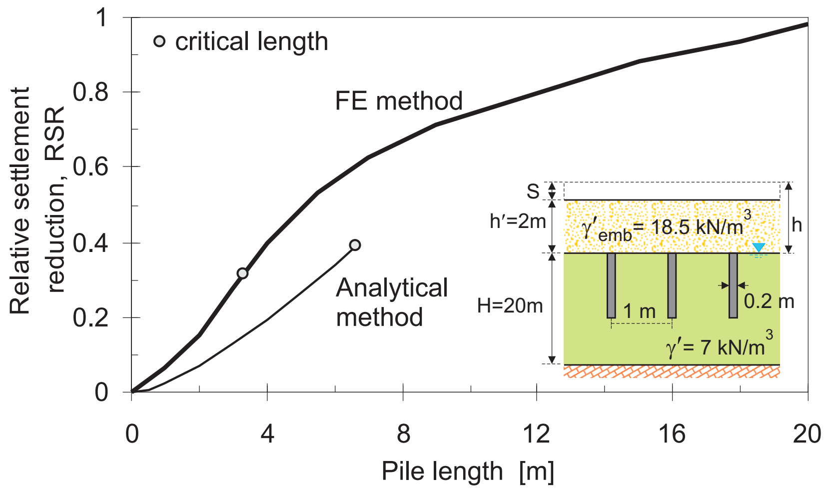

Figure 5.6: Comparison between RSR from analytical and FE methods

In Figure 5.6, the comparison of RSR against pile length curves obtained from analytical and FE methods is presented. Looking at the shape of the curves, both curves from analytical and FE methods show a similar concave shape up to the critical pile length. It is worth repeating that critical pile length is a certain pile length at which the entire embankment load is supported by the pile resistance. For the results of FE-analyses, the critical length $l_{crit,FE}$ is determined by the longest pile length with the entire skin friction along the pile is fully mobilized. For the specified embankment height above original soft soil surface $h' = 2$ m, the critical length is about 3 m and for h' of 1 m and 4 m, they are about 2 m and 4 m respectively. Beyond the critical length, the curve turns to be a convex shape where the increase rate of effectiveness becomes lower. Hence, the results of FE-analyses and analytical method are in agreement qualitatively but not quantitatively.

FE-analyses results show higher effectiveness of embankment on floating piles than what is suggested by analytical approach. This difference is due to the assumption of constant oedometer stiffness in the analytical approach, whereas in the FE-analyses, stress level dependent oedometer stiffness is applied. This is also indicated in Figure 5.6 that the difference of RSR becomes larger as the pile is longer. In addition to that, despite its small contribution in a floating pile, the base resistance of the floating pile is not considered in the analytical approach.

The relation between RSR with the ratio of pile length to the soft soil thickness (l/H) for different h' and different H is presented in Figure 5.7. In general, it is shown that the RSR values are higher than l/H. Moreover, comparing the amount of RSR to l/H, most gained effectiveness of embankment on floating pile is with pile length of about 0.3 to 0.5 times the thickness of soft soil, at least for the case where the soft soil is relatively uniform. Nevertheless, the corresponding settlements should be evaluated since at those lengths, the settlements may still significant.

5.3.3 Block settlement behaviour of floating piles

As a soft soil improvement, a group of floating piles in a certain area of soft soil is intended to act as a unity. This unity behaves like a mechanically improved block, which displaces uniformly. However, this behaviour is not achieved until the floating piles reach a certain length. Figure 5.8 presents vertical settlement shadings for different pile lengths showing block and non-block behaviour. For a long pile, the settlements of the soil in between the piles are uniform. In Figure 5.9, the comparison of vertical settlements in the soft soil along a vertical cross section at the middle of the pile spacing for different lengths of floating piles is presented. It can be seen that the longer the pile, the soft soil settlement along the pile becomes more uniform. Thus, up to a certain length of piles, block behaviour of the soft soil improved by the floating piles occurs.

It is of importance to find a general idea of at which length of floating piles that they begin to behave as a block with the surrounding soft soil. For this purpose, comparison

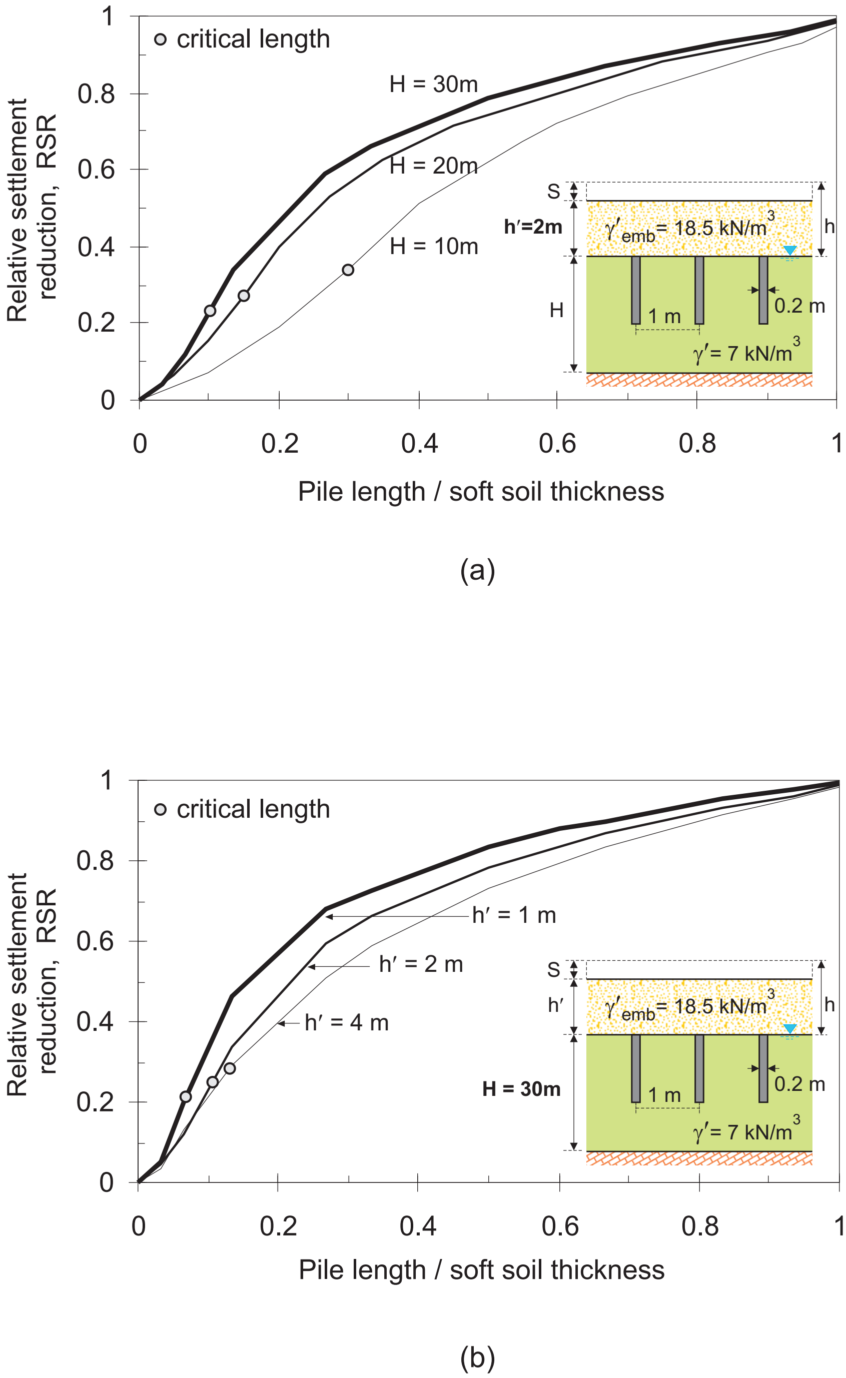

Figure 5.7: Relation between RSR and the ratio of pile length to soft soil thickness (a) Calculated RSR from different soft soil thickness H (b) Calculated RSR from different specified embankment height h'

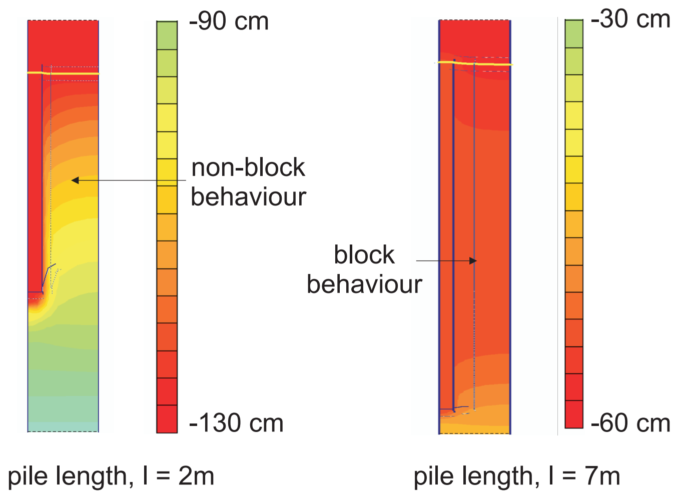

Figure 5.8: Vertical displacement shading for embankment with $h' = 2$m and different pile lengths

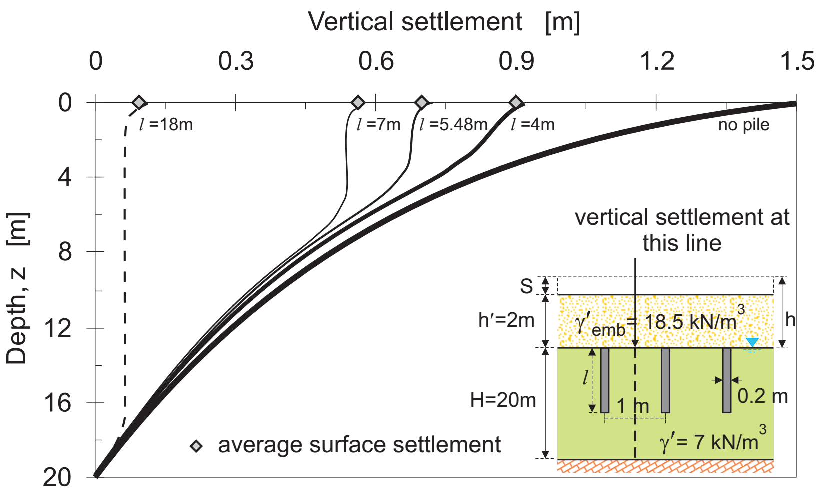

Figure 5.9: Vertical settlement of soft soil at the middle of pile spacing

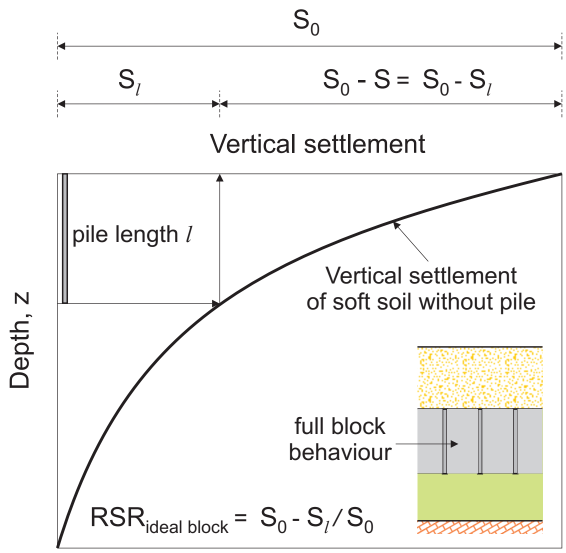

Figure 5.10: Description of the determination of $RSR_{ideal\,block}$

between RSR from FE-analyses with different pile length and from an ideal block behaviour are made. An ideal block behaviour is defined that when the settlement of the soft soil in between the pile is the same as the settlement of the pile-tip as illustrated in Figure 5.10. Hence, $RSR_{ideal\,block}$ is equal to $S_0 - S_l / S_0$. Figures 5.11 show the comparisons between RSR from FE-analyses with different pile lengths and $RSR_{ideal\,block}$ for different specified embankment height h' and soft soil thickness H of 30 m. Similar findings are also found from analyses with soft soil thickness H of 10 m and 20 m (see Appendix C). It is considered that block behaviour of the floating piles begins when the RSR curve from FE-analyses coincide or closely parallel to the $RSR_{ideal\,block}$. Considering the FE-analyses results as illustrated in Figures 5.11, it may be safely mentioned that at critical pile length as determined from analytical approach where $l_{crit} = \sqrt{2q_{emb}/(\beta \cdot \gamma')}$, block behaviour has taken place. However, as can be carefully observed in the figures, the block behaviour begins at pile length of about 20 to 25 percent shorter than the critical pile length l_{crit}. At this length, the skin resistance of the floating piles are not fully mobilized i.e. they are longer than $l_{crit,FE}$. Therefore, from the analyses results and practical point of view, it can be considered that floating piles with full block behaviour begins at pile length of about $0.75 \cdot l_{crit}$.

In addition to that, from the findings of this study, the design of floating piles foundation that fully behave as a block with the surrounding soft soil becomes simple. This simple method is presented in the next section.

5.3.4 Simple design method of floating piles with block behaviour

In a design of floating piles foundation especially for soft soil improvement, it is generally considered to have an acceptable amount of settlement as well as that the floating

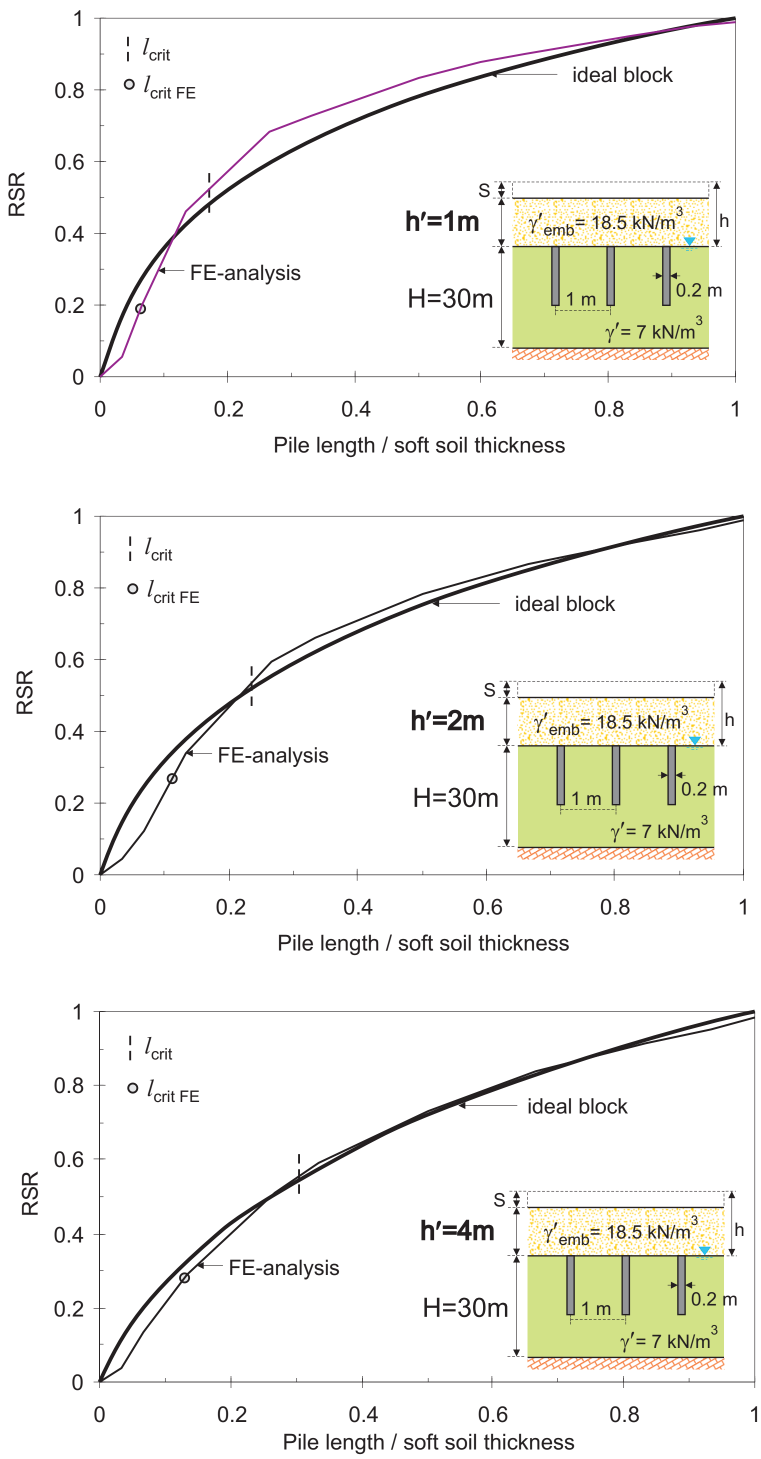

Figure 5.11: Comparison between RSR from FE-analyses with different h' and $RSR_{ideal\ block}$

piles behave fully as block with the surrounding soft soil. Hence, the entire embankment and external load is fully transferred to the soil below the pile-tip and the soft soil in between the piles experiences almost no compression due to embankment load. Indeed, from practical point of view and considering the construction cost, shorter piles might be preferable as long as the settlement requirement is fulfilled. Nevertheless, for this case the analyses of settlement and effectiveness of the floating piles are not simple. On the other hand, when considering floating piles with full block behaviour for example as a preliminary design, the analysis becomes simple. Based on the previous findings, the simple design procedure for a block behaving floating piles can be described in the following steps:

1. For a certain embankment and external load, Block behaviour is achieved when the length of the floating piles is chosen as equal to $0.75 \cdot l_{crit}$, where

   $$l_{crit} = \sqrt{\frac{2 \cdot (\gamma'_{emb} \cdot h + q)}{\beta \cdot \gamma'}}$$

   where q is the uniformly distributed load on the embankment surface. For a specified embankment height h', this is done iteratively.

2. Produce a curve of settlement against depth for unimproved soft soil due to embankment and external load. This can be done using one dimensional compression calculation.

3. Determine the settlement at the pile-tip S_l of the pile with the length of $0.75 \cdot l_{crit}$ as illustrated in Figure 5.10. For block behaviour the settlement of pile-tip is equal to the amount of settlement at a depth equal to $0.75 \cdot l_{crit}$ from the curve obtained in step 2.

4. Effectiveness of the floating piles can be determined by calculating the relative settlement reduction RSR.

When designing a floating pile foundation, it is common that the pile length is designed to a depth where the embankment and external load is far below the preconsolidation pressure of the soil at that depth. This is done so that only little settlement occurs due to higher compression modulus of the soil. A pile length, which is equal to this depth, is in general longer than the critical pile length depending on spacing of the piles. Therefore, the simple design procedure suggested above is considered very useful for practical engineers. Moreover, one needs to produce only a settlement curve against depth from one dimensional compression calculation. This can also be obtained without FE-calculation. the accepted amount of settlements must be judge in order to suit the financial and material availability for the embankment size and the pile length.

Apart from that, there is a concern on the risk of differential settlements on using floating piles due to the non-homogeneity of the soft soil. However, this risk should be small upon appropriate design length of the floating pile foundation. One might argue that end-bearing piles are more preferable to ensure no differential settlements occur.

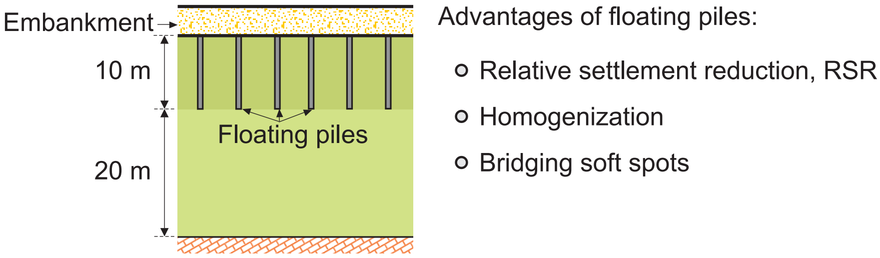

Figure 5.12: Advantages of floating piles for thick soft soils improvement

However, when considering an embankment on large soft soil thickness of for example 30 m, end-bearing piles are much too expensive. Hence, floating piles foundation is a realistic and safe way rather than without improving the soft soil. In addition, floating piles foundation is a familiar method that gives many advantages as shown in Figure 5.12.

Indeed, for a special case such as for bridge approach embankment where no differential settlements are allowed, long piles that are close to end-bearing piles need to be installed. The pile length can be reduced gradually as the embankment is in further distance from the bridge. In addition to that, a special connector is often applied between the bridge and the approach embankment to avoid sudden differential settlements.

5.4 Conclusions on settlement analysis of embankments on floating piles

On the design of embankments on floating piles, engineers have to deal with settlements. For that reason, settlement analysis needs to be performed to determined the effectiveness of the system based on the relative settlement reduction. Settlements become a problem when it implies differential settlements. The installation of floating piles reduce the total settlements of the piled embankments. No doubt that a reduction of total settlements will also reduce differential settlements. Moreover, the floating piles transfer the main embankment load to the deeper and stiffer stratum around the piles-tip. This gives the effect of bridging soft spots in the soft soil around the surface in between the piles. Hence, the floating piles render the soft soil in between the pile to become more homogeneous. This is apparently shown when the floating piles and the surrounding soft soil has reached a block behaviour.

Approaches for assessing the settlements and the effectiveness of embankments on floating piles using analytical and FE-method have been shown. It is found that, generally, an embankment on floating piles is an effective method for soft soil improvement.

Despite the use of simplifications, analytical approach is useful for understanding the general settlement behaviour of an embankment supported by floating piles and for the estimation of critical pile length. No doubt that the use of FE-method gives a more detailed and accurate prediction of the settlement behaviour.

Based on more accurate analyses using FE-method, the effectiveness of embankments supported by floating piles increases with pile length up to a design with end-bearing piles. The rate of effectiveness increases as the pile length closer to critical pile length and the rate of effectiveness decreases beyond pile critical length. The most cost effective construction is achieved when the ratio of pile length to the soft soil thickness is between 0.3 and 0.5. However, the corresponding embankment settlements should be carefully considered since at those lengths, the settlements may still be significant. Finally, a judgement must be taken on the accepted amount of settlements in order to suit the financial and material availability for the embankment size and the pile length.

Up to a certain pile length, soft soil improved by floating piles behave as a mechanically improved block, where the soft soil and the pile deform uniformly. It is found that the piles and the surrounding soft soil behave as a block when the pile length is about 75 percent of the estimated critical pile length l_{crit}. Furthermore, a simple method for the effectiveness of embankments on floating piles based on the concept of block behaviour has been presented. This method is very useful and easy to be used in practice.

Chapter 6

Case study of an embankment on floating piles

In this chapter, a three dimensional case study of an embankment on floating piles is described. The embankment is built on very thick and very soft clay layers, which are known to have a significant secondary settlement due to creep effect. In geotechnical engineering, the additional settlement of a soft soil in time under a constant load is referred to as pure creep. Apparently, creep also happens during the primary consolidation process where the load is not constant. Hence, in general, creep can be described as the viscous effect of soft soils under an effective stress, which causes secondary settlement. The creep behaviour of the soft clays are modelled using the Soft Soil Creep model (see also Appendix A.3). For that purpose, reliable material data for the Soft Soil Creep model are determined by back analyzing the constant rate of strain (CRS) oedometer tests data of several soft soil samples taken from different depths. The FE-analyses focus on the predicted settlement behaviour of the embankment on floating piles. Particular importance on the choice of pile lengths as used in the current embankment on floating piles related to the settlement is highlighted.

6.1 Nödinge test embankment on floating piles

For the development of infrastructure in western Sweden, a highway and a double railroad track for high-speed trains are being planned in the eastern part of the Göta river valley. Since the soil at the site is known for its deep deposit of very soft clays, soil improvement needs to be undertaken, so that the serviceability of the infrastructure is assured throughout its life time. In the preliminary design stage, soil improvement with floating piles is found to be the most suitable option (Olsson et al., 2008). To evaluate the settlement behaviour of the soft clays improved with floating piles and to improve the quality of the settlement calculation, several test-embankments on floating piles were constructed. One of them is located at Nödinge site and it is chosen for the back-analysis of a case study of an embankment on floating piles. Detail descriptions of the Nödinge test embankment and the settlement measurements have been reported by Alén et al. (2005) and Olsson et al. (2008).

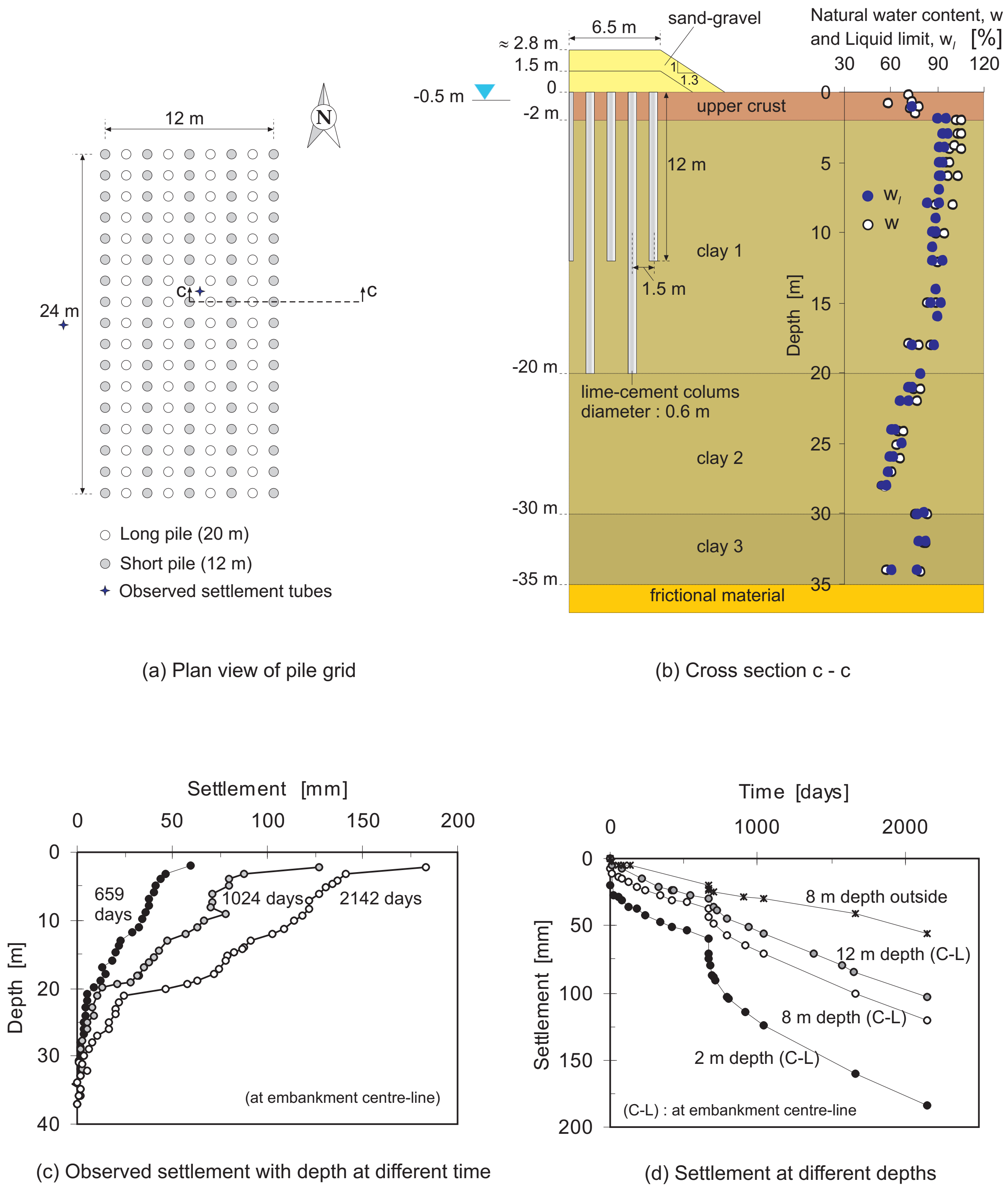

Figure 6.1: Nödinge embankment on floating piles configuration and measured settlements at settlement tubes (after Olsson et al., 2008)

Figures 6.1 illustrate the construction and the settlement measurements of the Nödinge test-embankment on very soft soils. The very soft soils at the Nödinge site are indicated by their natural water contents, which are almost the same as their liquid limit as shown in Figure 6.1b. The very soft soils consist of relatively homogeneous, thick and nearly normally consolidated clays up to a depth of about 35 m. Underneath the clays, there is a layer of a several metres of sandy soil underlain by bed-rock. The ground water level is around 0.5 m below the ground surface.

The floating piles for the soft soil improvement are made of lime-cement columns. A total of 153 lime-cement columns (LCCs) are installed in a square pattern as shown in Figure 6.1a. As illustrated in Figure 6.1b, the LCCs are installed with a length of 12 m in every other row and a length of 20 m for the row in between. The diameter of the LCCs is 0.6 m and they are spaced centre-to-centre of 1.5 m. The LCCs are constructed using dry mixing method. The mixture consists of 45 kg lime and 45 kg cement per cubic metre lime-cement-soil mixture. The installation of the LCCs was carried out in May 2001, about 7 months before the embankment construction. It is measured that the quality of the LCCs is relatively low down to a depth of 2 to 4 m and below that, the quality of the LCCs is very good. This is also indicated in Figure 6.1c. The main large settlements occurs at around 2 to 4 m depth of the LCCs-improved clay layers. The permeability k of the LCCs varies between $0.5{\cdot}10^{-8}$ to $5{\cdot}10^{-8}$ m/s.

The embankment has a crest length of 25 m and a crest width of 13 m. It is constructed in two stages. In the first stage, the embankment is raised to 1.5 m, which is equal to a load of 25 kPa on the soft soil surface and the piles. After one and a half years, the second stage of the embankment is constructed to give a total load of about 50 kPa on the soft soil surface. Several measurement devices, namely settlement hoses, piezometers and inclinometers are installed in the soft clay as well as in the lime-cement columns.

Measurements on settlements are performed during a period of 6 years. Figure 6.1c and d show the the measured settlements at the settlement hoses as indicated in Figure 6.1a. It can be seen that after almost six years, the settlements show no tendency to level off. The settlements will continue to progress for some time, which indicates that the creep process in the clay layers is significant. In 2007, the test embankment was removed due to the construction of a railway track.

6.2 Calibration of material properties

Typical soil data of Nödinge soils show that the average saturated unit weight $\gamma_{saturated}$ of the clays is about 15.5 kN/m^3. The clays have effective friction angle φ' around 29° to 31° and a low effective cohesion c', which is typically lower than 1 kPa except for the clay around the surface up to 2 m depth. This layer has a higher overconsolidation ratio OCR and a higher effective cohesion.

In Sweden, so-called constant rate of strain (CRS) oedometer tests are often used to determine the compression properties of soft soils (Larsson and Sällfors, 1986). In contrast

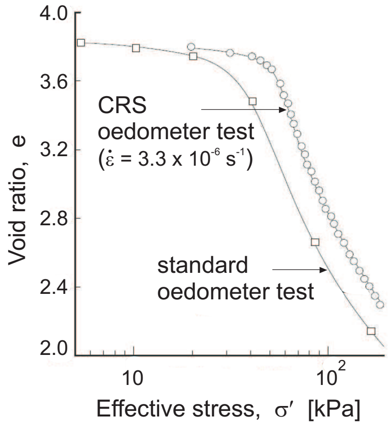

Figure 6.2: Comparison between the result of CRS and standard oedometer test (Hanzawa, 1989)

to the standard oedometer test, in CRS oedometer test, the soil sample is compressed continuously with a constant compression speed. Hence the rate of strain in the sample with respect to the original sample height is constant. The CRS oedometer test can be performed relatively quickly within one day, which is much faster than the standard oedometer test with 24 hours incremental loading steps that takes one to two weeks to complete. Hanzawa (1989) shows a typical comparison of void ratio e versus logarithmic effective stress $\log \sigma'$ curve from CRS oedometer test and from standard oedometer test as illustrated in Figure 6.2. It is shown that the $e - \log \sigma'$ curve from CRS oedometer test resembles the one from the standard oedometer test. The slope of the normally consolidated (NC) line from both curves are more or less the same. However, depending on the compression speed, the $e - \log \sigma'$curve from CRS oedometer test shifts horizontally compared to the one from standard oedometer test. As a consequence, it gives slightly different preconsolidation pressure from the standard oedometer test.

Despite that the material properties of the soft clays can be determined directly from the CRS oedometer results, the material properties as used for the Soft Soil Creep model are best obtained by back analyzing the results of the CRS oedometer tests, especially for the value of over consolidation ratio. Hence, the Soft Soil model with the calibrated properties can closely represent the real soft clays behaviour. The Soft Soil Creep model involves several parameters: the modified compression index $\lambda^\star$, the modified swelling index $\kappa^\star$, the modified creep index $\mu^\star$, effective friction angle φ', effective cohesion c' and unloading-reloading Poisson's ratio ν_{ur}[(1)]. For the calibration of the material parameters, FE-simulation of CRS oedometer tests are performed for several soil samples from different depths. The FE-back analyses focus on calibrating the calculated $\varepsilon_y - \ln \sigma'_y$ curves to the measured ones from CRS oedometer tests. The calculation procedure is described in the next section.

[1]a detailed description on the Soft Soil Creep model and its properties can be seen in Appendix A.3

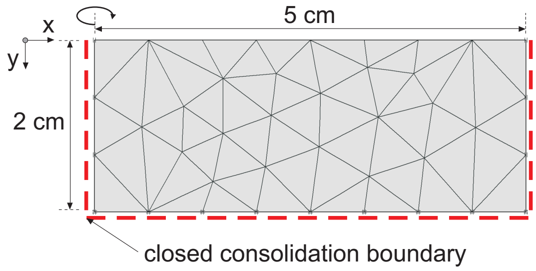

Figure 6.3: FE-mesh as used for the CRS oedometer test simulation

6.2.1 FE-back analyses of CRS oedometer tests

In order to simulate the CRS oedometer tests, axisymmetrical FE-mesh as shown in Figure 6.3 is used. The mesh consists of six-noded triangular elements with three Gaussian integration points. The mesh is 2 cm high and 5 cm wide. For the boundary conditions, at the side of the mesh, the horizontal displacement is prevented and at the bottom of the mesh both horizontal and vertical displacements are constrained. The phreatic water level is set at the soft soil surface. For consolidation calculation, closed consolidation boundary is set at the sides and the bottom of the mesh. Hence, the dissipation of excess pore water pressure is only allowed at the top of the mesh. Considering the CRS simulation which involves consolidation and creep analysis, the mesh as shown in Figure 6.3 was evaluated and it gives a converge result compared to using finer mesh.

The effective strength parameters of the clays are given and the stiffness parameter $\lambda^\star$ can be determined relatively accurately from the stress-strain curve obtained from the CRS oedometer tests. Based on the $\lambda^\star$ values, the $\kappa^\star$ and $\mu^\star$ values can be estimated based on the typical values, which are $\kappa^\star \approx \lambda^\star/10$ and $\mu^\star \approx \lambda^\star/30$. Hence, the FE-back analyses of the CRS oedometer tests are mainly for calibrating the overconsolidation ratio OCR of the clays.

The calculation procedure for the back analysis of the CRS oedometer test consists of six phases, which can be described as follows:

1. The initial condition is generated assuming a K_0^{NC}-condition for the soft clay, with K_0^{NC}-value according to Jaky's formula. In doing so, the Soft Soil creep properties for the soft clay sample are first assumed with typical values. In addition, the phreatic water pressure is also initialized.

2. An overburden load, which corresponds to the effective soil weight above the sample depth, is applied. This loading is performed very quickly and in drained condition.

3. The loaded sample is let creep for some time to achieve a trial value of OCR that is around the known value based on experience and measurement of typical soil in that area. For Nödinge clay, the typical value of OCR is around 1.1 to 1.3 (Olsson et al., 2008). It is known that the Nödinge clay has never been preloaded before. Hence, the lightly overconsolidated state of the soil is mainly due to creep.

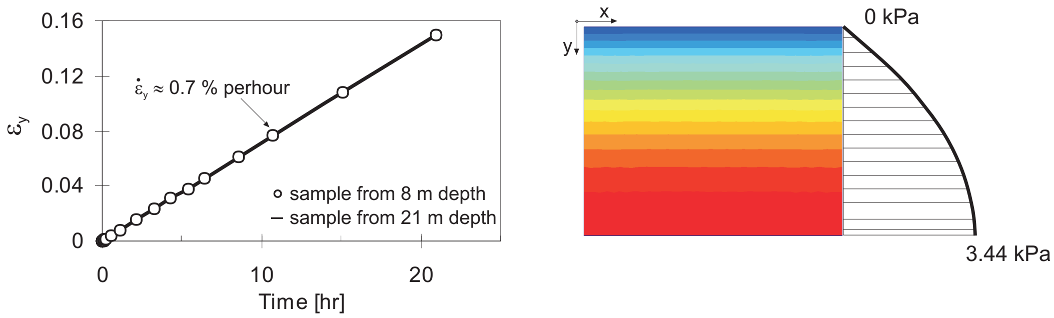

(a) Strain rate from FE-CRS simulation

(b) Excess pore water pressure after FE-CRS simulation

Figure 6.4: Calculation results of FE-CRS oedometer simulation

Table 6.1: Calibrated soil properties for the Soft Soil Creep model

Sample depth [m]	Soil layer [-]	$\lambda^\star$ [-]	$\kappa^\star$ [-]	$\mu^\star$ [-]	φ' [°]	c' [kPa]	OCR [-]	ν_{ur} [-]
2	Upper crust	0.28	0.028	0.014	29	2	1.95	0.15
8	Clay 1	0.26	0.017	0.0083	30	0.1	1.26	0.15
18							1.14	
21	Clay 2	0.26	0.017	0.0083	30	0.1	1.39	0.15

4. The overburden load is reduced down to the starting vertical stress as shown in the $\varepsilon_y - \ln \sigma'_y$ curve from the measured CRS oedometer test. This is done very quickly and in drained condition.
5. The sample settlement is set back to zero and it is followed by the simulation of CRS oedometer loading. The CRS oedometer tests are executed with a strain rate of 0.7 % per-hour. For a soil sample of 2 cm height, this gives a compression speed of 0.014 cm/hour. The CRS tests are loaded up to an axial strain of about 0.15. Hence, the final displacement of the soil sample is 0.3 cm in a testing duration of 21 hours. The FE-CRS loading is performed in consolidation analysis by applying a prescribed displacement of 0.3 cm on top of the soil sample within 21 hours time.
6. Repeat the procedure by varying the trial OCR value until a best fit calculated $\varepsilon_y - \ln \sigma'_y$ curve to the measured one is obtained.

As illustrated in Figure 6.4a, the ε_y − time curves from FE-calculations taken at a stress point in the middle of the sample are almost linear. This shows that a consistent strain rate of 0.7 % perhour is achieved in each calculation step. Figure 6.4b shows the excess pore water pressure shading at the end of FE-CRS loading, which resembles the typical excess pore water pressure distribution after a CRS oedometer test.

Figure 6.5 shows the calibration curves from FE-analyses compared to the CRS oedome-

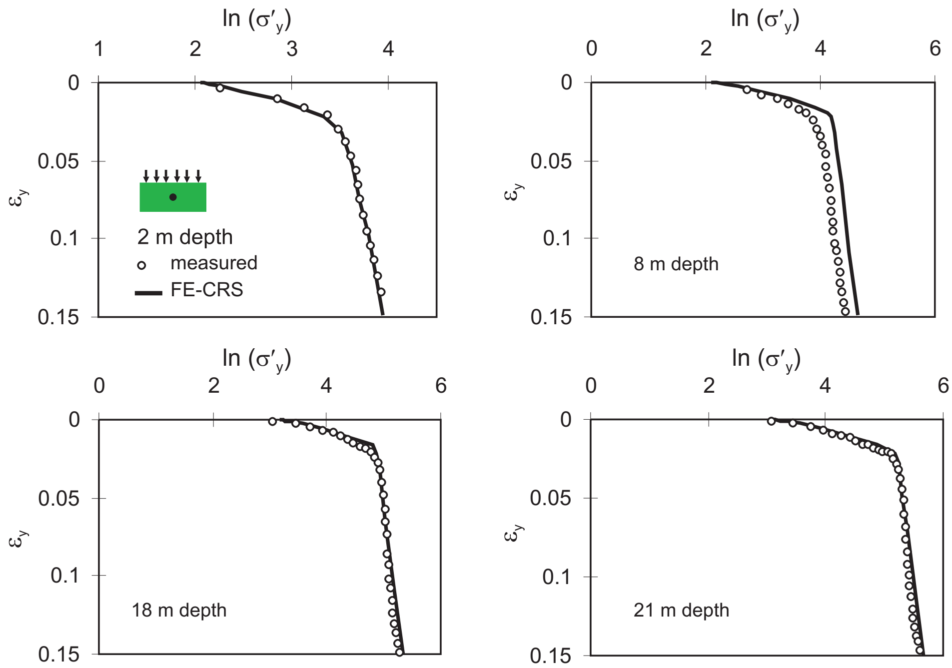

Figure 6.5: Calibration curves from FE-CRS oedometer simulations

ter test results. The calibrated soft clay properties as used in the Soft Soil Creep model are listed in Table 6.1. The soil sample from 8 m depth and 18 m depth belong to the same clay layer. Hence, the calibrated soil properties for both sample are taken the same. However, for sample depth of 8 m, perfect match of the calculated curve to the measured one cannot be obtained. As a consequence, it gives slightly higher OCR value compared to the measurement. Nevertheless, for this clay layer, an average OCR of 1.2, which is also the typical values from measurements can be considered. No doubt that general behaviour of the soil from experience and previous measurements should be bared in mind to confirm the reliability of the used input soil properties in numerical analysis.

6.3 FE-Creep analysis of Nödinge test embankment

The FE-creep analysis of the Nödinge test embankment on floating piles is performed three dimensionally using the mesh as shown in Figure 6.6. The 3D-mesh has a size of 38.5 m x 35 m x 1.5 m. About four thousand 15-noded wedge elements with six Gaussian integration points for each element are used. The average size of the elements is about 70 cm.

As for the boundary conditions, horizontal displacement is prevented and vertical displacement is let free at the side boundaries. Both horizontal and vertical displacements are prevented at the bottom boundary. For consolidation analysis, closed consolidation boundary is set at the sides of the mesh while the top and bottom boundaries are open

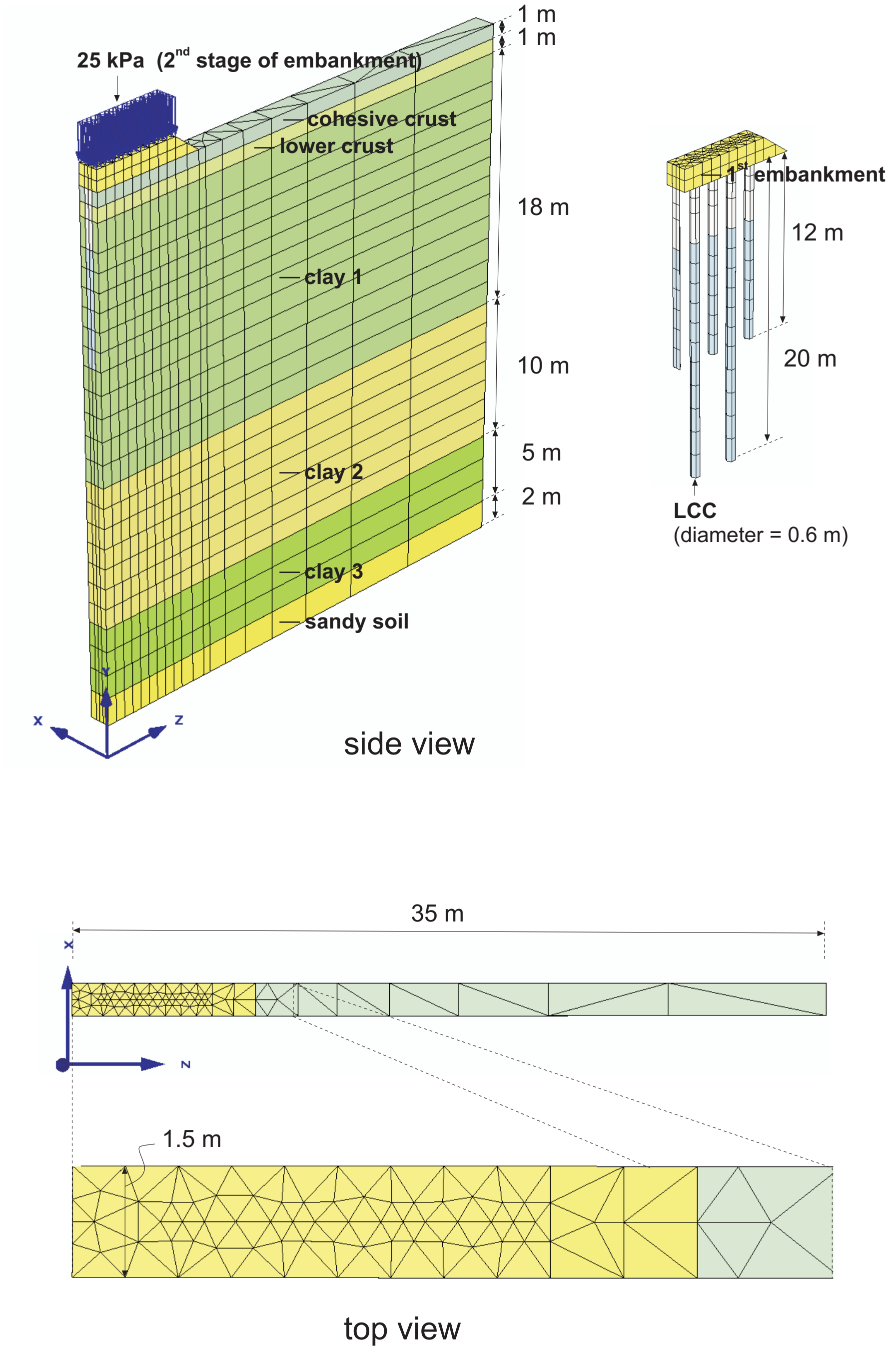

Figure 6.6: 3D FE-mesh as used for the Nödinge embankment on floating piles analyses

Table 6.2: Clay parameters as used for the Soft Soil Creep model

Properties		Cohesive crust	Lower crust	Clay 1	Clay 2	Clay 3
Thickness	[m]	1	1	18	10	5
$\gamma_{saturated}$	[kN/m^3]	15.5	15.5	15.5	15.5	15.5
φ'	[°]	30	29	30	30	31
c'	[kPa]	8	2	0.1	0.1	1
$\lambda^\star$	[-]	0.28	0.28	0.26	0.26	0.08
$\kappa^\star$	[-]	0.028	0.028	0.017	0.017	0.008
$\mu^\star$	[-]	0.014	0.014	0.0083	0.0083	0.0026
OCR	[-]	1.95	1.95	1.2	1.39	1.39
ν_{ur}	[-]	0.15	0.15	0.15	0.15	0.15
k	[m/day]	$1{\cdot}10^{-4}$	$1{\cdot}10^{-4}$	$1{\cdot}10^{-4}$	$1{\cdot}10^{-4}$	$1{\cdot}10^{-4}$

for the dissipation of excess pore water pressure.

The embankment material behaviour is modelled using the Hardening Soil model and the soft clays are modelled using the Soft Soil Creep model. For the dense sandy soil at the very bottom of the soil layers, the behaviour is modelled using the Mohr-Coulomb model. The material parameters as used in the FE-analysis of the embankment on floating piles are listed in Table 6.2 and Table 6.3. As can be seen in Table 6.2, the topmost clay layer down to 1 m depth has higher effective cohesion. This is assumed to account for higher cohesion due to thick vegetation as well as some preloading as a result of ground water fluctuation. The LCCs are assumed to behave elastically. It known that the quality of the upper part of the LCCs are low. Hence, the elastic stiffness of the LCCs is assumed to be 10 MPa down to 2m depth and it increases linearly to 160 MPa at 4m depth. Below a depth of 4 m, the elastic stiffness of the LCCs is constant of 160 MPa. The permeability k of the LCCs is chosen to be $8.7{\cdot}10^{-4}$ m/day, which is ten times larger than the permeability of the clay soils as also measured in the field.

For the initial conditions, the initial stresses are generated using K_0-procedure as described previously with K_0-value according to Jaky's formula. In addition to that, the phreatic water pressure is also generated.

The calculation stages follow the actual construction stages of the embankment on floating piles. After the generation of initial stresses conditions, the floating piles are installed. In Section 4.3, it is shown that installation process can be simulated using the K-Pressure method. The piles used for the Nödinge test-embankment consist of piles with different lengths, which require 3D analysis. For 3D analysis, there is a possibility of using the K-Pressure method indirectly by converting the calculation results into the pseudo displacement cavity expansion method. However, data on pile load tests are not available for back calculating the K-value. The lime cement columns are consi-

Table 6.3: Soil parameters for the embankment and bottom-most sandy soil

Properties		Embankment (HS model)	Sandy soil (MC model)
Thickness	[m]	1.5	2
$\gamma / \gamma_{saturated}$	[kN/m^3	17 / -	20 / -
φ'	[°]	45	40
c'	[kPa]	0.1	0.1
ψ	[°]	10	10
E_{50}^{ref}	[MPa]	70	-
E_{oed}^{ref}	[MPa]	70	-
E_{ur}^{ref} / E	[MPa]	280 / -	- / 120
k	[m/day]	2	2

dered as partial displacement piles with low degree of soil displacement. Hence, the increase of radial stress is low with the resulting K-value is close to the K_0-value of the soil. In present analysis, the K-value is assume to be the same as the K_0-value and the piles are installed wished in place. This calculation is performed under a drained condition since the real time lag between piles installation and the first embankment loading is about 7 months, which implies that excess pore water pressure due to piles installation is already dissipated. After that, the first embankment of 1.5 m high is applied in 8 hours under an undrained condition. This stage is followed by a 660 days consolidation calculation. In the next stage, the second embankment is applied. Due to some deformation and convergence problems in the numerical calculation, the second embankment fill is simulated using a uniformly distributed load of 25 kPa applied on top of the first embankment instead of applying another soil layer. This stage lasts 8 hours under an undrained condition. After that, a consolidation analysis is performed for 2142 days.

Figure 6.7 shows some of the calculation outputs after consolidation of 660 days. As can be seen in Figure 6.7a, b and c, the largest deformation after 660 days consolidation occurs around the slope at the side of the embankment. This is because the outer pile is installed half a metre inside the outer crest of the embankment. Hence, the embankment slope is not supported by pile. As a result, large vertical and horizontal deformations occur, which may lead to slope stability problem.

In Figure 6.7d, it can be seen that the excess pore water pressure in the soil has dissipated to 16 kPa from the initial excess pore water pressure of about 23 kPa after embankment construction. The residual excess pore water pressure concentrates at around the piles tip, where the embankment load is largely transferred by the piles.

Beside the creep analysis with the actual embankment on piles geometry as described above, several analyses are also performed with different uniform pile lengths and also without installing piles for settlement comparison.

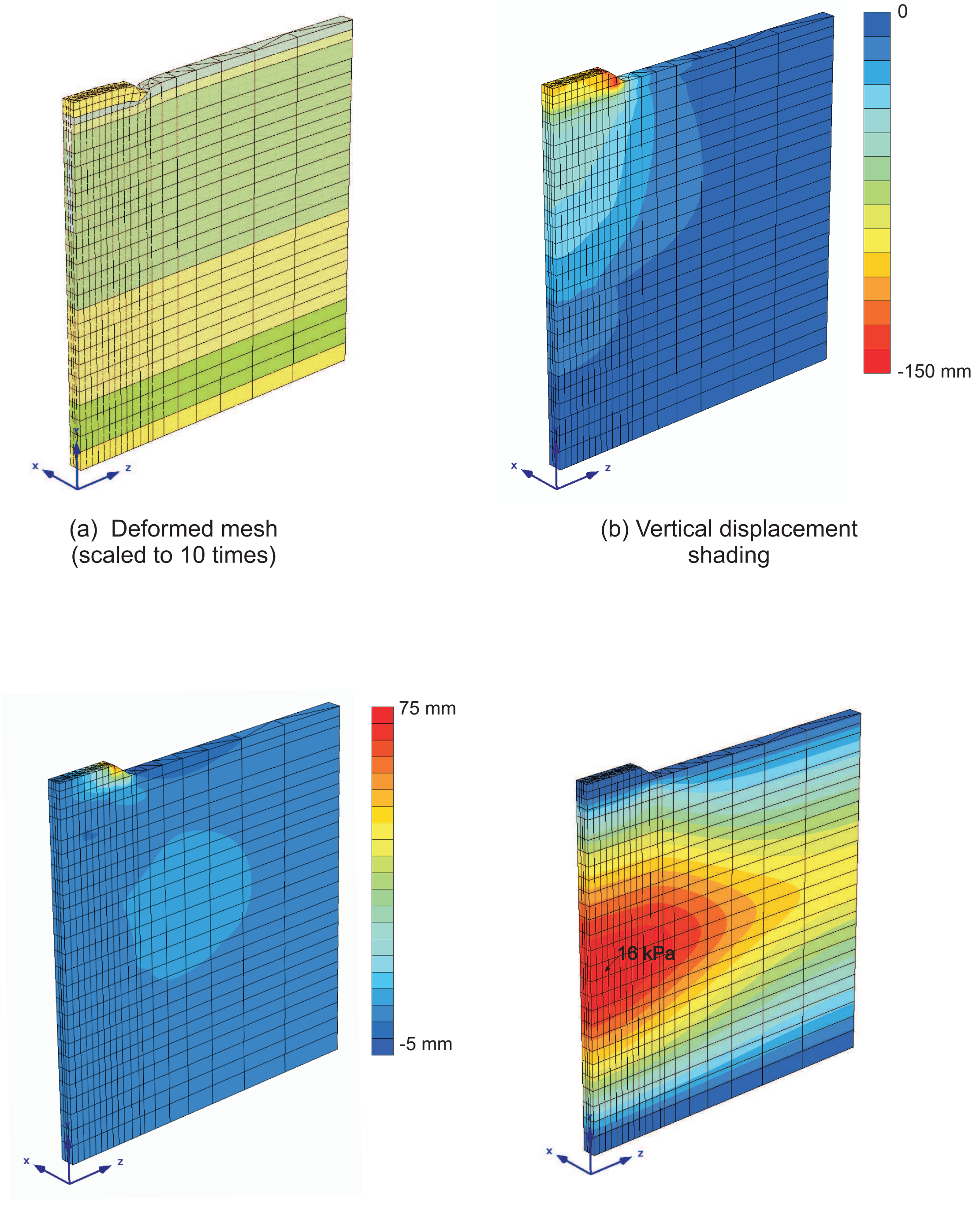

(a) Deformed mesh (scaled to 10 times)

(b) Vertical displacement shading

(c) Horizontal displacement shading (u_z)

(d) Excess pore water pressure

Figure 6.7: Calculation outputs for 1st stage of loading up to embankment height of 1.5 m after consolidation of 660 days

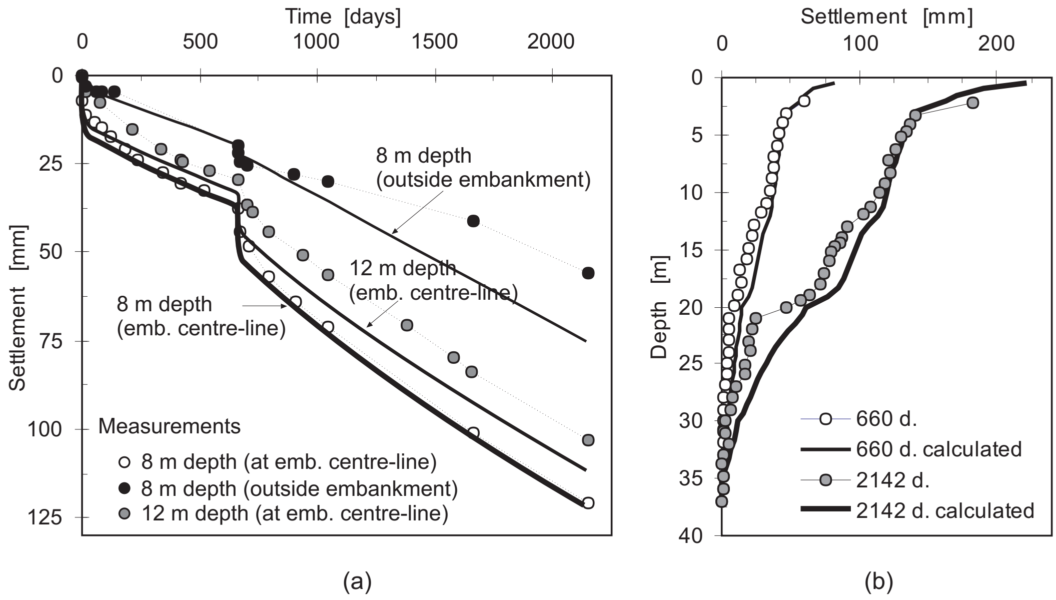

Figure 6.8: Calculated settlements at three different locations (a) Vertical settlement in time (b) Vertical settlement with depth at embankment centre-line

6.3.1 Settlement prediction

To be able to closely predict the settlement of the embankment on floating piles is very important. So that improvement measures can early be considered and applied on time. Figure 6.8a shows the calculated vertical settlements in time at three different locations compared to the corresponding measured settlement. It can be seen that the calculations give good agreements to measurements. The same case is also shown for the vertical settlements with depth as illustrated in Figure 6.8b. Nevertheless, the calculated amount of settlements at depth of 10 m to 25 m are slightly higher than the measurements. This may be due to variability of soil in the thick clay 1 and clay 2 layers. In the calculation, the thick clay layers are considered as homogeneous soil layers with each having a set of parameters. Despite this imperfection, it can be seen that overall, the FE-calculation can predict the measurements well.

Figure 6.9 shows the prediction of settlement in 40 years time. 40 years is a typical life time of a road embankment before maintenance such as embankment overlay is applied. It can be seen in the figure that the compression of the soil at around the surface after each embankment lift is significant compared to the overall settlement of the embankment on floating piles. This is mainly due to the low quality of the upper part of the LCCs as mentioned by Olsson et al. (2008). Hence, improvement on the method and control of the LCCs construction especially at the upper part around the ground surface need to be considered for a better settlement reduction.

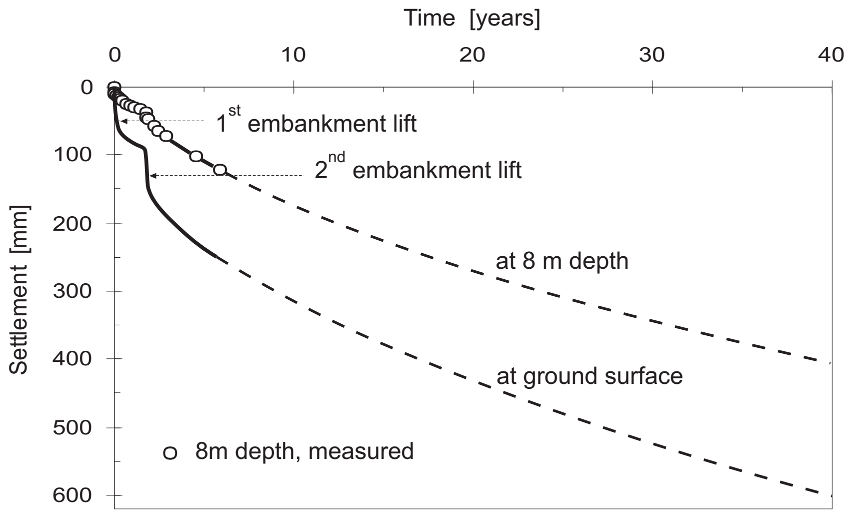

Figure 6.9: Settlement prediction in time at embankment centre-line

6.3.2 Influence of pile length

In the actual construction of the embankment on floating piles, the piles are installed with a length of 12 m in every other row and a length of 20 m for the row in between. It is of interest to evaluate the influence of the chosen pile length on the primary settlement and the secondary settlement behaviour due to creep process of the embankment on floating piles. For this reason, the results of stress distribution at the ground surface and settlement behaviour from the actual construction are compared to the ones from construction with uniform pile length of 12 m and 20 m.

When considering a skin friction floating pile as illustrated in Chapter 5, the required pile length so that the entire embankment load is supported by the pile, is at the pile critical length l_{crit}. For the 50 kPa embankment load in the Nödinge test embankment, the critical pile length l_{crit} can be calculated using Equation 5.11 to give l_{crit} of 9 m with K-value taken as equal to K_0^{NC}-value of the soil. Therefore, all piles are slightly over capacity and they can bear the entire load of the embankment. Based on the study in Section 5.3.3, full block behaviour has occurred for floating piles at the current lengths. Figure 6.10a shows the principal stresses in the embankment after 660 days consolidation from the actual construction. It indicates the development of arching action, which transfers the main part of the embankment load to the piles. As illustrated in Figure 6.10, the vertical stress distributions at the ground surface along line A-A from the actual construction and constructions with uniform pile lengths of 12 m and 20 m after consolidation of 660 days are almost the same. This suggests that the use of all short piles of 12 m is already adequate to support the embankment load.

However, the settlement in time as shown in Figure 6.11 highlights the importance of the current choice of pile lengths compared to the other constructions. It is shown that the actual applied pile lengths reduce the long-term settlement significantly compared

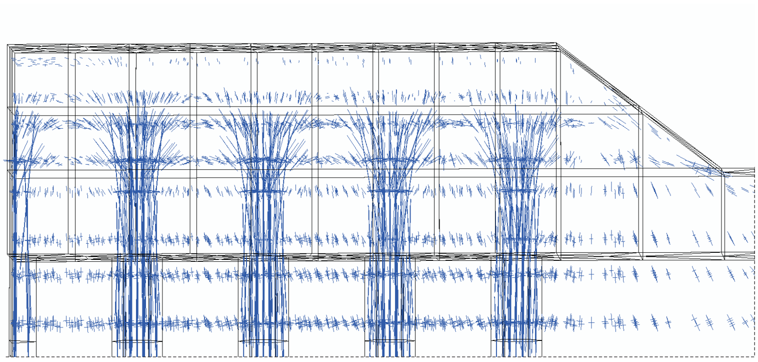

(a)

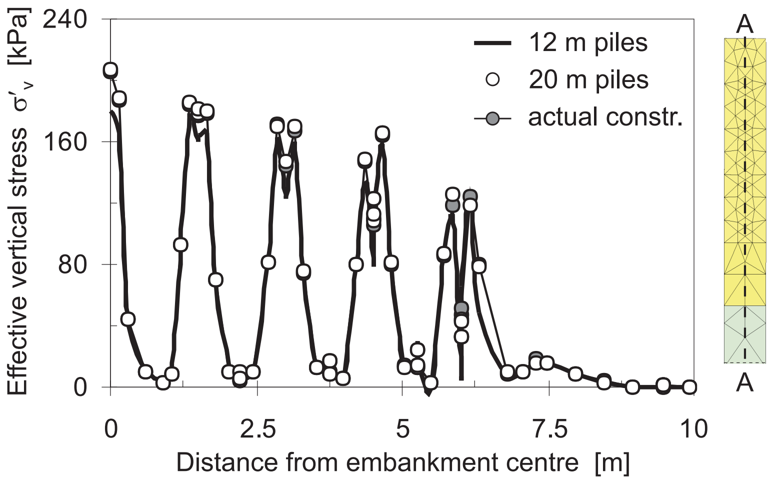

(b)

Figure 6.10: Developed arching action in the embankment after 660 days consolidation (a) Principal stresses (b) Comparison of vertical stress on the ground surface taken at along line A-A

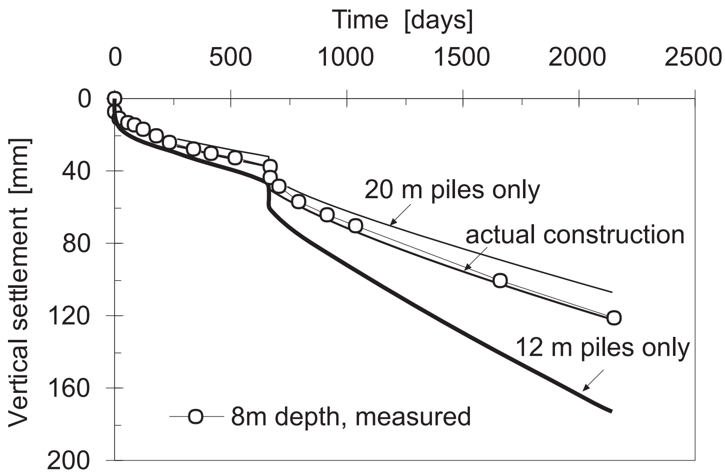

Figure 6.11: Comparison of vertical settlement at 8 m depth at the centre-line of the embankment from different pile lengths

to when using only short piles of 12 m. In addition to that, there is not much gain in settlement reduction when using only long piles of 20 m. Hence, the chosen actual pile lengths show a clear advantage of saving construction cost as well as obtaining an effective settlement improvement of the soft soil.

From this analysis, it is understood that the use of several long piles of 20 m is not intended for increasing the bearing capacity of the piles, but it is used for further long-term settlement reduction due to creep. It is known that the piles transfer the embankment load to the deeper soil around the pile tip. As shown by Vermeer and Neher (1999) and Leoni et al. (2008), creep rate depends on the degree of overconsolidation in the soil. For one dimensional creep, the rate of change in void ratio is written as

$$\dot{e} = -\frac{C_\alpha}{\tau \cdot \ln 10} \cdot \left(\frac{\sigma'}{\sigma'_p}\right)^{\beta} \qquad with \qquad \beta = \frac{C_c - C_s}{C_\alpha} \tag{6.1}$$

where C_c, C_s, C_α are the compression index, swelling index, and creep index obtained from the oedometer test respectively. τ is a particular reference time, which can mostly be taken equal to one day, σ' is the current effective stress in the soil and σ'_p is the preconsolidation pressure of the soil. Typical soft soil data give $C_s \approx C_c/10$ and $C_\alpha \approx C_c/30$. This gives β of about 27. The more embankment load is transferred to the deeper soil the higher the overconsolidation ratio (σ'_p/σ'). As a consequence, it yields lower rate of change in void ratio. Hence, the use of long piles reduce the long term settlement due to creep.

In Chapter 5, it is shown that the effectiveness of an embankment on floating piles can be assessed by the relative settlement reduction RSR. In order to evaluate the effectiveness of the actual construction, the settlement at the ground surface is compared to the one from embankment on the soft clays without piles. Figure 6.12 shows this comparison. It

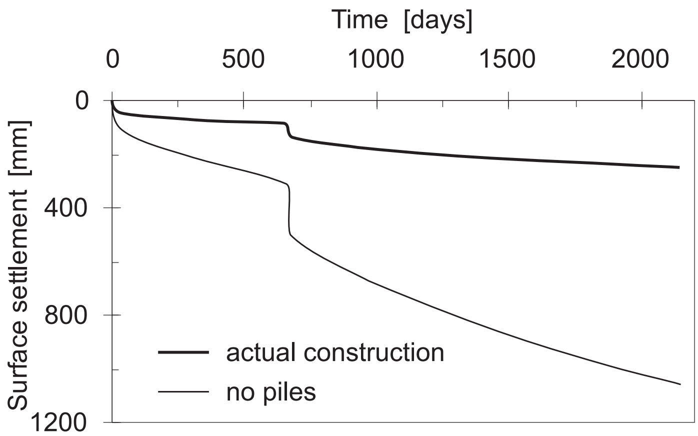

Figure 6.12: Comparison between ground surface settlements at embankment centre-line with actual construction and without installing piles

can be seen that the effectiveness of the actual construction after about 6 years is about 76 percent. The effectiveness continues to increase in time due to further creep settlement.

6.4 Conclusions on case study of an embankment on floating piles

Nödinge trial embankment on floating piles were built to validate the preliminary design calculations for the road and railway expansion project in Sweden. It provides actual data especially on the settlement behaviour of embankment on floating piles in time. The availability of data and advanced tools, namely FE-method and advanced soil constitutive models, enable the simulation of embankment construction and detail evaluation of its settlement behaviour in time.

The Nödinge test-embankment are built on floating piles with different lengths. For such case, the FE-analyses can not be performed using axisymmetrical geometry. Hence, 3D analysis is the only good way to simulate the case study.

FE-creep analysis of the Nödinge embankment has been performed. In the analysis, a procedure for calibrating soil parameters from the CRS oedometer test results has been shown. Furthermore, good agreements of the FE-creep analysis results and measurements are achieved. Based on this, further 40 years settlement prediction are made.

In addition to that, the advantage of the actual construction using a pile length of 12 m in every two rows and a longer pile length of 20 m for the row in between is highlighted. The use of several longer piles is essential for long term settlement reduction due to creep process. Through the comparison of the surface settlement with the construction without installing piles, the effectiveness of the soft soil improved by the actual floating piles is 76 percent after 6 years time. This effectiveness increases further due to further creep settlement.

Chapter 7

Conclusions and recommendations

In the framework of the research on numerical analysis and design criteria of embankment on floating piles, several research topics have been studied. The research can be divided into three main topics that include the numerical analysis of soil arching in a piled embankment, analysis of the effects of displacement pile installation and settlement analysis of embankment on floating piles. In addition, a case study of embankments on floating piles was performed to observe further settlement behaviour of an embankment on floating piles due to creep. The most important findings from this research are summarized in the following sections and followed by recommendations for further research on embankments on floating piles.

7.1 Conclusions on the numerical analysis of embankments on floating piles

The use of numerical analysis such as the finite element method has become more accessible and thereby more popular in geotechnical engineering. This trend also applies to the possibility of the design of embankments on floating piles. The finite element method is proven to be a reliable tool to simulate the complex soil-structure interaction related to the design of embankments on floating piles. However, the FE-method needs proper calculation procedures to obtain reliable results. The research that has been performed and presented in this thesis is aimed to establish a proper calculation procedure and highlight the important design criteria for the analysis of embankments on floating piles. The findings have been discussed in detail in the previous chapters, and they can be concluded in three categories:

On the numerical analysis of soil arching

- Analysis of soil arching in piled embankment in general can be performed numerically with 3D or axisymmetric geometrical idealizations. Both geometrical idealizations give equivalent results of soil arching analysis of one reference piled embankment cell. Because axisymmetrical analysis is much more efficient, this method is recommended.

- It is important to ensure the stability of soil arching action as a load transfer mechanism from the embankment to the piles. The stability of soil arching can be identified by observing the plasticity and shear strain conditions in the embankment soil stress points.
- The use of geotextile reinforcements improves embankment settlement and soil arching stability. When more than one layer of geotextiles is used, they should be placed within the lower half of the predicted arching height to ensure the effectiveness of the geotextile reinforcement. The arching height can be determined from the plane of equal vertical settlement in the embankment. In addition to that, more than one geotextile layer can be placed within the specified height to minimize the risk of punching failure.
- In numerical analysis of soil arching, the use of an advanced soil constitutive model such as the Hardening Soil model is recommended. It allows a more realistic choice of soil parameters, gives a better approximation of embankment settlement compared to reality and a clear identification of soil arching stability.
- Based on the consideration of soil arching stability and the rate of load transfer, numerical analysis results confirm the criterion of a minimum of 30° effective friction angle for the embankment material.
- Numerical analysis results suggest that it is advisable to use a capping ratio of at least 10 percent with a strong geotextile reinforcement. When no geotextile is applied, a conservative measure should be taken by using a much larger capping ratio. This is because of the high risk of soil arching collapse, which can lead to severe damage of the piled embankment.
- Based on the evaluation of punching failure indications, the following criteria for the design of a piled embankment are recommended to ensure a stable arching mechanism:
  - The embankment material has an effective friction angle $\varphi' \geq 30°$.
  - The embankment height are larger than arching height. This can be well estimated using the criteria from the German method EBGEO 2004 that is $h_a = 0.7 \cdot s_d$, where s_d is the diagonal spacing of the piles.
  - Pile capping ratio is larger than 10 percent.
  - One strong geotextile reinforcement.

On the analysis of the effects of displacement pile installation

- The main effect of displacement piles installation is the increase of radial stress around the pile, which increases the pile's bearing capacity. Apart from that, precast pile installations also create some residual skin friction and residual pile-tip pressure. However, for typical small and relatively short displacement piles installed in soft soils as in the case of embankments on floating piles, the residual skin friction and pile-tip pressure are insignificant.

- A clear procedure to simulate the effects of displacement piles installation, which is called $K - Pressure$ method, has been developed. The method is important especially for the analysis of displacement floating piles as used for soft soil improvement.
- The K-Pressure method has been developed for axisymmetric displacement pile analyses, which is based on stress controlled cavity expansion. The method is considered a sound method for displacement piles analysis and applicable within the realm of engineering practice. The applicability of this method is not limited to displacement piles, but can be also extended to other column type foundations.
- On using the K-Pressure method, the increase of radial stress due to pile installation is created by applying radial stresses on the cavity wall, with $p_r = K \cdot \sigma'_{v0}$. The constant K-value is back calculated from the load settlement measurements from pile loading tests. Hence, **the K-Pressure method requires calibration by pile loading tests**. Realistic stress fields after pile installation as well as after pile loading simulation are obtained up to an appropriate K-value, which is in the range of practical experience.
- The K-Pressure method is not only suitable for displacement pile analysis under drained conditions but also for analysis under undrained conditions. On applying the K-Pressure method under undrained conditions, excess pore water pressure develops around the pile within the plastic zone after pile installation simulation. When consolidation takes place afterwards, the excess pore pressure dissipates relatively rapidly as also observed from field experience.
- The resulting stress fields after applying K-Pressure under undrained conditions and followed by consolidation up to full dissipation of excess pore water pressure do not show significant differences compared to applying the K-Pressure procedure in drained conditions. Unfortunately, good data on excess pore water pressure after pile installation and pile loading are difficult to obtain for validation of the numerical analysis. Therefore, pile installation simulation with K-Pressure method in drained conditions, where the K-value is back-calculated from load-settlement measurements, is preferable.
- With the K-Pressure method, the option of using different advanced constitutive models in the numerical simulation are available. It is found that the resulting load settlement curve from displacement piles analysis with HS-Small model gives better agreement with the measurement compared to the ones from analyses with the HS model. Moreover, analyses with the HS-Small model show hysteresis when an unloading-reloading cycle is performed. Hence, the use of the HS-Small model gives better results especially when unloading-reloading is considered.

On settlement analyses of embankments on floating piles

- Approaches for assessing the settlements and the effectiveness of embankments on floating piles using analytical and FE-method have been shown. It is found that, generally, an embankment on floating piles is an effective method for soft soil improvement.
- Despite the necessity of simplifications, analytical approach is useful for understanding the general settlement behaviour of an embankment supported by floating piles and for the estimation of critical pile length, which is the length of pile at which the entire embankment load can be supported by the pile resistance.
- Based on more accurate analyses using the FE-method, the effectiveness of embankments supported by floating piles increases with pile length up to one hundred percent when the piles reach end-bearing piles. The rate of effectiveness increases rapidly as the pile length approach the critical pile length, and the rate of effectiveness decreases beyond the pile critical length. The most cost effective construction is achieved when using a pile length of one third to a half of the soft soil thickness. However, the corresponding embankment settlements should be carefully considered since at those lengths, the settlements may still be significant.
- Up to a certain pile length, soft soil improved by floating piles behaves as a mechanically improved block, where the soft soil and the pile deform uniformly. It is found that the piles and the surrounding soft soil begin to behave as a block when the pile length is about 75 percent of the estimated critical pile length l_{crit}.
- A simple method for estimating the effectiveness of embankments floating piles based on the concept of block behaviour has been presented. This method is very useful and easy to apply in practice.
- The use of long piles might be essential for reducing long-term settlement due to creep of soft soil. For economic considerations, a construction combining short and long piles as used in a case study of embankments on floating piles in Sweden has shown an optimization between cost and settlement reduction.

7.2 Recommendations for further research

The completed research topics on numerical analysis and design criteria of embankments on floating piles presented in this thesis covers mainly the behaviour of the middle part of the embankment on floating piles. Analyses focused on the design and the response of the sides of the embankment on floating piles due to loading have not been investigated. In addition, more uncertainties need to be clarified. Hence, further research related to the design of embankments on floating piles is required to investigate the following topics:

- The load transfer mechanism through soil arching action and settlement behaviour at the side of the embankment due to lateral thrust. This also leads to the geotextile tensile force requirement due to the lateral loading.
- The stability of soil arching action during cyclic loading and long-term availability of the arching action. In the current practice, the effect of cyclic loading is accounted for by factoring the applied static load. A closer observation of the response of soil arching action in the embankment due to cyclic loading, especially regarding stability, is necessary.
- The K-Pressure method can be extended to be applicable with data from field tests such as CPT data. For the construction of road and railway tracks, large areas of soft soil are involved. Generally, good data on the soft soil and pile load tests are not available for such large areas. However, often field test data such as CPT data are available because the cost of the test is low and it is simple to perform. Therefore, it is considered important to extend the applicability of the K-Pressure method based on CPT data. Several empirical correlations from CPT tests to the increase of radial stress around displacement piles are available. This involves a nonlinear K-Pressure distribution along the piles after installation.
- The K-Pressure procedure has been demonstrated in axisymmetrical analyses of displacement piles. It is necessary to implement the method in an analysis with 3D geometry, especially when considering the side part of the embankment on floating piles.
- The lateral resistance of floating piles with respect to pile embedment depth and the magnitude of lateral embankment thrust also calls for further investigation.
- The phenomenon of increasing displacement piles capacity in time (time set-up) after displacement piles installation is known. Many research findings based on field experiments have shown the time set-up phenomenon after displacement pile installation. However, its mechanical behaviour has not been fully understood.

Appendix A

Advanced constitutive models as used in this thesis

In the framework of research on numerical analysis and design criteria of embankments on floating piles, different advanced soil constitutive models have been incorporated, namely the Hardening Soil model, the Hardening Soil Small model and the Soft Soil Creep model. In this appendix, the main features of the advanced constitutive models are briefly described. For details on the constitutive modelling and its numerical implementations, further reference on the related publications are given. It should be mentioned that the Mohr-Coulomb (MC) constitutive model is also applied in the research. However, since the MC model is well known for geotechnical engineers, it is not presented again in this appendix. Nevertheless, the description of the elastic and perfectly plastic MC constitutive model can be seen for example in Möller (2006)

A.1 The Hardening Soil Model

The Hardening Soil (HS) model belongs to the group of double hardening model, which was developed by Schanz (1998) and Schanz et al. (1999) on the basis of a double hardening model by Vermeer (1978). The soil stress states are bounded by the Mohr-Coulomb failure stress criterion, which are simulated by means of shear strength parameters: effective cohesion c', effective friction angle φ' and dilatancy angle ψ. In addition to the Mohr-Coulomb failure surface, the HS-model uses hardening plasticity in the prefailure stress state instead of purely elastic behaviour as for example assumed in the MC model. The HS model uses two expandable yield surfaces namely shear hardening yield surface and compression hardening yield surface, by which the irreversible shear straining due to deviatoric loading as well as volumetric straining due to isotropic loading can be defined accurately. The stiffness of the soil is governed by three input stiffnesses: the triaxial loading stiffness E_{50}, the oedometer loading stiffness E_{oed} and the unloading-reloading stiffness E_{ur}. The formulation of these stiffnesses are advanced, adopting a stress dependent formulation according to the ideas of Ohde (1930). Through the use of E_{ur}, the soil stiffness is distinguished between first loading and unloading-reloading condi-

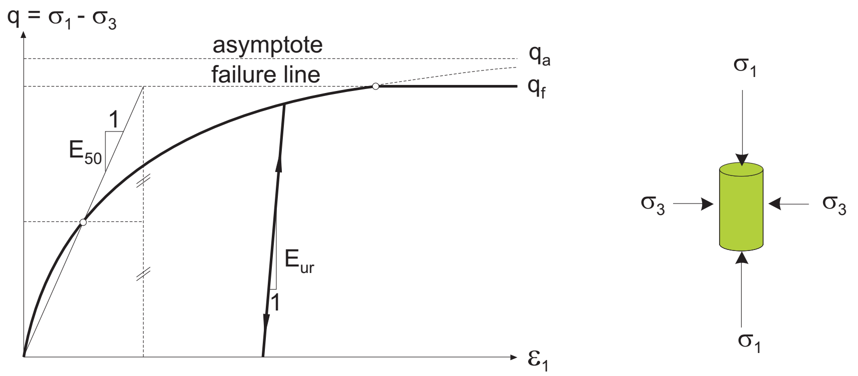

Figure A.1: Hyperbolic relationship between deviatoric stress and axial strain from a drained triaxial test

tion. Further details on the features of the HS model are described next with considering compression is positive.

Hyperbolic stress-strain relationship

When soil is subjected to primary deviatoric loading, as for example in the case of drained triaxial tests, a decrease in stiffness is observed and irreversible plastic strains develop. The typical shape of the stress-strain curve from a drained triaxial test resemble a hyperbola. Kondner and Zelasko (1963) were the first to formulate a hyperbolic relationship between the deviatoric stress $q = \sigma_1 - \sigma_3$ and the axial strain ε_1. Later, a hyperbolic model was presented by Duncan and Chang (1970). The HS model also adopt the hyperbolic stress-strain relationship as in the Duncan-Chang model. However, it supersedes the hyperbolic model by far. Firstly, by using the theory of plasticity rather than the theory of elasticity. Secondly, by introducing soil dilatancy and thirdly, by introducing compression yield surface (yield cap). The hyperbolic stress-strain relation can be written as

$$\varepsilon_1 = \frac{q_a}{2 \cdot E_{50}} \cdot \frac{q}{q_a - q} \tag{A.1}$$

where q_a is the asymptotic failure stress as illustrated in Figure A.1. The asymptotic failure stress q_a relates to the maximum failure stress q_f as follows

$$q_a = \frac{q_f}{R_f} \quad with \quad q_f = (c' \cdot \cot\varphi' + \sigma_3') \cdot \frac{2 \cdot \sin\varphi'}{R_f \cdot (1 - \sin\varphi')} \tag{A.2}$$

where $R_f = 0.9$ for many soils. While the maximum stress is determined by the Mohr-Coulomb failure criterion, the hyperbolic part of the curve can be defined using the stress-dependent secant modulus at 50 percent maximum stress, which is defined as

$$E_{50} = E_{50}^{ref} \cdot \left(\frac{c' \cdot \cot\varphi' + \sigma_3'}{c' \cdot \cot\varphi' + p^{ref}} \right)^m \tag{A.3}$$

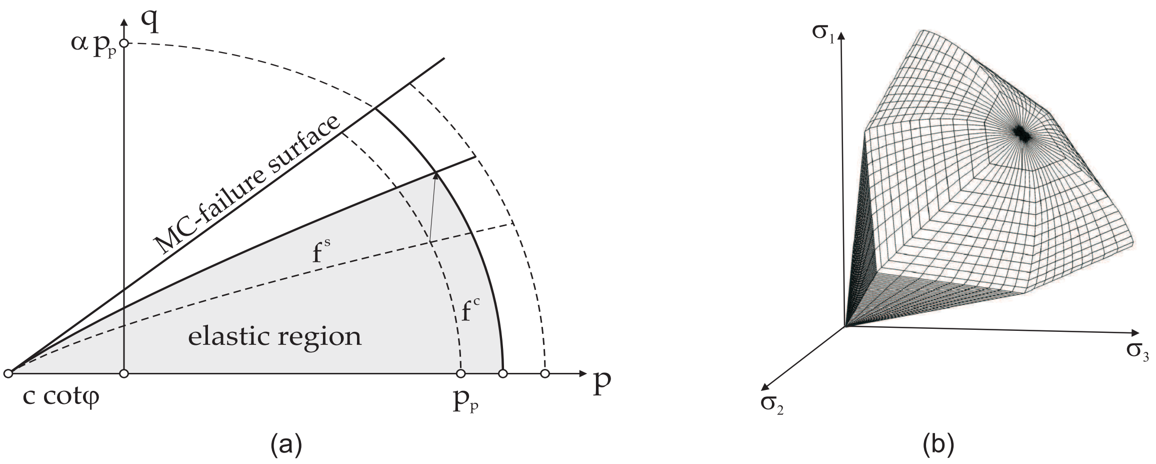

Figure A.2: Yield surface of the HS model (a) Successive yield loci for shear hardening and compression hardening in p-q space (b) Total yield contour in principal stress space

where E_{50}^{ref} is a reference secant triaxial loading stiffness corresponding to the reference confining pressure p^{ref}. Following the idea by Ohde (1930), the amount of stress dependency is governed by the exponent m, which can be measured both in oedometer tests and in triaxial tests. Von Soos (2001) shows that m values range between 0.4 and 1.0. A value of 0.5 is typical for sands and clays tend to have m = 1.0.

In contrast to E_{50}, which determines the magnitude of both the elastic and the plastic strains, E_{ur} is a true elasticity modulus. In conjunction with a Poisson's ratio ν_{ur}, it determines the ground behaviour under unloading and reloading; the subscript ur stands for unloading-reloading. Similarly to the E_{50}, E_{ur} is stress-level dependent and it is written

$$E_{ur} = E_{ur}^{ref} \cdot \left(\frac{c' \cdot \cot \varphi' + \sigma_3'}{c' \cdot \cot \varphi' + p^{ref}} \right)^m \tag{A.4}$$

where E_{ur}^{ref} is the reference Young's modulus, corresponding to the reference confining pressure p^{ref} .

In contrast to elastic perfectly-plastic MC model, in the HS model, plastic strains may already occur before the limit MC-failure stress is reached. The HS model incorporates two other yield surfaces, which are not fixed in principal stress space, but they may expand and soil hardening is simulated due to plastic straining. As illustrated in Figure A.2, distinction is made between two type of hardening, which are shear hardening and compression hardening. For the shear hardening law a yield function f^s is introduced, which is a function of the triaxial loading stiffness E_{50} and for the compression hardening a yield function f^c is formulated, being governed by the oedometer loading stiffness E_{oed}. As also displayed in Figure A.2, for unloading-reloading, elastic soil behaviour is assumed.

Shear hardening yield function f^s

The shear hardening yield function f^s adopted in the HS model has the formulation that can be written in the following equation

$$f^s = \bar{f} - \gamma^p \tag{A.5}$$

where

$$\bar{f} = \frac{1}{E_{50}} \cdot \frac{q}{1 - q/q_a} - \frac{2q}{E_{ur}} \tag{A.6}$$

is a function of stress and the hardening parameter

$$\gamma^p = \varepsilon_1^p - \varepsilon_2^p - \varepsilon_3^p = 2 \cdot \varepsilon_1^p - \varepsilon_v^p \approx 2 \cdot \varepsilon_1^p \tag{A.7}$$

is a function of plastic strains. The HS model adopts non-associated plasticity to determine the rates of plastic strain, which is generally done in soil constitutive modelling to achieve realistic dilation upon shearing. On doing so, in addition to the shear hardening yield function f^s, plastic potential functions g^s are employed. The plastic potential functions can be written as follows

$$g_1^s = \frac{1}{2} \cdot (\sigma_2' - \sigma_3') - \frac{1}{2} \cdot (\sigma_2' + \sigma_3') \cdot \sin\psi_m \tag{A.8}$$

$$g_2^s = \frac{1}{2} \cdot (\sigma_1' - \sigma_3') - \frac{1}{2} \cdot (\sigma_1' + \sigma_3') \cdot \sin\psi_m \tag{A.9}$$

$$g_3^s = \frac{1}{2} \cdot (\sigma_1' - \sigma_2') - \frac{1}{2} \cdot (\sigma_1' + \sigma_2') \cdot \sin\psi_m \tag{A.10}$$

ψ_m is the mobilized angle of dilatancy and it is calculated according to the so-called stress-dilatancy equation of Rowe (1962)

$$\sin\psi_m = \frac{\sin\varphi_m - \sin\varphi_{cv}}{1 - \sin\varphi_m \cdot \sin\varphi_{cv}} \tag{A.11}$$

The mobilized dilatancy angle depends on the mobilized friction angle φ_m, which is determined using the equation

$$\sin\varphi_m = \frac{\sigma_1' - \sigma_3'}{\sigma_1' + \sigma_3' + 2 \cdot c' \cdot \cot\varphi'} \tag{A.12}$$

and the critical state of constant-volume friction angle φ_{cv} is determined using the equation

$$\sin\varphi_{cv} = \frac{\sin\varphi' - \sin\psi}{1 - \sin\varphi' \cdot \sin\psi} \tag{A.13}$$

The mobilized dilatancy angle ψ_m is thus positive as soon as the mobilized friction angle φ_m exceeds the constant-volume friction angle φ_{cv}. Considering dense soils, contraction is excluded by taking $\psi_m = 0$ for $\varphi_m < \varphi_{cv}$.

The general elastic stress-strain relationship can be expressed as follow

$$\dot{\boldsymbol{\sigma}}' = \mathbf{D}^e \cdot \dot{\boldsymbol{\varepsilon}}^e \tag{A.14}$$

where $\dot{\sigma}$ is the stress rate, $\dot{\varepsilon}^e$ is the elastic strain rate and $\mathbf{D}^e$ is the elastic material stiffness matrix. The plasticity formulation decomposes strain rate $\dot{\varepsilon}$ into elastic and plastic part

$$\dot{\boldsymbol{\varepsilon}} = \dot{\boldsymbol{\varepsilon}}^e + \dot{\boldsymbol{\varepsilon}}^p \tag{A.15}$$

with $\dot{\varepsilon}^p$ is the plastic strain rate. Combining Equation A.14 and Equation A.15, one gets the basic plasticity formulation

$$\dot{\boldsymbol{\sigma}}' = \mathbf{D}^e \cdot (\dot{\boldsymbol{\varepsilon}} - \dot{\boldsymbol{\varepsilon}}^p) \tag{A.16}$$

The plastic strain rate due to shear hardening plasticity $\dot{\boldsymbol{\varepsilon}}^{ps}$ is defined as

$$\dot{\boldsymbol{\varepsilon}}^{ps} = \lambda^s \frac{\partial g^s}{\partial \boldsymbol{\sigma}'} \tag{A.17}$$

where λ^s is the plastic multiplier, which can be solved by using the consistency condition with $\dot{f}^s = 0$. Further description on the solution for the plastic multiplier can be seen for example in Möller (2006). The total strain rate can be calculated by combining Equation A.16 and Equation A.17 to give

$$\dot{\boldsymbol{\varepsilon}} = \dot{\boldsymbol{\varepsilon}}^e + \dot{\boldsymbol{\varepsilon}}^{ps} = \mathbf{D}^{-1}\dot{\sigma}' + \lambda^s \frac{\partial g^s}{\partial \boldsymbol{\sigma}'} \tag{A.18}$$

Compression hardening yield function f^c

Another important feature in the HS model is the compression hardening, which is formulated by means of cap-type yield surfaces. By using this feature, it makes the model both suitable for hard soils as well as soft soils. The cap-type yield function has the formulation

$$f^c = \frac{q^2}{\alpha^2} - p^2 - p_p^2 \tag{A.19}$$

where parameter α is an internal program parameter. Together with the isotropic preconsolidation pressure p_p, they form the size and the shape the cap yield surface. p is the mean effective stress defined as $p = 1/3 \cdot (\sigma_1' + \sigma_2' + \sigma_3')$. The preconsolidation pressure is used as the hardening parameter, which is expressed as

$$\dot{p}_p = 2 \cdot \lambda^c \cdot H_\beta^{ref} \cdot p \cdot \left(\frac{p}{p^{ref}}\right)^m \tag{A.20}$$

Similar to α, the parameter H_β^{ref} is also an internal program parameter that influence the shape of the cap yield surface. The parameter α relates to the lateral earth pressure

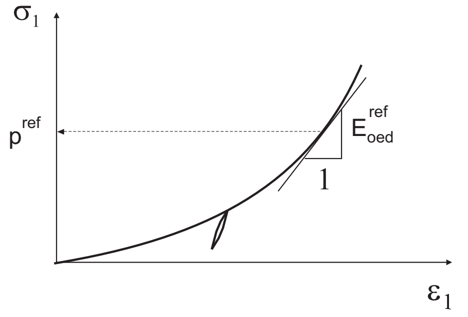

Figure A.3: Typical stress-strain curve from an oedometer test

at rest K_0^{NC}, E_{50}^{ref} and E_{oed}^{ref} , whereas the parameter H_β^{ref} is linked to the E_{oed}^{ref}, which can be determined from an oedometer test as illustrated in Figure A.3. Hence both internal parameters are not used as input parameters. Further details on the internal parameters α and H_β^{ref} as well as on the plastic multiplier λ^c can be found in Benz (2007). In contrast to the shear hardening flow rule, associated flow rule is applied for determining the strain rate in the compression hardening. Hence, the potential function $g^c = f^c$. The plastic volumetric strain rate is determined as

$$\dot{\varepsilon_v}^{pc} = \lambda^c \frac{\partial f^c}{\partial \sigma'} \tag{A.21}$$

the plastic multiplier is solved by the use of consistency condition $\dot{f}^c = 0$. Further detail on the solution for the plastic multiplier is given for example by Möller (2006).

In total eight parameters are required for the HS model, which consist of shear strength parameters namely: effective friction angle φ', effective cohesion c' and dilatancy angle ψ, stiffness parameters namely: triaxial loading stiffness E_{50}^{ref}, oedometer loading stiffness E_{oed}^{ref}, unloading-reloading stiffness E_{ur}^{ref} and unloading-reloading Poisson's ratio ν_{ur}. The superscript ref denotes that the stiffnesses are measured at a reference pressure p^{ref}, which is generally taken as 100 kPa. In addition to that, another input parameter is the power law m. For more information on the formulation and the implementation of the HS model, the reader is referred to Schanz et al. (1999) and Brinkgreve (2002).

A.2 The HS-Small Model

The HS-Small model is an extension of the HS model to incorporate the small strain stiffness behaviour of soils. The behaviour of soil at small strains has been studied by many researchers for example Seed and Idriss (1970), Burland (1989), Atkinson (2000), Benz (2007) and it is found to be an important phenomenon in geotechnical engineering problems. At small strain levels, most soils exhibit a higher stiffness than at engineering strain levels. This stiffness varying non-linearly with strain. The soil stiffness decays as

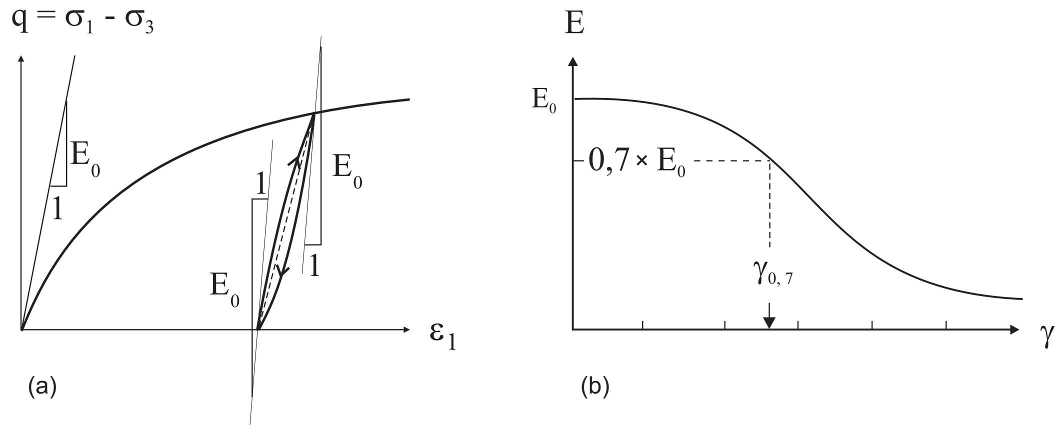

Figure A.4: HS-Small model (a) Description of initial stiffness modulus in a triaxial test E_0 (b) Small strain parameters E_0 and $\gamma_{0.7}$

the strain increases. The importance of the high stiffness at small strains and its use in geotechnical engineering has also been shown by Benz (2007). His work has lead to the development of the Hardening Soil Small (HS-Small) model.

As an extension of the HS model, all the features described Appendix A.1 also hold true for the HS-Small model. In addition to the HS model, the HS-Small model incorporates a formulation of the small strain stiffness. As displayed in Figure A.4a, small unloading-reloading stress-strain paths result in a considerably higher elasticity modulus E_0. In fact, maximum soil stiffness is observed at very low strain levels, e.g. strains smaller than 10^{-5} (Atkinson and Sällfors, 1991). The strain levels considered here, are far below conventional laboratory testing. It requires special measuring devices such as dynamic methods or local strain gauges to identify the stiffness at this strain. A simple correlation for E_0 is given by Biarez and Hicher (1994) for quartz sand in the following equation

$$E_0 = \frac{140}{e} \cdot \left(\frac{p}{p^{ref}} \right)^{0.5} \tag{A.22}$$

where e is the void ratio of the soil and p is the mean stress. Another possibility for preliminary estimation of the E_0 is given by Alpan (1970).

The decay of stiffness with increasing strain level is described by means of a modified hyperbolic formulation after Hardin and Drnevich (1972)

$$E = \frac{E_0}{1 + \frac{3}{7} \cdot \frac{\gamma}{\gamma_{0.7}}} \tag{A.23}$$

where E is the actual secant modulus at the corresponding shear strain γ, E_0 is the initial stiffness of the soil and $\gamma_{0.7}$ is the shear strain at which E has decayed to 70 percent from the initial stiffness E_0 as illustrated in Figure A.4b. The initial shear modulus G_0 is determined from the relation with E_0 and and Poisson's ratio ν as in the following equation

$$G_0 = \frac{E_0}{2 \cdot (1+\nu)} \tag{A.24}$$

The shear strain is expressed using the strain invariant

$$\gamma = \frac{1}{\sqrt{2}} \cdot \sqrt{(\varepsilon_1 - \varepsilon_2)^2 + (\varepsilon_2 - \varepsilon_3)^2 + (\varepsilon_3 - \varepsilon_1)^2} \tag{A.25}$$

According to the formulation of the HS model, stiffness degradation due to plastic straining is modelled by involving material hardening. Therefore, before reaching plastic material behaviour, the formulation of the small strain stiffness is cut off at the unloading-reloading stiffness E_{ur}.

Besides the input parameters as introduced for the HS model, two additional input parameters are required for the HS-Small model: the elastic small strain shear modulus G_0^{ref} at reference pressure p^{ref} and the curve-decay value $\gamma_{0.7}$ in primary loading. A more detailed explanation of the HS-Small model can be found in Benz (2007).

A.3 The Soft Soil Creep Model

The most significant behaviour of soft soils is their high degree of compressibility. Typically, a normally consolidated soft soil is ten times softer than a normally consolidated sand. In addition to that, another important behaviour of soft soils is that they continue to settle in time under a constant load. The latter is also known as secondary compression and it is referred to as pure creep. Apparently, creep also happens during the primary consolidation process where the load is not constant. Hence, in general, creep can be described as the viscous effect of soft soils under an effective stress, which causes secondary settlement. Creep has been observed in laboratory as well as in fields (Buisman, 1936, Bjerrum, 1967). In soil mechanics, creep has primarily been studied for one-dimensional compression. Buisman (1936) was probably the first to propose a creep law for clay after observing that soft soil settlements could not be fully explained by classical consolidation theory. The work on 1D secondary compression was continued by researchers including, for example, Garlanger (1972) and Mesri and Choi (1985). A more mathematical lines of research in the area were followed by, for example, Adachi and Okano (1974), Borja and Kavaznjian (1985), Vermeer and Neher (1999) and Leoni et al. (2008).

1D creep model

The Soft Soil Creep model described here is on the basis of the work done by Vermeer and Neher (1999) on elastic visco-plastic creep model. For the one dimensional creep,

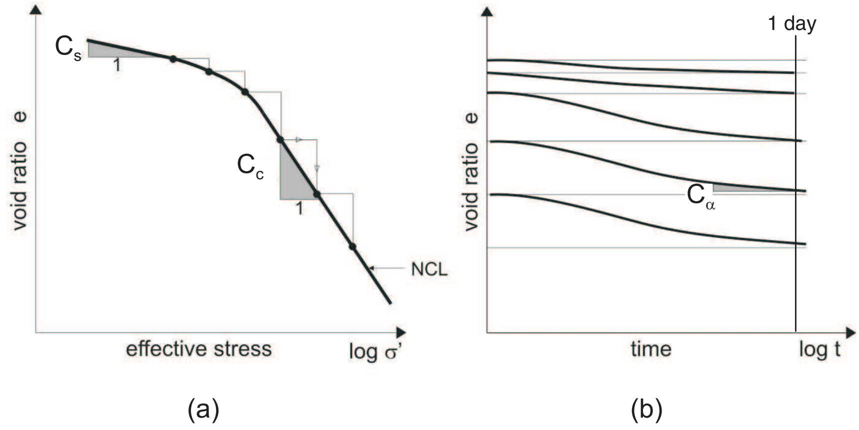

Figure A.5: Standard oedometer test data (a) Stepwise loading in $e - \log \sigma$ curve (b) evolution of void ratio with time

two strain components need to be modelled. First of them is the more or less elastic deformation, as directly observed in unloading and reloading condition. The other component of strain is irreversible and time dependent. Volumetric strain implies a change of void ratio and it is convenient to formulate the deformation in terms of void ratio (e) as shown by Vermeer et al. (2006). Hence, the change of void ratio is written as

$$\dot{e} = \dot{e}^e + \dot{e}^c \tag{A.26}$$

where the superscripts e and c refer to the elastic and creep components respectively. The elastic change of void ratio is formulated as follows considering compression is positive as the usual convention in soil mechanics

$$\dot{e}^e = -\frac{C_s}{\ln 10}\frac{\dot{\sigma}'}{\sigma} \tag{A.27}$$

where C_s is the swelling index, which is sometimes called the unloading-reloading index and denoted as C_{ur}. The creep deformation is modelled by the power law

$$\dot{e}^c = -\frac{C_\alpha}{\tau \cdot \ln 10}\left(\frac{\sigma'}{\sigma_p}\right)^\beta = -\frac{C_\alpha}{\tau \cdot \ln 10}\left(\frac{1}{OCR}\right)^\beta \quad with \quad \beta = \frac{C_c - C_s}{C_\alpha} \tag{A.28}$$

where τ is a particular reference time, which can mostly be taken equal to one day. C_α is the secondary compression index that is also referred to as the creep index and C_c is the compression index obtained from an oedometer test as illustrated in Figure A.5. Equation A.28 shows that the creep rate depend on the OCR value. Typical soft soil data give $C_s \approx C_c/10$ and $C_\alpha \approx C_c/30$. This gives β of about 27. As a consequence, creep rate decrease exponentially with the increase of OCR.

The preconsolidation stress σ_p increases during creep according to the differential equation

$$\frac{\dot{\sigma}_p}{\sigma_p} = -\frac{\ln 10}{C_c - C_s} \cdot \dot{e}^c \tag{A.29}$$

for a constant temperature. The integrated form of Equation A.29 is

$$\sigma_p = \sigma_{p0} \cdot \exp - \frac{\ln 10 \cdot \Delta e^c}{C_c - C_s} \quad \textit{with} \quad \Delta e^c = e^c - e^c_0 \tag{A.30}$$

where σ_{p0} is the initial preconsolidation stress for $e^c = e^c_0$ and subscript 0 denotes the initial value. Combining Equation A.30 to Equation A.28, one obtains the differential creep rate formulation

$$\dot{e}^c = - \frac{C_\alpha}{\tau \cdot \ln 10} \left(\frac{\sigma'}{\sigma_{p0}} \right)^\beta \exp \frac{e^c - e^c_0}{C_\alpha / \ln 10} \tag{A.31}$$

The effective stress σ' may be either larger or smaller than σ_{p0} and it does not need to be constant. In the simplest case of creep at constant effective stress, the creep rate reduces monotonically due to the decreasing void ratio in the exponential term. For the special case of a constant effective stress, the differential creep formulation in Equation A.31 can be integrated analytically to obtain the logarithmic creep law

$$\Delta e^c = e^c - e^c_0 = -C_\alpha \log \left(1 + \frac{t}{\tau^\star} \right) \tag{A.32}$$

where $t = 0$ for $e = e_0$, and

$$\tau^\star = \tau \cdot \left(\frac{\sigma_{p0}}{\sigma'} \right)^\beta = \tau \cdot OCR^\beta_0 \tag{A.33}$$

3D Soft Soil Creep model

On extending the 1-D model to general states of stress and strain, the well-known stress invariants p and q for mean and deviatoric stress are adopted. These invariants are used to define a new stress measure named p^{eq} that is

$$p^{eq} = p' + \frac{q^2}{M^2 p'} \tag{A.34}$$

with

$$p' = \frac{1}{3} \left(\sigma'_1 + \sigma'_2 + \sigma'_3 \right) \quad \textit{and} \quad q = \frac{1}{\sqrt{2}} \cdot \sqrt{(\sigma'_1 - \sigma'_2)^2 + (\sigma_2 - \sigma_3)^2 + (\sigma_2 - \sigma_2)^2} \tag{A.35}$$

p_{eq} is an equivalent stress defining a unique Modified Cam Clay ellipse in p-q plane as introduced by Roscoe and Burland (1968). The ellipses of Modified Cam Clay are taken as contours of volumetric creep rate in p-q plane as illustrated in Figure A.6. Hence the same volumetric creep rate applies to all stress states which lie on a particular ellipse.

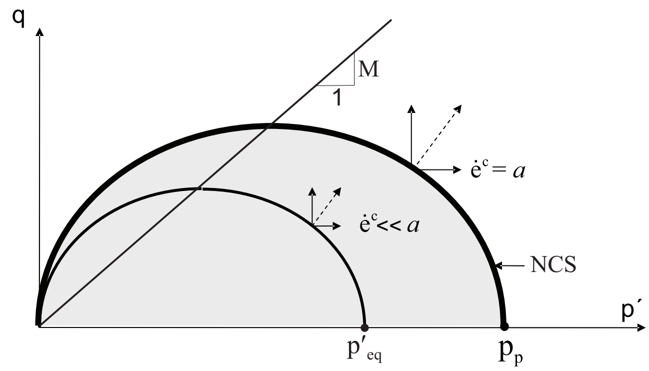

Figure A.6: Ellipses of Modified Cam Clay as contours for constant rate of volumetric strain

The ellipse, which intersects with the p-axis in p_p is referred to as the normal consolidation surface (NCS). The soil parameter M represents the slope of the so-called *critical state line* as also indicated in Figure A.6 and it is defined as

$$M = \frac{6 \cdot \sin \varphi_{cv}}{3 - \sin \varphi_{cv}} \tag{A.36}$$

where φ_{cv} is the constant volume friction angle, also referred to as critical-state friction angle. The preconsolidation pressure changes during creep according to the law

$$p_p = p_{p0} \cdot \exp \frac{\triangle \varepsilon^c_{vol}}{\lambda^\star - \kappa^\star} \tag{A.37}$$

where $\lambda^\star$ and $\kappa^\star$ are a modified compression index and a modified swelling index respectively. It yields for small strain

$$\lambda^\star = \frac{C_c}{\ln 10} \cdot \frac{1}{1 + e_0} \tag{A.38}$$

and

$$\kappa^\star \approx \frac{3(1-\nu)}{1+\nu} \cdot \frac{C_s}{\ln 10} \cdot \frac{1}{1+e_0} \approx \frac{2C_s}{\ln 10} \cdot \frac{1}{1+e_0} \tag{A.39}$$

For a derivation of the approximate relation between $\kappa^\star$ and C_s, the reader is referred to Vermeer and Neher (1999). With the definition of Equation A.34 in mind, the 1D creep rate as written in Equation A.28 is modified to define the volumetric creep strain rate

$$\dot{\varepsilon}^c_{vol} = \frac{\mu^\star}{\tau} \cdot \left(\frac{p_{eq}}{p_p} \right)^{\frac{\lambda^\star - \kappa^\star}{\mu^\star}} \quad with \quad \mu^\star = \frac{C_\alpha}{\ln 10} \cdot \frac{1}{1+e_0} \tag{A.40}$$

As for the elastic volumetric strain rate $\dot{\varepsilon}^e_{vol}$, it depends on the stress dependent bulk modulus being defined as $K_{ur} = p'/\kappa^\star$. Hence, the elastic volumetric strain rate can be written as

$$\dot{\varepsilon}^e_{vol} = \frac{\dot{p}'}{K_{ur}} = \kappa^\star \frac{\dot{p}'}{p'} \tag{A.41}$$

The total volumetric strain rate in 3D Soft Soil Creep model can be written as

$$\dot{\varepsilon}_{vol} = \dot{\varepsilon}^{e}_{vol} + \dot{\varepsilon}^{c}_{vol} = \kappa^{\star}\frac{\dot{p}'}{p'} + \frac{\mu^{\star}}{\tau} \cdot \left(\frac{p_{eq}}{p_p}\right)^{\frac{\lambda^{\star}-\kappa^{\star}}{\mu^{\star}}} \tag{A.42}$$

For further details on the formulation of the 3D Soft Soil Creep model and its numerical implementation, the reader is referred to Vermeer and Neher (1999), Vermeer et al. (2006) and Leoni et al. (2008).

The Soft Soil Creep model is an isotropic model being the ellipses are symmetric with respect to the p-axis. The creep model involves dilation and associated softening for stress states on the dry side (left of the intercept of the critical state line) as shown in Figure A.7. However, in numerical analyses, softening cannot easily be simulated as it leads to mesh-dependency and possible numerical instabilities. In order to remain within the framework of a classical continuum and to avoid numerical difficulties, the dry side of critical state is modelled by a fixed Mohr-Coulomb failure surface with a slope

$$M_{MC} = \frac{6 \cdot \sin\varphi'}{3 - \sin\varphi'} \tag{A.43}$$

as indicated in Figure A.7. In the figure, it would suggest that tensile stresses are possible, but this can be omitted by using a tension cut off option. In this way, two extra model constants, i.e. the effective cohesion c' and the effective friction angle φ' are used. In total, eight parameters are required for the parameters that are required for the Soft Soil Creep model and their rough estimations are listed in Table A.1. As shown in the table, input of OCR or preoverburden pressure POP is required to define the state of preconsolidation stress σ_p as illustrated in Figure A.8.

An important feature of the isotropic Soft Soil Creep model is a relatively steep NC-surfaces can be used by adopting relatively large values for M_{CS}, which is different from the slope M. This is done by selecting the value of φ_{cv} for the Equation A.36, which correspond to a realistic K_0^{NC}. No doubt, M_{CS} may be equal to M, but the model gives the possibility to use M_{CS} values well beyond M as in the Modified Cam Clay model. On doing so we deviate from the Modified Cam Clay model, as this model tends to give too large horizontal stresses in oedometric loading. In order to make sure that the model predicts realistic K_0^{NC}-values, quite large M_{CS} values need to be used, and consequently, relatively steep normal consolidation ellipses in p-q plane are obtained.

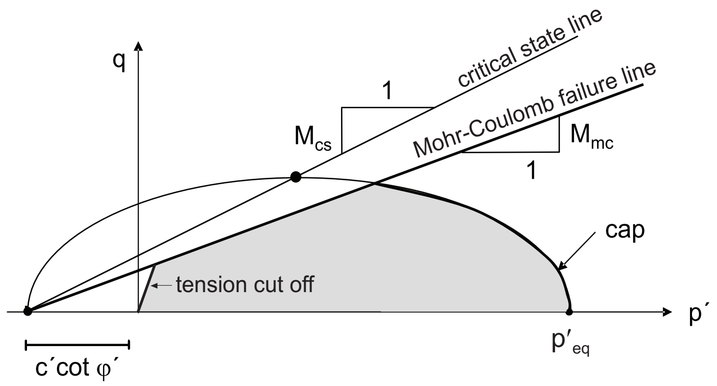

Figure A.7: Isotropic Soft Soil Creep model

Table A.1: Material parameters for the Soft Soil Creep model

$\lambda^\star$	a modified compression index
$\kappa^\star \approx \lambda^\star/10$	a modified swelling index
$\mu^\star \approx \lambda^\star/30$	a modified creep index
$\nu_{ur} \approx 0.15$	elastic Poisson's ratio
c'	effective cohesion
φ'	effective friction angle
$K_0^{NC} \Leftrightarrow M_{CS}$	height of the normal consolidation surface
$OCR \Leftrightarrow POP$	the state of preconsolidation stress

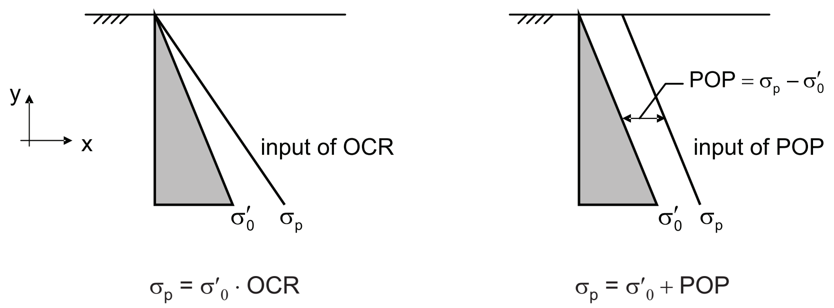

Figure A.8: Influence of input OCR and POP on the initialization of geostatic stress state

Appendix B

Interface element

Many geotechnical engineering problems relate to the analysis of soil-structure interaction. For example in the research on pile installation and loading analysis, the behaviour of contact zone between the pile and the soil plays an important role. In this zone, the soil is considerably distorted due to shearing takes place. When performing an FE-analysis of such problem, the contact zone is simulated by means of interface elements. The advantages of using interface elements for soil-structure interactions have been shown by several researchers. For example to suppress stress singularity around the corner points (Van Langen, 1991) and to reduce sensitivity to mesh refinement in pile loading analysis Wehnert and Vermeer (2004).

Figure B.1a shows an interface element connected to a continuum element. In this case, for the six noded continuum element, a three pairs noded interface element is applied. In the figure, the interface element is shown to have a finite thickness, but in the finite element formulation, the coordinates of each node pair are identical, which means that the interface has zero thickness. However, in each interface element a virtual thickness t_{in}, which is an imaginary dimension, is assigned to define its material behaviour. In the used FE program, the interface virtual thickness is by default taken as ten percent of the average elements size. However, this value can be specified independently.

The Mohr-Coulomb interface model

The interface elements follow Mohr-Coulomb constitutive behaviour. Figure B.1b and c describe interface stress-strain behaviour and its deformation mechanism for a constant normal stress. For the Mohr-Coulomb constitutive model, the interface uses five parameters c_{in}, φ_{in}, ψ_{in}, ν_{in} and E_{in}, which are the interface effective cohesion, effective friction angle, dilatancy angle, Poison's ratio and elastic stiffness respectively. Another important parameter for the interface element is the virtual interface thickness t_{in}. As for the interface stiffness, it can be specified as a constant elastic stiffness or stress-dependent elastic stiffness. If stress-dependent is used, it follows the power law formulation with E_{in} proportional to the effective normal stress σ'_{in} as expressed below:

$$E_{in} = E_{in}^{ref} \cdot \left(\frac{c_{in} \cdot \cot \varphi_{in} + \sigma'_{in}}{c\prime_{in} \cdot \cot \varphi_{in} + p^{ref}} \right)^{m} \tag{B.1}$$

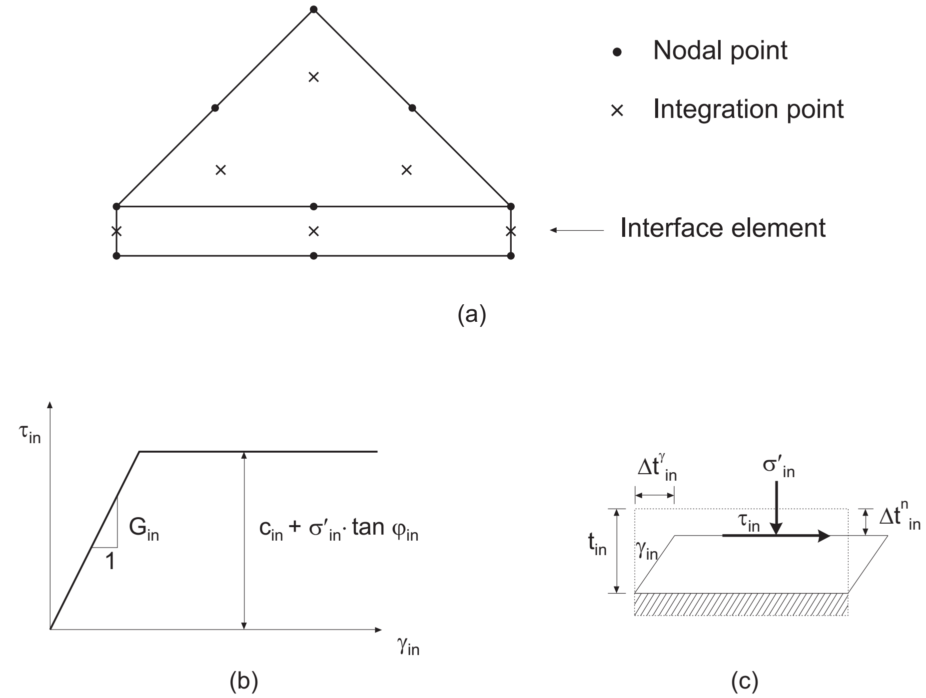

Figure B.1: Interface with MC-model (a) Interface element connected to continuum element (b) Interface stress-strain relationship (c) Deformation mechanism

where E_{in}^{ref} is an input elastic stiffness that corresponds to a reference pressure p^{ref}. The elastic interface incremental strains can be expressed in terms of incremental interface stresses as follows:

$$\dot{\boldsymbol{\varepsilon}}_{in}^{e} = \mathbf{C}_{in}^{e} \cdot \dot{\boldsymbol{\sigma}}_{in} \tag{B.2}$$

or in a matrix form

$$\begin{bmatrix} \dot{\varepsilon}_{in}^{e} \\ \dot{\gamma}_{in}^{e} \end{bmatrix} = \begin{bmatrix} 1/E_{in}^{oed} & 0 \\ 0 & 1/G_{in} \end{bmatrix} \cdot \begin{bmatrix} \dot{\sigma}_{in}^{e} \\ \dot{\tau}_{in}^{e} \end{bmatrix} \tag{B.3}$$

where ε_{in}^{e} is the elastic interface normal strain, γ_{in}^{e} is the elastic interface shear strain and $\mathbf{C}_{in}^{e}$ denotes the elastic compliance matrix expressed in term of interface oedometer (constrained) modulus E_{in}^{oed} and interface shear modulus G_{in} with

$$G_{in} = \frac{E_{in}}{2 \cdot (1 + \nu)} \qquad and \qquad E_{in}^{oed} = 2 \cdot G_{in} \cdot \frac{1 - \nu_{in}}{1 - 2\nu_{in}} \tag{B.4}$$

The elasto-plastic behaviour follows the Mohr-Coulomb yield function with non associated plastic potential as expressed in following equation

$$f_{in} = \sigma'_{in} \cdot \tan \varphi_{in} + c_{in} - \tau_{in}, \quad g_{in} = \sigma'_{in} \cdot \tan \varphi_{in} - \tau_{in} \tag{B.5}$$

Following the basic equation of elasto-plastic modelling, one can write that

$$\begin{bmatrix} \dot{\varepsilon}_{in} \\ \dot{\gamma}_{in} \end{bmatrix} = \begin{bmatrix} \dot{\varepsilon}_{in}^{e} \\ \dot{\gamma}_{in}^{e} \end{bmatrix} + \begin{bmatrix} \dot{\varepsilon}_{in}^{p} \\ \dot{\gamma}_{in}^{p} \end{bmatrix} \tag{B.6}$$

where ε_{in} is the total interface normal strain, defined as $\varepsilon_{in} = \Delta t^{n}_{in}/t_{in}$ with Δt^{n}_{in} is the interface normal displacement. γ_{in} is the total interface shear strain, which is defined as $\gamma_{in} = \Delta t^{\gamma}_{in}/t_{in}$ with Δt^{γ}_{in} is the interface slip displacement. Figure 2.3b shows the deformation mechanism of the interface element. The plastic part of the interface strains ε^{p}_{in} and γ^{p}_{in} can be expressed in following formulae:

$$\dot{\varepsilon}^{p}_{in} = \lambda \frac{\partial g_{in}}{\partial \sigma'_{in}} \quad and \quad \dot{\gamma_{in}}^{p} = \lambda \frac{\partial g_{in}}{\partial \tau_{in}} \tag{B.7}$$

where λ is the plastic multiplier. Hence, the total incremental stress-strain formulation can be written as follows:

$$\dot{\boldsymbol{\sigma}}_{in} = \mathbf{D}^{e}_{in} \cdot (\dot{\boldsymbol{\varepsilon}}_{in} - \dot{\boldsymbol{\varepsilon}}^{p}_{in}) = \mathbf{D}^{e}_{in} \cdot (\dot{\boldsymbol{\varepsilon}}_{in} - \lambda \frac{\partial g_{in}}{\partial \boldsymbol{\sigma}_{in}}) \tag{B.8}$$

where $\mathbf{D}^{e}_{in}$ is the elastic interface stiffness matrix as follows

$$\mathbf{D}^{e}_{in} = \begin{bmatrix} E^{oed}_{in} & 0 \\ 0 & G_{in} \end{bmatrix} \tag{B.9}$$

In order to solve the plastic multiplier λ, a consistency equation is needed. For the case of perfect plasticity, it is expressed as below:

$$\dot{f}_{in} = \frac{\partial f_{in}}{\partial \boldsymbol{\sigma}_{in}}^{T} \cdot \dot{\boldsymbol{\sigma}}_{in} = 0 \tag{B.10}$$

thus, it yields

$$\lambda = \frac{1}{d} \frac{\partial f_{in}}{\partial \boldsymbol{\sigma}_{in}}^{T} \mathbf{D}^{e}_{in} \cdot \dot{\boldsymbol{\varepsilon}}_{in} \quad with \quad d = \frac{\partial f_{in}}{\partial \boldsymbol{\sigma}_{in}}^{T} \mathbf{D}^{e}_{in} \frac{\partial g_{in}}{\partial \boldsymbol{\sigma}_{in}} \tag{B.11}$$

which gives the final result for the total stress-strain relationship as follows

$$\dot{\boldsymbol{\sigma}}_{in} = \mathbf{M}_{in} \cdot \dot{\boldsymbol{\varepsilon}}_{in} \quad with \quad \mathbf{M}_{in} = \mathbf{D}^{e}_{in} - \frac{\alpha}{d} \mathbf{D}^{e}_{in} \frac{\partial g_{in}}{\partial \boldsymbol{\sigma}_{in}} \frac{\partial f_{in}}{\partial \boldsymbol{\sigma}_{in}}^{T} \mathbf{D}^{e}_{in} \tag{B.12}$$

where α is equal to 0 in elastic condition and equal to 1 in elasto-plastic condition. Equation B.12 can be written in matrix form as below

$$\begin{bmatrix} \dot{\sigma}_{in} \\ \dot{\tau}_{in} \end{bmatrix} = \frac{1}{t_{in}} \cdot \mathbf{M}_{in} \cdot \begin{bmatrix} \Delta \dot{t}^{n}_{in} \\ \Delta \dot{t}^{\gamma}_{in} \end{bmatrix} \tag{B.13}$$

When assuming a rough contact surface, the interface shear strength is considered equal to the soil shear strength. This implies that c_{in} and φ_{in} are equal c′ and φ' of the soil respectively. If the interface is not entirely rough then the interface shear strength is less than the soil shear strength. The value of interface Poisson's ratio is set fix to be 0.45 within the used FE program. There are two possibilities of applying the interface input parameters, i.e. as direct input or indirect input of interface properties. Direct input of interface parameters gives flexibility on the input of the parameters. This is particularly important for pile analysis in a very cohesive soil, as the interface cohesion should always be close to zero considering a remoulded contact zone due to pile installation. When no direct input parameter is applied, the interface properties uses the properties of the surrounding soil with the so-called interface strength reduction factor parameter R_{inter}. It yields:

$$
\begin{gathered}
G_{in} = R_{inter}^2 \cdot G_{ur} \quad with \quad G_{ur} = \frac{E_{ur}^{ref}}{2 \cdot (1 + \nu_{ur})} \\
c_{in} = R_{inter} \cdot c' \quad and \quad \tan \varphi_{in} = R_{inter} \cdot \tan \varphi' \\
\psi_{in} = \begin{cases} 0^\circ & for \;\; R_{inter} < 1 \\ \psi & for \;\; R_{inter} = 1 \end{cases}
\end{gathered} \tag{B.14}
$$

Appendix C

Comparison of RSR curves

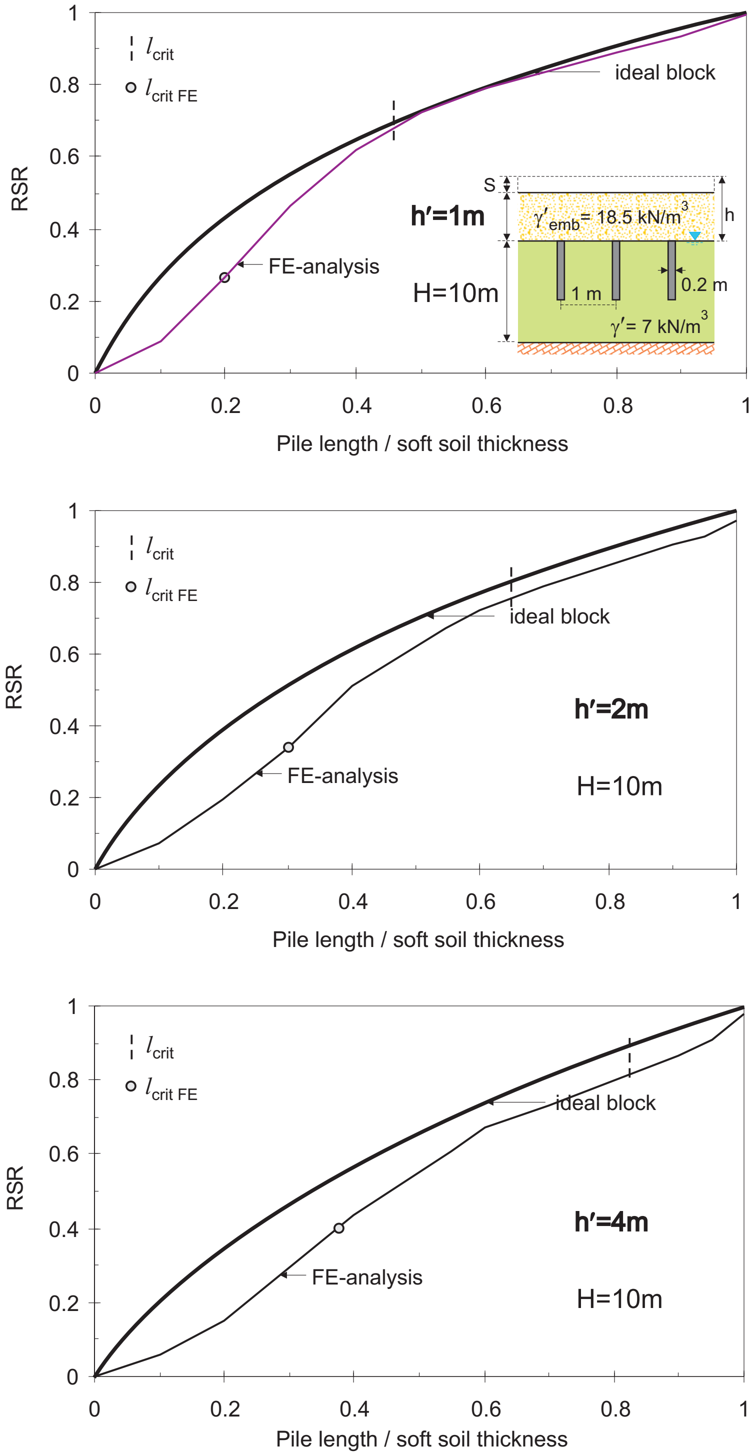

Figure C.1: Comparison between RSR from FE-analyses and $RSR_{ideal\ block}$ for H = 10 m

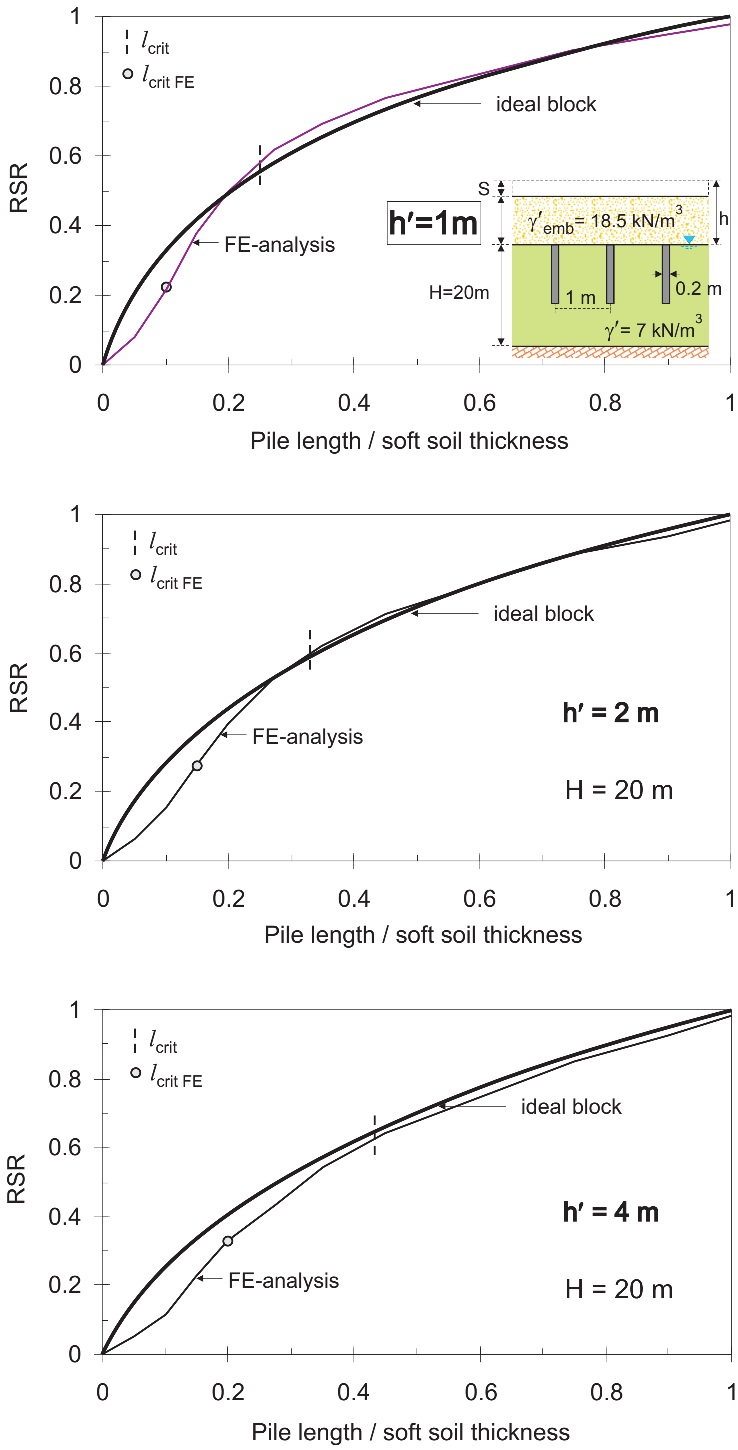

Figure C.2: Comparison between RSR from FE-analyses and $RSR_{ideal\ block}$ for H = 20 m

Bibliography

Adachi, T. and Okano, M. (1974). "A constitutive equation for normally consolidated clay." *Soils and Foundations*, 14(4), 55–73.

Alawneh, A. and Malkawi, A. I. H. (2000). "Estimation of post-driving residual stresses along driven piles in sand." *Geotechnical Testing Journal*, 23(3), 313–326.

Alén, C., Baker, S., Ekström, J., Hallingberg, A., Svahn, V., and Sälfors, G. (2005). "Test embankments on lime/cement stabilized clay." *Proceedings of Deep Mixing'05*. 213–219.

Alpan, I. (1970). "The geotechnical properties of soils." *Earth-Science Reviews*, 6, 5–49.

Arwanitaki, A. and Triantafyllidis, T. (2006). "Mehrlagig mit Geogittern bewehrte Erdkorper uber pfahlartigen Gründungselementen." *Bautechnik*, 83(10), 695–707.

Atkinson, J. H. (2000). "Non-linear soil stiffness in routine design." *Géotechnique*, 50, 487–508.

Atkinson, J. H. and Sällfors, G. (1991). "Experimental determination of soil properties." *Proceedings of 10th ECSMFE*, Vol. 3, Florence. 915–956.

Baligh, M. M. (1985). "Strain path method." *Journal of Geotechnical Engineering*, 111(9), 1108–1136.

Benz, T. (2007). "Small strain stiffness of soils and its numerical consequences," PhD thesis, Institute of Geotechnical Engineering, University of Stuttgart.

Bergado, D. T. and Long, P. V. (1994). "Numerical analysis of embankment on subsiding ground improved by vertical drains and granular piles." *Proceedings of the XIII International Conference on Soil Mechanics and Foundation Engineering*, Vol. 4, Morgantown, WV, USA. A.A. Balkema, 1361–1366.

Biarez, J. and Hicher, P.-Y. (1994). *Elementary Mechanics of Soil Behaviour*. Balkema.

Bjerrum, L. (1967). "Engineering geology of norwegian normally-consolidated marine clays as related to settlements of buildings." *Géotechnique*, 17, 81–118.

Borja, R. I. and Kavaznjian, E. (1985). "A constitutive model for the stress-strain-time behaviour of wet clays." *Géotechnique*, 35, 283–298.

Briaud, J. L. and Tucker, A. M. (1984). "Piles in sand : A method including residual stresses." *Journal of Geotechnical Engineering*, 110(11), 1666–1680.

R. B. J. Brinkgreve, ed. (2002). *PLAXIS 2D Version 8*. A. A. Balkema.

BSI (1995). "Bs 8006: Code of practice for strengthened/reinforced soils and other fills.

Buisman, A. (1936). "Results of long duration settlement tests." *1st International Conference on Soil Mechanics and Foundation Engineering*, Cambridge. 103–107.

Burland, J. B. (1973). "Shaft friction of piles in clay -a simple fundamental approach." *Journal of Ground Engineering*, 3, 30–42.

Burland, J. B. (1989). "Small is beautiful - the stiffness of soils at small stains." *Canadian Geotechnical Journal*, 26, 499–516.

Carlsson, B. (1987). *Reinforced soil, principles for calculation.* Terratema AB, Linköping.

CGTDSM (1958). "Glossary of terms and definitions in soil mechanics." *Journal of the Soil Mechanics and Foundations Division, ASCE*, 84(4), 1–43.

Chandler, R. J. (1968). "Shaft fricion of piles in cohesive soils in term of effective stress." *Civil Engineering and Public Works Review*, 68, 48–51.

Chopra, M. B. and Dargush, G. F. (1992). "Finite element analysis of time-dependent large-deformation problems." *International Journal for Numerical and Analytical Method Geomechanics*, 16, 101–130.

CUR (2001). *Guideline road construction over peat and organic soils*. The Netherlands.

DGGT (2004). *EBGEO: Bewehrte Erdkörper auf punkt- oder linienförmigen Traggliedern*, chapter 6.9.

DIN-1054 (2005). "Baugrund-Sicherheitsnachweise im Erd- und Grundbau.

Dumas, C. (2002). "Piles supported embankments for accelerated construction." FHWA Resource centre.

Duncan, J. M. and Chang, C. Y. (1970). "Nonlinear analysis of stress and strain in soils." *Journal of Soil Mechanics and Foundation Division*, 96(5), 1629–1652.

Eissautier, M. (1986). "Frottement latéral des pieux en milieu pulvérulent.," PhD thesis, Institut National Polytechnique de Grenoble.

Emde, O. (1995). "Der unterspannte schubsteife Balken - Ein mechanisches Modell für geotextilbewerhte Tragschichten." *Report No. 15*, Grundbau, Bodenmechanik und Unterirdisches Bauen, Bergische Unversität Gesamthochschule Wuppertal.

FOND. (1972). "Fondations courantes d´ouvrages d´art. LCPC-SETRA.

Garlanger, J. (1972). "The consolidation of soils exhibiting creep under constant effective stress." *Géotechnique*, 22, 71–78.

Guido, V. A., Kneupel, and Sweeny, M. A. (1987). "Plate loading tests on geogrid-reinforced earth slabs." *Proceedings of Geosynthetics Conference*. 216–225.

Han, J. and Gabr, M. A. (2002). "Numerical analysis of geosynthetic-reinforced and pile-supported earth platforms over soft soil." *Journal of Geotechnical and Geoenvironmental Engineering*, 128(1), 44–53.

Handy, R. L. (1985). "The arch in soil arching." *Journal of Geotechnical Engineering, ASCE*, 111(3), 302–318.

Handy, R. L. (1987). "Closure of discussions of the arch in soil arching." *Journal of Geotechnical Engineering, ASCE*, 113(3), 275–277.

Hanzawa, H. (1989). "Evaluation of design parameters for soft clays as related to geological stress history." *Soils Foundation*, 29, 99–111.

Hardin, B. O. and Drnevich, V. P. (1972). "Shear modulus and damping in soils: Measurement and parameter effects." *Journal of Soil Mechanics and Foundation Divisions*, 98, 602–624.

Henke, S. and Grabe, J. (2006). "Simulation of pile driving by 3-dimensional finite-element analysis." *Proceedings of 17th European Young Geotechnical Engineers' Conference*, Szavits-Nossan, ed.

Hewlett, W. J. and Randolph, M. F. (1988). "Analysis of piled embankments." *Ground Engineering*, 21(3), 5.

Holtz, R. D. and Massarsch, K. R. (1976). "Improvement of the stability of an embankment by piling and reinforced earth." *Proceedings of 6th european conference on soil mechanics and foundation engineering*, Vol. 1.2. 473–478.

Holtz, W. G. and Lowitz, C. A. (1965). "Effects of driving displacement piles in lean clay." *Journal of Soil Mechanics and Foundation Division*, 91, 1–13.

Jardine, R. J., Standing, J. R., and Chow, F. C. (2006). "Some observation of the effects of time on the capacity of piles driven in sand." *Geotechnique*, 56(4), 227–244.

Jenck, O., Dias, D., and Kastner, R. (2007). "Two-dimensional physical and numerical modeling of a pile-supported earth platform over soft soil." *Journal of Geotechnical and Geoenvironmental Engineering*, 133(3), 295–305.

Jones, C. J. F. P., Lawson, C. R., and Ayres, D. J. (1990). "Geotextile reinforced piled embankments." *Proceedings of the 4th International Conference on Geotextiles, Geomembranes and Related Products*, Vol. 1, The Hague. A.A. Balkema, 155–160.

Kempton, G., Russell, D., Pierpoint, N. D., and Jones, C. J. F. P. (1998). "Two- and three-dimensional analysis of the performance of piled embankments." *Proceeding of 6th International Conference in Geosynthetics*, Rowe, ed., Atlanta. 767–772.

Kondner, R. L. and Zelasko, J. S. (1963). "A hyperbolic stress-strain formulation for sands." *2nd Pan-American Conference of Soil Mechanics and Foundation Engineering*, Vol. 1. 289–394.

Kulhawy, F. H. (1984). "Limiting tip and side resistance: Fact or fallacy." *Proceeding of Symposium on Design and Analysis of Pile Foundation*, New York. ASCE, 80–98.

Lancellotta, R. (1995). *Geotechnical Engineering*. A.A.Balkema, Rotterdam.

Larsson, R. and Sällfors, G. (1986). "Automatic continuous consolidation testing in sweeden." *Consolidation of Soils : Testing and Evaluation*, ASTM Special Technical Publication 892.

Leoni, M., Karstunen, M., and Vermeer, P. A. (2008). "Anisotropic creep model for soft soils." *Géotechnique*, 58(3), 215–226.

Love, J. and Milligan, G. (2003). "Design methods for basally reinforced pile-supported embankments over soft ground." *Ground Engineering*, 36(3), 39–43.

Mabsout, M. E., Reese, L. C., and Tassoulas, J. L. (1995). "Study of pile driving by finite-element method." *Journal of Geotechnical Engineering*, 121(7), 535–543.

Mesri, G. and Choi, Y. (1985). "Settlement analysis of embankments on soft clays." *Journal of Geotechnical Engineering*, 4(111), 441–464.

Möller, S. C. (2006). "Tunnel induced settlements and structural forces in lining," PhD thesis, Institute of Geotechnical Engineering, University of Stuttgart.

Morison, M. J. (1984). "Insitu measurement on a model pile in clay," PhD thesis, MIT.

Naughton, P. J. (2007). "The significance of critical height in the design of piled embankments." *Geotechnical Special Publication*, number 172 in Geotechnical Special Publication, Denver, CO, United States. American Society of Civil Engineers, Reston, VA 20191-4400, United States.

Ohde, J. (1930). "Zur Theorie der Druckverteilung im Baugrund." *Bauingenieur*, 20, 451–459.

Olsson, M., Edstam, T., and Alén, C. (2008). "Some experiences from full-scale test embankments on floating lime-cement columns." *Geotechnics of Soft Soils - Focus on Ground Improvement*, London. Taylor & Francis Group, 77–85.

O'Neil, M. W. and Reese, L. C. (1972). "Behaviour of bored piles in Beaumont clay." *Journal of the Soil Mechanics and Foundation Division*, 98, 195–213.

Pestana, J. M., Hunt, C. E., and Bray, J. D. (2002). "Soil deformation and excess pore pressure field around a closed ended pile." *Journal of Geotechnical and Geoenvironmental Engineering*, 128, 1–12.

Plomteux, C. and Porbaha, A. (2004). "Cmc foundation system for embankment support - a case history." *Proceeding of Geosupport, ASCE*.

Poulos, H. G. (2007). "Design charts for piles supporting embankments on soft clay." *Journal of Geotechnical and Geoenvironmental Engineering*, 133(5), 493–501.

Puech, A., Foray, P. Boulon, M., and Desreus, J. (1979). "Calcul des pieux à l´arrachement à partir d´un modèle numérique en contraintes effectives. premiers résultats.." *Proceeding of the 7th European Conference on Soil Mechanics and Foundation Engineering*, Vol. 1. 227–233.

Rahardjo, P. P. (2005). *Ground improvement case histories : The use of bamboo and bakau piles for soil improvements and applications of piled raft system for the construction of embankment on peats and soft soils*, chapter 31, 899–922. Elsevier.

Randolph, M. F. and Wroth, C. P. (1979). "An analytical solution for the consolidation around a driven pile." *International Journal for Numerical and Analytical Method Geomechanics*, 3, 217–229.

Rathmayer, H. (1975). "Piled embankment supported by single pile cap." *Proceeding of Conference on Soil Mechanics and Foundation Engineering*, Istanbul. 283–290.

Roscoe, K. H. and Burland, J. B. (1968). "On the generalised stress-strain behaviour of wet clay." *Engineering Plasticity*, Vol. 1, London, UK. Cambrigde University Press, 535–609.

Roy, M., Blanchet, R., Tavenas, F., and La Rochelle, P. (1981). "Behaviour of a sensitive clay during pile driving." *Canadian Geotechnical Journal*, 18, 67–85.

Ruse, N. M. (2004). "Räumliche Betrachtung der Standsicherheit der Ortsbrust beim Tunnelvortrieb," PhD thesis, Institut für Geotechnik, Universität Stuttgart.

Russel, D. and Pierpoint, N. (1997). "Assessment of design methods for piled embankments." *Ground Engineering*, 30(10), 39.

Russo, G. (2004). "Full-scale load tests on instrumented piles." *Proceeding of the Institution of Civil Engineers, Geotechnical Engineering 157*, GE3. 127–135.

Said, I. (2006). "Comportement des interfaces et modélisation des pieux sous charge axiale," PhD thesis, Ecole Nationale des Ponts et Chaussées.

Satibi, S., Abed, A., Yu, C., Leoni, M., and Vermeer, P. A. (2007). "Finite element simulation of installation and loading of tube-installed pile." *Report No. 29*, Institute for Geotechnical Engineering, University of Stuttgart.

Satibi, S., Van der Meij, R., and Leoni, M. (2007). "Piled embankments: literature review and required further research using numerical analysis." *Report No. 34*, IGS, Universität Stuttgart.

Schanz, T. (1998). "Zur Modellierung des mechanischen Verhaltens von Reibungsmaterialien." *Report No. 45*, Institut für Geotechnik, Unversität Stuttgart.

Schanz, T., Vermeer, P. A., and Bonnier, P. G. (1999). "The hardening soil model: Formulation and verification." *Beyond 2000 in Computational Geotechnics - 10 years of Plaxis*, Rotterdam. Balkema.

Seed, H. B. and Idriss, I. (1970). "Soil moduli and damping factors for dynamic response analyses." *Report no.*, Earthquake Engineering Research Center, University of California, Barkeley.

Smoltczyk, U. (1976). "Pile foundation of a railway embankment." *Proceedings of 6th european conference on soil mechanics and foundation engineering*, Vol. 1.2. Gistel & Cie., Wien, 473–478.

Spangler, M. G. and Handy, R. L. (1982). *Soil engineering*. Harper and Row, Inc., New York.

Tan, S. B., Tan, S. L., Yang, K. S., and Chin, Y. K. (1985). "Soil improvement method in singapore." *Proceedings of 3rd International Geotechnical Seminar on Soil Improvement Methods*. NTI, Singapore, 249–272.

Terzaghi, K. (1936). "Stress distribution in dry and in saturated sand above a yielding trap-door." *Proceedings of the International Conference on Soil Mechanics and Foundation Engineering*, Vol. Bd.1, Cambridge. 307–311.

Terzaghi, K. (1941). *Theoritical soil mechanics*.

The, B. H. P. A. M., Tauuffic, R., Moeljani, D., Suhaimi, D., Shouman, Teunissen, E., and Deutekom, J. (2002). "The bereng bengkel test site." *Report no.*, RWS-DWW and IRE.

Totani, G., Calabrese, M., and Monaco, P. (1994). "Shaft resistance of piles driven in clay: Field study of an instrumented full scale pile." *Piled Foundations Experimental Investigations, Analysis and Design*, Napoli. 199–253.

Touma, F. T. and Reese, L. C. (1974). "Behaviour of bored pile in sand." *Journal of the Geotechnical Engineering Devision*, 100(GT7), 749–761.

Van der Stoel, A. E. C., Klaver, J. M., T., B. A., and de Lange, A. P. (2006). "Numerical design, installation and monitoring of a load transfer platform (ltp) for a railway embankment near rotterdam." *Proceeding of Numerical Methods in Geotechnical Engineering*, H. F. Schweiger, ed. 463–469.

Van Eekelen, S. J. M., Bezuijen, A., and Alexiew, D. (2008). "Piled embankments in the netherlands, a full scale test, comparing 2 years of measurements with design calculations." *Proceeding of 4th European Geosynthetics Conference*.

Van Eekelen, S. J. M., Bezuijen, A., and Oung, O. (2003). "Arching in piled embankments; experiments and design calculations." *BGA International Conference on Foundations, Innovations, Observations, Design and Practice*, BGA International Conference on Foundations, Innovations, Observations, Design and Practice, Dundee, United Kingdom. Thomas Telford Services Ltd, London, United Kingdom, 885–894.

Van Impe, W. F. (1994). "Influence of screw pile installation parameters on th overall pile behaviour." *Workshop on Piled Foundation: Full Scale Investigations, Analysis and Design.*, Naples.

Van Langen, H. (1991). "Numerical analysis of soil-structure interaction," PhD thesis, T.U. Delft.

Van Langen, H. and Vermeer, P. A. (1991). "Interface elements for singular plasticity points." *International Journal for Numerical and Analytical Method Geomechanics*, 15, 301–315.

Vermeer, P., Leoni, M., Karstunnen, M., and Neher, H. (2006). "Modelling and numerical simulation of creep in soft soils." *Proceedings of the 4th International Conference on Soft Soil Engineering (ICSSE)*, Vancouver. 57–71.

Vermeer, P. A. (1978). "A double hardening model for sand." *Géotechnique*, 28(4), 413–433.

Vermeer, P. A. and Neher, H. P. (1999). "A soft soil model that accounts for creep." *Proceeding of International Symposium Beyond 2000 in Computational Geotechnics*. Balkema, 249–261.

Vermeer, P. A., Punlor, A., and Ruse, N. (2001). "Arching effects behind a soldier pile wall." *Computers and Geotechnics*, 28, 379–396.

Vermeer, P. A. and Schad, H. (2005). "Hsp pile loading tests in wijchen: Inspection report." *Report no.*, Institut for Geotechnical Engineering, University of Stuttgart.

Vermeer, P. A., Schweiger, H., and Zweschper, B. (1999). "Assessment of influence of constitutive models in finite element analysis of deep excavations." *Report No. 12*, Institute for Geotechnical Engineering, University of Stuttgart.

Vermeer, P. A. and Sutjiadi, W. (1985). "The uplift resistance of shallow embedded anchors." *Proceedings of the 11th International Conference on Soil Mechanics and Foundation Engineering*, San Fransisco. 1635–1638.

Vesic, A. S. (1963). "Bearing capacity of deep foundation in sand." *Highway Research Record*, number 39, National Academy of Sciences, National Research Council, 112–153.

Vesic, A. S. (1970). "Test on instrumented piles, Ogeechee river site." *Journal of the Soil Mechanics and Foundation Devision*, 96, 561–584.

Vesic, A. S. (1972). "Expansion of cavities in infinite soil mass." *Journal of the Soil Mechanics and Foundation Devision*, 98(3), 265–290.

Von Soos, P. (2001). *Eigenschaften von Boden und Fels - ihre Ermittung im Labor : Gundbau-Taschenbuch*, Vol. 1, chapter 1.4, 117–201. Ernst und Sohn, Berlin.

Wehnert, M. and Vermeer, P. A. (2004). "Numerical analyses of load tests on bored piles." *Proceedings 9th Symposium on Numerical Models in Geomechanics (NUMOG IX)*, Ottawa, Canada. A.A. Balkema Publishers, 505–511.

Wichert, H. W. (1988). "Einfluß der Alterung auf die Tragfähigkeit von historischen Spickpfahl-Gründungen," PhD thesis, Technische Unversität Braunschweig.

Wieckowsky, Z. (2004). "The material point method in large strain engineering problems." *Computer Methods in Applied Mechanics and Engineering*, 193, 4417–4438.

Wood, H. J. (2003). "The design and construction of pile-supported embankments for the A63 selby bypass." BGA International Conference on Foundations, Innovations, Observations, Design and Practice. Thomas Telford Services Ltd, London, United Kingdom, 941–950.

Zaeske, D. (2001). "Zur Wirkungweise von unbewehrten und bewerhrten mineralischen Tragschichten über pfahlartigen Gründungselementen," PhD thesis, Universität Gh Kassel.

Curriculum Vitae

08.10.1976	Geboren in Bengkalis (Indonesien)
1995-2000	Institut Teknologi Bandung (Indonesien) Diplom in Bauingeniurwesen
2000-2001	University of Newcastle Upon Tyne (United Kingdom) Master in Geotechnik
Seit 2002	University of Riau (Indonesien) wissenschaftlicher Mitarbeiter
2005-2009	Universität Stuttgart Doktorand im Rahmen des ENWAT Doktoral program

Mitteilungen des Instituts für Geotechnik

Nr. 01	Thamm, B. R.	(1974)	Anfangssetzungen und Anfangsporenwasserüberdrücke eines normalverdichteten wassergesättigten Tones. € 5,11
Nr. 02	Gußmann, P.	(1975)	Einheitliche Berechnung von Grundbruch und Böschungsbruch. € 2,56
Nr. 03	Feeser, V.	(1975)	Die Bedeutung des Kalziumkarbonats für die bodenphysikalischen Eigenschaften vom Löß. **Vergriffen**
Nr. 04	Du Thin, K.	(1976)	Standsicherheit von Böschungen: Programm-Dokumentation. **Vergriffen**
Nr. 05	Smoltczyk, U. / Pertschi, O. / Hilmer, K.	(1976)	Messungen an Schleusen in der UdSSR. Schleusennorm der UdSSR (SN 30365). **Vergriffen**
Nr. 06	Hilmer, K.	(1976)	Erddruck auf Schleusenkammerwände. € 9,20
Nr. 07	Laumans, Q.	(1977)	Verhalten einer ebenen, in Sand eingespannten Wand bei nichtlinearen Stoffeigenschaften des Bodens. € 9,20
Nr. 08	Lächler, W.	(1977)	Beitrag zum Problem der Teilflächenpressung bei Beton am Beispiel der Pfahlkopfanschlüsse. **Vergriffen**

Nr. 09	Spotka, H.	(1977)	Einfluß der Bodenverdichtung mittels Oberflächenrüttelgeräten auf den Erddruck einer Stützwand bei Sand. **Vergriffen**
Nr. 10	Schad, H.	(1979)	Nichtlineare Stoffgleichungen für Böden und ihre Verwendung bei der numerischen Analyse von Grundbauaufgaben. **Vergriffen**
Nr. 11	Ulrich, G.	(1980)	Verschiebungs- und kraftgesteuerte Plattendruckversuche auf konsolidierenden Böden.
	Gußmann, P.		Zum Modellgesetz der Konsolidation. € 10,23
Nr. 12	Salden, D.	(1980)	Der Einfluß der Sohlenform auf die Traglast von Fundamenten. € 12,78
Nr. 13	Seeger, H.	(1980)	Beitrag zur Ermittlung des horizontalen Bettungsmoduls von Böden durch Seitendruckversuche im Bohrloch. € 12,78
Nr. 14	Schmidt, H. H.	(1981)	Beitrag zur Ermittlung des Erddrucks auf Stützwände bei nachgiebigem Baugrund. € 12,78
Nr. 15	Smoltczyk, U. / Schweikert, O.	(1981)	Vorstudie über bauliche Alternativen für Durchgangsstraßen in Siedlungen. € 6,14
Nr. 16	Malcharek, K. / Smoltczyk, U.	(1981)	Vergleich nationaler Richtlinien für die Berechnung von Fundamenten. € 7,67
Nr. 17	Gruhle, H. D.	(1981)	Das Verhalten des Baugrundes unter Einwirkung vertikal gezogener Ankerplatten als räumliches Problem des Erdwiderstandes. **Vergriffen**
Nr. 18	Kobler, W.	(1982)	Untersuchungen über Böschungs- und Grundbruch bei begrenzten Lastflächen. € 12,78
Nr. 19	Lutz, W.	(1983)	Tragfähigkeit des geschlitzten Baugrunds neben Linienlasten. € 12,78

Nr. 20	Smoltczyk, U.	(1983)	Studienunterlagen Bodenmechanik und Grundbau; überarbeitete Ausgabe 1983. € 20,45
Nr. 21	Schweikert, O.	(1984)	Der Einfluß des Böschungswinkels auf die Berechnung des aktiven Erddrucks. € 10,23
Nr. 22	Vogt, N.	(1984)	Erdwiderstandsermittlung bei monotonen und wiederholten Wandbewegungen in Sand. **Vergriffen**
Nr. 23	Buchmaier, R.	(1985)	Zur Berechnung von Konsolidationsproblemen bei nichtlinearem Stoffverhalten. € 12,78
Nr. 24	Schad, H.	(1985)	Möglichkeiten der Böschungssicherung bei kleinen Baugruben.
	Smoltczyk, U. / Schad, H. / Zoller, P.		Sonderkonstruktionen der Böschungssicherung. € 17,90
N. 25	Gußmann, P.	(1986)	Die Methode der Kinematischen Elemente. € 10,23
Nr. 26	Steinmann, B.	(1985)	Zum Verhalten bindiger Böden bei monotoner einaxialer Beanspruchung. **Vergriffen**
Nr. 27	Lee, S. D.	(1987)	Untersuchungen zur Standsicherheit von Schlitzen im Sand neben Einzelfundamenten. **Vergriffen**
Nr. 28	Kolb, H.	(1988)	Ermittlung der Sohlreibung von Gründungskörpern unter horizontalem kinematischen Zwang. € 12,78
Nr. 29	Ochmann, H.	(1988)	Ebene Grenzzustände von Erdböschungen im stochastischen Sicherheitskonzept. € 12,78
Nr. 30	Breinlinger, F.	(1989)	Bodenmechanische Stoffgleichungen bei großen Deformationen sowie Be- und Entlastungsvorgängen. € 15,34

Nr. 31	Smoltczyk, U. / Breinlinger, F. / Schad, H. / Wittlinger, M. y	(1989)	Beitrag zur Bemessung von Tunneln in offener Bauweise. € 12,78
Nr. 32	Gußmann, P. / Schanz, T. / Smoltczyk, U. / Willand, E.	(1990)	Beiträge zur Anwendung der KEM (Erddruck, Grundbruch, Standsicherheit von Böschungen) **Vergriffen**
Nr. 33	Gruhle, H. D.	(1990)	Der räumliche Erdwiderstand vor überwiegend horizontal belasteten Ankerplatten. **Vergriffen**
Nr. 34	Henne, J.	(1995)	Zur Bewehrung von verformten Bodenschichten durch Einsatz zugfester Geokunststoffe. € 15,34
Nr. 35	Wittlinger, M.	(1994)	Ebene Verformungsuntersuchungen zur Weckung des Erdwiderstandes bindiger Böden. € 15,34
Nr. 36	Schad, H.	(1992)	Zeit- und geschwindigkeitsabhängiges Materialverhalten in der Geotechnik – Experimentelle Erfassung und numerische Analyse. € 15,34
Nr. 37	Belz, I.	(1992)	Zur Ermittlung dynamischer Bodenkennwerte in situ aus der Systemantwort des Erregers. € 15,34
Nr. 38	Ma, J.	(1994)	Untersuchungen zur Standsicherheit der durch Stützscheiben stabilisierten Böschungen. € 15,34
Nr. 39	Smoltczyk, U.	(1994)	Sonderheft: 25 Jahre Lehre und Forschung in der Geotechnik. € 15,34
Nr. 40	Rilling, B.	(1994)	Untersuchungen zur Grenztragfähigkeit bindiger Schüttstoffe am Beispiel von Lößlehm. € 17,90
Nr. 41	Vermeer, P. A.	(1996)	Deponiebau und Geotechnik. € 17,90

Nr. 42	Vermeer, P. A.	(1997)	Baugruben in Locker- und Festgestein. € 17,90
Nr. 43	Brinkmann, C.	(1998)	Untersuchungen zum Verhalten von Dichtungsübergängen im Staudammbau. € 17,90
Nr. 44	Fiechter-Scharr, I.	(1998)	Beeinflussung von Erdbaustoffen durch Beimischen eines organophilen Bentonits. € 17,90
Nr. 45	Schanz, T.	(1998)	Zur Modellierung des mechanischen Verhaltens von Reibungsmaterialien. € 17,90
Nr. 46	Akinrogunde, A. E.	(1999)	Propagation of Cement Grout in Rock Discontinuities Under Injection Conditions. € 17,90
Nr. 47	Vogt-Breyer, C.	(1999)	Experimentelle und numerische Untersuchungen zum Tragverhalten und zur Bemessung horizontaler Schraubanker. € 17,90
Nr. 48	Vermeer, P. A.	(1999)	Neue Entwicklungen in der Geotechnik. € 17,90
Nr. 49	Marcher, T.	(2002)	Resultate eines Versuchsprogramms an Beaucaire-Mergel. € 17,90
Nr. 50	Marcher, T.	(2003)	Nichtlokale Modellierung der Entfestigung dichter Sande und steifer Tone. € 17,90
Nr. 51	Ruse, N. M.	(2004)	Räumliche Betrachtung der Standsicherheit der Ortsbrust beim Tunnelvortrieb. **Vergriffen**
Nr. 52	Beutinger, P. H.	(2005)	Ein geotechnischer Beitrag zur Standsicherheit mobiler Baumaschinen. € 17,90
Nr. 53	Wehnert, M.	(2006)	Ein Beitrag zur drainierten und undrainierten Analyse in der Geotechnik. € 17,90
Nr. 54	Möller, S. C.	(2006)	Tunnel induced settlements and structural forces in linings. € 17,90

Nr. 55	Benz, T.	(2007)	Small-Strain Stiffness of Soils and its Numerical Consequences. € 17,90
Nr. 56	Abed, A.	(2008)	Numerical Modeling of Expansive Soil Behavior. € 17,90
Nr. 57	Hintner, J.	(2008)	Analyse der Fundamentverschiebungen infolge vertikaler und geneigter Belastung. € 17,90
Nr. 58	Russeli, C.	(2008)	Probabilistic Methods applied to Bearing Capacity Problem. € 17,90
Nr. 59	Olarte, A. A. P.	(2008)	Influence of Particle Shape on the Global Mechanical Response of Granular Packings: Micromechanical Investigation of the Critical State in Soil Mechanics. € 17,90
Nr. 60	Neher, H. P.	(2008)	Zeitabhängiges Materialverhalten und Anisotropie von weichen Böden - Theorie und Anwendung. € 17,90
Nr. 61	Vermeer, P. A.	(2008)	Von der Forschung zur Praxis: Symposium anlässlich des 80. Geburtstags von Prof. U. Smoltczyk € 17,90
Nr. 62	Satibi, S.	(2009)	Numerical Analysis and Design Criteria of Embankments on Floating Piles € 17,90